

Enhancing Motor Cortical Theta and Gamma Oscillations Using Closed-loop Phase-dependent Optogenetic Stimulation

A thesis submitted for the degree of

Doctor of Philosophy

August 2024

Jessica Louise Myatt

Keble College

MRC Brain Network Dynamics Unit

Nuffield Department of Clinical Neurosciences

University of Oxford

Oxford, UK

Abstract

Neuronal oscillations are a prominent feature of motor cortical local field potentials (LFPs) and abnormalities in oscillatory activity have been linked to several disorders. Theta-modulated gamma-frequency pulses of alternating current stimulation are known to modulate motor learning in humans; however, it is unclear how these frequencies modulate motor cortical activity at the cellular microcircuit level.

Here, we aimed to develop a method for bidirectionally modulating theta and gamma coupled oscillations in the motor cortex using closed-loop optogenetic stimulation of parvalbumin (PV)-expressing inhibitory interneurons or excitatory pyramidal neurons. To achieve this, motor cortical LFPs were recorded in PV-Cre and RBP4-Cre (retinol-binding-protein-4) mice, in which these neurons were transfected with Channelrhodopsin-2 (ChR2). Using our recently developed phase-tracking system (OscillTrack), blue-light pulses were delivered at four phases of the ongoing motor cortical theta oscillation in awake, head-fixed mice. Optogenetic stimulation was delivered over a quarter of the theta cycle, either as a continuous pulse, a burst of three pulses at gamma frequency (75Hz), or a burst of three pulses where the gamma rhythmicity was slightly altered – random gamma.

Both continuous and gamma stimulation significantly modulated motor cortical theta power in a phase-dependent manner compared to controls, with continuous stimulation of excitatory cells leading to strongest modulation. Phase-dependent amplification during stimulation of excitatory vs inhibitory neurons was offset by 90°, in line with predictions from computational models of excitatory and inhibitory circuits. These effects did not occur when previously recorded closed-loop stimulation patterns were replayed to the mice, suggesting that the effects on theta power were not due to the stimulation patterns alone, but rather due to the real-time interaction with underlying theta phase. While gamma oscillations were broadly modulated by all stimulation types for excitatory neurons, the strongest effect was induced by gamma stimulation, leading to a clear 75Hz peak. These results were not dependent on the phase of theta oscillation targeted.

These findings demonstrate that phase-dependent modulation of theta power can be mediated by stimulation of excitatory or inhibitory neurons, and that the effect of specific stimulation phases is likely to be the result of interactions between these populations. Moreover, theta phase-dependent optogenetic stimulation of excitatory, but not inhibitory, neurons could be a more effective method of driving cortical gamma power. This approach can be used to inform the development of brain stimulation methods to modulate these activities in humans.

Acknowledgements

First, I must thank my supervisors, Andrew Sharott and Charlotte Stagg for their patience, guidance and kindness throughout this project. For creating welcoming research environments and for supporting me in applications to broaden my research knowledge, opportunities and indulge in my passion to travel, either at international conferences or through my research placement in Canada.

In particular, this project relied on the OscillTrack algorithm for real-time phase tracking, previously developed in the Sharott group by Colin McNamara. Many thanks to Robert Toth who integrated OscillTrack with Intan to provide a graphical user interface (GUI) which allowed us to set and visualise real-time phase-tracking capabilities simultaneously with optogenetics – this project would not have been possible without this. In addition to this, I thank Robert for his help in writing the pre-processing scripts for data analysis as well as the initial plotting scripts for visualising our data. I would also like to acknowledge Andreia Madalena and Naomi Berry for training me in surgery techniques and head-fixed recordings when I first joined the group; their previous supervision and patience allowed me to hit the ground running when I started my DPhil project. I also thank Jane Westcott and Rae Dolman for expert animal care, Ben Micklem for microscopy support and help acquiring the confocal images using an oil immersion objective lens, and Brook Perry for technical support in the lab. I also thank all members, past and present of both the Sharott lab and the Physiological Neuroimaging Group (PiNG) for their friendship, advice and support throughout my DPhil, as well as the wider members of the BNDU.

Special thanks also go to the friends I made within Oxford, who have been on this unpredictable journey alongside me. As well as the friends I made during my undergraduate degree in Manchester, who were always there for me when needed, either at the end of the phone or willing to book a last-minute flight or trip to escape reality with me, and to always remind me that anything is possible if you believe in it. I would also like to thank my friends from home, for always sending words of encouragement and picking me back up when I didn't believe in myself. Finally, I must thank my partner and family for their unconditional love and constant belief in me. Completing this thesis is a testament to their unwavering support over the course of this journey and I submit this thesis with great pride.

Contents

ABSTRACT ..... **I**

ACKNOWLEDGEMENTS ..... **III**

CONTENTS ..... **IV**

TABLES ..... **IX**

FIGURES ..... **IX**

ABBREVIATIONS ..... **XIII**

1. GENERAL INTRODUCTION **1**

1.1 CEREBRAL CORTEX 1

1.1.1 Anatomy & Function of the Motor Cortex *1*

1.1.2 Cellular anatomy & connectivity of the motor cortex *5*

1.1.2.1 Glutamatergic Pyramidal Neurons 5

1.1.2.2 GABAergic Interneurons 7

1.1.2.3 Layer 5 circuitry 11

1.1.3 Neural Circuitry & Pathways *13*

1.1.4 Disorders & Dysfunction of the Motor Cortex *15*

1.2 OSCILLATIONS 17

1.2.1 Quantifying oscillation via the local field potential *17*

1.2.2 Introduction to neural oscillations *21*

1.2.3 Function of neural oscillations *27*

1.2.4 Role of theta & gamma oscillations *31*

1.2.5 How we can study oscillations using in vivo electrophysiology *41*

1.2.6 Rationale for acute electrophysiology *42*

1.2.7 Oscillations & disease *43*

1.3 BRAIN STIMULATION 46

1.3.1 Brain stimulation & current uses *46*

1.3.2 Benefits & Drawbacks of Deep Brain Stimulation *48*

1.3.3 Rationale for closed-loop brain stimulation *49*

1.3.4 Examples of phase-locked stimulation in humans *53*

1.3.5 Phase-locked stimulation in animal models *56*

1.3.6 Non-phased-locked closed loop stimulation approaches *60*

1.3.7 Neuroplasticity & therapeutic applications of closed-loop brain stimulation *60*

1.4 THE ROLE OF OPTOGENETICS 61

1.4.1 Background of optogenetics *62*

1.4.2 Genetic engineering for optogenetics *64*
1.4.3 Rational, relevance & pitfalls of optogenetics *68*
1.4.4 Complexities of in vivo optogenetic studies *70*
1.5 AIMS 72
2 METHODS 74
2.1 ANIMALS 74
2.2 STEREOTAXIC SURGERIES 74
2.2.1 Unilateral Stereotaxic Viral Injection *74*
2.2.2 Headplate Surgery *76*
2.3 HABITUATION & ELECTROPHYSIOLOGICAL RECORDINGS 77
2.4 CLOSED-LOOP ELECTROPHYSIOLOGY 79
2.5 STIMULATION PROTOCOL 81
2.6 OPEN-LOOP ELECTROPHYSIOLOGY 83
2.7 HISTOLOGY - IMMUNOHISTOCHEMISTRY 85
2.8 CLOSED-LOOP ALGORITHM & IMPLEMENTATION WITH INTAN RHD2000 87
2.9 DATA ANALYSIS 88
2.9.1 Pre-processing *88*
2.9.2 Statistical Analyses *90*
2.10 BREAKDOWN OF EXPERIMENTAL MICE 93
3 MODULATION OF INHIBITORY INTERNEURONS 96
3.1 INTRODUCTION 96
3.2 METHODS 100
3.3 RESULTS 102
3.3.1 ChR2-GFP expression was localised to PV-interneurons *102*
3.3.2 Accurate phase-targeting of the ongoing theta oscillations *104*
3.3.3 Closed-loop gamma stimulation *106*
3.3.3.1 Closed-loop gamma stimulation of the motor cortex results in phase-specific modulation of theta power in PV-Cre mice 109
3.3.3.2 Gamma stimulation leads to phase-specific effects on theta power in opsin mice but not control mice 111
3.3.3.3 Gamma stimulation in opsin mice results in phase-specific effects on theta power only when stimulation is on 112
3.3.4 Closed-loop continuous stimulation *112*
3.3.4.1 Closed-loop continuous stimulation of the motor cortex results in phase-specific modulation of theta power in PV-Cre mice 113
3.3.4.2 Continuous stimulation leads to phase-specific effects on theta power in opsin but not control mice 115
3.3.5 Open-Loop Stimulation *117*

3.3.5.1 Stimulation patterns resulting from closed-loop stimulation do not underly phase-dependent changes in theta power. 117
3.3.5.2 Open-loop gamma and continuous stimulation do not significantly modulate theta power in opsin mice 120
3.4 DISCUSSION 124
3.4.1 Accuracy of phase tracking does not depend on the phase of stimulation 125
3.4.2 Closed-loop is more effective than open-loop for modulation of theta phase 126
3.4.3 Heterogeneity of optogenetically stimulated cells 127
3.4.3.1 Stimulated PV interneurons are spread across cortical layers 127
3.4.3.2 Stimulated cells may not all be FS 127
3.4.4 Phase-specificity may be a property of the underlying microcircuitry 129
3.4.5 Phase-specific optogenetic stimulation outside motor cortex leads to behavioural effects 130
3.4.6 Response of PV+ interneurons to optogenetic stimulation 131
3.4.7 Conclusions 132
4 MODULATION OF EXCITATORY PYRAMIDAL NEURONS 133
4.1 INTRODUCTION 133
4.2 METHODS 135
4.3 RESULTS 137
4.3.1 ChR2-GFP expression localised to cell bodies in layer 5 137
4.3.2 Accurate phase targeting of ongoing theta oscillations 139
4.3.3 Closed-loop gamma stimulation 141
4.3.3.1 Closed-loop gamma stimulation of the motor cortex results in phase-specific modulation of theta power in RBP4-Cre mice 142
4.3.3.2 Gamma stimulation leads to phase-specific effects on theta power in opsin but not control mice 146
4.3.3.3 Gamma stimulation in opsin mice results in phase-specific effects on theta power only when stimulation is on 147
4.3.4 Closed-loop continuous stimulation 147
4.3.4.1 Closed-loop continuous stimulation of the motor cortex results in phase-specific modulation of theta power in RBP4-Cre mice 148
4.3.4.2 Continuous stimulation leads to phase-specific effects on theta power in opsin but not control mice 152
4.3.4.3 Continuous stimulation in opsin mice leads to phase-specific effects of theta power only when stimulation is on 153
4.3.5 Open loop stimulation 153
4.3.5.1 Stimulation patterns resulting from closed-loop stimulation do not underly phase-dependent changes in theta power 153

4.3.5.2 Open-loop gamma and continuous stimulation modulate theta power in opsin mice, but only when consistently stimulated 157
4.3.6 Determining the role of gamma rhythmicity 164
4.3.6.1 Gamma rhythmicity does not affect phase-dependent theta power modulation 166
4.3.6.2 No significant differences in theta power modulation by stimulation pattern 167
4.3.6.3 Gamma and random gamma stimulation resulted in significant phase-dependent modulation of theta power when stimulation was on 168
4.3.6.4 Closed-loop random gamma stimulation pattern does not underly phase-specific theta modulation 169
4.4 DISCUSSION 173
4.4.1 Accuracy of phase-tracking is not dependent on the phase of stimulation 173
4.4.2 Closed-loop is more effective than open-loop stimulation for theta-phase modulation 174
4.4.3 Phase-specific modulation is not dependent on stimulation pattern 175
4.4.4 Pyramidal neuron subtypes potentially involved in theta modulation within L5 176
4.4.5 Interneuron subtypes potentially involved in theta modulation within L5 178
4.4.6 Pyramidal neurons can respond to gamma frequency optogenetic stimulation 179
4.4.7 Theta-gamma coupling is unlikely to play a role in theta power modulation in this experimental set-up 179
4.4.8 Conclusions 180
5 CELL-TYPE DEPENDENT MODULATION OF GAMMA POWER 182
5.1 INTRODUCTION 182
5.2 METHODS 185
5.3 RESULTS 186
5.3.1 Theta phase-specific stimulation of inhibitory interneurons 186
5.3.1.1 No significant theta phase modulation of gamma oscillations in PV-Cre mice 186
5.3.1.2 Phase-specific theta stimulation of PV-Cre ChR2 mice does not significantly modulate gamma power compared to control mice 190
5.3.2 Theta phase-specific modulation of excitatory pyramidal cells 192
5.3.2.1 No significant theta phase modulation of gamma oscillations in RBP4-Cre mice 192
5.3.2.2 Phase-specific theta stimulation of pyramidal neurons significantly modulates gamma power 196
5.3.2.3 Stimulation patterns resulting from closed-loop stimulation modulate gamma power to a lesser extent than when phase-locked 199
5.3.2.4 Theta phase-specific stimulation patterns differentially modulate gamma power when targeted to pyramidal neurons 203
5.3.2.5 Rhythmic gamma stimulation most significantly modulates gamma power 204
5.3.2.6 Gamma power modulation varies significantly across all three stimulation patterns 207

5.3.2.7 Resultant random gamma closed-loop stimulation pattern leads to significantly less modulation of gamma power 207
5.4 DISCUSSION 210
5.4.1 Gamma stimulation did not lead to increased gamma power when targeting PV+ interneurons 210
5.4.2 Gamma and continuous stimulation lead to increased gamma power when targeting RBP4+ pyramidal neurons 211
5.4.3 The rhythm of gamma stimulation is important for the modulation of gamma power 212
5.4.4 Open-loop replay of theta-phase locked stimulation modulated gamma power to a lesser extent 212
5.4.5 Optogenetic stimulation led to modulation of gamma power in both control and opsin PV+ mice 213
5.4.6 75Hz is a key frequency in the motor cortex 216
5.4.7 Conclusions 217
6 GENERAL DISCUSSION 219
6.1 OVERVIEW 219
6.1.1 Inhibitory and excitatory neurons have a 90-degree offset in phase-dependent amplification, indicating neuronal synchronisation 219
6.1.2 Optogenetic modulation of gamma power is not theta phase-specific 223
6.1.3 Stronger phase-specific modulation of theta power in RBP4+ mice than PV+ mice .. 224
6.1.4 Lack of a bi-directional modulation of oscillatory power 225
6.1.5 Open-loop stimulation less effective 226
6.1.6 Speed of optogenetic approaches 226
6.2 TECHNICAL LIMITATIONS 231
6.2.1 Experimental 231
6.2.2 Heating effect of lasers 233
6.2.3 Probes 236
6.2.4 Inclusion of female mice 238
6.3 TRANSLATIONAL APPLICATIONS 239
6.4 FUTURE DIRECTIONS 240
6.5 OUTLOOK 242
6.6 CONCLUDING REMARKS 243
REFERENCES 244

Tables

Table 2.1: Stimulation patterns used for closed-loop optogenetic electrophysiology 82

Table 2.2: Stimulation patterns used for open-loop optogenetic electrophysiology 84

Table 2.3: Primary and secondary antibodies 86

Table 2.4: Total subject list 93

Table 2.5: PV-mice session number breakdown 94

Table 2.6: RBP4-Cre mice session number breakdown: Experiment 1 95

Table 2.7: RBP4 ChR2 session number breakdown: Experiment 2 95

Figures

Figure 1.1 Location of the rodent motor cortex 3

Figure 1.2 Dendritic morphology and location of cortical pyramidal neurons 6

Figure 1.3 Classification of cortical GABAergic interneurons 9

Figure 1.4 Recording and characteristics of the LFP 19

Figure 1.5 Cre-dependent mouse line and AAV injection for optogenetics 67

Figure 2.1 Experimental procedures timeline for *in vivo* electrophysiology with optogenetics 76

Figure 2.2 Simplified experimental setup for *in vivo* awake head-fixed electrophysiological recordings 80

Figure 2.3 Stimulation patterns and targets 82

Figure 2.4 Formulation of open-loop replay control recordings 83

Figure 3.1 Localised expression of ChR2-GFP in PV-expressing neurons 103

Figure 3.2 Accurate phase-targeting of ongoing theta oscillation with gamma stimulation 105

Figure 3.3 Accurate phase-targeting of ongoing theta oscillation with continuous stimulation 106

Figure 3.4 Phase-dependent effect in local LFP following closed-loop gamma stimulation of PV+ interneurons 108

Figure 3.5 Gamma stimulation of PV+ interneurons lead to phase-dependent effects on theta power 110

Figure 3.6 Phase-dependent effect in local LFP following closed-loop continuous stimulation of PV+ interneurons 114

Figure 3.7 Continuous stimulation of PV+ interneurons lead to phase-dependent effects on theta power 116

Figure 3.8 Local theta LFP and z-scored change in theta power following continuous closed-loop stimulation and its open-loop replay & the z-scored difference in theta power between the most and least amplifying closed-loop phases 119

Figure 3.9 Local power spectra and z-scored change in theta power of PV-Cre opsin mice demonstrate no modulation of theta power following open-loop stimulation 122

Figure 4.1 Localised expression of ChR2-GFP and no overlap with PV-expressing neurons 138

Figure 4.2 Accurate phase-targeting of ongoing theta oscillation with gamma stimulation 140

Figure 4.3 Accurate phase-targeting of ongoing theta oscillation with continuous stimulation 141

Figure 4.4 Phase-dependent effect in local LFP following closed-loop gamma stimulation of RBP4+ pyramidal neurons 143

Figure 4.5 Gamma stimulation of RBP4+ pyramidal neurons lead to phase-dependent effects on theta power 145

Figure 4.6 Phase-dependent effect in local LFP following closed-loop continuous stimulation of RBP4+ pyramidal neurons 149

Figure 4.7 Continuous stimulation of RBP4+ pyramidal neurons lead to phase-dependent effects on theta power 151

Figure 4.8 Local theta LFP and z-scored change in theta power following gamma and continuous closed-loop stimulation and their open-loop replays..... 156

Figure 4.9 Z-scored difference in theta power between the most and least amplifying closed-loop phases identified following gamma and continuous stimulation and their open-loop replay counterparts 157

Figure 4.10 Local power spectra of RBP4-Cre opsin and control mice following open-loop stimulation patterns 160

Figure 4.11 Open loop stimulation patterns can modulate theta power in RBP4-Cre opsin mice..... 161

Figure 4.12 Phase-dependent effect in local LFP of opsin mice following all three closed-loop stimulation patterns 165

Figure 4.13 Local power spectra and z-scored change in theta power following gamma and random gamma closed-loop stimulation and their open-loop replays..... 171

Figure 4.14 Z-scored difference in theta power between the most and least amplifying closed-loop phases identified following gamma and random gamma stimulation and their open-loop replay 172

Figure 5.1 Local gamma LFP following closed-loop gamma stimulation targeted to the theta oscillation in PV-Cre mice 187

Figure 5.2 Local gamma LFP following closed-loop continuous stimulation targeted to the theta oscillation in PV-Cre mice 189

Figure 5.3 Gamma stimulation targeted to the theta oscillation leads to increased effects on gamma power in PV-Cre control and opsin mice, but not continuous stimulation 191

Figure 5.4 Local gamma LFP following closed-loop gamma stimulation targeted to the theta oscillation of RBP4+ pyramidal neurons..... 193

Figure 5.5 Local gamma LFP following closed-loop continuous stimulation targeted to the theta oscillation of RBP4+ pyramidal neurons 195

Figure 5.6 Gamma and continuous stimulation targeted to the theta oscillation lead to increased effects on gamma power in RBP4-Cre Opsin mice 197

Figure 5.7 Local gamma LFP and z-scored change in gamma power following closed-loop gamma and continuous stimulation targeted to the theta oscillation and their open-loop replays in RBP4-Cre opsin mice 201

Figure 5.8 Modulation of local gamma LFP in response to gamma, random gamma, and continuous stimulation in RBP4-Cre opsin mice 205

Figure 5.9 Local gamma LFP and z-scored change in gamma power following closed-loop gamma and random gamma stimulation and their open-loop replays in RBP4-Cre opsin mice 209

Abbreviations

#

5HT3aR	5-hydroxytryptamine (serotonin) receptor 3a

A

AAV	adeno-associated virus
aDBS	adaptive deep brain stimulation
ALM	anterior lateral motor cortex
Arch	archaerhodopsin
ASD	autism spectrum disorder

B

BOLD	blood-oxygen-level-dependent

C

cDBS	conventional deep brain stimulation
CFC	cross frequency coupling
ChR1	channelrhodopsin-1
ChR2	channelrhodopsin-2
CPu	caudate putamen
CT	corticothalamic
CTC	communication-through-coherence

D

DBS	deep brain stimulation
DIO	double-floxed inverted open reading frame
dmPFC	dorsal medial prefrontal cortex

E

ECoG	electrocorticograms
ECT	electroconvulsive therapy
EEG	electroencephalogram
EI	excitatory-inhibitory
EPSCs	excitatory post-synaptic currents
eYFP	enhanced yellow fluorescent protein

F

fMRI	functional magnetic resonance imaging
FS	fast spiking

G

GABA	gamma-aminobutryric acid
$GABA_AR$	$GABA_A$ receptor
GFP	green fluorescent protein

I

IT	intratelencephalic

L

L1	layer 1
L2/3	layer 2/3
L4	layer 4
L5	layer 5
L6	layer 6
LEDs	light emitting diodes

LFP	local field potential

M

M1	primary motor cortex
M2	secondary motor cortex
MB	multipolar bursting

O

OCD	obsessive compulsive disorder

P

PAC	phase amplitude coupling
PD	Parkinson's Disease
PT	pyramidal tract
PT_{lower}	pyramidal tract lower
PT_{upper}	pyramidal tract upper
PV	parvalbumin
PV+	parvalbumin positive

R

REM	rapid eye movement
RBP4	retinol binding protein 4

S

S1	somatosensory cortex
SST	somatostatin
STN	subthalamic nucleus

T

tACS	transcranial alternating current stimulation
TBI	traumatic brain injury
tCDS	transcranial direct current stimulation
TMS	transcranial magnetic stimulation

V

vGluT1	vesicular glutamate transporter 1
VIP	vasointestinal peptide
VL	ventrolateral thalamic nucleus

1. General Introduction

1.1 Cerebral Cortex

The cerebral cortex is made up of two hemispheres, within each are four lobes – the frontal, parietal, temporal and occipital lobe. Each lobe processes different information types which allows the cortex to engage in higher level processes such as memory, learning, problem-solving, cognition & emotions.

In development, the migration of neurons into the neocortex forms six cortical layers. The deepest cortical layers form from the earliest migrating neurons, while later migrating neurons form the more superficial layers, known as inside out migration (Cooper 2008; Stiles and Jernigan 2010). These neurons differentiate into distinct neuronal subtypes depending on cues they receive and become part of neural networks, communicating with other neurons. In mammals, the neocortex is organised so that the most superficial and dorsal layer is known as layer 1 (L1), as you progress ventrally through the cortical layers you reach the final layer, layer 6 (L6). The individual cortical layers vary in size both between layers and regions, and some are further subdivided into a more superficial (a) and deeper (b) layer. Each layer has its own distribution of neurons and connections to cortical and subcortical regions. Vertically, the cortex is divided into cortical columns that encompass these layers.

1.1.1 Anatomy & Function of the Motor Cortex

The motor cortices are responsible for planning, executing, and controlling voluntary movements of the body, integrating sensory information to both generate plans, and execute them for fine or gross motor control (Ebbesen and Brecht 2017; Guo et al.

2015). The motor cortices are also involved in motor learning and plasticity and can adapt motor behaviour in response to environmental changes (Karni et al. 1998; Kawai et al. 2015; Sanes and Donoghue 2000). The acquisition of novel motor skills is essential in day-to-day life; for example, learning a musical instrument or how to drive a car. However, after a brain injury such as a stroke, re-acquisition of motor skills is vital for re-learning daily tasks, such as eating or brushing your teeth.

Motor skill acquisition is defined as the capability of adjusting and refining movement in response to environmental input. Through practice, motor learning can result in motor memory formation, through which motor skills are improved and associated with lasting neuronal changes (Karni et al. 1998; Kawai et al. 2015; Sanes and Donoghue 2000). While the hippocampus is heavily involved in learning and memory consolidation, motor skill acquisition is commonly thought to be an example of non-hippocampal-dependent learning (Gould et al. 2002; Kleim et al. 1996). Instead, skill acquisition primarily relies on the primary motor cortex (M1).

In rodents, the motor cortex is comprised of the primary motor cortex (M1) and secondary motor cortex (M2) which are located in the frontal cortex. M1 is located anterior to the somatosensory cortex (S1), while M2 is anterior to M1 (Figure 1.1). The boundaries of these regions within the literature vary, but in the experiments in this thesis I will define them based on the boundaries given in the mouse brain atlas (Paxinos and Franklin 2019). M1 is responsible for generating signals that direct movement in response to sensory stimuli, via inputs from the frontal and parietal cortex, such as the somatosensory cortex as well as the thalamus and M2 (Hooks et al. 2013; Mao et al. 2011; Muñoz-Castañeda et al. 2021). The primary output pathway

of M1 in mice is the corticospinal tract, to innervate motor neurons in the spinal cord, as well as other brainstem nuclei involved in motor coordination and motor output (Hooks et al. 2013; Muñoz-Castañeda et al. 2021).

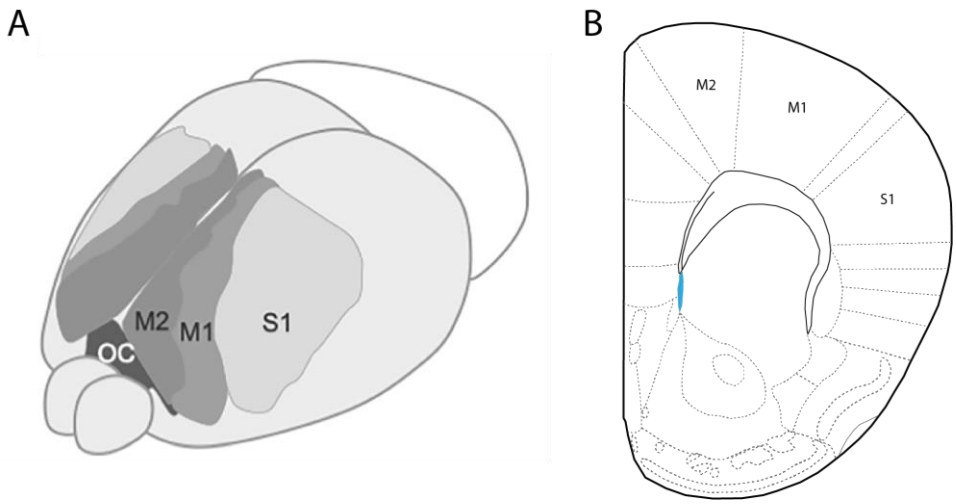


Figure 1.1 Location of the rodent motor cortex

The primary (M1) and secondary (M2) motor cortices in mice are located within the frontal cortex (**A**). In this thesis the boundaries are defined using the Paxinos and Franklin atlas (2019). M1 is located anterior to the somatosensory cortex (S1) and M2 is anteriorly located to M1 (**A & B**). Adapted from Fig 1, Lee et al, 2022 (A) and traced from Paxinos and Franklin, 2019 (B).

Meanwhile, M2 activity has been associated with learning of complex motor skills, as lesioning or inactivation of M2 has been found to interfere with this (Cao et al. 2015; Makino et al. 2017). M2 also receives sensory feedback from S1 as well as inputs from association cortices that are involved in higher-order motor planning like the prefrontal cortex and parietal cortex (Hooks et al. 2013; Hovde et al. 2019; Manita et al. 2015; Yamawaki, Radulovic, and Shepherd 2016). Similarly, M2 sends afferents to the corticospinal tract as well as other subcortical structures like the thalamus and striatum (Hooks et al. 2013; Macías et al. 2022; Rothwell et al. 2015). Additionally, it has recently been revealed that as motor learning progresses neuronal activity of M1 and M2 become increasingly correlated, with activity in M2 preceding that of M1 in rats (Veuthey et al. 2020). Disruption to M2 was also found to minimally affect the local

dynamics of M1, affecting, instead cross-area dynamics and skilled reaching behaviour after learning (Veuthey et al. 2020). These two regions are reciprocally connected (Lee, Kim, and Kaang 2022), therefore indicating a division of labour between the regions and that while M2 can modulate activity of M1, M1 also has intrinsic circuitry and mechanisms to function independently depending on the context. There is some evidence of functional subdivisions within M2: a specific subregion in the anterior pole of M2 is also known as the anterior lateral motor cortex (ALM) in the literature and is heavily linked to movement preparatory activity (Chen et al. 2017; Guo et al. 2014; Li et al. 2016).

Rodent motor lesion studies have demonstrated that motor cortical lesions (forelimb regions contralateral to the dominant limb) lead to impairment, primarily of skilled movement and skilled learning; however, there is not total loss of movement and such cases have often shown substantial recovery (Alaverdashvili and Whishaw 2008; Kawai et al. 2015; Whishaw 2000). Contrastingly, motor cortical lesions in non-human primates and humans can abolish the ability to move, depending on the size and location of the lesion, although this may be partially regained with training (Murata et al. 2008), as there is evidence of reorganisation within the motor cortex (Biernaskie and Corbett 2001; Ramanathan, Conner, and Tuszynski 2006).

These differences between species may be due to the relative complexity of the brain. Briefly, primates, including humans, show a broad somatotropic organisation of the motor cortices, in which different regions of the motor cortex innervate different body parts. This is depicted by the motor cortex homunculus, which portrays a distorted human body represented by relative cortical area devoted to each part for motor

processing (Penfield and Boldrey 1937; Roux et al. 2020). This idea has more recently evolved to encompass an interleaved map in humans, which contains effector regions with concentric organisation (mouth, hand and foot) similar to previous evidence in primates (Kwan et al. 1978), and additional inter-effector regions involved in coordination of actions with strong functional connectivity (Gordon et al. 2023; Roux et al. 2020). The organisation of the rodent motor cortex, however, appears less rigid and spatially separated than that of primates.

1.1.2 Cellular anatomy & connectivity of the motor cortex

1.1.2.1 Glutamatergic Pyramidal Neurons

In the neocortex, the most abundant neuronal cells are excitatory pyramidal neurons, which comprise of around 70-80% of neurons, while the remaining population consists of GABAergic neurons (Markram et al. 2004; Rudy et al. 2011). Pyramidal neurons are the principal projection neurons in the cerebral cortex, releasing the excitatory neurotransmitter glutamate upon an action potential. This allows for detection through vGluT1 expression, a vesicular glutamate transporter. Expression of glutamate transporters infers the amount of glutamate involved in neurotransmission, by determining the amount that can be loaded into vesicles and released upon an action potential (Wojcik et al. 2004). With the exception of layer 1, pyramidal neurons are distributed across all cortical layers, with neurons in each layer distinguishable through specific patterns of long-range axonal connections (Harris and Shepherd 2015). Pyramidal neurons are spiny neurons which can be divided into three main groups depending on their axonal targets, these are intratelencephalic (IT), pyramidal tract (PT) and corticothalamic (CT) neurons, see Figure 1.2. However, each group

remains heterogenous with their own subclasses of neurons. Each of these classes has a characteristic laminar distribution, but some layers have an intermixed composition (Harris and Shepherd 2015; Muñoz-Castañeda et al. 2021).

IT neurons are found in layers 2-6 and their axons project to areas within the telencephalon, including other cortical areas, striatum and amygdala (Harris and Shepherd 2015; Shepherd 2013; Winnubst et al. 2019). Those in layers 2/3 (L2/3) typically have corticocortical projections; while those in layers 5A, 5B and 6 collectively have both corticocortical and corticostriatal connections (Shepherd 2013). These excitatory neurons are the only type to project to the contralateral cortex via the corpus callosum and anterior commissure as well as ipsilaterally (Harris and Shepherd 2015; Hooks et al. 2013; Winnubst et al. 2019).

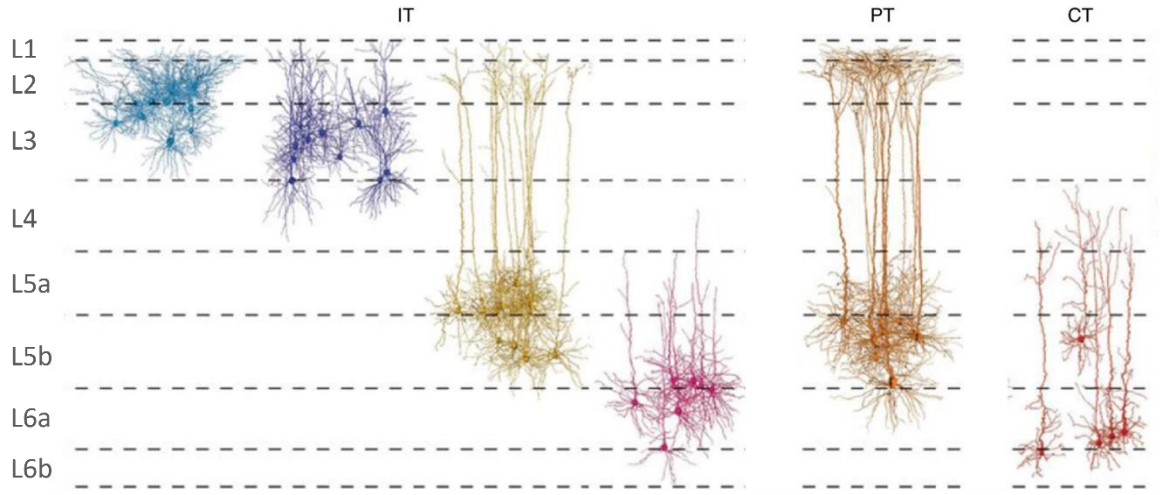


Figure 1.2 Dendritic morphology and location of cortical pyramidal neurons

Dendritic morphology of L2-6 intratelencephalic (IT) neurons, L5b pyramidal tract (PT) neurons and L6 corticothalamic tract (CT) neurons. Pyramidal neurons are located across all cortical layers with the exception of layer 1. PT neuron cell bodies and CT neurons are restricted to layers 5b and L6 respectively, whereas IT neurons are found across layers 2-6. (Adapted from fig 1; Harris & Shepherd, 2015).

PT neuron cell bodies are restricted to layer 5b of the cortex. These are large spiny neurons that send axon collaterals to the brainstem and spinal cord, as well as to the

ipsilateral cortex and subcortical regions like the thalamus and striatum (Harris and Shepherd 2015; Shepherd 2013; Winnubst et al. 2019). Within the motor cortex of mice, it appears PT neurons consist of 2 subtypes with distinct gene expression and projections. These have been referred to as PT_{upper} and PT_{lower} neurons, which have axons projecting to the thalamus and premotor centres in the medulla respectively. ALM recordings indicate a role in motor planning for PT_{upper} neurons, while PT_{lower} neurons instead have a role in execution of movement (Economo et al. 2018). Other studies have similarly identified two subtypes of PT neurons in the motor cortex. The first of which corresponds with this finding (Winnubst et al. 2019); the other partly corresponds, identifying PT neurons that project only to the medulla, like PT_{lower} neurons, however, conversely found the second subtype to project to both the thalamus and medulla (Jiang et al. 2020).

CT neurons are found in layer 6 of the cortex and primarily project to the ipsilateral thalamus (Harris and Shepherd 2015; Hooks et al. 2013). There is a hierarchical organisation between these excitatory neurons, by which IT neurons have reciprocal connections to each other as well as projections to PT neurons. However, PT neurons do not have connections to IT neurons (Hooks et al. 2013; Kiritani et al. 2012; Shepherd 2013). This aligns with the finding that PT neurons tend to have more focal dendritic arbors compared to IT neurons (Hooks et al. 2013).

1.1.2.2 GABAergic Interneurons

The other neuronal class critical in shaping neocortical circuits are inhibitory interneurons. Interneurons are a highly heterogeneous population, that instead release the inhibitory neurotransmitter GABA. Multiple different subtypes can be

identified through their differing morphology, connectivity, synapses, intrinsic membrane properties and expression of different molecular markers (Ascoli et al. 2008; Markram et al. 2004; Mazuir, Fricker, and Sol-Foulon 2021; Rudy et al. 2011). These subtypes have various electrophysiological properties revealed by recordings, including, fast-spiking, bursting, regular-spiking, delayed and irregular-spiking (Ascoli et al. 2008; Markram et al. 2004). Interneurons can therefore be divided based on electrophysiological properties, morphology or neurochemical markers, all of which contribute different information about these cell types.

Basket cells comprise the majority (~50%) of all inhibitory interneurons (Markram et al. 2004). Identified through their distinct morphology of axonal arborisations, these can be further subdivided into separate groups expressing different neurochemical markers (Markram et al. 2004). In contrast with pyramidal neurons, mature interneurons tend to have aspiny dendrites (Markram et al. 2004). Although interneurons represent the minority of neurons in the cortex – only around 10-20% in rodents, they precisely control the entire cortical neuronal population by controlling the firing timing of pyramidal neurons as well as other interneurons, allowing synchronisation of network activity and cortical rhythm generation. Dysregulation of GABAergic neurons has been implicated in a wide range of disorders such as epilepsy, autism, and schizophrenia, which are often described as an imbalance of excitatory and inhibitory cortical neurons.

Figure adapted from {Mazuir et al, 2021} - removed for copywrite reasons

Figure 1.3 Classification of cortical GABAergic interneurons

Three distinct classes of cortical interneurons can be classified by immunochemical markers – parvalbumin-expressing (PV+), somatostatin-expressing (SST+) and ionotropic serotonin receptor-expressing (5HT3aR+). PV+ basket cells are the most abundant interneuron type in the neocortex, these are fast spiking cells. Chandelier cells are another PV+ type, which synapse onto the axon initial segment of pyramidal neurons unlike PV+ basket cells which innervate the soma and proximal dendrites. PV+ interneurons are located through cortical layers 2-6. A small proportion of PV+ interneurons also express SST+. SST+ neurons can be divided into two main types, Martinotti cells which synapse with pyramidal neuron dendrites and are more abundant in deeper cortical layers and non-Martinotti cells which project over long distances. The final subgroup are 5HT3aR+ expressing, just under half of these additionally express vasointestinal peptide (VIP). 5HT3aR+ expressing neurons are predominantly located within the superficial cortical layers. (Adapted from Fig 1, Mazuir et al, 2021).

Throughout the mouse neocortex three distinct classes of interneurons can be reliably identified by their immunochemical markers, each with a different embryonic origin. These are parvalbumin (PV), somatostatin (SST) and serotonin receptor (5HT3aR), see Figure 1.3 (Rudy et al. 2011; Xu, Roby, and Callaway 2010). PV-positive (PV+) neurons account for approximately 40% of GABAergic neurons and include fast-spiking basket and chandelier cells (Ascoli et al. 2008; Rudy et al. 2011). Basket cells typically have a multipolar morphology and form synapses at the soma and proximal dendrite of neuronal targets, meanwhile chandelier cells instead target the axon initial segment of pyramidal neurons (Rudy et al. 2011). Fast-spiking (FS) cells give rise to sustained brief action potentials in high-frequency trains and are known to have the fastest

membrane time constant of all interneurons, making them efficient in their role with fast synaptic responses (Ascoli et al. 2008; Rudy et al. 2011). PV+ interneurons are distributed throughout cortical layers 2-6, with a higher proportion distributed in deeper cortical layers (Xu et al. 2010).

PV+ basket cells have been implicated in the establishment and maintenance of cortical gamma oscillations in layer 5 (Rudy et al. 2011). While limited research has been conducted on them, multipolar bursting (MB) neurons are an additional subtype of PV+ interneuron currently found in the frontal and somatosensory cortex. MB neurons were shown to innervate FS neurons, but there was no evidence of a reciprocal connection. Instead, MB neurons are coupled to each other and reciprocally connected with pyramidal neurons of layers 2/3 (Blatow et al. 2003; Tremblay, Lee, and Rudy 2016). These neurons comprise a unique inhibitory network that under cholinergic stimulation can produce rhythmic and synchronised theta activity (Blatow et al. 2003).

SST-positive neurons account for around 30% of GABAergic neurons, this subtype includes Martinotti cells as well as some neurons that specifically target layer 4 (L4) of the cortex and innervate layer 4 PV+ interneurons (Rudy et al. 2011; Tremblay et al. 2016). Martinotti cells are more abundant in deeper layers than in superficial layers, but are found distributed throughout all cortical layers and connect to other interneuron subtypes but not to each other (Rudy et al. 2011; Tremblay et al. 2016; Xu et al. 2010). These interneurons have arborizing axons that spread horizontally in layer 1 and innervate dendritic tufts of pyramidal neurons, as well as sending collaterals that synapse onto the apical and basal dendrites of pyramidal neurons in deeper

layers (Rudy et al. 2011). Martinotti cells tend to form synapses located on spines and dendritic shafts and have a strongly facilitating response to excitatory input (Rudy et al. 2011).

The final 30% of interneurons are a heterogeneous population known as the ionotropic serotonin receptor (5HT3aR-positive) neurons, of which just under half (40%) of these additionally overlap with vasointestinal peptide (VIP) expression (S. H. Lee et al. 2010; Rudy et al. 2011). Morphologies of 5HT3aR+ interneurons include bipolar, multipolar and bitufted cells and they also have heterogenous electrophysiological properties and express different markers (Rudy et al. 2011). All subtypes are potently modulated through ionotropic serotonin receptors and receive glutamatergic input – both of which mediate local and long-range input, but also express nicotinic receptors which enables for cholinergic modulation (S. H. Lee et al. 2010; Rudy et al. 2011). The majority of 5HT3aR+ interneurons are situated in superficial layers, where they constitute the majority (Rudy et al. 2011).

1.1.2.3 Layer 5 circuitry

Layer 5 (L5) is the major output layer of the motor cortex, and oscillations in L5 of the motor cortex arise from the complex interactions of these excitatory and inhibitory neurons. There is, therefore, substantial research aimed at understanding the functional significance, mechanisms and clinical implications of layer 5 oscillations. It therefore seems important to briefly consider the composition and interactions of these cell types within L5.

The majority of neurons in L5 are pyramidal cells. IT neurons are distributed throughout L5 while L5b predominantly contains more PT type large pyramidal

neurons that project to subcortical targets (Harris and Shepherd 2015; Shepherd 2013). In L5, PV+ FS basket cells exert strong inhibitory control through perisomatic synapses via both local axons to other cells, as well as translaminar axons providing inhibition across other cortical layers, they are known to connect strongly to other PV+ interneurons (Tremblay et al. 2016). Other interneuron subtypes include chandelier cells, Martinotti cells and non-Martinotti cells that express SST. Some of these SST subtypes have often been found to have a low-threshold spiking pattern while others show regular or burst spiking patterns. On the other hand, the non-Martinotti SST subtype typically demonstrate low input resistance and higher frequency brief spiking more comparable to FS basket cells, however, show greater firing frequency adaptation than these (Tremblay et al. 2016). Martinotti cells have been linked to a wiring principle whereby they cause disynaptic inhibition of local L5 pyramidal neurons via pyramidal cell activation – a central mechanism of cortical activity regulation as well as ascending inhibition to L2/3 and L4 (Kätzel et al. 2010; Silberberg and Markram 2007).

The combination of inhibitory interneurons and excitatory pyramidal neurons control cortical activity, maintaining an excitatory and inhibitory balance that allows for information transfer and synchronisation of activity, which in turn, enables the effective generation of cortical oscillations (Adrian and Matthews 1934; Buzśaki and Wang 2012; Fries et al. 2001; Singer 1993). Understanding more about the role excitatory and inhibitory cells play individually within these circuits will be useful for elucidating effective treatments for disorders affected by disturbances to these cells and the oscillations they give rise to.

1.1.3 Neural Circuitry & Pathways

Traditionally, the distinct though interconnected layers within the motor cortex are grouped into L2/3 - a prominent source of intracortical excitation to L5 and recurrent activity – and L5, the strong output layer transmitting signals to subcortical structures to drive movement. Pyramidal neurons allow for integration of information between different cortical layers through long-distance axonal connections. Thalamocortical inputs tend to target neurons in L2/3 through to L5b but do not target L6. Sensory inputs from S1 or sensory related thalamic regions for example, targeted neurons in the upper layers – L2/3 as well as L5a (Hooks et al. 2013). M2 sends inputs predominantly from upper cortical layers into L5b of M1 and fewer into L6, including excitatory inputs to pyramidal tract neurons (Hooks et al. 2013). Therefore, sensory-related cortical and thalamic regions preferentially target neurons in the upper cortical layers, which project to the cortex and striatum, and may be important in sensorimotor processing (Hooks et al. 2013). On the other hand, other areas associated with movement, like M2, inputs directly to PT and IT neurons that project to the brainstem with collaterals that, in turn go to the thalamus and striatum (Hooks et al. 2013).

PT neurons, which are only found in L5b receive few inputs from interlaminar pyramidal neurons (Hooks et al. 2013; Mao et al. 2011). Furthermore, pyramidal neurons in the main layers 2/3 and 5 have different evoked firing rates indicative of the differences in the roles they play within different cortical layers. L2/3 pyramidal neurons have low spontaneous and evoked rates (<1 spike per second (s)), whilst in contrast, L5 pyramidal neurons fire at a higher rate (5-15 spikes/s) (Harris and Mrsic-Flogel 2013). Interlaminar connections such as those from L2/3 to L5 are dependent

on pyramidal neuron identity and location within layer 5, whereby L2 neurons project to IT neurons and L3 neurons project to PT, implying information to each type is from separate upstream cortical targets (Shepherd 2013).

Recent work combining optogenetics with functional magnetic resonance imaging (fMRI) has interrogated the role of different layers of M1 in driving local and brain wide networks (Chan et al. 2022). The combination of optogenetics in this manner can allow examination of the contribution and influences of genetically defined populations of neurons. Through specific mouse lines targeting different M1 layers, activating different layers resulted in different spatiotemporal brain wide evoked responses. Optogenetic stimulation (5Hz, 30-50mW/mm^2) targeted to L2/3 (Drd3+ neurons) only activated ipsilateral M1. Targeting optogenetic stimulation to neurons (Scnn1a+) in layer 4 also activated ipsilateral M1 as well as some small negative blood-oxygen-level-dependent (BOLD) responses to the contralateral M1, bilateral caudate putamen (CPu) and ipsilateral ventrolateral thalamic nucleus (VL). Targeting stimulation to layer 5 RBP4+ neurons was able to evoke strong activation in ipsilateral M1, bilateral CPu – although this peaked after the stimulation ended, ipsilateral VL as well as the ipsilateral posterior nucleus and parafascicular thalamic nucleus. Additionally, some small BOLD responses to L5 stimulation were detected in the contralateral M1. Finally, stimulation targeting layer 6 (Ntsr1+ neurons) evoked the strongest activation to ipsilateral VL, ipsilateral posterior nucleus, ipsilateral parafascicular thalamus and both bilateral CPu and M1 responses, in which the BOLD signal transitions from negative during stimulation to positive following stimulation. Activation of L5 (RBP4) evoked significantly stronger effects than activation of L2/3

(Drd3) or L4 (Scnn1a). Histology later confirmed long-range axonal projections from L5 and L6 of the M1 to the CPu and VL as expected (Chan et al. 2022).

Relatively similar effects, but not identical, were demonstrated when applying 10, 20 and 40Hz stimulation to test how the network characteristics changed in a spatiotemporal manner, relative to stimulation frequency and no effects were detected in a naïve animal. Furthermore, local field potential (LFP) recordings were also obtained in this study under the same experimental conditions, evoked responses correlated with the previously obtained BOLD-fMRI responses. Overall, these data suggest that stimulation to upper cortical layers (L2/3) evoke local M1 responses, whereas stimulation to L5 evokes both local and brain-wide responses (Chan et al. 2022).

1.1.4 Disorders & Dysfunction of the Motor Cortex

A number of clinical conditions can lead to motor dysfunction in humans. Stroke is a leading cause of disability worldwide. If a stroke is located in the motor cortex, it can lead to deficits of motor function affecting mobility, daily activities, and ability to return to work. Strokes can either be ischemic, due to a restriction or stoppage of blood supply to parts of the brain leading to cell death due to lack of oxygen and nutrients, or haemorrhagic, which is caused by a bleed on the brain that increases pressure leading to cell damage due to a blood vessel leaking or bursting. Neurological recovery after stroke presents a nonlinear logarithmic manner, but the majority of recovery is reported to happen within the first 3 months following a stroke (Langhorne, Bernhardt, and Kwakkel 2011). A key part of neuro-recovery is rehabilitation, to try and re-learn motor tasks as a result of the new motor deficits.

Traumatic brain injury (TBI) is another disorder that can cause damage to the motor cortex resulting in motor impairments such as weakness, poor coordination, and balance and in severe cases even paralysis or reduced fine motor control. This can be caused by anything that could lead to a violent blow or jolt to the head or body; for example, something seemingly as minor as a fall (an increasing risk in the elderly) or as major as a traffic accident. While TBI was once believed to be an acute event in a subset of individuals, it has now been shown that such incidents can lead to long lasting disability, similar to those affected by a stroke, significantly impacting an individual's quality of life and ability to work and maintain relationships. As with a stroke, rehabilitation in the acute stage can be key in improving outcomes (Corrigan, Wee, and Collins-Praino 2023; Walker and Pickett 2007).

A final example of another common disorder leading to dysfunction in the basal-ganglia thalamocortical circuitry affecting motor control and coordination is Parkinson's Disease. This goes in hand with movement disorders, which can manifest as tremors, dystonia or problems with gait. Parkinson's Disease will be discussed in greater detail later in this thesis, however current treatments only target the symptoms and can result in other side-effects that further burden patients.

Treatments that could more effectively target these oscillations and circuits within the brain involved in these disorders, could potentially improve re-learning as part of neurorehabilitation or reduce off target side effects in already existing treatments. Therefore, could be hugely beneficial worldwide and reduce the burden of those living with such conditions.

1.2 Oscillations

Neuronal activity is the fundamental mechanism by which the brain processes information, involving dynamic interactions among interconnected neurons. Communication in this way is facilitated via the movement of ions across neuronal membranes which lead to changes in transmembrane currents. In this way, neurons generate rhythmic patterns of activity that are referred to as neuronal oscillations (Buzsáki, Anastassiou, and Koch 2012). These can be thought of as the brain's natural rhythms and they have key roles in processes such as cognition, perception and motor control. This is achieved through coordinating the timing of neural communication across brain regions (Buzśaki and Wang 2012; Fries 2015; Siegel, Donner, and Engel 2012).

1.2.1 Quantifying oscillation via the local field potential

Neural oscillations characterised by rhythmic fluctuations in activity give rise to an extracellular potential known as the local field potential (LFP) (Figure 1.4A). This measures the summed electrical activity from a group of neurons within a specific brain region, providing insights into the synchronous firing of neurons. Research indicates that excitatory post-synaptic currents (EPSCs) are the primary contributor to LFPs (Buzsáki et al. 2012). Measuring the LFP allows researchers to gain insight into the collective activity of neuronal populations and network dynamics in a local brain area or the connectivity among brain areas.

These changing electric fields can be monitored through a variety of different techniques, with extracellular traces remaining remarkably similar. The LFP can be measured with a time resolution of sub-milliseconds using inserted micro/depth-

electrodes, intracerebral or scalp electrocorticograms (ECoG) and scalp electroencephalography (EEG). Higher frequency components have greater resolution and greater changes in amplitude are demonstrated for inserted or intracerebral methods in comparison to recording over the scalp (Buzsáki et al. 2012; Katzner et al. 2009; Logothetis, Kayser, and Oeltermann 2007). Advances in micro-electrode technology (silicon-based polytrodes, Neuropixels) allow high density recordings *in vivo*, providing extraordinary coverage and resolution of the underlying processes involved in LFP generation. Furthermore, simultaneous recordings of LFP alongside other large-scale measures of neural activity such as functional MRI could further enhance our understanding of how networks interact across multiple levels (Einevoll et al. 2013).

The extracellular field is the output of all electrical currents within a specific location. This means any type of transmembrane current contributes irrespective of origin, to both intracellular and extracellular voltage changes. Synchrony within the spatial field will also play a key role in shaping the extracellular field. Characteristics of the LFP will also depend on the contribution of these sources and brain tissue properties, determined by the distance from the recording electrode. Additional contributors to extracellular field include synaptic activity, fast action potentials (unit/spike activity), calcium spikes, intrinsic currents, cell-type and architecture and synchrony (Buzsáki et al. 2012; Einevoll et al. 2013; Glickfeld et al. 2008; Kamondi, Acsády, and Buzsáki 1998; Llinás 1988). For example, large transmembrane currents are produced as a result of action potentials in the vicinity of the cells somata. If in the vicinity of the electrode there are many active neurons, the electrode records from all, and it is only

possible to identify and separate a given neuron by moving the electrode closer to the specific neurons cell body, than to other neurons (Buzsáki 2004). Increasing numbers of electrodes, increases the yield of the population of neurons that can be simultaneously recorded from, for instance, across different cortical layers. Due to the numerous potential sources of the LFP, this can be more difficult to interpret (Einevoll et al. 2013). Increased power in the high frequency components of the LFP have been found to represent synchronous activity from multiple spiking neurons. The LFP can therefore be used to acquire valuable information about the temporal structure of spiking neuronal populations (Buzsáki et al. 2012).

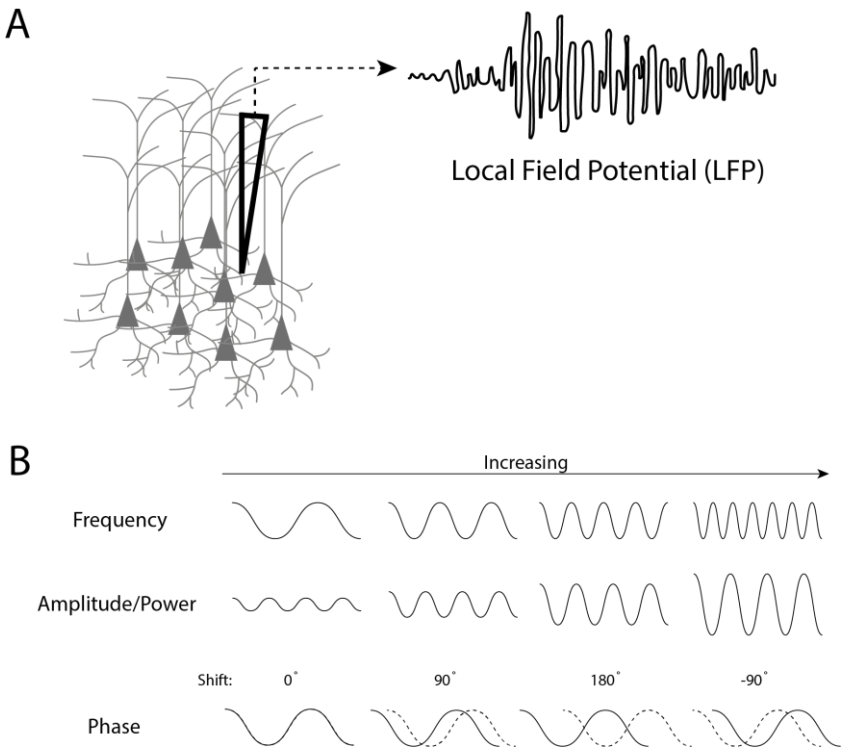


Figure 1.4 Recording and characteristics of the LFP

An extracellular electrode can be placed within brain tissue to record the summed extracellular field potential – the LFP (**A**). This is an overview of all electrical currents within a given location. To gain insights into oscillations we can determine their characteristics (**B**), such as frequency (number of cycles per unit time; Hz), amplitude or power and their phase relationship (degrees).

LFPs can have certain characteristics which help us to gain insight into oscillations within the brain. Two such characteristics are frequency and amplitude (Figure 1.4B).

As previously discussed, oscillations have been separated into various frequency bands, that broadly seem to reflect activity in specific circuits underlying certain behaviours. LFPs enable us to measure the frequency and amplitude of oscillatory activity within these different frequency bands and this helps to characterise activity associated with various cognitive processes. By measuring LFPs across time, we can additionally examine the temporal dynamics of how oscillations evolve and change in frequency, phase or amplitude over time, which can elucidate to their ongoing relationship and functional significance to cognitive processes, behaviours, tasks, or stimuli. Furthermore, as mentioned above, synchronisation between neuronal oscillations in different brain regions is crucial for coordinating information across neural networks and facilitating communication between different regions of the brain. Another advantage of recording the ongoing LFP is to study synchronisation and phase relationships between oscillations of differing frequencies which may infer network dynamics, functional connectivity, transfer of information or cognitive processes. Finally, being able to recognise abnormalities in the LFP can be indicative of underlying pathophysiology, such as neurological or psychiatric disorders. Thus, the LFP could be used as a clinical indicator and biomarkers for diagnosis and monitoring response to treatments in such cases.

Methodological considerations also play a crucial role in accurate recording and interpretation of LFP data. Electrode placement is one key consideration as location and electrode configuration can influence spatial resolution and specificity. One must ensure optimal coverage of the brain region of interest, while minimising possible artifacts or signal contamination from other nearby structures. Proper filtering is also

necessary to extract meaningful LFP signals and remove background noise or artifacts. Other signal processing methods can then be utilised to ensure data quality and reliability, such as spectral analysis, feature extraction and statistical analysis.

1.2.2 Introduction to neural oscillations

Throughout mammalian evolution, the hierarchy of brain oscillations has remained remarkably preserved regardless of brain size across species (Buzsáki, Logothetis, and Singer 2013), allowing effective communication both within and across neural networks across multiple time scales. Within the nervous system, rhythms are found everywhere. In more simple systems, neurons have central pattern generators which promote rhythmic activity within particular frequency ranges (Grillner 2006). In increasingly complex systems, oscillations are created by specific microcircuits particularly influenced by inhibition (Buzsáki and Chrobak 1995; Whittington, Traub, and Jefferys 1995).

Oscillatory activity within the brain is, therefore, an effect of synchronous action potentials resulting in rhythmic patterns of neural activity, with periods of enhanced and reduced excitability (Adrian and Matthews 1934; Buzśaki and Wang 2012; Fries et al. 2001; Singer 1993). Coordinated network activity emerges from the dynamic interplay between excitatory (pyramidal neurons) and inhibitory (interneuron) input, which creates a fluctuating excitatory-inhibitory (EI) balance (Adrian and Matthews 1934; Buzśaki and Wang 2012; Shu, Hasenstaub, and McCormick 2003; Singer 1993). Disruption to the balance of inhibition and excitation, whereby excitation dominates, which is demonstrated by an increase in excitatory neuronal firing could result in hyper-excitation and potential pathological activity (Isaacson and Scanziani 2011;

Yizhar, Fenno, Prigge, et al. 2011). Conversely, neuronal activity could be completely silenced if inhibition were to dominate (increased activity of interneurons decreasing the likelihood of other neurons to fire) (Isaacson and Scanziani 2011). Precise EI balance therefore enables neurons to fire in a timely manner shaped by excitatory and inhibitory inputs, tightly regulating the underlying spiking activity of neurons and thus allowing oscillatory activity to emerge (Isaacson and Scanziani 2011; Shu et al. 2003; Van Vreeswijk and Sompolinsky 1996). Across brain regions, synchronisation of oscillations is a consequence of long-range connections, allowing for co-ordinated network activity (Siegel et al. 2012). It has been established that oscillatory activity, both locally and across networks, correlates with motor, cognitive and sensory processing (Buzsáki and Draguhn 2004; Fries 2015; Siegel et al. 2012).

Oscillations are dependent on behavioural brain state, can be observed across various frequencies within the brain and different frequencies have been associated with different functions (Penttonen and Buzsáki 2003). Temporal aspects of oscillatory activity alongside their behavioural correlates have been well conserved across mammals and seem to reflect functional requirements (Buzsáki et al. 2013). Broadly, oscillations have been separated into the following frequencies: delta (0.5-4Hz), theta (~4-8Hz), alpha (~8-12Hz), mu (~8-13Hz), beta (~12-30Hz) and gamma (>30Hz) (Buzsáki and Draguhn 2004). Typically, oscillations are most easily observed in humans by electroencephalography (EEG), a non-invasive method which measures activity through scalp electrodes, however this predominantly captures cortical oscillations. Alternatives include magnetoencephalography (MEG) another non-invasive technique, functional magnetic resonance imaging (fMRI) which can capture

activity patterns across the brain, or invasive methods such as electrodes directly in the brain.

Infra-slow oscillations are the slowest oscillation observed in the brain – these are typically between 0.01-0.1Hz (Aladjalova 1957; Penttonen et al. 1999). Infra slow oscillations are believed to play crucial roles in modulation of higher frequency oscillations and synchronising neural networks over widespread brain regions (Leopold, Murayama, and Logothetis 2003; Monto et al. 2008). Following these are delta oscillations, prominent during deep sleep stages and associated with memory consolidation and restorative processes (Kim, Gulati, and Ganguly 2019; Knyazev 2012). Theta oscillations are commonly observed in states of arousal, attention, exploration, and rapid eye-movement sleep. Theta is particularly prominent in the hippocampus and has been linked to episodic memory retrieval, spatial learning, and sensory integration (Colgin 2013, 2016; Cornwell et al. 2008; Dupret, O'Neill, and Csicsvari 2013; Korotkova et al. 2018; O'Keefe and Recce 1993; Tan et al. 2024). Alpha oscillations are prominent during relaxed wakefulness and have been inversely associated to visual attention in the occipital cortex (Clayton, Yeung, and Cohen Kadosh 2018; Jasper and Penfield 1949; Schürmann and Başar 2001). Meanwhile, beta oscillations are observed during active wakefulness and are linked to alertness, concentration, and motor function. Often present in the motor cortex, beta oscillations are involved in motor planning, execution, and coordination (Baker 2007; Jasper and Penfield 1949; Pfurtscheller and Aranibar 1977). Gamma oscillations are the fastest frequency observed in the brain and are associated with various cognitive processes. Oscillations in the gamma frequency are believed to represent

synchronised activity across distributed neural populations (Buzśaki and Wang 2012; Engel, Fries, and Singer 2001; Fries 2009; Gray et al. 1989; Jensen, Kaiser, and Lachaux 2007). Various methods can be used to record oscillations (EEG, MEG, fMRI, LFPs) allowing us to observe them within different brain regions including both cortical and subcortical regions.

An additional rhythm is the mu oscillation, which is also known as the sensorimotor rhythm as it is particularly prominent in the sensorimotor cortex and exhibits characteristic changes in amplitude due to attenuation or desynchronisation linked to motor tasks or motor imagery (Cochin et al. 1998, 1999; Gastaut and Bert 1954). Mu typically oscillates at alpha frequency (8-13Hz) and these oscillations are limited to brief durations of 0.5-2 seconds, which are maximal when an individual is at rest. Due to the overlap in frequencies with alpha oscillations, these two oscillations have previously been difficult to separate or are misidentified. In contrast to alpha oscillations that are desynchronised when eyes are open, mu oscillations are not affected by the eye opening or closing (Pineda 2005). Furthermore, the mu oscillation has been functionally compared to mirror neurons that are found in monkeys. Mirror neurons fire not only when a monkey performs an action, but also during observation of the same action (Rizzolatti, Fogassi, and Gallese 2001).

Many oscillations co-occur within a brain state or interact with each other. In this case, the interaction tends to be hierarchical, in that the phase of the slower neuronal oscillation typically modulates the power of a faster oscillation (Buzśaki and Wang 2012; Penttonen and Buzsáki 2003). This is known as phase-amplitude coupling (PAC) in which the amplitude of a faster oscillations at one frequency is modulated by the

phase of oscillations at another slower frequency, thus differing frequencies interacting to coordinate activity. Over time, slower oscillations impose a temporal bias on faster oscillations, which leads to synchronisation of the amplitude of the faster oscillation so that it represents the temporal structure of the slower oscillation. As a result of this, there will be synchronised changes in power across different frequency bands, however, the phase relationship remains stable across time (Buzsáki et al. 2013; Jensen and Colgin 2007).

In the primary motor cortex, the most prominent neuronal oscillations are beta and gamma. Beta is known to dominate during periods of rest where there is increased beta power and a reduction in beta power is commonly observed prior to and during voluntary movements (Jurkiewicz et al. 2006; Murthy and Fetz 1996). Meanwhile, increases in gamma power are detected just before the onset of movement and during execution (Akkad et al. 2021; Muthukumaraswamy 2010; Nowak et al. 2017). Theta oscillations of 6Hz are also found in the human motor cortex (Canolty et al. 2006). Additionally, there is substantial evidence linking theta and gamma coupling in the motor cortex in both animal models and humans (Canolty et al. 2006; Igarashi et al. 2013; Johnson et al. 2017; Rustamov et al. 2022; Spooner et al. 2022).

The power distributions of different frequencies of neuronal oscillations display a 1/f appearance over long temporal scales when plotted logarithmically - a type of signal in which the power spectrum is inversely proportional to the frequency (f). This means that lower frequencies have more power than higher frequencies, creating a characteristic slope within the power spectrum (Buzsáki and Draguhn 2004). This characteristic shape of the power spectrum relates to aperiodic or arrhythmic neural

activity (He 2014) and can be related back to fast and slow neural oscillations. As slow oscillations tend to generate large, synchronised membrane voltage fluctuations in many neurons across networks, leading to relatively high power, whereas faster oscillations in contrast have lower power, as they are associated with smaller changes in membrane voltage and more restricted neuronal synchronisation (Buzsáki et al. 2012, 2013). The resultant slope is more negative if the neuronal population is highly correlated and flatter if more units within the population spike asynchronously (Voytek et al. 2015). The aperiodic component has been demonstrated to change with age, cognitive states and task demands (Dave, Brothers, and Swaab 2018; Donoghue et al. 2020; Voytek et al. 2015). Additionally, the characteristic shape has been found to represent the excitatory to inhibitory ratio which is a result of neural firing and overall synchronisation. As such, increased excitation relative to inhibition steepens the PSD slope (Gao, Peterson, and Voytek 2017). Furthermore, when a particular oscillation frequency becomes dominant, perhaps a result of the brain engaging in particular functions, a peak appears in the power spectrum at the respective frequency band. This represents an increase of power at that frequency and may be indicative of heightened neural activity, increased neural synchronisation, or engagement of brain regions for specific tasks or functions.

Ongoing research into oscillatory activity is exploring the pivotal role of oscillations in both brain health and dysfunction. Emerging areas of research encompass implications in regulation of sleep, consciousness, involvement in neurological disorders such as epilepsy or Parkinson's disease as well as relevance to various psychiatric disorders.

1.2.3 Function of neural oscillations

Pioneering work in 1875 linked to the discovery of the electroencephalogram (EEG), a type of non-invasive recording first lay the foundations for studying neuronal oscillations (Whittington, Traub, and Adams 2018). In the following decades researchers built upon this foundational work to create the field of neuronal oscillations. Neural oscillations are fundamental to the brain and orchestrate the complex interplay of information processing, communication, and coordination across vast neuronal networks. Oscillations play a pivotal role in the functioning brain, from roles in basic sensory and motor processes, to higher order cognitive functions like decision-making, memory, and attention. The brain has evolved to support these increasingly complex behaviours through effective information transmission and integration, coordinating and facilitating communication between different brain regions using neural oscillations and the interaction between different frequencies of oscillations. Understanding more about these complex dynamics could allow us to harness their intrinsic power during periods of neurological or cognitive impairment.

Buzsáki is a leading figure in the study of neural oscillations, and central to his ideas is the concept that oscillations serve as fundamental building blocks in the brain, facilitating neural communication and information processing. His theory emphasises the role of oscillations in coordination of neuronal assemblies (Buzsáki 2010). Synchronised oscillatory activity enables rhythmic firing of neurons leading to communication and exchange of information between distant brain regions. Diversity of membrane properties and resonant oscillatory features enable neurons to discriminate inputs based on their frequency profiles, which can be further refined

through phase biasing. This ultimately coordinates activity across regions of the brain, facilitating information transfer. Neuronal assemblies are thus organised and synchronised through oscillations allowing for functional circuits that support ongoing cognitive processes and behaviours (Buzsáki and Draguhn 2004).

A key contribution to the oscillation field was the identification of the functions associated with different frequency bands. For example, theta oscillations for example are prominently observed in the hippocampus during spatial navigation and rapid eye movement (REM) sleep and are therefore linked to memory encoding and retrieval (Buzsáki 2002; Buzsáki and Moser 2013). Similarly, Buzsaki's work revealed the presence of gamma oscillations during sensory processing tasks and cognitive tasks that required attention, highlighting the role of this oscillation in attention and information transfer and integration in local neural networks (Buzśaki and Wang 2012). Different frequencies allow for diversity of patterns and the specific role they play, which through coordinated neuronal activity results in cognitive functions. It was later proposed that oscillations occur within a nested structure in the brain, whereby slower oscillations provide a framework across large brain regions or networks for the organisation of faster oscillations (Belluscio et al. 2012; Buzsáki and Draguhn 2004; Csicsvari et al. 2003). Hierarchical organisation of oscillations across brain structures has been proposed to promote multi-scale communication both within and across networks, allowing efficient information processing at greater temporal scales with lower energy costs. This means in local networks, slower oscillations modulate the timing and amplitude of faster oscillations, which provides temporal windows suitable for information processing (Buzsáki and Draguhn 2004; Buzsáki and Schomburg

2015). These ideas suggest oscillations play a pivotal role in orchestrating information flow across multiple spatial and temporal dimensions, which permit adaptive and flexible behaviour in relation to complex environments.

While also believing oscillations play a large role in processing and communication, Fries proposes that neural communication is facilitated by neuronal coherence and synchronisation. Rhythmic fluctuations in excitability and inhibition due to the synchronisation of neurons firing, enables intrinsic temporal scales for communication (Fries 2005; Lewis et al. 2021). Neuronal groups can then effectively interact via phase-locking and neurons synchronised in this way allow for cognitive flexibility. Conversely the absence of coherence, when neuronal inputs arrive during random phases of an excitability cycle, prevents communication. This is known as the 'communication-through-coherence' (CTC) hypothesis. Fries based these ideas on the fact that groups of neurons have an intrinsic drive to oscillate and that these rhythmic oscillations affect spiking and sensitivity to synaptic input in short temporal windows (Fries 2005). This means, communication between brain regions is most effective when it occurs during a period of increased excitability or synchronisation with pre- and post-synaptic neuronal populations. Fries proposes a delay in the timing of synchronisation, referred to as entrainment with delay, in which the post-synaptic population of neurons adjusts ongoing activity after a slight delay. This allows for more precise coordination of neural activity as the population is then ready to process incoming signals effectively (Fries 2015). Modulating timing in this way, by which neural inputs arrive during specific oscillatory phases therefore controls the flow of

information within neural networks, which can enable flexible and adaptive processing to meet environmental demands.

In Fries' hypothesis, gamma oscillation synchronisation via CTC are crucial for prefrontal computations and coordinate activity between brain regions (Fries 2005, 2009). He suggests that coherent oscillations in the gamma frequency range is fundamental for activated cortical networks, enabling them to establish exclusive communication both within and between neuronal groups (Fries 2005). Synchronisation of gamma oscillations between neuronal groups rapidly modulates excitation to effectively activate post-synaptic neuron firing, information transfer is then most favourable when gamma cycles are highly synchronised between regions (Fries 2005, 2009). This hypothesis is supported by the fact that driving FS-interneurons using optogenetics in the somatosensory cortex with a 40Hz pulse train not only induces gamma oscillations, but the timing of sensory input relative to gamma altered evoked neuronal responses (Cardin et al. 2009). FS cells, therefore, are highly implicated in driving dynamic information transfer through rhythmic synchronicity and modulation of synaptic inputs through gamma oscillations.

Since these seminal papers were published, the communication-through-coherence hypothesis, has evolved as such other neuronal oscillations and their interplay, across a range of frequency bands, are also important for neural communication. For instance, both gamma and beta rhythms playing a role regulating incoming signals and facilitating efficient connectivity through coherence (Fries 2015). There is also a potential role of selective coherence, in which certain neuronal populations can become synchronised in activity while others do not, depending on the relevance of

the information or stimuli being processed (Fries 2015). This finding suggests that coherence can vary in response to task demands or cognitive processes, selectively enhancing or attenuating coherence based on relevance.

Ultimately, different frequency bands have been associated with different roles and functions. The precise frequency, phase and amplitude of oscillatory activity is therefore likely to be important in encoding specific aspects of neural information, this may additionally be further subdivided within each frequency further increasing the complexity. These theories help to emphasise the different aspects of neuronal oscillation functions. Abnormalities in oscillatory activity have been linked to many neurological and neuropsychiatric disorders, further highlighting the vital importance of these oscillations and the complex role they play within the brain.

1.2.4 Role of theta & gamma oscillations

As mentioned above, theta oscillations are rhythmic oscillations, typically defined as occurring at a frequency of between 4-8Hz. They have been linked to memory and learning, spatial navigation and attention as well as emotional regulation (Colgin 2013, 2016; Cornwell et al. 2008; Dupret et al. 2013; Korotkova et al. 2018; O'Keefe and Recce 1993; Tan et al. 2024). Within the rodent brain, the hippocampal theta oscillation is one of the most widely studied oscillations mainly found during active exploration or during REM sleep. Arising from synchronous neural activity, these large amplitude fluctuations in LFP represent the sum of the activity of many synchronised neurons and the hippocampus contains a large volume of densely packed neurons that can facilitate this. Theta oscillations in the hippocampus vary and are characterised by rhythmic changes in both phase and amplitude according to depth

and subregion (Buzsáki 2002). This spatial modulation of theta reflects the underlying complexity of the hippocampal circuitry and its significance in coordinating widespread activity. Moreover, neuronal spiking in several other brain regions is phase-locked to the hippocampal theta oscillation, such as the prefrontal and entorhinal cortex (Buzsáki 2002; Colgin 2016).

Consistent with the previously mentioned circuitry, pyramidal neurons and interneurons both modulate and generate hippocampal theta oscillations. GABAergic neurons within the medial septum are believed to function as local 'theta' pacemakers, they target other interneurons within the hippocampal formation thus facilitating rhythmic theta firing (Colgin 2013, 2016; Nuñez and Buño 2021). Besides this, it has also been suggested theta oscillations can emerge from local hippocampal interactions and intrinsic properties in the absence of the medial septum, although this can be linked to deficits in theta rhythmicity (Buzsáki 2002; Colgin 2013, 2016; Goutagny, Jackson, and Williams 2009; Mitchell et al. 1982; Nuñez and Buño 2021; Wang et al. 2014). Therefore, it is likely, that complex interactions between these different components underscore theta oscillations in the hippocampus and their role within cognitive processes (Nuñez and Buño 2021). Additionally, distinct classes of interneurons within the hippocampus are known to be phase-locked to different phases of the ongoing hippocampal theta oscillation (Buzsáki 2002; Somogyi et al. 2014) which may reflect distinct functions. Coherence has been demonstrated between theta oscillations in the hippocampus and cortex, suggestive of functional coupling and communication (Benchenane et al. 2010; Colgin 2013; Jones and Wilson 2005; Siapas, Lubenov, and Wilson 2005; Sirota et al. 2008). However, there is

additional evidence that local theta generators exist in the neocortex (Carracedo et al. 2013; David et al. 2023; Florez et al. 2015; Kahana, Seelig, and Madsen 2001; Silva, Amitai, and Connors 1991).

Previous work, however, demonstrates a multipolar subtype of PV-interneurons - the multipolar-bursting (MB) cells - contribute to theta generation within the neocortex. Named after their firing pattern and morphology these neurons have been found in the frontal and somatosensory cortex in layers 2/3 (Blatow et al. 2003). They differ in both morphology and functional properties to the commonly found FS-interneurons, for instance, have a typical resting membrane potential of ~-60mV in comparison to FS-interneurons which are around -73mV (Blatow et al. 2003). Additionally, MB cells were found to have a firing frequency of ~12.8Hz compared to ~38Hz for FS-interneurons (Blatow et al. 2003). Interconnected by both chemical and electrical synapses forming an inhibitory network, MB neurons are well suited for their role in theta generation and receive a small amount of excitatory input from L2/3 pyramidal neurons, although, this input is not required for theta generation. Furthermore, following induced theta (4-7Hz) frequency oscillations, MB neurons were found to evoke synchronised inhibition of local pyramidal neurons (Blatow et al. 2003). Caution may need to be observed when inferring from this study, however, as the mice used were relatively young (14-days old) compared to most studies within the field, and whole-cell recordings were undertaken at room temperature. Moreover, beyond the scope of this study, this type of interneuron has not been extensively studied to interrogate further their potential role in neocortical theta oscillation generation or existence within the motor cortex.

In humans in the neocortex, theta oscillations are found naturally at approximately 6Hz (Canolty et al. 2006). Some studies have additionally linked theta oscillations to motor learning, more specifically motor sequence learning in humans (van der Cruijsen et al. 2021; Meissner et al. 2018). Moreover, in support of this, neurofeedback (a real-time visual signal relating to changes in target band power from a single scalp electrode) has previously been used to modulate electroencephalogram (EEG) activity following a motor sequence task involving finger tapping on a keyboard, increasing theta power in this way was shown to improve performance (Rozengurt et al. 2016). While the neurofeedback was for the most part from the 'Fz' electrode, a frontal midline site, theta modulations were observed over most scalp locations (Rozengurt et al. 2016). It is also possible that theta oscillations within the motor cortex are associated with sensorimotor integration or movement planning and execution. In addition to this, studies in humans have suggested a role of increased theta activity within the cortex in relation to movement suppression (Brier et al. 2010; Zavala et al. 2018), which may align with theta activity presence within the motor cortex of head-fixed mice as they suppress movement activity. In rodents the theta oscillation can be induced in the primary motor cortex *in vitro* (Johnson et al. 2017) as well as being found *in vivo* in head-fixed rodents, although the origin of which is not yet clarified (Igarashi et al. 2013), these have, however, been shown to be coupled to gamma oscillations.

Commonly observed during both awake and sleep states throughout many regions of the brain, gamma oscillations have been associated with various cognitive processes such as sensory perception and integration, motor coordination, attention, decision making and memory encoding (Buzśaki and Wang 2012; Engel and Fries 2010; Engel

et al. 2001; Fries 2009; Fries, Nikolić, and Singer 2007; Gray et al. 1989; Jensen et al. 2007). Gamma oscillations demonstrate similar kinetics throughout the brain regions they have been associated with, such as the neocortex, hippocampus, entorhinal cortex, and amygdala. In many regions of the brain such as the cortex and hippocampus, gamma oscillations are driven by local networks of reciprocally connected parvalbumin-containing basket cells and pyramidal neurons (Bartos, Vida, and Jonas 2007; Buzśaki and Wang 2012). In the thalamus and striatum, the mechanism of gamma oscillations differs however and involve more complex interactions with different neuronal subtypes that have unique intrinsic properties and may be synchronised through cortical regions (Berke 2009; Pinault and Deschênes 1992). In the striatum, for instance, while striatal FS interneurons have a natural tendency to resonate at gamma frequency, it is believed gamma oscillations are driven through external mechanisms with other brain structures (Berke 2009; Carmichael, Gmaz, and van der Meer 2017; Popescu, Popa, and Paré 2009). Generally, the consistency of the excitatory-inhibitory (EI) mechanism implies the widespread presence of inhibitory interneurons mediated through the decay time constant of $GABA_AR$ synapses and the involvement of this oscillation in processing throughout the brain. Neural assemblies can exhibit recurring activity across successive cycles of gamma or different assemblies can alternate in a sequential manner. This oscillation subtype tends to be short-lived, but the coordination of excitation and inhibition can still be detected in the LFP (Buzśaki and Wang 2012). Occurring typically at frequencies ranging from 30Hz-100Hz, gamma oscillations can be subdivided into slow-gamma (30-50Hz), mid-gamma (50-90Hz) and high-gamma (>90Hz). Within the hippocampus there is temporal separation in their association with theta oscillations,

this indicates that these subdivisions of gamma may have different mechanisms for gamma generation and differential distribution (Belluscio et al. 2012; Buzśaki and Wang 2012). Meanwhile, in the cortex, EI mechanisms are believed to predominate (Adesnik and Scanziani 2010; Cardin et al. 2009; Sohal et al. 2009; Sohal and Cardin 2016).

The synchronised firing of local neural ensembles involved in gamma oscillations is believed to facilitate integration, communication, and plasticity across large distances throughout the brain. Although gamma oscillations have been implicated in long-range network dynamics, these oscillations typically arise locally (Buzśaki and Wang 2012). As discussed above, gamma oscillations emerge through coordinated neural networks which are shaped by excitatory and inhibitory input balance, network connectivity, intrinsic membrane properties and additional neuromodulatory influence. FS-interneurons play a crucial role in the timing of gamma oscillations, alongside recurrent pyramidal neuron connections that receive inhibitory feedback (Bartos et al. 2007; Buzśaki and Wang 2012; Cardin et al. 2009; Whittington et al. 1995). PV-basket cells additionally, have previously been shown to be precisely phase locked to gamma oscillations and generate action potentials approximately at a rate of 1 per gamma cycle (Bartos et al. 2007; Bragin et al. 1995; Csicsvari et al. 2003). Furthermore, gamma oscillations are robustly induced in the barrel cortex of mice when driving channelrhodopsin-2 (ChR2) in FS-interneurons (Cardin et al. 2009). Driving these neurons within the 20-80Hz range, led to a significant increase at those frequencies in the power of the LFP, contrastingly, this was not seen with lower frequencies. This demonstrates the ability if this circuit to resonate at gamma

frequency, with the most significant changes in power seen when FS-In were driven at 40Hz (Cardin et al. 2009). This is further supported via inhibition of FS-In leading to suppression of gamma (Sohal et al. 2009). Besides this, pyramidal neurons can also be optogenetically driven to generate gamma oscillations (Adesnik and Scanziani 2010). Overall, these data support excitatory and inhibitory circuits in the generation of gamma oscillations.

Gamma oscillations are widely implicated in cross frequency coupling (CFC), particularly interactions with the theta oscillation. Theta-gamma CFC is linked to information transfer within or across brain regions. Through modulation of gamma power by the phase of a slower oscillation such as theta, slower gamma temporal coordination can be achieved (Buzśaki and Wang 2012). A particularly well studied co-occurring oscillation is theta-gamma phase-amplitude coupling in hippocampus, which is important for hippocampal learning (Buzsáki and Moser 2013; Colgin 2015; Lasztóczi and Klausberger 2014; Lopes-dos-Santos et al. 2018). It has been hypothesised, that cross frequency coupling, enables local networks generating gamma to be coupled via long range connections (Buzśaki and Wang 2012). This is because oscillations of low frequency facilitate synchrony over long distances as a result of conduction delays, whereas this happens more locally for faster frequency oscillations. As such, this aids communication as information arriving in phase is preferentially processed and is more effective facilitating coherent communication, meanwhile out of phase information is integrated less effectively (Buzśaki and Wang 2012; Jensen and Colgin 2007).

During active behaviours such as engagement in a task or movement, prominent theta activity emerges in the hippocampus, unlike during periods of inactivity where there is lack of motion, such as resting (Vanderwolf 1969). This increase in theta, together with the finding that bursts of gamma activity occur within each theta cycle, raised the possibility that these interactions are an integral part of hippocampal network dynamics (Colgin 2015; Lasztóczi and Klausberger 2014). Following on from this, theta-gamma coupling has been found to support memory processes in both rodents and humans (Canolty et al. 2006; Colgin 2015; Lopes-dos-Santos et al. 2018). Whereby, different theta nested gamma frequencies have different roles, slow gamma may promote memory retrieval, while mid-gamma is associated with learning and fast gamma might facilitate memory encoding (Colgin 2015; Lopes-dos-Santos et al. 2018).

While more research is needed to elucidate the role of theta-gamma coupling in contexts other than hippocampal dependent plasticity, as previously mentioned, there is evidence from both animal models and human studies that associate theta and gamma oscillations to the motor cortex (Canolty et al. 2006; Igarashi et al. 2013; Johnson et al. 2017; Rustamov et al. 2022; Spooner et al. 2022). One recent study (Akkad et al. 2021) demonstrated that in humans, transcranial alternating current stimulation (tACS) can significantly improve learning of a thumb abduction task when applied over the contralateral primary motor cortex. The improvement correlated to gamma stimulation applied to the theta peak, simulating theta-gamma coupling as compared to the control targeted to the theta trough and sham conditions (Akkad et al. 2021). Robust coupling in the neocortex between theta and high gamma has also

previously been shown in patients, it was also observed that the theta oscillation amplitude can affect the strength of coupling, not just the theta phase (Canolty et al. 2006). Additionally, CFC of theta-gamma oscillations in the motor cortex has also been linked to movement execution in healthy individuals, this was however, more specific to power-power interactions as opposed to phase (Spooner et al. 2022).

Further, there is evidence of theta-gamma coupling in the motor cortex in animal studies. In layer 5 of the rat motor cortex for instance, CFC of theta and gamma was demonstrated through an *in vitro* study, which also found that these oscillations were generated through distinct mechanisms (Johnson et al. 2017). This is important, as it is already well known that layer 5 of the motor cortex drives movement through subcortical structures. It was found that at the peak of the theta oscillation there were packets of gamma waveform activity (Johnson et al. 2017).

Pharmacological manipulation was further used to dissect the circuitry underlying these two induced oscillations. Gamma oscillations were dependent on both excitatory or inhibitory recurrent synaptic transmission, theta oscillations contrastingly, were not dependent on these mechanisms (Johnson et al. 2017). Both oscillations were dependent however, on the presence of gap junctions and could be modulated via metabotropic glutamate receptors (Johnson et al. 2017).

Theta-gamma coupling in the forelimb region of the motor cortex of head-fixed rodents during a behavioural forelimb reaching task has been observed, and specific neuronal types were seen to fire at specific phases of the theta oscillation, dependent on behavioural state of the animal, in a cortical layer-dependent manner (Igarashi et al. 2013). Neuronal spiking (juxtacellular) and LFP were recorded and both regular spiking

(putative pyramidal) neurons and putative FS-interneurons, phase-locked preferentially to the trough of fast and slow gamma oscillations and the tendency to phase-lock was strongest when the amplitude of the ongoing oscillation was larger. Theta phase-locking of putative pyramidal neurons demonstrated dependence on cortical layer: in superficial layers putative pyramidal neurons fired at the theta trough, while in deep layers putative pyramidal neuron spiking was distributed broadly over the theta cycle (Igarashi et al. 2013). Putative FS-interneurons meanwhile fired near the theta oscillation trough in all motor cortical layers (Igarashi et al. 2013). This provides additional evidence that head-fixed rodents can demonstrate increases in gamma power. This may be associated with movement such as body repositioning, however, not just a behavioural task consistent with studies in which gamma increases during movement (Muthukumaraswamy 2010; Nowak et al. 2017; Pfurtscheller and Lopes Da Silva 1999), or other cognitive processes such as sensorimotor integration that gamma oscillations have been associated with (Engel and Fries 2010).

This may be indicative of the different pyramidal neuronal subtypes across cortical layers phase locking preferentially to different phases of the theta oscillation. Only IT neurons are found in more superficial layers, whereas deeper layers also contain either PT or CT pyramidal neurons (Harris and Shepherd 2015; Hooks et al. 2013; Shepherd 2013). Theta oscillations within this study were shown to coordinate slow and fast gamma oscillations and were essential in structuring motor related activity with neurons encoding different stages of sequential movement implicated in firing at particular phases of theta, particularly within deeper layers (Igarashi et al. 2013).

Unlike in the hippocampus, this study indicated no evidence for theta phase-progression (Igarashi et al. 2013) which may reflect physiological differences between these circuits and their associated roles.

These data demonstrate that theta-gamma phase coupling could be a key mechanism for motor learning. Utilising the development of these methods as a possible therapy, could be facilitated through understanding of the mechanisms involved by which entraining oscillations and the role of different frequencies can improve learning. To facilitate this at a level of the underlying microcircuitry requires animal models in which you can manipulate specific cell types to elucidate their role.

1.2.5 How we can study oscillations using in vivo electrophysiology

Electrophysiology is a branch of neuroscience that enables us to study oscillations and neuronal activity within the brain. The electrical signals generated by cells while they communicate and function are measured and analysed, then used to inform insights into neural communication and underlying neural processes. While there are multiple methods to measure electrophysiology, the technique I will focus on are the use of multi-electrode arrays. This technique is useful in studying network activity as they consist of arrays of small electrodes that can be placed inside the brain to simultaneously record electrical activity across multiple cells. As already mentioned, this technique is readily combined with optogenetics, both of which offer unique temporal and spatial resolution. Data acquired can then be used to advance understanding of neuronal and cellular functions.

In utilising *in vivo* electrophysiology, we can measure the low-frequency components of extracellular signals (LFP) which give insight into the collective activity of a neuronal population, reflecting temporal summation of both excitatory and inhibitory post-synaptic currents as well as multi-unit potentials. It is therefore also possible to detect single/multi-unit activity using spike sorting techniques. This is the recording of action potentials representing the fundamental units of communication between different neurones. In doing this, not only the firing rates of neurons can be determined, but spike timing and synchrony within the population as well. This could enable newfound insights into the coordination, communication and temporal dynamics within a neural network.

1.2.6 Rationale for acute electrophysiology

Acute electrophysiology using silicon probes can leave the tissue relatively undisturbed, preserving some neural integrity without the need for implants in the tissue. Acute set-ups are limited to a certain timeframe in which experiments can be performed. While it could be said that this is a disadvantage, as a result it likely minimises changes via neuronal plasticity over such short timeframes and is therefore more representative of localised baseline neural activity while allowing study of a brain region with a more minimal invasive approach. This method is useful when combining transient optogenetic stimulation via an optrode for an experiment, as it can capture insights into the effects. Finally, acute set ups allow for more versatility and flexibility with regard to experimental changes than chronic approaches and can be undertaken in awake, head-fixed animals.

Recording population dynamics of hundreds of neurons using extracellular electrophysiology can be achieved in a way which is simply not possible using intracellular recordings which tend to have low yields and can only record a few cells at once. However, this methodology prevents localisation of cell types involved in signal generation and can only be attributed to either fast spiking (putative parvalbumin) neurons or regular spiking (putative excitatory) neurons without the use of additional complementary techniques such as optogenetics.

1.2.7 Oscillations & disease

Oscillations are understood to be a key mechanism for a normal healthy functioning brain. Therefore, understanding the role oscillations play in health and disease is an important goal within neuroscience. Abnormal oscillations have been implicated in a large range of brain disorders, with impairments in different memory and cognitive functions for instance, closely correlating to core symptoms (Uhlhaas and Singer 2010).

A well-known hallmark of Parkinson's Disease is dopamine depletion, alongside a robust elevation of beta power in the basal ganglia - a group of nuclei involved in motor control (Brown et al. 2001; Sharott et al. 2005). There is, however, growing evidence for a role of multiple frequency bands, for instance in the gamma frequency and their interactions in contributing to components of both motor & non-motor impairments (Muthuraman et al. 2020; Swann et al. 2016).

In addition, there is increasing evidence that disturbances in oscillations are present in a number of psychiatric disorders. One such disorder that has been well studied is

schizophrenia and patients that experience psychosis, in which aberrant gamma activity has been linked (Uhlhaas and Singer 2006, 2010). This is not the only affected oscillation though, it has also been reported that beta coherence is diminished in comparison to healthy controls (Uhlhaas and Singer 2006), as well as changes in the theta frequency that can be linked to deficits in verbal memory (Kirihara et al. 2012).

Considering well-known interactions, oscillations like these have not been affected singularly, and patients have also been found to have altered theta-gamma coupling. One study suggested theta-gamma coupling is impaired during a working memory task in patients with Schizophrenia (Barr et al. 2017), meanwhile another contrastingly indicated elevated coupling in relation to attention and hyper-focusing (An et al. 2024). Furthermore, studies have also demonstrated reduced phase-synchronisation across the beta and gamma frequencies (Krishnan et al. 2005; Uhlhaas et al. 2006; Uhlhaas and Singer 2006). These dysfunctions of neural synchrony may result from deficits in GABAergic transmission, which are vital for the generation of synchronised oscillatory activity (Lewis, Hashimoto, and Volk 2005; Uhlhaas and Singer 2010). There is also evidence that aberrant oscillatory activity like that suggested here, could be related to the core schizophrenia symptoms such as hallucinations or thought disorder. While a lot of data indicates decreases in power and synchrony in relation to psychiatric disorders, in contrast, some positive symptoms such as hallucinations have been associated with increased oscillatory activity (Uhlhaas and Singer 2010). The role of multiple oscillations and underlying circuitry in such disorders remains complex and under investigation.

Moreover, it has previously been shown that oscillations are altered in those with autism spectrum disorder (ASD). Some studies have reported altered gamma oscillations, other studies have indicated reduced alpha oscillations particularly during tasks requiring attention or cognitive control as well as alterations in both theta and beta have also been observed (Kessler, Seymour, and Rippon 2016; Larrain-Valenzuela et al. 2017; Orekhova et al. 2007; Simon and Wallace 2016; Zeng et al. 2017). Furthermore, there is evidence of disruptions to synchronisation and connectivity across brain regions in individuals with ASD (Simon and Wallace 2016; Uhlhaas and Singer 2006; Zeng et al. 2017). There is, therefore, growing evidence of an abnormal role of oscillations that may contribute to cognitive and behavioural phenotypes of those with ASD.

Ultimately, oscillations have been associated with numerous disorders and I have presented just a few examples to support this. Oscillations, synchrony of oscillations and the correlations between their dynamics and disorders ultimately opens an avenue for therapeutic interventions targeting these. A mechanism which could help further understand the function of oscillations within the brain are brain stimulation paradigms. Closed-loop stimulation paradigms that use oscillations as a biomarker for manipulation are of even greater importance and may be crucial in advancing what we already know regarding these oscillations and the importance they play in a functioning brain.

Therefore, to fully investigate the role of oscillations and the underlying circuitry, it would be advantageous to modulate different frequencies bidirectionally. A method

of bidirectionally modulating oscillations is through the use of brain stimulation techniques.

1.3 Brain stimulation

1.3.1 Brain stimulation & current uses

Brain stimulation methods can be used to alter neuronal activity within the brain. These methods enable the investigation of brain function, as well as providing treatment options for neurological and psychiatric disorders, for example. In humans, brain stimulation can be split into two main different types, invasive and non-invasive stimulation, the former of which requires direct access to the brain. Examples of non-invasive brain stimulation methods include transcranial magnetic stimulation (TMS) which uses magnetic fields to induce electrical activity within a brain area, transcranial direct current stimulation (tCDS) which modulates brain activity through application of a low electric current to the scalp, as well as transcranial alternating current stimulation (tACS) which uses alternating currents to influence brain activity. Non-invasive techniques, like repetitive TMS (rTMS), which delivers magnetic pulses repeatedly are increasingly being used as a treatment, for example in major depressive disorder, in which several studies show reductions in the Hamilton Depression rating Scale scores between real and sham rTMS groups (Fitzgerald et al. 2018; Lefaucheur et al. 2020). It also shows high efficacy for other disorders, reducing pain scores in studies of neuropathic pain and in promoting motor recovery in the post-acute stage of a stroke (Lefaucheur et al. 2020). There is, however, still a need for more rigorously designed and substantially larger studies, to determine the continuing impact of these therapeutic treatments, which may have already been approved by regulatory

agencies, to ensure they are clinically relevant. An additional powerful non-invasive method is electroconvulsive therapy (ECT) where brief controlled electrical currents are used to induce seizure activity.

Invasive brain stimulation is more complex because it requires direct access to the brain, for implantable devices which involves surgical procedures. An example of this is deep brain stimulation (DBS) in which electrodes that deliver electrical pulses are implanted into specific regions of the brain. Modern deep brain stimulation has revolutionised the treatment of movement disorders since the chance discovery in the late 1980s that higher frequency stimulation could reduce some motor symptoms of Parkinson's Disease (PD) (Gardner 2013). Approved as a treatment for essential and severe tremor in 1996 by the FDA (Gardner 2013) and later for treatment in the UK by the early 2000s.

Deep brain stimulation has now long been recognised as a useful treatment for Parkinson's Disease. Here, the implanted electrodes deliver electrical impulses to a specific region (e.g. subthalamic nucleus (STN)) independent of ongoing activity, to disrupt the abnormal circuitry activity that presents itself as the symptomology we see (Guidetti et al. 2021). Whilst DBS is primarily used as a treatment for movement disorders, the potential role of deep brain stimulation in a much larger number of disorders is becoming more and more apparent. The technique has shown itself to be useful in other clinical populations, such as those with obsessive compulsive disorder (OCD) and depression (Figee et al. 2022; Rapinesi et al. 2019; Rosson et al. 2022; Sheth et al. 2022), as well as in medically refractory focal epilepsy (Fisher et al. 2010; Salanova et al. 2015; Zangiabadi et al. 2019). More recently, its role as a therapeutic in

other neurological and psychiatric disorders such as schizophrenia (Corripio et al. 2020, 2022; Nucifora et al. 2019) and anorexia nervosa (Braeutigam et al. 2022; Oudijn et al. 2023; Scaife et al. 2022) are also being investigated.

1.3.2 Benefits & Drawbacks of Deep Brain Stimulation

Deep brain stimulation has shown significant effectiveness in alleviating common symptoms of neurological disorders, in the case of Parkinson's Disease, for instance, improvement of motor control and reducing tremors. Many medications that are used in the treatment of neurological and psychiatric conditions have several side effects; these can prevent the success of medications due to patients discontinuing them (Brown & Bussell, 2011; Semahegn et al., 2020; Velligan et al., 2017). However, following the implantation of a DBS device, overall reliance on medications may be reduced helping to limit other side effects. Additionally, DBS can be used as an alternative treatment in patients that are drug-resistant or in cases where the drug effectiveness diminishes over time. An example of this is Levodopa, used for dopamine replacement in Parkinson's patients, while effective, the effects have been reported to wear off in 40-50% of patients treated for 5 years, increasing to two-thirds by 10 years (Mizuno, Shimoda, and Origasa 2018).

Additionally, DBS tends to be used as a last resort because of the surgical risks involved in the procedure. As previously mentioned, DBS involves brain surgery to implant a device which comes with additional risks such as infection and possible damage or bleeding in surrounding tissue. Furthermore, as a surgical procedure, this is costly, requires follow-up care - only physicians can adjust the settings, and battery changes over time. While DBS is known to help manage symptoms associated with

disorders, it does not cure the disorder and can cause its own adverse side effects (Appleby et al. 2007; Hariz et al. 2008), due to current devices stimulating using constant settings in an uninterrupted manner, independent of need. In PD patients, for example, too much stimulation can result in dyskinesia (involuntary movements) or uncontrolled movements that can increase risk of falls as well as speech impairments (Guidetti et al. 2021). This highlights the fact current high frequency DBS treatments do not interact with ongoing neural activity, which is likely to substantially reduce these treatments effectiveness.

Currently, the most documented side effects are those from movement disorder patients due to the increased length of therapeutic use in this clinical population. For furthering the development of deep brain stimulation therapeutics, it is necessary to gain greater understanding of the mechanisms that underly the circuitry involved in these disorders. This would enable enhanced patient selection & target identification, which could help mitigate the poor results DBS treatment can have in some patients. This would also allow for greater predictions of patients that could benefit from treatment and define a more specific criteria for those who could be treated effectively in this way. Moreover, the effects of continuous brain stimulation in the long term remain unknown. Therefore, ongoing research into adaptive brain stimulation which responds to ongoing brain activity to appropriately deliver stimulation may help mitigate some of these drawbacks.

1.3.3 Rationale for closed-loop brain stimulation

While neural oscillations can be supressed using a variety of pharmacological and stimulation methods (McConnell et al. 2012; Osinski et al. 2018; Tachibana et al.

2008), amplification is more difficult. It has however, previously been shown that perturbing specific phases of oscillations has the capacity to either energise or dampen ongoing neural LFP activity (Cagnan et al., 2017; Holt et al., 2019; McNamara et al., 2022). This is possible using advanced methods of brain stimulation.

Closed-loop brain stimulation represents an advanced neuromodulation approach. Unlike traditional open-loop brain stimulation methods which provide continuous stimulation regardless of brain state, closed-loop methods aim to enhance therapeutic efficacy through synchronisation of stimulation to precise points in the underlying neural signals. Thus, creating therapeutics that harness temporal dynamics through their interaction with ongoing activity. This can be achieved using closed-loop circuitry, regulated via feedback from intrinsic oscillations which can allow for more precise manipulation of neuronal oscillations. Temporal dynamics can then be used to drive neuronal processes into a desired state when required, instead of independently consistently at the same rate.

Adaptive deep brain stimulation (aDBS) or closed-loop DBS is a technique more recently developed that fine-tunes signals through feedback from the brain itself. This is based on the theory that stimulation should in fact, only be delivered when required, for instance around the onset of symptoms. Whilst this is an improvement, it should be stated that further interaction with the oscillation on a more physiological level using precise manipulation could be even more beneficial.

Overall, this could substantially decrease the amount of stimulation delivered to the brain by these treatments, as well as improve specificity of stimulation, which in turn could reduce unwanted stimulation side effects which tend to be due be driven by

stimulation effects to other ongoing oscillations (Kumari and Kouzani 2021). This could allow for more consistent effects of stimulation and ensure a more powerful output for those treated. Over time neurological disorders tend to get progressively worse, alongside this is often a change in associated symptomology (Maetzler, Liepelt, and Berg 2009). Fluctuations in symptoms can therefore alter the effectiveness of treatment. A system that can continuously adapt to these fluctuations would therefore be hugely beneficial in both long-term treatment and patient orientated treatment.

These newer aDBS devices can modulate brain activity similarly to conventional DBS (cDBS) devices, however, additionally monitor ongoing brain activity. A small study comparing feasibility of constant and adaptive approaches (based off cortical gamma in relation to dyskinesia) in patients with Parkinson's disease found that there were no differences reported in regard to movement improvement, however, the efficacy of stimulation, due to the nature of adaptive stimulation was in fact far more energy efficient (Swann et al. 2018). Previous work similarly in Parkinson's patients, compared aDBS using brain-computer-interface feedback from the beta-LFP in the STN and were able to demonstrate both better efficacy and efficiency of aDBS (Little et al. 2013). Furthering this, Little et al (2016) demonstrated that aDBS was more effective in improving motor function than cDBS using the same parameters, and could significantly reduce unwanted side effects of stimulation (speech intelligibility) seen with cDBS. This study demonstrates the potential for not only improved efficacy, but reduction of side effects associated with cDBS treatment, although further work needs to be undertaken in chronically implanted patients (Little et al. 2016).

Additionally, it has been shown that use of neurostimulation earlier on in the stage of disease can improve patients' quality of life (Schuepbach et al. 2013), this could be further improved using aDBS technologies that can both improve efficacy and reduce unwanted side effects.

While this body of work primarily focuses on invasive brain stimulation, non-invasive brain stimulation techniques will similarly benefit from the use of closed-loop methods. While these open-loop approaches have already proved effective in treating neuropsychiatric disorders (Kuo et al., 2014; Lefaucheur et al., 2020), and can modulate cortical plasticity safely, currently they still have limitations. The heterogeneity of effects that is seen between individual responses to non-invasive brain stimulation is one such limitation (Hamada et al. 2013; López-Alonso et al. 2014; Maeda et al. 2000; Wiethoff, Hamada, and Rothwell 2014). Repetitive TMS for instance, which tends to follow either an 'excitatory' or 'inhibitory' protocol, can result in the opposite effect to what was expected, or absent responses in as many as 50% of individuals (Hamada et al. 2013; López-Alonso et al. 2014; Ziemann and Siebner 2015). This number varies depending on stimulation type, but it is possible these effects have been underestimated in earlier literature.

Many factors are thought to contribute to the heterogeneity seen in response to rTMS, for example differences in brain anatomy and function, individual differences in baseline activity, the recruitment of different neuronal populations (Hamada et al. 2013; L. M. Li, Uehara, and Hanakawa 2015; Ridding and Ziemann 2010). It is likely that all non-invasive techniques are influenced by this variability, as whilst the techniques work through different mechanisms to induce effects, the underlying resultant

changes are similar. Tailoring stimulation for these therapeutic applications through closed-loop stimulation could help to reduce the heterogeneity of effects, improving the overall efficacy of treatment. An additional difficulty in finding effective stimulation protocols, is linked to the fact it is likely brain states of patients are altered in respect to healthy controls. This could result in stimulation protocols that don't exert the same effects in both populations of individuals and are only optimal under certain conditions, challenging our ability to truly define optimal protocols.

1.3.4 Examples of phase-locked stimulation in humans

Stimulation can be phase-locked, this is a technique in which stimulation is synchronised to specific phases of an ongoing oscillation. In doing this, we can aim to maximise the efficacy of stimulation which could enhance therapeutic outcomes and reduce unwanted side effects.

As previously mentioned, Akkad and colleagues demonstrated the role of gamma stimulation (tACS) targeted to the theta peak in improving motor learning. An improvement in learning was only observed when gamma stimulation was targeted to the theta peak which simulated theta-gamma coupling, as opposed to the sham condition in which it was applied to the theta trough, or the control condition (Akkad et al. 2021). Stimulation in this study was not locked to the underling theta phase as the protocol applied predefined coupling of these two rhythms and thus does not interact with individuals naturally occurring oscillations. However, it still infers the potential benefits studies that apply phase-locking techniques could achieve.

Furthermore, it has been shown that phase-locked tACS is able to reduce amplitude of tremor. This was first shown with tremor in Parkinson's patients, when targeting the M1 phase-locked to the individuals tremor frequency, it was possible to achieve approximately 50% suppression of tremor, inducing a phase cancellation on the tremor rhythm itself (Brittain et al. 2013). More recently, the amplitude of the pathological beta oscillation in Parkinson's patients was shown to be suppressed by up to 40% when stimulation was delivered on a patient specific beta phase (Holt et al. 2019). Similar work targeting the cerebellum for essential tremor in a tremor phase-locked manner, was also able to significantly reduce tremor amplitude (Schreglmann et al. 2021). As was tremor phase-locked stimulation delivered to the ventrolateral thalamus in essential tremor patients that demonstrated up to 87% tremor suppression (Cagnan et al. 2017).

Other non-invasive brain stimulation techniques have also been investigated for the use of phase-locked stimulation. For instance, one study utilised EEG recording of the human M1 to deliver mu-rhythm phase-specific TMS pulses using a customised real-time signal processing algorithm. This system was triggered when a pre-determined power threshold was reached as well as simultaneous crossing of a specified phase angle. This demonstrates phase modulation of the ongoing sensorimotor mu-rhythm results in changes in corticospinal excitability. Stimulation targeted to the mu trough, representing a state of high-excitability, increases corticospinal excitability in a long-term potentiation manner, while targeting the mu peak, a state of low-excitability, or at random phases results in no changes in corticospinal excitability (Zrenner et al. 2018). While this technique is not completely adaptive in controlling stimulation and

should not be called closed-loop, it is an example of a study that takes brain state as an online marker to provide adapted stimulation. This study indicates the impact of targeted stimulation in a brain state dependent manner being more favourable in producing longer-term changes. This could be utilised in humans to help improve the efficacy of inducing neuroplasticity in studies. Not all studies have found a significant effect of phase-locked stimulation however, a study by Mansouri et al (2019) for example, compared theta tACS to phase-locked (peak & trough) transcranial pulsed current stimulation and sham stimulation for modulation of the salience network during a task. They reported no significant effects in electrophysiological or behavioural measures between the different stimulation conditions and sham condition (Mansouri et al. 2019). However, it is not clear whether the stimulation parameters were appropriate for the area of the brain targeted, and the authors used a task which hadn't been used in combination with brain stimulation before. The authors therefore remained hopeful that future work with these types of stimulation of the salience network could be used for therapeutic purposes in treatment of neuropsychiatric disorders.

Currently, whilst we can study single neurons in freely moving animals, this is a limitation of human studies as participants in these types of studies are immobile. Implanted neural devices, as previously mentioned, do not have the capability to allow for single neuron recording or to customise parameters of neural stimulation. To try and overcome these limitations, one group has investigated the potential of a wearable platform for closed-loop stimulation. Known as the 'Neuro-stack', a miniature recording and stimulation system that can be used in humans with

implanted electrodes, during stationary and ambulatory types of behaviour. This device can deliver phase-locked closed-loop stimulation, while recording single units and LFP and is highly flexible in terms of the programming options available (Topalovic et al. 2023). This could substantially enhance the types of research questions that could be investigated. Whilst there are still challenges for this type of wearable technology such as reducing artifacts, this highlights the possibilities of such advancing technology and the ability to record both LFP and single neurons in moving patients. This could one day enable greater insights into pathology of the brain in patients in more naturalistic settings.

Technical challenges in implementing phase-locked closed-loop stimulation, such as employing real-time phase-tracking algorithms and occurrence of stimulation artifacts presents difficulties for adopting these methods. The studies mentioned here, indicate a small breadth of research currently investigating phase-locked methodologies in humans. Further research in this field, could enable precise control of the effect of stimulation (i.e. direction) as well as improving consistency of effects both within and across different individuals.

1.3.5 Phase-locked stimulation in animal models

Whilst closed-loop devices are gaining traction in humans, there is still a lot that is unknown in regard to the best biomarkers to target and the temporal dynamics of stimulation. To more precisely interrogate this, animal studies which can target the endogenous oscillation are vital. A new closed-loop phase-locking system was recently pioneered in the basal ganglia of chronically implanted Parkinsonian rats (lesioned with 6-hydroxydopamine) (McNamara et al., 2022). These rats displayed a

pathological beta oscillation, typical of those with Parkinson's, which could be targeted at 8 evenly spaced phases across the cycle. Modulation of the ongoing pathological beta oscillation was then demonstrated in a phase-dependent manner. Electrical stimulation targeting the mid-descending phase resulted in maximal amplification of the pathological beta oscillation, while targeting the mid-ascending phase showed maximal suppression of beta power (McNamara et al., 2022). Phase-dependent stimulation could additionally produce changes in ongoing behaviour (McNamara et al., 2022). This indicates the importance of precise temporal manipulations and the resulting output.

To manipulate circuits even more precisely requires further specificity, this is possible using optogenetics. Previous *in vitro* studies on phase sensitivity have often focused on theta oscillations in the hippocampus. It has previously been demonstrated that gamma oscillations in an *in vitro* hippocampal slice set-up, can be entrained by optogenetic sinusoidal stimulation of pyramidal neurons, with a strong frequency-dependent phase relationship between optogenetic stimuli and the response generated (Akam et al. 2012). Moreover, Nicholson et al (2018) showed phase-locked stimulation of gamma oscillations bi-directionally modulating gamma frequency and amplitude without altering the overall firing rate of the neurons, instead altering the synchronicity of pyramidal cell firing (Nicholson et al. 2018).

Even more relevant however, are studies testing phase-locked closed-loop stimulation systems with optogenetics *in vivo*. Siegle & Wilson (2014) demonstrated endogenous theta phase-specific manipulation of freely moving mice within the dorsal CA1 region of the hippocampus using optogenetics. Inhibition through the

activation of PV interneurons, targeted to different phases of the endogenous hippocampal theta rhythm could improve performance of different aspects of a spatial navigation task. Inhibition targeted to the theta peak was able to improve performance of the encoding segment of the task, while inhibition directed to the trough improved the retrieval performance in the task (Siegle and Wilson 2014). This closed-loop design was able to interrogate the roles that phase, and task segment play in task relevant information processing. Moreover, Dejean et al. (2016) identified a prominent 4Hz oscillation that develops in relation to a conditioned fear response in the dorsal medial prefrontal cortex (dmPFC) mediated by recruitment of neural assemblies. The authors then used optogenetics to demonstrate selective activation/inhibition of neurons in the dmPFC at different phases of the 4Hz oscillation. During the ascending phase, inhibition of pyramidal neurons through the activation of PV-interneurons (reducing assembly recruitment) reduces freezing behaviour, while activating pyramidal neurons and thereby increasing neuronal assembly recruitment increases freezing behaviour. When instead targeting the descending phase, inhibition of pyramidal neurons increases freezing behaviour, the opposite effect to inhibition at the ascending phase, while activation of pyramidal neurons does not affect behaviour. This study identifies a phase-specific coding mechanism for the fear response in mice using optogenetic phase-locked stimulation, through dynamic regulation of neuronal assemblies in the dmPFC (Dejean et al. 2016).

Kanta et al, (2019) more recently demonstrated work utilising a system for closed-loop optogenetics in the basolateral amygdala of rats. Based on the prominent gamma oscillations in the basolateral amygdala during contextual memory consolidation,

they tracked bouts of this endogenous gamma oscillation and delivered optogenetic stimulation in and out of the preferred firing phase of these neurons. Firstly, they confirmed that during contextual memory consolidation in a rat, the basolateral amygdala has prominent mid-gamma oscillations (40-70Hz). Then, that boosting or diminishing this gamma oscillation with optogenetic stimulation targeted to the gamma trough (gamma LFP phase with high network excitability) and peak (gamma LFP phase with low network excitability) respectively, during memory consolidation, was subsequently able to either enhance or impair memory strength, an effect not seen with random stimulation (Kanta, Pare, and Headley 2019).

Building on previous techniques, Zaaimi et al (2023) used closed-loop optogenetics to manipulate neural dynamics in non-human primates under terminal anaesthesia. The optogenetic method utilised in this study does not restrict expression of excitatory opsins to a specific neuronal subtype but should restrict to neuronal populations of cells in the primary motor cortex. Quantification of green fluorescent protein (GFP)-expressing cells primarily identified cells positive for neuronal markers, inhibitory interneuron expression was found only a small fraction of cells. The authors did however confirm, that in response to one of the viruses used there was additionally relatively high expression of the virus in astrocytes positive for glial fibrillary acidic protein. Prior to this, the authors gained information from their *in vitro* experiment in mice hippocampal slices, in which they determine how to fine tune their closed-loop optogenetic stimulation based on a post hoc cross-correlation between the LFP and underlying neural activity. This indicates that a phase shift of 0-90° relative to the gamma envelope can drive oscillations, while at 180-270° there were minimal

oscillations. Utilising this knowledge, they then showed effective neural enhancement and suppression through optogenetic closed loop stimulation in non-human primates which is not seen under control conditions. While this study gains valuable insights to a more naturalistic and complex brain, these observations are taken in a state of unconsciousness (under anaesthesia) and therefore may not fully represent the ever-changing dynamics of the awake brain so caution must be taken in interpreting these results (Zaaimi et al. 2023).

1.3.6 Non-phased-locked closed loop stimulation approaches

There are examples of closed-loop approaches that do not involve specific phase-locking of stimuli, but nevertheless have relevance for the work contained in this thesis. One such recent study, for example, demonstrated the potential of closed-loop optogenetics in freely moving epileptic mice. Using their closed-loop system, they were able to intervene and manipulate activity based on the recognition of pre-seizure neural EEG activity to suppress seizures before turning the stimulation off when activity returns to baseline (Du et al. 2024).

1.3.7 Neuroplasticity & therapeutic applications of closed-loop brain stimulation

Ultimately, a long-term aim of closed-loop brain stimulation techniques are to improve therapeutic applications by providing more precise and effective brain stimulation. This could be beneficial to a wide range of conditions such as Parkinson's Disease, depression, epilepsy as well as other neurological and psychiatric disorders that could be treated using either implantable brain stimulation devices or non-invasive brain stimulation applications. Many conditions like these can change over time, therefore, a system which can continuously adapt to changing brain states is

likely to be more advantageous long-term. Additionally, acquisition of data in this way which includes real-time monitoring of ongoing oscillations is also likely to advance our understanding of neural circuits and pathological brain states.

Furthermore, it is possible that timing stimulation to specific phases of oscillatory activity could maximise the potential for inducing neuroplastic changes. Promoting neuroplasticity within the brain, which is the ability to alter activity in response to either internal or external stimuli leading to reorganisation of structure, function or connections (Mateos-Aparicio and Rodríguez-Moreno 2019), is particularly important following injury, such as a stroke. Non-invasive brain stimulation techniques have already been found to modulate neuroplasticity, with effects that can persist in some cases beyond the stimulation sessions themselves (Lefaucheur et al. 2020). For instance, rTMS studies in the postacute stage after a limb motor stroke have demonstrated motor improvement to be sustained for at least 3 months after the last stimulation session (Du et al. 2016; Long et al. 2018). An example outside of this, in healthy controls, was demonstrated by Akkad and colleagues (2022) in which theta-gamma peak tACS enhanced motor skill acquisition which was maintained for at least 75 minutes following the stimulation period. Therefore, more precisely matched stimulation to individuals underlying physiological signals could further enhance these effects.

1.4 The role of Optogenetics

In this thesis, we have developed and utilised a technique using optogenetic closed-loop phase-locked brain stimulation to further interrogate motor cortical circuitry in mice.

1.4.1 Background of optogenetics

Microbiologists first discovered microorganisms that were able to produce visible light-gated proteins with the ability to regulate ion flow across the plasma membrane in the early 1970's (Deisseroth 2010). Following on from this, yellow-light activated halorhodopsins were first described in 1977 (Matsuno-Yagi and Mukohata 1977), while channelrhodopsins (ChR1 & ChR2) from the species Chlamydomonas reinhardtii activated by blue light were identified in 2002 (Nagel et al. 2002). It took years, however, to bridge the gap between these identified microbial opsins and the now well-known field of optogenetics. First introduced into neuroscience in 2005 as a readily targetable single component, optogenetics is where light-sensitive ion channels are inserted into specific cell types which allow for millisecond precision control of excitation or inhibition of neuronal populations while not altering other populations (Boyden et al. 2005; Deisseroth 2010). As a result of vertebrate tissue already containing the necessary co-factor (all-trans retinal) essential in allowing photonic control, these can be used *in vitro* but also in freely moving mammals (Deisseroth et al. 2006; Tsai et al. 2009). Thus, allowing interrogation of a large range of neuroscientific questions that we couldn't previously answer as we lacked precise temporal control and greater insight into the complexity of the brain in both healthy and unhealthy conditions.

Rodent optogenetics therefore is a promising technique to increase the specificity of closed-loop brain stimulation as mentioned previously. Different microbial opsins are used to achieve the opposite effects - channelrhodopsins for example conduct inward cation currents to depolarise the neuronal membrane upon light stimulation, while

halorhodopsins conduct negatively charged chloride ions to hyperpolarise neurons, thereby positively modulating neuronal firing and inhibiting firing respectively (Zhang et al. 2007).

Since their discovery, the optogenetic toolbox has greatly expanded and diversified, now including dozens of proteins, activated by various wavelengths of light, with lots of different properties (Deisseroth 2010; Fenno, Yizhar, and Deisseroth 2011; Gunaydin et al. 2010; Mattis et al. 2011). Neural silencing can also be achieved through Archaerhodopsin (Arch), a class of outward proton pumps reliably driven by light and spontaneously recover function in seconds (Chow et al. 2010). BiPOLES (Bidirectional Pair of Opsins for Light-induced Excitation and Silencing) have also been reported, which induce either excitation or inhibition, based on the wavelength of light stimulation (Vierock et al. 2021).

To utilise optogenetics one must also have a method of light delivery. While both *in vitro* and *in vivo* studies tend to use lasers or light-emitting diodes (LEDs), *in vivo* stimulation tends to be trickier, as it often requires implanting cannulas, to insert optical fibers. Lasers are widely used to deliver light as they can facilitate multimodal control and application of a narrow bandwidth of light delivery through optical fibers. Optic fiber delivery can enable specific targeting of even deep brain structures and achieve temporal patterns of stimulation, while versatility of the fiber type (e.g. flat/tapered) can provide even more tailored delivery and alter tissue damage acquired through this invasive method (Pisanello et al. 2014; Pisano et al. 2019). LEDs are a low-cost alternative, can be readily modulated and do not require complex electronic systems, however, there are less efficient methods of coupling than with an optic fiber

and generation of heat can be a problem (Yizhar, Fenno, Davidson, et al. 2011). The small size of LEDs, as well as not requiring too much power can make them useful, however, for targeting multiple different sites, as well as portability in freely moving animals (Guru et al. 2015; Stark, Koos, and Buzsáki 2012). Care must be taken when designing experiments to minimise tissue heating and damage as much as possible while achieving optimal neuronal activation.

It is also important to be able to measure and determine the effects of manipulating neural activity in this way. This can be done in numerous ways depending on the experimental question being asked, for instance using electrophysiological recordings, functional imaging techniques or behavioural observations can be used in combination with optogenetics (Ledochowitsch et al. 2015; J. H. Lee et al. 2010; Siegle and Wilson 2014; Sohal et al. 2009).

1.4.2 Genetic engineering for optogenetics

To introduce light sensitive proteins into biological systems, genetic engineering techniques are employed. One powerful technique to achieve this is the Cre/loxP system (Dymecki and Kim 2007), where a combination of transgenic mice and injection of a virus are used to target discrete populations of cells enabling great flexibility (Figure 1.5). Viral vectors are typically used within neuroscience, which have been genetically modified to deliver a gene to a cell (knock-in). Adeno-associated viruses (AAV) are commonly used as they achieve high penetration and contain the transgene of interest that we would like to express in specific cell types, as well as often a fluorescent reporter protein either fused to the transgene of interest or inserted in a reading frame itself, for example ChR2-eYFP (enhanced yellow fluorescent

protein). These additional fluorescent reporter proteins tend to exhibit strong expression that allows later visualisation of viral expression.

One limitation of reporter expression, however, is that exposure to fixatives or high temperatures for instance in tissue processing can result in weak expression (Alkaabi, Yafea, and Ashraf 2005; Bokman and Ward 1981). Antibodies against the reporter protein can later be used to help circumvent this and improve expression visualisation for histology. The transgene and reporter are also flanked by loxP sites, these are short sequences of DNA that act as recognition sites. The other aspect in this technique are transgenic mice - a large number of transgenic mouse models have been created, that selectively express Cre-recombinase in particular cell-types (Gong et al. 2007; Madisen et al. 2009; Taniguchi et al. 2011). Cre-recombinase is an enzyme that catalyses recombination between two Lox-P sites and ultimately enables expression of the transgene of interest (Fischer, Collins, and Callaway 2019). This strategy has enabled the neuroscientific community to deliver optogenetic stimulation to precisely defined cell types *in vivo* (Figure 1.5).

To try to prevent off-target expression, the double-floxed inverted open-reading frame (DIO) system was developed. DIO viruses contain two sets of loxP sites, both of which Cre-recombinase can bind to and the transgene of interest is inserted in reverse orientation flanked by both sets of loxP sites. In the presence of Cre-recombinase, upon binding to one of the sets of loxP sites, the orientation of the flanked transgene will be inverted leading to its expression and production of the light sensitive protein (Figure 1.5A). This inversion also results in the unused loxP site being flanked by a pair of loxP sites that are orientated in the same direction, which signals for this DNA to be

excised. This leaves the transgene of interest between two different loxP sites which prevents it from reverting back into the original state preventing expression (Fenno et al. 2011; Sohal et al. 2009). Conversely, when Cre-recombinase is not present, no recombination occurs, and the promotor drives the expression of the gene as it is, therefore, even though the virus has infected the cell it does not express the transgene of interest.

Whilst some studies have reported viral expression to be robust and off-target effects undetectable (Sohal et al. 2009) others found that they could be leaky (Botterill et al. 2021; Fischer et al. 2019). After investigation, it was identified that a reason for some off-target expression was due to spontaneous recombination between homologous pairs of loxP sites before viral vector packaging, but this is believed to occur at a low rate (Fischer et al. 2019). Furthermore, new generation sequencing is also being developed to help standardise and quality control assays and check for any cross-contamination or recombination events, while also confirming the identity of adeno-associated virus preparations (Guerin et al. 2020).

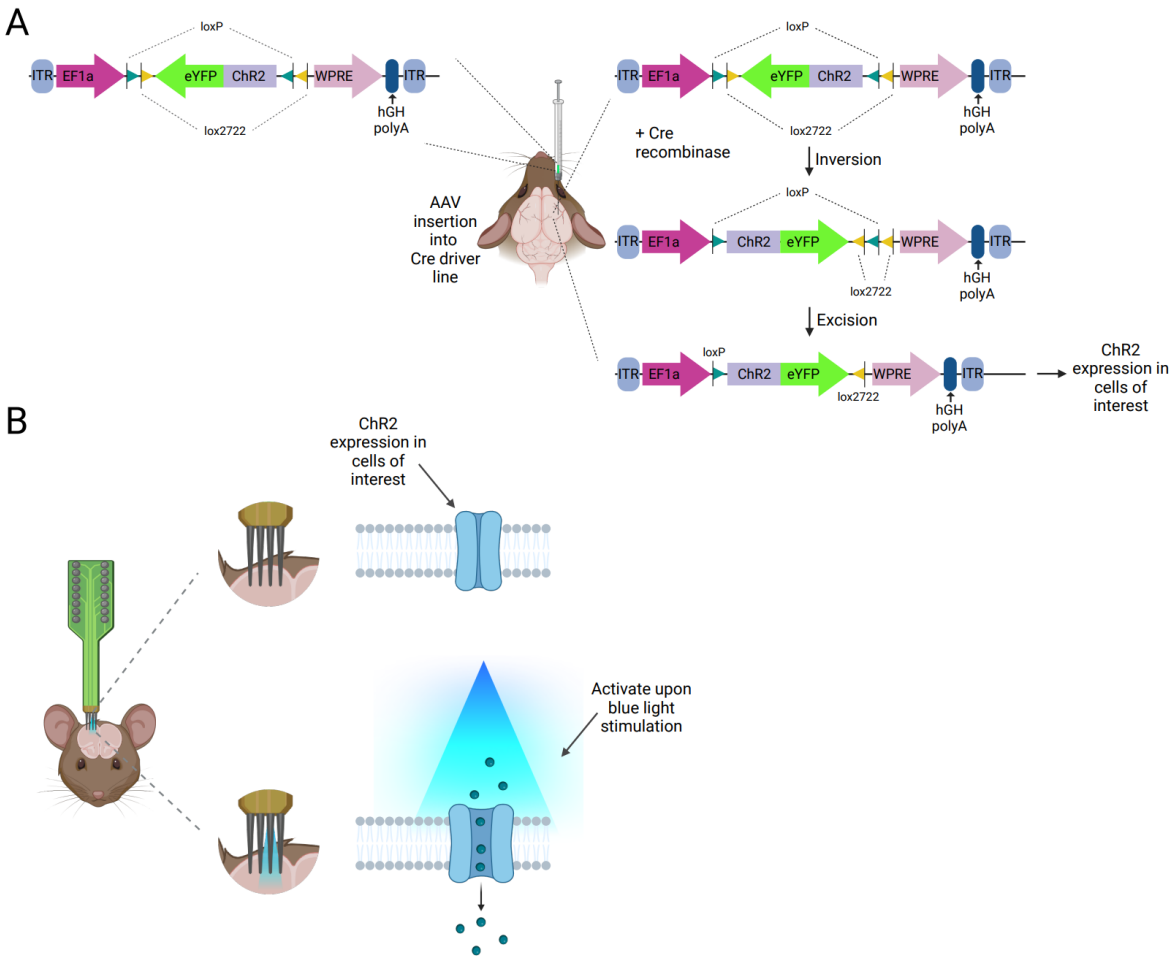


Figure 1.5 Cre-dependent mouse line and AAV injection for optogenetics

This demonstrates the Cre/loxP system (**A**). The adeno-associated virus (AAV) has two loxP sites surrounding the gene of interest (DIO: double-floxed inverted open-reading frame) - in this case 'ChR2-eYFP', a light sensitive protein. The transgenic mouse line expresses Cre-recombinase in the cell types of interest. When there is overlap between a cell that expresses Cre-recombinase that has also up taken the AAV, Cre-recombinase will bind to a pair of loxP sites inverting the relevant gene and excising DNA between two loxP sites orientated the same way. The gene is then expressed by the cell, so the light sensitive protein is produced, and this ion channel is inserted into the cell's membrane. Upon light stimulation (476nm blue light) the light sensitive protein activates resulting in neuronal cell depolarisation (**B**). (Figure created with BioRender.com).

In this thesis I have utilised two well-known transgenic mouse lines: PV-Cre (Hippenmeyer et al. 2005) and RBP4-Cre (Gerfen, Paletzki, and Heintz 2013; Harris et al. 2014). These lines target Cre-recombinase to either parvalbumin (PV) expressing interneurons or retinol-binding-protein-4 (RBP4) expressing pyramidal neurons in our area of interest respectively. I have combined this with a standard adeno-associated virus (AAV) to deliver an ultrafast opsin (ChR2(E123T/T159C)), known to display fast

kinetics allowing rapid repolarisation of the membrane following an action potential as well as robust membrane insertion (Berndt et al. 2011; Stahlberg et al. 2019).

1.4.3 Rational, relevance & pitfalls of optogenetics

Optogenetics is of significant importance to the neuroscientific community and has allowed us to expand the questions we can ask with our studies. A substantial body of work has already been undertaken utilising these techniques to show reliable activation of neurons for studies investigation functional mapping, modelling of disease, behaviour studies and neurophysiology to name a few (Kravitz et al. 2010; Ledochowitsch et al. 2015; J. H. Lee et al. 2010; Siegle and Wilson 2014; Sohal et al. 2009). As previously mentioned, the main advantages of optogenetics are the spatial and temporal precision it allows, the flexibility and reversibility. These advantages are what lend itself to leveraging its potential through closed-loop optogenetic stimulation.

Optogenetics does however, have some pitfalls that should be considered. Optogenetics is an invasive technique and injection of the virus, the method of light delivery *in vivo* (i.e. cannulas/optrodes) and tissue heating generated via light delivery can contribute to tissue damage. Experimental methods can be optimised to minimise such damage, such as by using smaller injection pipettes, injecting the virus at small volumes with a slow rate and using low laser powers to prevent tissue heating. Use of chronically implanted cannulas for light delivery, however, will result in areas of damage, but the optic fiber shape can be considered to help reduce that damage in the area of interest. For instance, tapered fibers can reduce tissue damage compared to the previously standardly used flat fibers and supports more even distribution of

light within a tissue (Owen, Liu, and Kreitzer 2019). It is also possible to use optrodes either acutely or chronically that combine a recording method with light delivery to minimise the number of required insertions into the tissue and decrease some of the associated tissue damage.

Not only can light delivery cause tissue damage, but optogenetics can also lead to heating of the tissue which could in turn lead to significant physiological changes as many neuronal processes like synaptic transmission or ion channel conductance are dependent on temperature (Owen et al. 2019; Yizhar, Fenno, Davidson, et al. 2011). Indeed, suppression of neural firing has been shown in acute whole cell recordings (Owen et al. 2019). Moderate suppression of pyramidal neurons in cortical layer 5 has previously been demonstrated, as well as stronger suppression of fast-spiking interneurons (Owen et al. 2019). On the other hand, previous *in vivo* work has shown temperature changes due to light can increase cortical activity dependent on the of the laser power used (Stujenske, Spellman, and Gordon 2015). In both of these studies, the wavelength of light used was the same (532nm).

The difference between *in vivo* and *in vitro* studies in this regard also highlights the complexity of *in vivo* work, which although may be more representative of true physiological function, presents challenges in disentangling effects and the discrepancies that can arise between different techniques. It is important to note that the time constant for heating neuronal tissue via light is much slower than the time constant by which optogenetic proteins affect neural activity, this can ultimately be used to help differentiate effects that are a result of the opsin opposed to experimental artifacts like tissue heating (Owen et al. 2019). The main way to combat tissue heating

is to use lower light stimulation powers, pulsed stimulation over continuous stimulation, longer wavelengths of light that generate less heat and experiments have additionally suggested that larger fiber diameters could also reduce temperature changes near the fiber tip (Arias-Gil et al. 2016; Cardin et al. 2010; Owen et al. 2019; Stujenske et al. 2015).

1.4.4 Complexities of *in vivo* optogenetic studies

There are a number of potential difficulties for *in vivo* optogenetic studies. Firstly, the penetration of light into the brain in *in vivo* studies can be limited, and access to different brain areas can be challenging. The brain is biological tissue which results in absorption and scattering (photons deflected from their path of travel) of light, affected by tissue composition and differences in optical properties of cells (Al-Juboori et al. 2013). Transmission properties also depend on the wavelength of light, as increasing wavelengths scatter less and so penetrate more deeply into the tissue (Yizhar, Fenno, Davidson, et al. 2011). This means the blue light used for ChR2 stimulation will penetrate less through the brain than yellow light. Finally, light could cause non-specific neural responses e.g. sensory responses through the retina, due to light escaping from the delivery apparatus or alternatively via scattering in the tissue itself (Yizhar, Fenno, Davidson, et al. 2011). Control experiments are therefore paramount in helping to distinguish these effects.

Additionally, when utilising the Cre/loxP system in the form of a viral vector, it is unlikely that there will be uniform expression across all cells in the area targeted, even though AAV viruses can penetrate cells widely. Similarly, when delivering light to the targeted neuronal population, it is unlikely to be uniform. Combining these effects, it

is likely different cells will have different ranges of activity elicited by light and only a subset of these will be modulated (Guru et al. 2015).

A further challenge of optogenetics is that while technology has advanced to allow us to stimulate a particular subset of cells, stimulation of the targeted population can result in synchronous neural activity which itself is not normally observed from a physiological perspective. This can cause changes in individual neuronal firing patterns within the population and so physiological differences usually observed such as spiking rate and phase with respect to the LFP can be lost (Guru et al. 2015). Depending on the questions being asked, care should be taken when interpreting results. Likewise, when recording activity with a technique like electrophysiology, collective neural activity is recorded, not just those that have been optogenetically manipulated, but those indirectly recruited as well and not necessarily all neurons that may express the virus. This can undoubtedly be helpful for interpreting signals at a population level, but due to spiking latencies of cells *in vivo* being highly variable as a result of intensity of illumination differences, caution should still be observed at a neuron level (Yizhar, Fenno, Davidson, et al. 2011).

Finally, advances in neuro-engineering contributed to the development of optrodes which we have utilised in this thesis. This allows multichannel readouts of electrophysiological data as well as optogenetic stimulation through a fiber and thus allows multiple cells to be simultaneously recorded and stimulated. While not as challenging as electrical artifacts, this technique can lead to photoelectric artifacts, which can make interpretation of the data difficult. Although newer silicon optrodes are designed to minimise artifacts, this can still be an experimental confound

distorting the signal and needs to be carefully controlled in *in vivo* studies of the type presented in this thesis.

1.5 Aims

Inhibitory interneurons and pyramidal neurons play a vital role in maintaining an excitatory and inhibitory balance necessary to drive neuronal oscillations through coordinated rhythmic activity which ultimately drives sensory, motor and cognitive processes. To determine more about the precise role these neurons play within the microcircuit, they can be optogenetically manipulated and the global response to manipulation can then be measured using the LFP. Recent work has shown that closed-loop phased-locked stimulation, which more precisely modulates the circuit using feedback from intrinsic oscillations may lead to more specific changes in the circuitry improving effectiveness and can also drive changes in behavioural performance (McNamara et al., 2022; Siegle & Wilson, 2014). Therefore, we wanted to bring this technique together with optogenetics to determine whether we can effectively modulate the circuitry in the motor cortex.

The aims of my DPhil thesis are:

Aim 1: Confirm feasibility of an optogenetic closed-loop experimental set-up in head-fixed mice.

Aim 2: Assess the theta global response (LFP) of optogenetic motor cortical theta stimulation in different neuronal subtypes.

Aim 3: Assess whether we can not only modulate the local theta oscillation, but whether gamma frequency theta stimulation is able to successfully modulate gamma power when targeting either of the neuronal subtypes in our study.

To address these aims, we first needed to confirm the feasibility of motor cortical optical stimulation whilst utilising a new closed-loop stimulation approach to both record LFPs and stimulate specific phases of the ongoing oscillation. To achieve this, we combined electrophysiology with optogenetic stimulation in a closed-loop system.

Once feasibility was confirmed, we used *in vivo* awake head-fixed probe recordings in different mouse lines to determine whether closed-loop brain stimulation could modulate cortical theta activity (LFP). This was assessed in PV-Cre mice, a line targeting inhibitory interneurons as well as RBP4-Cre which targets layer 5 pyramidal neurons. The experimental methods and results of this aim are described in the following two chapters.

Finally, to address my last aim we studied whether there were any additional changes in the motor cortical gamma oscillation when undertaking closed-loop theta targeted optogenetic stimulation. This was assessed when targeting inhibitory interneurons and pyramidal neurons in the two separate mouse lines. The results of this aim are described in Chapter 5.

2 Methods

All experimental chapters in this thesis used very similar methods. I have therefore described the methods for all chapters in detail here. Specifics, such as the number of mice used in each analysis, are detailed within each chapter.

2.1 Animals

Adult mice (male) either B6;129P2-Pvalb$^{tm1(cre)Arbr}$ (PV-Cre, heterozygous on a C57BL/BJ background, Jackson Laboratories) or Tg(RBP4-Cre)KL100Gsat (RBP4-Cre, heterozygous with a C57BL/BJ background, Jackson Laboratories) weighing 23-43g were used for all experimental procedures. Mice were housed with their littermates where possible, then singularly housed after headplate surgery. Animals were kept in a 12-hour light/dark cycle at both a constant temperature and humidity in ventilated cages, with food and water provided *ad libitum*. All studies performed were in accordance with institutional guidelines and the Animal (Scientific Procedures) Act, 1986 (United Kingdom).

2.2 Stereotaxic surgeries

2.2.1 Unilateral Stereotaxic Viral Injection

All surgeries were performed aseptically. Anaesthesia was induced at 4% isoflurane in oxygen, then maintained through a nose mask at 1-2%. The anaesthetised animal had its head shaved, then was secured in a stereotaxic frame (David Kopf Instruments). The body temperature of the animal was maintained using a probe and heating pad around 37±0.5°C. To provide analgesia Buprenorphine (Vetergesic - 0.08mg/kg in sterile saline) was administered subcutaneously after anaesthesia was

induced. The shaved scalp was cleaned using chlorhexidine and sterile saline, before, Marcain (2mg/kg) was injected subcutaneously into the scalp to provide local anaesthesia. 8-10 minutes later, an incision was made along the midline with a scalpel. If necessary, the skull was levelled, through minor adjustments to the stereotaxic equipment. Using bregma as a reference, the site of the craniotomy was located, and a drill was used to make a small craniotomy (~1.5mm^2). A prefilled pulled glass micropipette (tip diameter 15-20µm) loaded with the virus was moved to the desired coordinates then lowered manually into the brain. The brain was allowed to settle for 5 minutes before the virus was pressure-injected at a rate of ~60nl/min, following the injection the pipette then remained in the brain for 5-10 minutes to allow viral diffusion before removal. The skin was brought together and sutured using non-continuous stitches (coated Vicryl suture 5-0) before adhering using Vetbond skin glue (3M, Minnesota, USA). Prior to moving the animal to its pre-heated home cage, a subcutaneous injection of 0.4ml pre-warmed isotonic glucose solution was given along with supplementary food in the cage. Animals were monitored until they regained full ambulatory capability, followed by every 24-hours post-operatively until they were fully recovered and within 5% of their original pre-surgery weight.

To allow optogenetic stimulation of either PV-expressing interneurons or RBP4-expressing pyramidal neurons, 100nl of a Cre-dependent virus (AAV5-Ef1a-DIO-ChR2(E123T/T259C)-eYFP ~6.2x10^{12} vg/ml; Deisseroth, Vector Core, University of North Carolina) expressing a 'double-floxed' mutant of ChR2 was injected unilaterally into the right motor cortex (AP +1.5, ML +1.3, DV +0.8) of a PV-Cre or RBP4-Cre mouse respectively. In both cases, control mice were injected unilaterally into the right motor

cortex (AP +1.5, ML +1.3, DV +0.8) with 100nl of a Cre-dependent virus that does not express ChR2 (AAV5-Ef1a-DIO-eYFP ~4x10^{12} vg/ml; Deisseroth Vector Core).

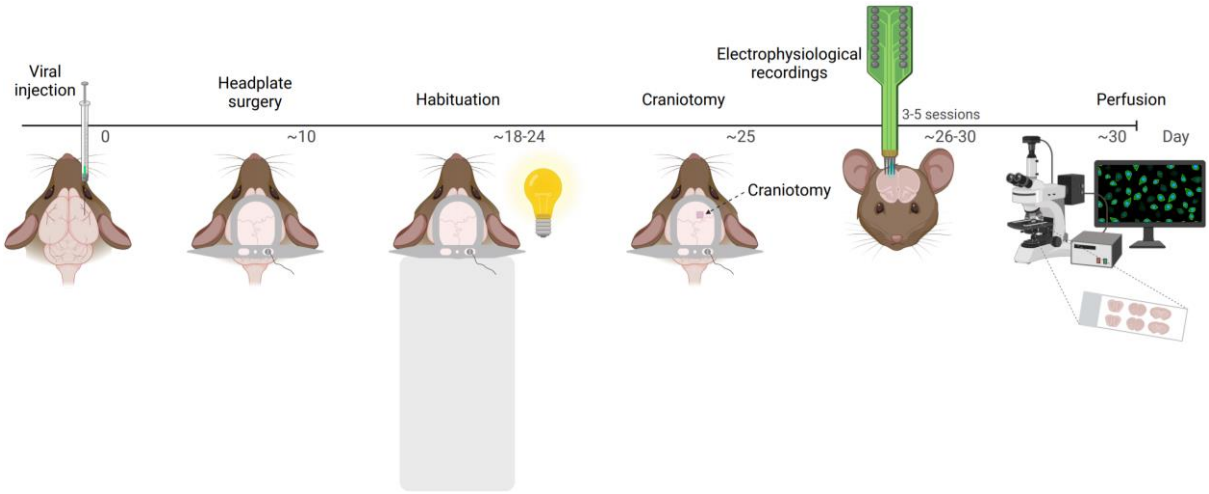


Figure 2.1 Experimental procedures timeline for *in vivo* electrophysiology with optogenetics

Firstly, the mouse was injected with either a Cre-dependent ChR2 or control virus into layer 5 of the motor cortex, before being implanted with a headplate and habituated to the recording rig set up. The day prior to starting the recordings the mouse underwent craniotomy surgery, before up to 5 recording sessions were acquired from the motor cortex. After the final session the mouse was perfused so that the brain could be collected for post hoc immunohistochemistry (Figure created with BioRender.com).

2.2.2 Headplate Surgery

Animals were implanted with a titanium custom-made headplate (Get It Made Ltd, London) (0.7g, internal diameter 9mm) at least 10 days prior to recordings, usually around 7-14 days after the initial viral injection surgery. After induction of anaesthesia as previously described for viral injection surgery, the skin was cleared from the skull. The skull was washed with hydrogen peroxide (3%, H_20_2 in dH_20) to remove debris and a scalpel was used to etch the skull for improved adhesion. Vetbond (3M, Minnesota, USA) was used to glue the edges of the skin to the skull before the headplate was aligned to bregma and lambda, then stuck to the skull with a few drops of superglue. Clear dental cement (Super Bond C&B, Parkell) was used to bond the headplate to the skull as well as provide a thin layer over the entire exposed skull surface. A small

reference screw (Precision Technology, East Grinstead) wrapped in wire was placed in one hemisphere over the cerebellum, ipsilateral to the injection site. Dental cement (Jet Denture Repair Powder: Lang Dental, Illinois, USA; Meadway Repair Liquid: MR. Dental, Surrey) was used over the reference screw. As in the previous recovery surgery, subcutaneous glucose was given, the mouse's nails were trimmed, and the animal was put in a heated recovery cage until fully ambulatory. Following recovery, animals were singly housed and regularly monitored.

The day prior to recording, anaesthetised recovery surgery (as described for the stereotaxic viral injection) was carried out to perform a small craniotomy (~1.5mm^2) above the recording site (see Figure 2.1). Dura gel (Cambridge Neuro Tech) and silicone (Body Double, Smooth-On) were placed over the craniotomy to form a barrier and protective layer over the exposed brain tissue.

2.3 Habituation & Electrophysiological Recordings

In vivo probe recordings were made in awake, head-fixed mice, untrained in any behavioural task. Prior to recordings, mice were handled to become comfortable with the experimenter then habituated to the recording set up usually over a period of 5-10 days. This was done by applying head-fixation for increasing time durations until the mouse could sit comfortably for an hour. While head-fixed, mice were habituated to the microscope light and a piezo and periodically given a 20% sucrose solution orally using a syringe. To head-fix the mouse, the bars of the implanted headplate were fixed into clamps and fastened using thumb screws, whilst the mouse sat in a cardboard tube combined with a 3D printed insert lined with cork, supported by a caddy. A Faraday cage surrounded the rig to shield it from electromagnetic signals in the

external environment. After every head-fixation session the mouse would be held for around 5-10 minutes to ensure it remained habituated to and comfortable with the experimenter.

Recording sessions were performed either twice a day for a maximum duration of 3 hours or once per day for a maximum duration of 4 hours. Mice had a maximum of 5 sessions in total. If the mouse appeared uncomfortable or restless the session would be stopped earlier. The probe was moved to slightly different coordinates from bregma in every subsequent recording session, to avoid re-entering at the same place for each insertion. At the end of each recording session the mouse was held for up to 15 minutes to remain comfortable with the experimenter, then returned to the home cage.

Acute recordings were undertaken using linear four shank silicon probes, which had 32 channels across the 4 shanks, 100µm between contacts and 200µm between shanks (A4x8-100-200-177-OA32; NeuroNexus, Michigan, USA). This probe had an integrated optic fiber on its second shank, 200µm above the top contact site. In the last set of experiments (n=5 mice), I used a newer probe with an additional coating: 'Z-coat' (NeuroNexus, Michigan, USA) - technology to reduce impedance, noise and photoelectric artifacts, as well as improve recording capability and signal detection of low amplitude signals.

An electrode holder was used to support the probe which was positioned above the desired coordinates using a stereotaxic frame and arm (Kopf Instruments, California, USA). The probe was lowered manually into the motor cortex at a depth of between 1000-1300µm and allowed to settle for a period of ~10 minutes to allow for more stable

and reliable recordings by minimising noise from the mechanical insertion and tissue responses and for unit activity to therefore become visible. The probe depth was adjusted as necessary until there were visible cortical units. In the last recording session, a fluorescent lipophilic membrane stain 1,1'-dioctadecyl-3,3,3',3'-tetramethylcarbocyanine perchlorate (DiI; Invitrogen, California, USA; 1mg/ml in isopropanol) was used to mark the probe tracts. A cortical headstage (64-channel; Intan Technologies, California, USA) was attached to the probe with an adaptor (Adpt-A32-OM32, Omnetics, Minnesota, USA) and connector (OM32, NeuroNexus) as well as to both a grounding wire and the cerebellar reference screw.

A camera was positioned in front of the mouse to monitor the animal's welfare throughout the recording session. Periodically throughout the session, the mouse was given a sucrose (20%) reward hand-delivered via a syringe, to ensure it remained settled. To guarantee the craniotomy remained moist for the entirety of the recording, sterile saline was also periodically applied and at the end of the recording dura gel and silicone were re-applied to cover the craniotomy.

2.4 Closed-loop Electrophysiology

The closed-loop system (OscillTrack) described in McNamara et al (2022) (McNamara and Sharott 2022) was used to track the phase of 6Hz theta activity in the motor cortical LFP, detect specific target phases and use this information to drive a laser connected to an optic fiber on the silicon probe (see Figure 2.2). Throughout this thesis, all closed-loop electrophysiology was phase-locked to the 6Hz theta oscillation.

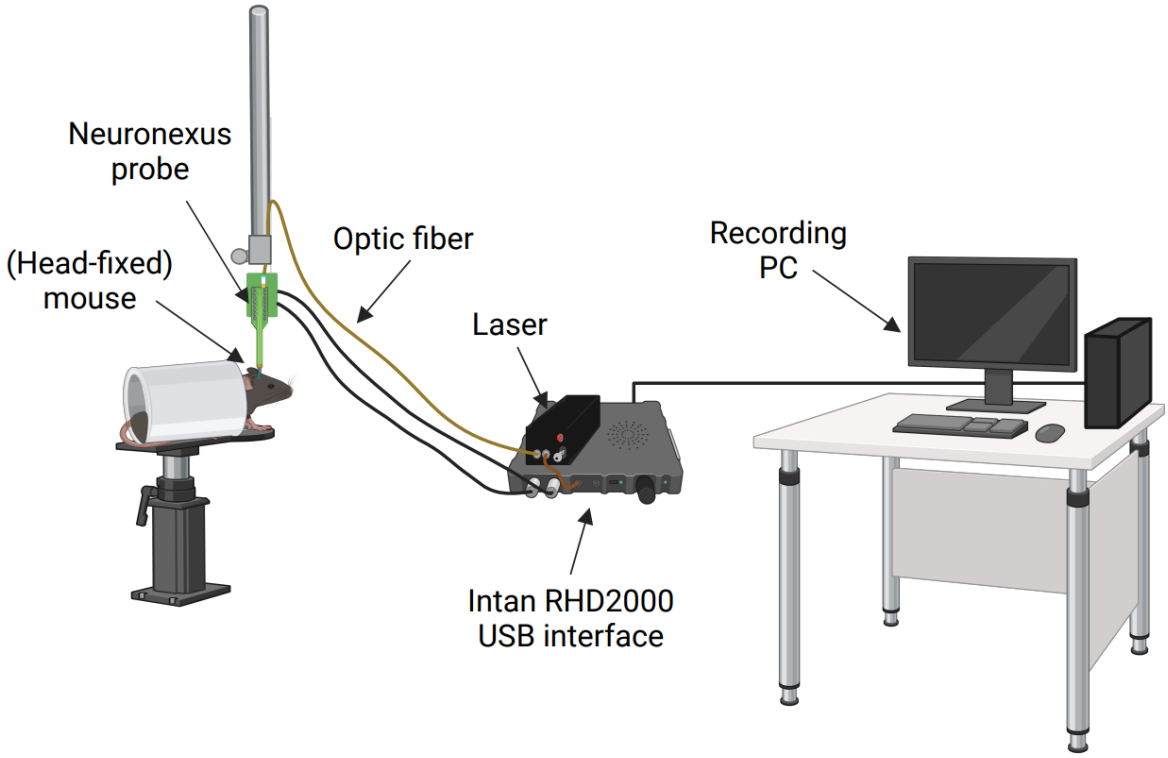


Figure 2.2 Simplified experimental setup for *in vivo* awake head-fixed electrophysiological recordings

The mouse was head-fixed in a Faraday cage using a custom titanium headplate (not drawn for simplicity). The Neuronexus probe and head stage were held by a holder for insertion into the motor cortex of the mouse. The Neuronexus probe used for electrophysiological recordings was a 4-shank probe (32 channels) with an integrated optic fiber. Closed-loop recordings were undertaken using the custom Intan RHD2000 interface which recorded and tracked the phase of the 6Hz theta oscillation. This additionally drove the laser which controls stimulation output via the optic fiber. When 'stimulation off' recordings were carried out, the key to control the laser was removed. This prevented laser output but still allowed theta phase tracking and electrophysiological recording. All recording outputs were saved on the recording PC. (Figure created using BioRender.com).

In these experiments, the closed-loop algorithm was implemented on a custom-made interface programmed on the Intan RHD2000 USB interface board (Robert Toth, Sharott group) that allowed target phase and stimulation output to be selected on a GUI. Electrophysiological recordings were made using the same Intan system at a sampling rate of 20kHz. An optic fiber (105µm core, 200µm, 0.22NA, Thorlabs, New Jersey, USA) was attached to the probe and used to deliver optogenetic stimulation at a wavelength of 473nm (Cobolt Laser, Sweden). Optical stimulation was driven through the Intan software in a closed-loop manner from the channel that displayed

the best spikes at the start of each session. While the depth of the electrode used to track the phase varied slightly across mice and probes, the mean (±SD) depth was 1045±127μm, suggesting phase differences in tracking as a result of depth would be minimal. Laser power was verified and adjusted before every recording session using a power meter interface (PM100USB, Thorlabs) alongside a sphere photodiode power sensor (S140C, Thorlabs).

2.5 Stimulation protocol

Stimulation patterns (Table 2.1) were delivered over 4 different phases (Figure 2.3) of the 6Hz theta cycle, in a randomised order at a combination of different laser powers (0mW, 1mW, and 2mW) to the motor cortex (Figure 2.3D). Each protocol was delivered over a period of ~2.5-7 minutes, this was dependent on the number of conditions to be recorded within each individual session and the limitation of the maximum recording time for the welfare of the animal. The continuous pattern (Figure 2.3B) consisted of a single, uninterrupted pulse delivered centred around the target phase for a duration of approximately ¼ of the 6Hz theta cycle. The gamma and random gamma patterns delivered 3 short pulses of stimulation. For gamma stimulation these pulses were at 75Hz with the middle pulse aligned to the target phase (Figure 2.3A). We included the random gamma pattern to interrogate the effect of gamma rhythmicity on the circuits. In this condition, the first and last pulses were identical to the original gamma condition, however, the middle pulse varied in its position between these two pulses (Figure 2.3C).

Stim Pattern	Stim length (us)	Pulse on (us)	Pulse off (us)	Timeout (us)	Number of pulses
Gamma	33335	6667	6667	133333	3
Continuous	41667	41667	0	133333	1
Random gamma	33335	6667	Random interval	133333	3

Table 2.1: Stimulation patterns used for closed-loop optogenetic electrophysiology

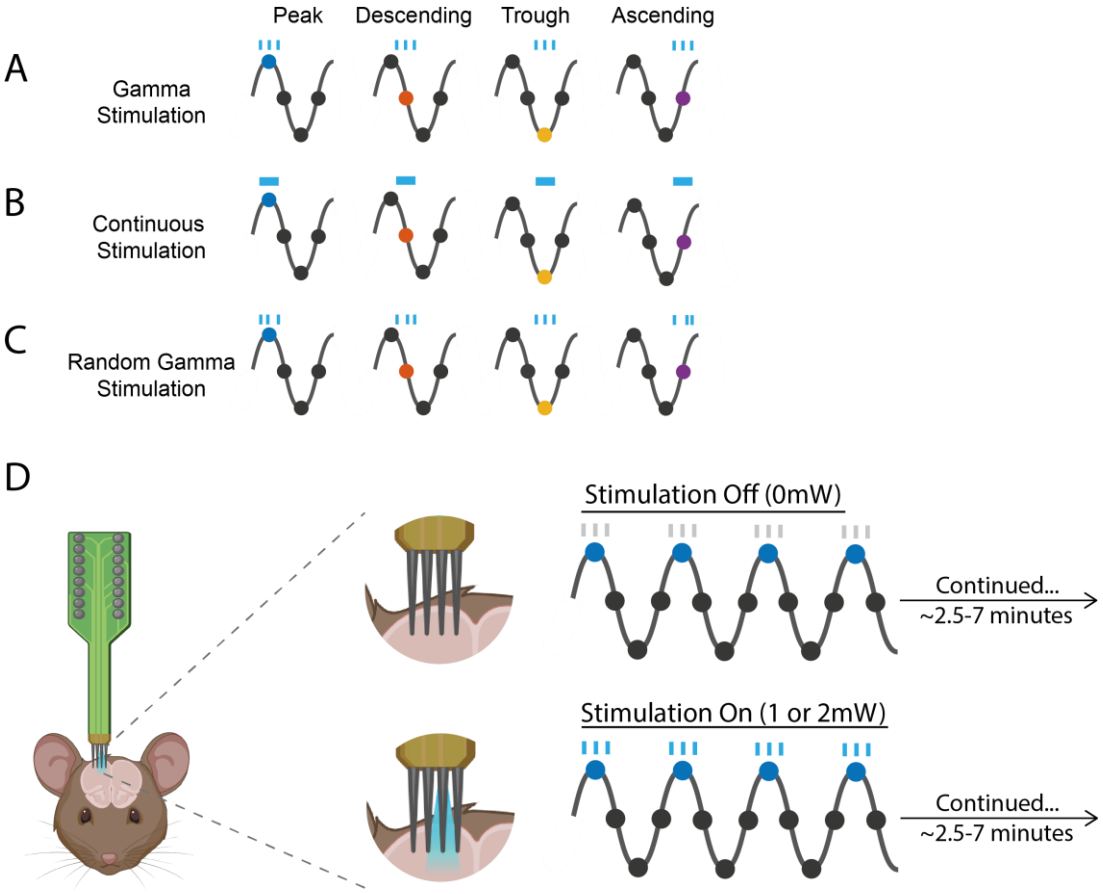


Figure 2.3 Stimulation patterns and targets

Two optogenetic stimulation patterns were devised to interrogate whether there was differential modulation over 4 different phases of the theta cycle (**A & B**). The first was a burst of 3 pulses at gamma frequency (75Hz), the middle pulse centred to the phase (**A**), and the second a simple ON/OFF pattern over ¼ of the theta cycle (41.667ms) (**B**). In some experiments, the gamma pattern was altered to create random gamma, to interrogate the importance of gamma rhythmicity in the circuit (**C**). In this case, the two outside pulses stayed the same as gamma stimulation and the middle pulse was moved around from a library of positions, resulting in 3 pulses that were spaced within the total duration of 3 gamma cycles, but at random interstimulus intervals. For each recording within a session, a stimulation pattern, stimulation phase and stimulation on (1 or 2mW) or off (0mW) were chosen in a randomised order then stimulated and recorded for between ~2.5-7 minutes. Example of phase tracking and optogenetic stimulation targeted to the peak of the theta oscillation during a recording session when stimulation was either off or on (**D**). The 6Hz theta oscillation was tracked using the OscillTrack algorithm on a custom Intan RHD2000 USB interface, used for both stimulation and electrophysiological recordings. (Figure created with the help of BioRender.com).

2.6 Open-loop Electrophysiology

In later closed-loop recording sessions (see tables 2.5-2.7), 'open-loop replay' trials were introduced (Figure 2.4), an approach used in McNamara et al (2022). These were pre-recorded (Intan data files) stimulation patterns from earlier on within the same session (details as noted above).

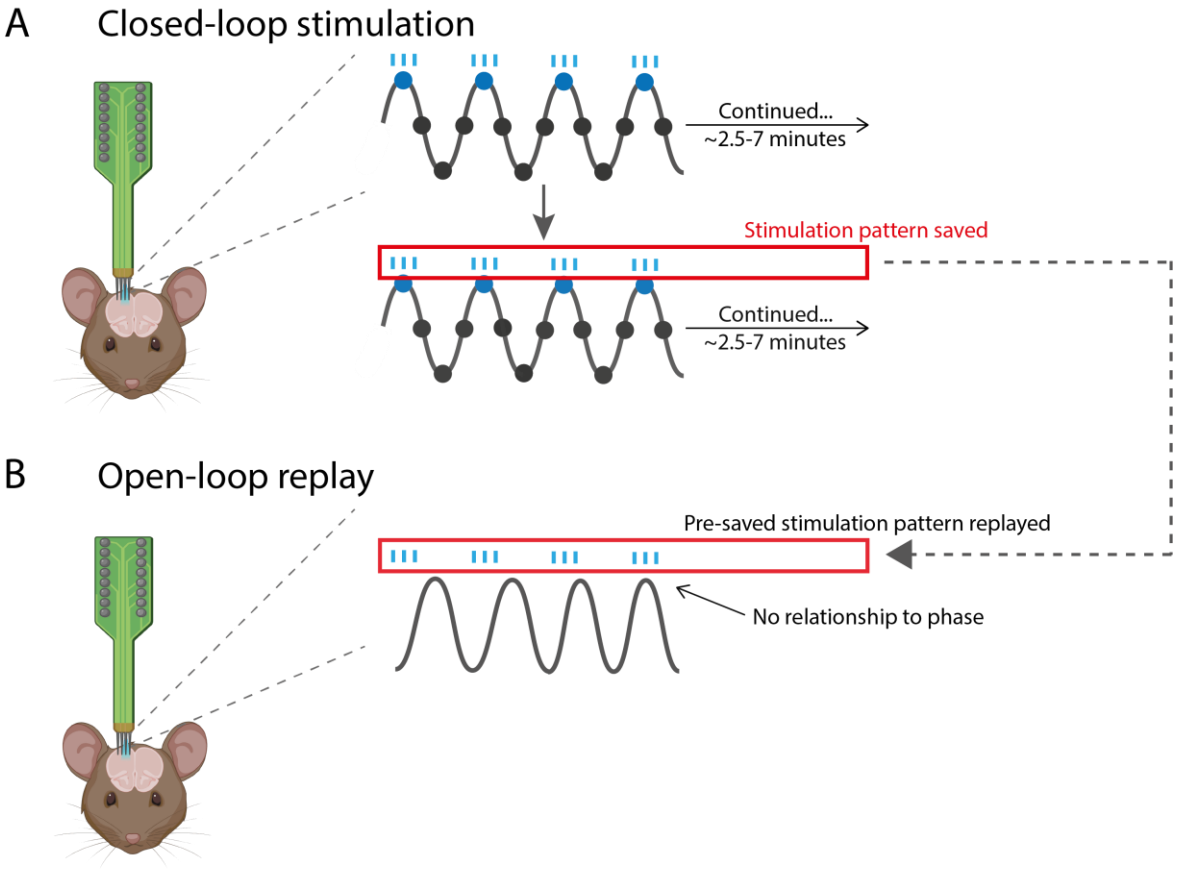


Figure 2.4 Formulation of open-loop replay control recordings

During each session all closed-loop stimulation patterns (targeting the 6Hz theta oscillation to a particular phase) were recorded (**A**), in later sessions these specific patterns were transferred to an SD card to replay them to the mouse later within the same session. These recordings were called 'open-loop replay' (**B**). Care was taken to replay them at the correct stimulation amplitude as the original closed-loop recording (1 or 2mW). Open-loop replay recordings were electrophysiological recordings that were the same length as the original closed-loop recordings, using the exact same stimulation pattern. These recordings, however, did not have any relationship to phase like the original closed-loop recording, as no phase-tracking of the ongoing theta oscillation took place during acquisition of these recordings. (Figure created with the help of BioRender.com).

These previously phase-specific patterns of laser activity were then re-played to the mouse, by loading the Intan digital output files onto a micro-SD card and playing them

through an Arduino-compatible microcontroller (Teensy 3.6; PJRC Ltd, Sherwood, Oregon, USA). The files were randomly played back to the mouse using the Arduino software to replay the datafile while triggering the Intan to record the electrophysiological data, care was taking to ensure the original laser power was used.

Additionally, within these later closed-loop recording sessions, mice also had open-loop (OL) stimulation for comparison of OL effects with the effects of closed-loop stimulation. Open-loop stimulation was also applied using the Arduino set up and therefore was not phase-locked to the ongoing theta oscillation. The length of open-loop stimulation epochs was matched in terms of the number of pulses, and length to closed-loop stimulation patterns, however, stimulation was given continuously throughout the recording period, with 167ms between subsequent stimuli instead of stimuli targeted to a specific theta-phase. A variation of these two OL patterns was also devised which had randomised 1-1.2 second gaps interleaved between every 6 stimulation pulses, these were subsequently named gamma gaps and continuous gaps (Table 2.2).

Stim pattern	Stim length (us)	Pulse on (us)	Pulse off (us)	Time between subsequent stimuli (ms)	Number of pulses	Randomised gap length following 6 stim bursts (ms)
OL-Gamma	33335	6667	6667	166.667	3	N/A
OL-Continuous	41667	41667	0	166.667	1	N/A
OL-Gamma gaps	33335	6667	6667	166.667	3	1000-1200
OL-Continuous gaps	41667	41667	0	166.667	1	1000-1200

Table 2.2: Stimulation patterns used for open-loop optogenetic electrophysiology

2.7 Histology - Immunohistochemistry

Mice were anaesthetised upon completion of recordings with a terminal pentobarbital IP injection (200mg/kg) and then transcardially perfused with ~20ml 0.1 M phosphate buffered saline (PBS; pH 7.4) followed by ~40ml 4% paraformaldehyde solution (PFA) in PBS. The whole brain was extracted and post-fixed overnight at 4°C in PFA before washing in PBS and storing in PBS-Azide (PBS with 0.05% sodium azide, PBS-Az). Coronal sections (50μm) were later taken using a vibrating microtome and stored in PBS-Az. To confirm the location of the injection site and assess viral spread as well as verify probe location, every 1 in 3 sections were taken from around AP +2.57 to AP -0.49. An antibody was used to enhance native signal of GFP, alongside other antibodies useful in helping delineate cortical layers in the case of all PV-Cre sections and some RBP4-Cre sections. For details of antibodies used, see Table 2.3. A neuronal marker for RBP4+ pyramidal neurons itself is lacking, therefore some sections were mounted without undergoing immunohistochemistry as we could still confirm the presence of GFP and identify probe tracts.

Free floating PV-Cre or RBP4-Cre sections were washed in PBS-Triton-azide (PBS-Tx, 0.3% Triton (v/v), 0.02% sodium azide (w/v)) for 3x 10 minutes to permeabilize the tissue. Sections were then blocked in 20% v/v normal donkey serum (NDS, Vector Laboratories, California, USA) in PBS-Tx for one hour at room temperature. Following this, sections were incubated in primary antibody solution in PBS-Tx with 1% NDS overnight at room temperature before 3x 10-minute washes in PBS. Sections were subsequently incubated in secondary antibodies (raised in Donkey) diluted in PBS-Tx and 1% NDS either for 4 hours at room temperature, or overnight at 2-4°C. Following 3

final 10-minute washes in PBS, sections were mounted on glass microscope slides. Coverslips were applied with an aqueous mounting medium (Vectashield, Vector laboratories).

Primary Antibodies				
Antigen	Species, clonality	Dilution	Company	Catalogue No.
Green fluorescent protein (GFP)	Chicken	1:500	Aves	GFP-1020
Parvalbumin	Guinea Pig	1:1000	Synaptic Systems	195-004
FoxP2	Goat	1:500	Santa Cruz	SC-21069
Necab-1	Rabbit	1:1000	Life Technologies	PA554849
Secondary Antibodies				
Fluorophore	Species Reactivity	Dilution	Company	Catalogue No.
Alexa-488	Chicken	1:1000	Jackson	703-545-155
AMCA	Guinea pig	1:250	Jackson	706-155-148
Alexa-647	Goat	1:250	Jackson	705-605-147
Cy3	Rabbit	1:400	Jackson	711-165-152

Table 2.3: Primary and secondary antibodies

Images were taken on an Axio Imager M2 epifluorescent microscope (Zeiss), equipped with Plan-Apochromat objective lenses, a Hamamatsu Flash 4.0 LT camera (C10600) and Colibri LEDs. ZEN Blue software was used to acquire tiled single plane images with a 10x objective. A Zeiss LSM 880 Axio Imager 2 laser scanning confocal microscope was used to take higher resolution images. ZEN Black software was used in acquisition of tile-scans using a 5x or 20x Plan-Apochromat air objective lens (NA 0.16 & NA 0.8 respectively). Images were stitched offline using ZEN Blue software. Neuronal specificity images were acquired using a 63x Plan-Apochromat oil objective lens (NA 1.46). AMCA, Alexa-488, Cy3 & Alexa-647 fluorescence were imaged using excitation from a Diode 405nm laser, Argon 488nm laser, and HeNe 543nm laser and HeNe 633nm laser, with MBS-405 and MBS-488/543/633 beamsplitters respectively.

2.8 Closed-loop Algorithm & Implementation with Intan RHD2000

We have implemented the OscillTrack algorithm (McNamara et al. 2022) previously developed in the lab which allows us to perform real-time oscillatory phase tracking. In brief, the algorithm is a partial implementation of a modified Kalman filter. This approach aims to align the observed signal with a predetermined fixed model consisting of a pair of sine and cosine waves with constant frequencies, enabling the generation of a signal estimate. For real-time phase tracking, data was downsampled (49x, reference wave resolution of 68 points per cycle) and a first order digital high pass filter implemented with a cut off frequency of 4Hz (See McNamara et al., 2022 for more details). In these experiments a real-time trigger at the target phase was only generated if more than 80% of the period of a 6Hz theta cycle had passed (Timeout: 133.333ms). If the current phase estimate was imprecise, this value allows for successful stimulation in subsequent oscillatory cycles and helps to reduce erroneous triggering.

We integrated this application of OscillTrack with the use of the commercial Intan RHD2000 USB evaluation board with a graphical user interface (GUI). The interface was configured for phase-tracking and the GUI customised with a new 'Phase' tab, to allow us to set and visualise real-time phase tracking capabilities – demonstrating the raw magnitude estimate and phase of the signal. A source signal channel was selected in each recording, based on a channel with consistent units following the probe settling and recording of the baseline. Phase-tracking options on the GUI include a choice of high-pass filtering settings, selection of a target frequency, shift gain and target phase as well as stimulation waveform settings which include stimulation

length, pulse on/off and the timeout period. During an experiment the stimulation state can be verified on one of the 16 digital input channels which allows real-time visualisation.

2.9 Data Analysis

Meta tables were created to contain all of the meta-data associated with these experiments, these include a table identifying each individual recording, a block table which identifies a recording block, a subject table, a probe table and stimulation table. Matlab (R2023b) was used to process all electrophysiological data. Custom scripts were written to analyse the local field potential, phase and amplitude of the oscillations.

2.9.1 Pre-processing

At the beginning of each session an impedance measurement was taken for each channel on the recording probe. We have utilised this measurement to maximise the number of channels taken from each recording by filtering channels based on the impedance measurement to allow us to exclude broken or bad channels. The first probe type had a threshold set with a range of 0.3MΩ either side of the expected channel impedance value based on impedance data that came from the company as well as checking the overall impedance values across all sessions with this probe type, which was 1.1MΩ. The second probe type, which had the additional Z-coating, as expected had much lower impedance values, this meant we could not use the same threshold as the first type and there is greater tolerance for impedance values in this lower range. Instead, a threshold was set from 0.01-0.08MΩ, capturing the nominal 0.05MΩ value. The four channels closest to the optic fiber have been

excluded from all analyses as a result of artifact. Additionally, measuring the impedance value of each channel in every recording and using these individual values helps to correct for any potential bias and variance between channels.

Data from the remaining channels then went through pre-processing which involved calculating a Welch power spectral density estimate with a 0.25Hz resolution using 4000 sample Fourier transforms, tapered with the Hann window function and 50% overlap between subsequent windows. For analysis in the gamma frequency range, a 2.0Hz resolution Welch power spectral density estimate was calculated using 500 sample Fourier transforms, tapered using the Hann window function with 50% overlap between subsequent windows. This was done on signals down sampled to 1kHz for efficiency. For each recording a Welch file was output using this custom preprocessing script. Post-hoc phase analyses were established by filtering down sampled extracellular potentials of all remaining channels between 4.5-7.5Hz using an offline zero-phase 4^{th} order Butterworth filter then calculating the Hilbert transform. For each individual recording within a session that wasn't identified as a baseline recording, these processed outputs were subsequently used for stimulation-based analyses. The stimulation pattern delivered was identified, processed into sampling points and stimuli too close to the beginning or the end of the signal were removed. Time slices were taken as -170ms pre and post stimulation, 0ms was taken as the centre of stimulation.

Using the Welch power spectral density estimate of remaining channels, all recorded data was plotted for blinded manual visual inspection. Blocks containing fewer than ¼ of remaining Channels (<7) after accounting for the removal of the four channels

containing optogenetic artifacts from all datasets, were excluded from further analysis (n=4 sessions; 3 x 5-Ch + 1 x 0-Ch) as well as any sessions demonstrating abnormal power spectra across all channels in the majority of recordings, indicative of a ground fault or artifact throughout a recording session (n=5 sessions). If the spectra from single recordings from within a session looked like artifact these were also excluded (n=1 recording from 1 session). A new 'visually inspected excluded' meta table was then created to account for any additional exclusions in all further analysis of the data. Two mice were additionally excluded from all analyses, one because of a ground fault through all sessions and the other due to a severe lesion noticed in post hoc microscopy. Finally, 1 session was excluded from analyses due to missing impedance data, which was necessary for the pre-processing step.

Additional custom scripts were then used to compute a session baseline file for each type, using the baseline recorded at the beginning of each recording as well as each additional unstimulated recording throughout a session. Baseline files were used to remove session baseline from each individual recording from that session, using all remaining channels in a channel-to-channel manner, before extracting and outputting tables which contained the mean of all remaining channel's power spectral density estimate between 4.5-7.5Hz and 56.25-93.75Hz.

2.9.2 Statistical Analyses

These tables were then reformatted using Matlab to import into R (4.3.2) for all statistical analyses using linear mixed effects (LME) models. LME models were chosen as they can model longitudinal data with interactions and are also able to account for missing values across subjects. LME models were always undertaken when possible,

however, in the case that there was insufficient data to use a LME model, paired t-tests were occasionally used as an alternative. Custom R scripts were written to test specific questions from our data.

Data were collected using two laser power amplitudes, 1 & 2mW. LME models were used to determine if there was a significant difference between the two at any given phase in either mouse group (control or opsin). We found no significant differences of amplitude as a main effect or any of the interaction terms in PV-Cre or RBP4-Cre mice. As a result, throughout this thesis all data collected at both 1 & 2mW has been combined into a 'stimulation on' condition. This means the same recording sessions can have data going into the analyses collected for both amplitudes at each phase and different stimulation patterns.

Following this, the data were split into their respective genotypes and stimulation types then checked for normality using QQ plots and running Shapiro-Wilk tests across all combinations. As a result of some of the data within each test having a p-value <0.05, and hence being significantly non-normally distributed, all data were z-scored before running linear mixed effect models and creating boxplots. Prior to z-scoring within the script, an additional check was run to identify any outliers based on a value outside of 1.5x the interquartile range for each subset of data. All outliers identified in the theta range using R were extracted into a table which allowed re-visual inspection of these specific plots of the spectra using Matlab to double check nothing abnormal was missed in the first visual inspection. There were no grounds for excluding any further data points, as such, all data was included for all statistical analysis, however, these 'outliers' have been identified on plots accompanying the

statistics by plotting these points in a lighter colour for differentiation and have not been included in plotting the boxplot.

All linear mixed effects models in this thesis contained random effects to appropriately account for variance within the model. These random effects were subject (each mouse) and date (extracted from each block which denotes a session). Random effects are included to help account for variability within the data that arises from grouping of observations. In these experiments, mice were used across several days, meaning each subject was repeated, as well as commonly recording from multiple subjects across the same date. These two random effects could not be combined as then each subject repeated on a different date would have been counted as separate which they are not, as well as wanting to account for recording different subjects on the same dates. As such, we are controlling for the variation in these random effects while determining if there are associations between the fixed effects of the model. Fixed effects were determined by the question being asked. P-values were obtained by likelihood ratio tests of the full model with the effects in question against null models without these effects. In this case, REML (restricted maximum likelihood) was set to false as ML (maximum likelihood) was used instead as this estimates both fixed and random effects. Using ML rather than REML means models with different fixed effects can still be compared as the model is simplified, however, this estimator doesn't account for the bias introduced by estimating fixed effects.

Subsequently, to follow up on significant interactions ($p<0.05$) and determine differences in theta power between individual stimulation phases, pairwise t-tests

were undertaken (Tukey adjustment for multiple comparisons). Throughout this thesis: *p<0.05, **p<0.01, ***p<0.001.

2.10 Breakdown of experimental mice

Table 2.4 states all the mice used for data collected throughout this thesis. This is further broken down into separate tables for the PV-Cre and RBP4-Cre mice with session numbers for different stimulation types (Tables 2.5-2.7).

Table 2.4: Total subject list

Mouse ID	**Genotype**	**Notes**
JM006	PV ChR2	
JM008	PV ChR2	
JM009	PV ChR2	
JM010	PV ChR2	Data from 1 session only (subject used to trial other experimental conditions)
JM016	PV ChR2	Excluded (Cortical lesion)
JM017	PV ChR2	Excluded (Grounding issue identified)
JM018	PV Control	
JM019	PV Control	
JM020	PV Control	
JM021	PV Control	
JM022	PV ChR2	
JM023	PV ChR2	
JM024	PV ChR2	Data from 1 session only
JM028	RBP4 ChR2	
JM029	RBP4 ChR2	
JM030	RBP4 ChR2	
JM031	RBP4 ChR2	
JM032	RBP4 Control	
JM033	RBP4 Control	
JM034	RBP4 Control	
JM035	RBP4 Control	
JM036	RBP4 ChR2	
JM037	RBP4 ChR2	
JM038	RBP4 ChR2	
JM039	RBP4 ChR2	
JM040	RBP4 ChR2	
NB162	RBP4 ChR2	

To assess changes in LFP power when targeting inhibitory interneurons 4 PV-Cre mice were injected with a control virus and 7 PV-Cre mice were injected with ChR2. These mice are highlighted in Table 2.5. This table lists the number of sessions containing the different types of stimulation – gamma, continuous, any sessions containing open-loop replay and finally sessions that contained open-loop stimulation. No sessions that were excluded are included in this table.

Table 2.5: PV-mice session number breakdown

(Data used in Chapters 3 & 5)

Mouse ID	Genotype	# Gamma sessions	# Continuous sessions	# Sessions with open-loop replay	# Sessions with open-loop
JM006	PV ChR2	3	0	0	0
JM008	PV ChR2	3	0	0	0
JM009	PV ChR2	2	2	0	0
JM010	PV ChR2	1	1	0	0
JM018	PV Control	4	4	0	0
JM019	PV Control	3	3	0	0
JM020	PV Control	4	5	2	0
JM021	PV Control	4	4	2	0
JM022	PV ChR2	3	3	1	3
JM023	PV ChR2	3	3	2	3
JM024*	PV ChR2	1	1	1	1

*Excluded from gamma frequency range analyses (Chapter 5) due to the presence of 50Hz noise.

To assess changes in LFP power when targeting excitatory pyramidal neurons, 4 RBP4-Cre mice were injected with a control virus and 10 RBP4-Cre mice were injected with ChR2. These mice are listed in Table 2.6 & Table 2.7. This table details the number of sessions containing the different types of stimulation – gamma, continuous and random gamma, as well as the sessions containing open-loop replay of any of these stimulation types. Additionally, sessions that contained open-loop stimulation are listed. Only sessions not excluded from analyses have been included in these tables.

Table 2.6: RBP4-Cre mice session number breakdown: Experiment 1

(Data used in Chapters 4 & 5)

Mouse ID	Genotype	# Gamma sessions	# Continuous sessions	# Sessions with open-loop replay*	# Sessions with open-loop
NB162	RBP4 ChR2	4	4	0	0
JM028	RBP4 ChR2	4	4	3	2
JM029	RBP4 ChR2	5	5	4	4
JM030	RBP4 ChR2	4	4	3	3
JM031	RBP4 ChR2	4	4	4	4
JM032	RBP4 Control	4	4	3	3
JM033	RBP4 Control	3	3	2	2
JM034	RBP4 Control	4	4	3	3
JM035	RBP4 Control	4	4	2	2

*NB: Some open-loop replay sessions only include open-loop replay of one stimulation pattern.

Table 2.7: RBP4 ChR2 session number breakdown: Experiment 2

(Data used in Chapters 4 & 5)

Mouse ID	# Gamma sessions	# Random Gamma sessions	# Continuous sessions*	# Sessions with open-loop replay**
JM036	4	4	4	2
JM037	4	4	4	2
JM038	4	4	4	3
JM039	4	4	4	2
JM040	4	4	4	3

*Continuous data collected only for stimulation on & for a shorter time period (Exception: JM039 – 1 day recorded 0mW continuous).

**Open-loop replay: Only for gamma & random gamma stimulation; sessions with '3' have both types in the first two sessions and only replay gamma stimulation in the third session.

3 Modulation of Inhibitory Interneurons

3.1 Introduction

Inhibitory interneurons that are responsible for releasing the neurotransmitter GABA are involved in helping to precisely control the firing of excitatory pyramidal neurons and other inhibitory (GABAergic) interneurons (Rudy et al. 2011). Neocortical circuits are thus largely shaped by inhibition provided by these neurons, one particular subset are parvalbumin (PV) interneurons (Rudy et al. 2011). PV-positive (+) interneurons within the neocortex can be categorised into fast spiking-basket cells and chandelier cells, based on morphological and functional characteristics (Ascoli et al. 2008; Rudy et al. 2011). While a higher proportion of PV+ interneurons are found within deeper cortical layers, they are distributed throughout cortical layers 2-6 (Xu et al. 2010). In comparison to FS basket neurons, chandelier cells are mainly found in layers 2 & 6 only, and exclusively target the axon initial segment of local pyramidal neurons (Howard, Tamas, and Soltesz 2005; Tremblay et al. 2016). Within the frontal and somatosensory cortices, an additional PV+ subtype has been identified, known as multipolar bursting (MB) neurons that innervate FS subtypes (Blatow et al. 2003; Tremblay et al. 2016). However, it is unknown whether they exist within the motor cortex.

The balance between inhibitory and excitatory neurons is extremely important in neuronal oscillation generation (Adrian and Matthews 1934; Buzśaki and Wang 2012; Fries et al. 2001; Singer 1993). Oscillations are generated as a result of synchronous action potential firing leading to fluctuations in excitability (Buzsáki et al. 2012). These oscillations can be synchronised across brain regions to allow for coordinated

network activity (Siegel et al. 2012). Aberrant neuronal oscillations have been linked to numerous brain disorders (Simon and Wallace 2016; Uhlhaas and Singer 2006, 2010; Zeng et al. 2017), therefore stressing the importance of better understanding of the dynamics of these oscillations.

Inhibitory interneurons such as PV+ FS basket cells have consistently been linked to the generation of layer 5 cortical gamma oscillations (Rudy et al. 2011). The majority of L5 neurons are pyramidal neurons which project to subcortical targets to drive movement, making it the major output layer in the motor cortex (Harris and Shepherd 2015; Shepherd 2013). PV+ FS basket cells within L5 have been shown to exert strong inhibition locally and across cortical layers (Tremblay et al. 2016). This means that these neurons can influence neighbouring cortical layers to facilitate the maintenance and generation of neuronal oscillations and control of motor function. The less-studied MB subtype of PV-interneurons have also been shown to contribute to the generation of theta oscillations in L2/3. MB neurons receive excitatory input from L2/3 pyramidal neurons and evoke synchronised inhibition of local pyramidal neurons in the neocortex (Blatow et al. 2003). Layers 2/3 are targeted by thalamocortical and sensory inputs (Hooks et al. 2013), indicating a role in sensory integration.

The role and function of chandelier cells within the circuit remain unclear, with limited, contrasting evidence. On one hand, it has been suggested that chandelier cells produce depolarising synapses that drive activity in postsynaptic neurons (Szabadics et al. 2006), while on the other hand, they have been shown to have hyperpolarising inhibitory role (Glickfeld et al. 2008). More recently, one study has found chandelier cells to be capable of both promoting and inhibiting postsynaptic potentials as a result

of membrane potential under quiescent conditions (Woodruff et al. 2011). Whereas, during *in-vivo* like conditions the postsynaptic effect was predominately inhibitory (Woodruff et al. 2011). This suggests these neurons may be capable of promoting contrasting effects on surrounding pyramidal neurons based on their level of activity.

Optogenetic modulation of neurons can be used to alter neuronal excitability, and fluctuations in excitability can be measured by changes in the local field potential. Optogenetics therefore allows us to gain insight into the collective dynamics of a neuronal population by looking at changes in amplitude and frequency. Closed-loop stimulation is more dynamic than open-loop stimulation, using feedback to precisely control and dynamically adjust stimulation. Combining optogenetics with closed-loop stimulation may help us elucidate the role that PV+ inhibitory interneurons play within the microcircuit and in the generation of neuronal oscillations. PV-interneurons have more commonly been optogenetically manipulated within the hippocampus.

For example, one study used theta phase-specific optogenetic modulation of freely moving mice in the dorsal CA1 region (Siegle and Wilson 2014). This was carried out in the context of a spatial navigation task, where the authors determined that stimulation of PV-interneurons at different phases was linked to the improvement of different task aspects. Moreover, theta peak stimulation resulted in inhibition that could improve task encoding, while theta trough stimulation improved retrieval performance in the task (Siegle and Wilson 2014). Similarly, another study manipulated PV-interneurons using phase-specific optogenetics in the dorsal medial prefrontal cortex and identified a theta phase-mediated response in freezing behaviour as part of the fear response linked to neuronal assembly recruitment (Dejean et al. 2016). Both of these studies

relied on a computer for online analysis of phase-tracking. This effectively results in latency between analysis and triggering of stimulation. For instance, Dejean et al, (2016) identified a maximum of 30ms for laser onset, including data retrieval (10ms) and computation (5-20ms). Therefore, it is also essential to employ online phase-tracking methods which allow instantaneous stimulation. These studies, while important in paving the way for the use of effective closed-loop stimulation methods combined with optogenetics for more precise manipulation, primarily interpret their results in terms of changes in behavioural output. To understand more about the impact specific neuron types have on closed-loop manipulation, and the role they play within the microcircuit, it is vital to investigate how closed-loop manipulation can alter neuronal oscillations.

In this chapter, we first set out to demonstrate the feasibility of optogenetically stimulating the motor cortex while recording the local field potential using a new closed-loop stimulation approach. This was possible using a genetic mouse model (PV-Cre) that targets Cre-recombinase to parvalbumin (PV) interneurons and mice were first injected with a Cre-dependent optogenetic virus. We then used electrophysiological recordings as an input to a highly responsive closed-loop system (OscillTrack) that provides continuous online phase estimation, to deliver phase-dependent stimulation to PV+ interneurons in the motor cortex. We then aimed to determine whether phase-dependent stimulation of PV+ interneurons modulated ongoing cortical theta oscillations.

Finally, we investigated whether the precise stimulation pattern was important for phase-dependent modulation to occur. To test this, we devised two different patterns

of optogenetic stimulation for our study, namely gamma stimulation and continuous stimulation. Additionally, we designed a control experiment in which precise stimulation patterns from specific phases of closed-loop stimulation were used to deliver open-loop replay of the same stimulation patterns.

3.2 Methods

In brief, PV-Cre mice were injected with either a control or ChR2-containing virus before *in vivo* electrophysiological recordings were undertaken. During electrophysiological recordings, we used optogenetics to manipulate inhibitory interneurons using closed-loop stimulation targeted to the 6Hz theta oscillation. Initial experiments verified the presence of a 6Hz oscillation that could be tracked in the mouse motor cortex. All closed-loop stimulation performed throughout this thesis was phase locked to the theta oscillation. Two different stimulation patterns were utilised to determine how these can influence changes in local theta power. These were targeted to four different phases of the ongoing theta oscillation (peak, descending, trough & ascending).

To ensure appropriate controls, as well as using control mice, for each stimulation condition we performed no stimulation control recordings for both control and opsin mice. Additionally, to control for the stimulation patterns received during closed-loop phase-specific stimulation we later implemented a stimulation control, in which previous closed-loop stimulation patterns were utilised for 'open-loop replay'. These replicated previously delivered trains of stimulation at each phase. In addition, similar open-loop stimulation was delivered with no relationship to the theta oscillation.

As mentioned in Chapter 2, optogenetic stimulation was performed at two different amplitudes – 1 & 2mW. We examined whether there were any significant differences in theta power modulation between the two, for each group and phase, to investigate whether we could combine these stimulation amplitudes for subsequent analyses. We, therefore, created a linear mixed effects (LME) model with fixed effects of group, phase and laser power (1mW and 2mW only) and their interactions, alongside random effects of subject and date.

When targeting gamma stimulation to the theta oscillation there was no significant main effect of laser power ($F(1,213)=0.49$, $p=0.49$), and no significant interaction between laser power and other variables [group*laser power ($F(1,213)=0.64$, $p=0.42$); phase*laser power ($F(3,206)=1.84$, $p=0.14$)] suggesting that there was no significant difference between the effects of 1mW and 2mW on the degree of theta power modulation.

As with gamma stimulation, for continuous stimulation there was no significant main effect of laser power ($F(1,185)=0.67$, $p=0.42$) nor the interactions between laser power and other variables [group*laser power ($F(1,185)=1.41$, $p=0.24$); phase*laser power ($F(3,184)=0.16$, $p=0.92$)] suggesting that there were no significant differences between the two laser powers (1mW and 2mW) on theta power. We therefore combined these laser powers for all further analyses ("stimulation on").

In this chapter, data was collected in 4 PV-Cre control mice as well as 7 PV-Cre ChR2 (gamma) and 5 PV-Cre ChR2 (continuous). For a full summary of the methods and breakdown of mice used, please refer to Chapter 2.

3.3 Results

3.3.1 ChR2-GFP expression was localised to PV-interneurons

Firstly, to verify the expression of channelrhodopsin-2 (ChR2) in PV-interneurons. We targeted PV-positive (PV+) inhibitory interneurons in layer 5 of the motor cortex with an excitatory opsin (ChR2) fused to green fluorescent protein (GFP). Cre-dependent viruses were used in conjunction with a PV-Cre mouse line (see methods), to permit specificity of neuronal activation. Visual inspection of histology demonstrated that virus expression was limited to the cortex (Figure 3.1) and relatively localised to the injection coordinates (AP 1.5, ML 1.3, DV 0.8). We could also visually identify probe tracts with DiI in some sections, used primarily on the last day of recording. If DiI was present, sections could be compared to the Allen Brain Atlas to identify location in comparison to theoretical injection site targeted to confirm we were recording within the motor cortices. Necab-1 and FoxP2 expression were used to delineate cortical layers, as they show strong expression in layer 4 and layer 6 respectively (Figure 3.1A). Overlap between cells expressing ChR2-GFP and PV demonstrates specific ChR2 expression in PV-interneurons (Figure 3.1B-C).

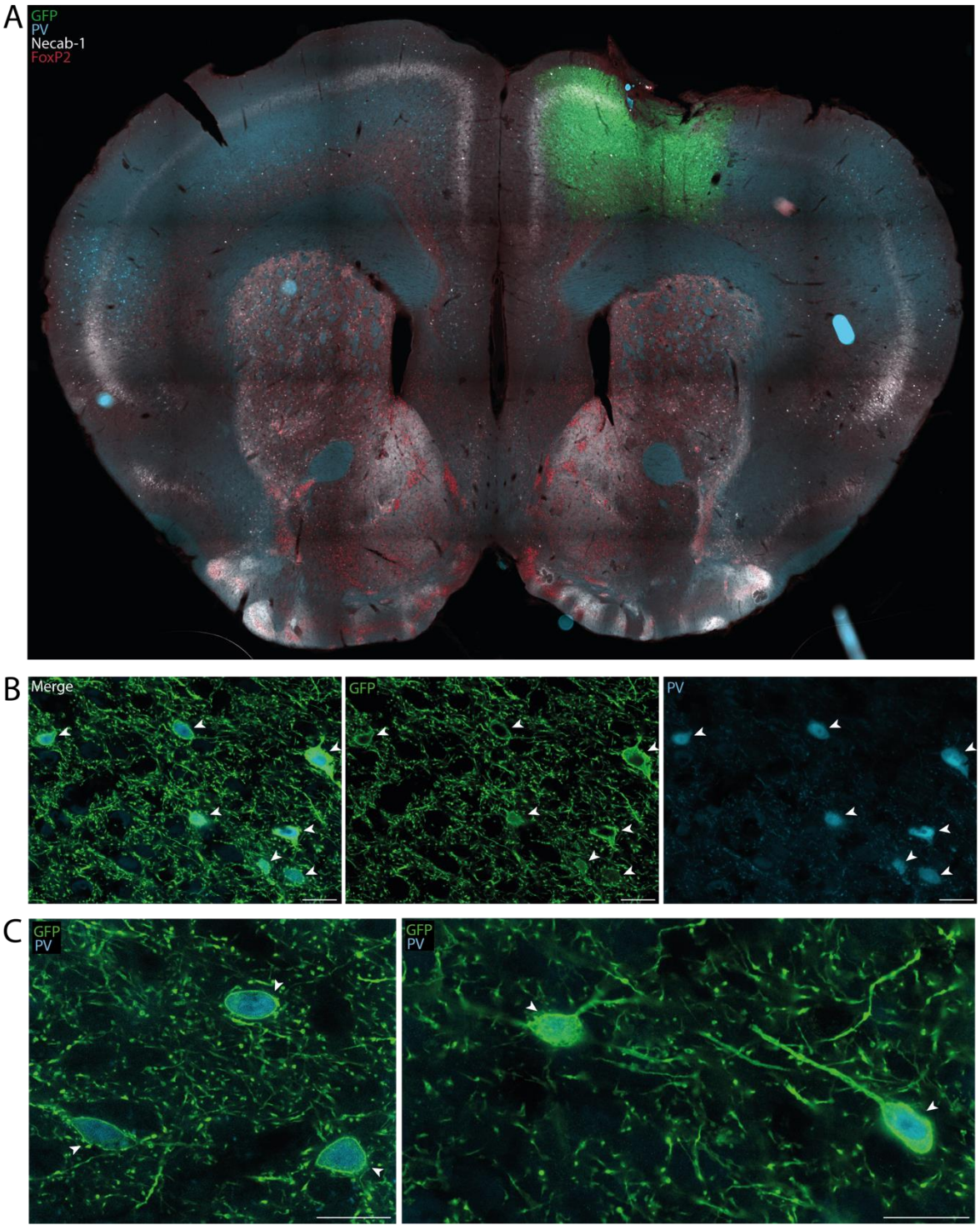


Figure 3.1 Localised expression of ChR2-GFP in PV-expressing neurons

PV-Cre mice were injected either with a Cre-dependent control virus (GFP) or a virus containing ChR2-GFP. Low magnification image of PV, ChR2-GFP, Necab-1 and FoxP2 immunoreactivity on a whole brain coronal section (**A**) ~1.41mm from bregma (Paxinos & Franklin's Mouse Atlas – Figure 19). The Cre-dependent virus remains within the cortex and does not spread to deeper structures. (**B-C**) Higher magnification confocal images of ChR2-GFP & PV expression from a section of layer 5 within the motor cortex. Scale bar represents 20μm. There is extensive overlap between cells expressing both green fluorescent protein (GFP) and the calcium-binding protein Parvalbumin (PV), identified by white arrows. This confirms expression of PV-Interneurons with the Cre-dependent ChR2 virus.

3.3.2 Accurate phase-targeting of the ongoing theta oscillations

Next, we verified that we could accurately target different phases of an oscillation in an awake head-fixed *in vivo* experimental set-up. To investigate this, while monitoring the LFP from one channel and using it as an input for phase-tracking of the ongoing theta oscillation, we then simultaneously performed targeted closed-loop optogenetic stimulation whilst recording the LFP. An experimental set-up was devised in which we could deliver optogenetic stimulation targeted to four distinct phases of the ongoing theta oscillation (Figures 3.2 & 3.3). Post hoc analysis demonstrated accurate phase targeting of all four stimulation phases regardless of stimulation type (Figures 3.2 & 3.3).

These demonstrate that the centre-point of stimulation (0ms, dotted line) in the evoked potential (triggered average of the LFP) is phase-specific for both gamma (Figure 3.2) and continuous stimulation (Figure 3.3). In addition, the centre-point of the stimulation pattern has a high degree of alignment with our target phase, and we can separate out our four target phases. This was observed in the control mice (Figures 3.2A & 3.3A), as well as when stimulation was off in the opsin mice (Figures 3.2B & 3.3B) for both stimulation patterns. When stimulation was on in the opsin mice (Figures 3.2B & 3.3B), the phase accuracy appears to be similar in some phases to the control and stimulation off conditions (descending & ascending phases), however, slightly more or less accurate in the other two phases (trough and peak respectively). This is fairly consistent across the two stimulation patterns; however, the descending phase also appears to be slightly less accurate with continuous stimulation in opsin

mice (Figure 3.3B). This variability is likely due to the stimulation effect on the LFP itself.

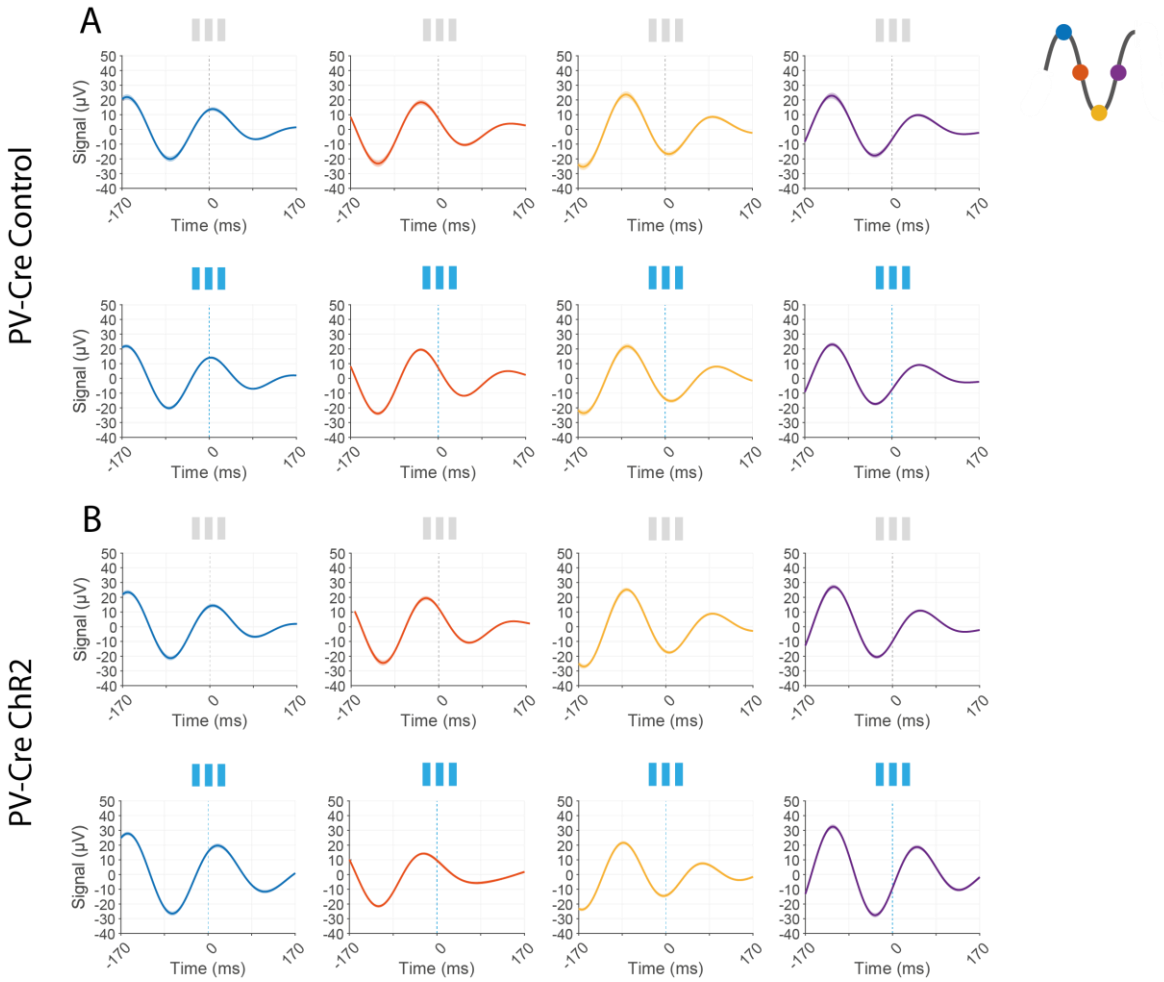


Figure 3.2 Accurate phase-targeting of ongoing theta oscillation with gamma stimulation

Stimulation triggered averages of local field potentials in response to closed-loop optogenetic gamma stimulation in PV-Cre mice (n=4 control (**A**); n=7 ChR2 (**B**)). The four columns denote each of the four targeted phases: peak, descending, ascending and trough, identified with a colour-coded key. These are provided for both stimulation off (0mW; grey pulses) and stimulation on (1 or 2mW; blue pulses). The dotted line at '0' on the x-axis (Time (ms)) represents the centre-point of stimulation, which falls immediately prior to the targeted phase of the ongoing theta oscillation. This is plotted across two theta cycles one on either side of the stimulation centre-point. Mean activity in the 6±1.5Hz theta band was filtered offline with a zero-phase 4th order Butterworth filter. The coloured lines represent the mean of all the sessions for each combination of stimulation on/off and phase. Lighter shading represents the standard error of the mean (SEM). The total number of sessions used to calculate the mean & SEM in control mice was n=15 (13-14 recordings per phase stimulation off, n=28-30 recordings per phase stimulation on). In opsin mice, this was n=16 (15-16 recordings per phase stimulation off, n=28-29 recordings per phase stimulation on).

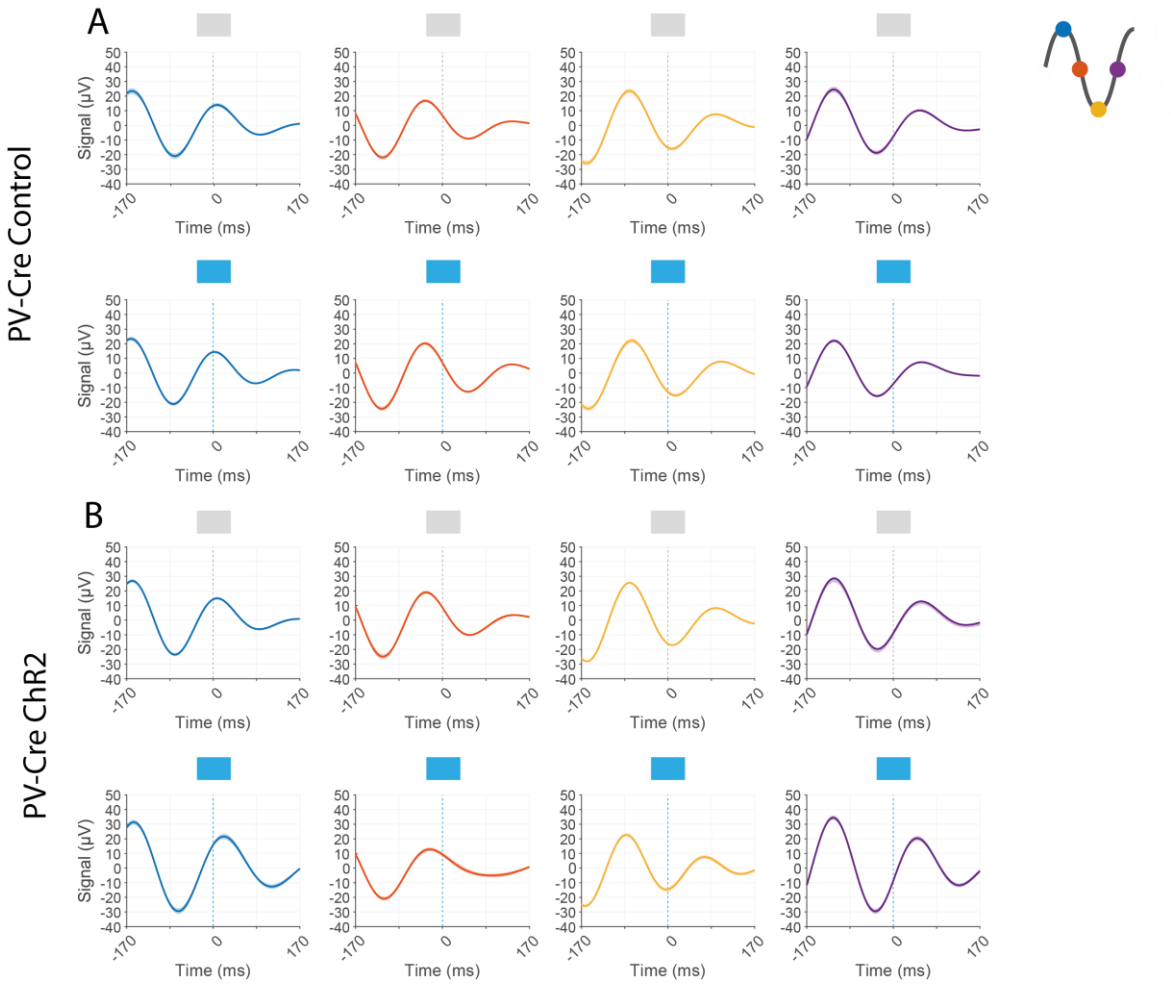


Figure 3.3 Accurate phase-targeting of ongoing theta oscillation with continuous stimulation

Stimulation triggered averages of local field potentials in response to closed-loop optogenetic gamma stimulation in PV-Cre mice (n=4 control (**A**); n=5 ChR2 (**B**)). The four columns denote each of the four targeted phases: peak, descending, ascending and trough, identified with a colour-coded key. These are provided for both stimulation off (0mW; grey pulses) and stimulation on (1 or 2mW; blue pulses). The dotted line at '0' on the x-axis (Time (ms)) represents the centre-point of stimulation, which falls immediately prior to the targeted phase of the ongoing theta oscillation. This is plotted across two theta cycles one on either side of the stimulation centre-point. Mean activity in the 6±1.5Hz theta band was filtered offline with a zero-phase 4th order Butterworth filter. The coloured lines represent the mean of all the sessions for each combination of stimulation on/off and phase. Lighter shading represents the standard error of the mean (SEM). The total number of sessions used to calculate the mean & SEM in control mice was n=16 (16 recordings per phase stimulation off, n=31 recordings per phase stimulation on). In opsin mice, this was n=10 sessions (9-11 recordings per phase stimulation off, 20 recordings per phase stimulation on).

3.3.3 Closed-loop gamma stimulation

Having established the ability to target different phases of the ongoing theta oscillation and cell type-specific manipulation, we proceeded to evaluate whether closed-loop optogenetic stimulation could modulate the power of the ongoing motor cortical theta

oscillation and whether this modulation was phase-dependent. Additionally, we determined whether the frequency and pattern of optogenetic stimulation were important in altering theta power. To do this, we devised two different patterns of stimulation, the first of which we refer to as gamma stimulation (Figure 2.3 - see methods, Chapter 2), which consisted of 3 pulses at gamma frequency (75Hz) to simulate theta-gamma coupling, the centre pulse of which was centred to the target phase. Closed-loop stimulation was targeted to the ongoing 6Hz theta frequency oscillation and LFPs were measured using a Neuronexus probe.

Data for the gamma pattern of stimulation were collected when the stimulation was off (0mW) and on (1 & 2mW) (Control: n=4 mice, 15 sessions; Opsin: n=7 mice, 16 sessions).

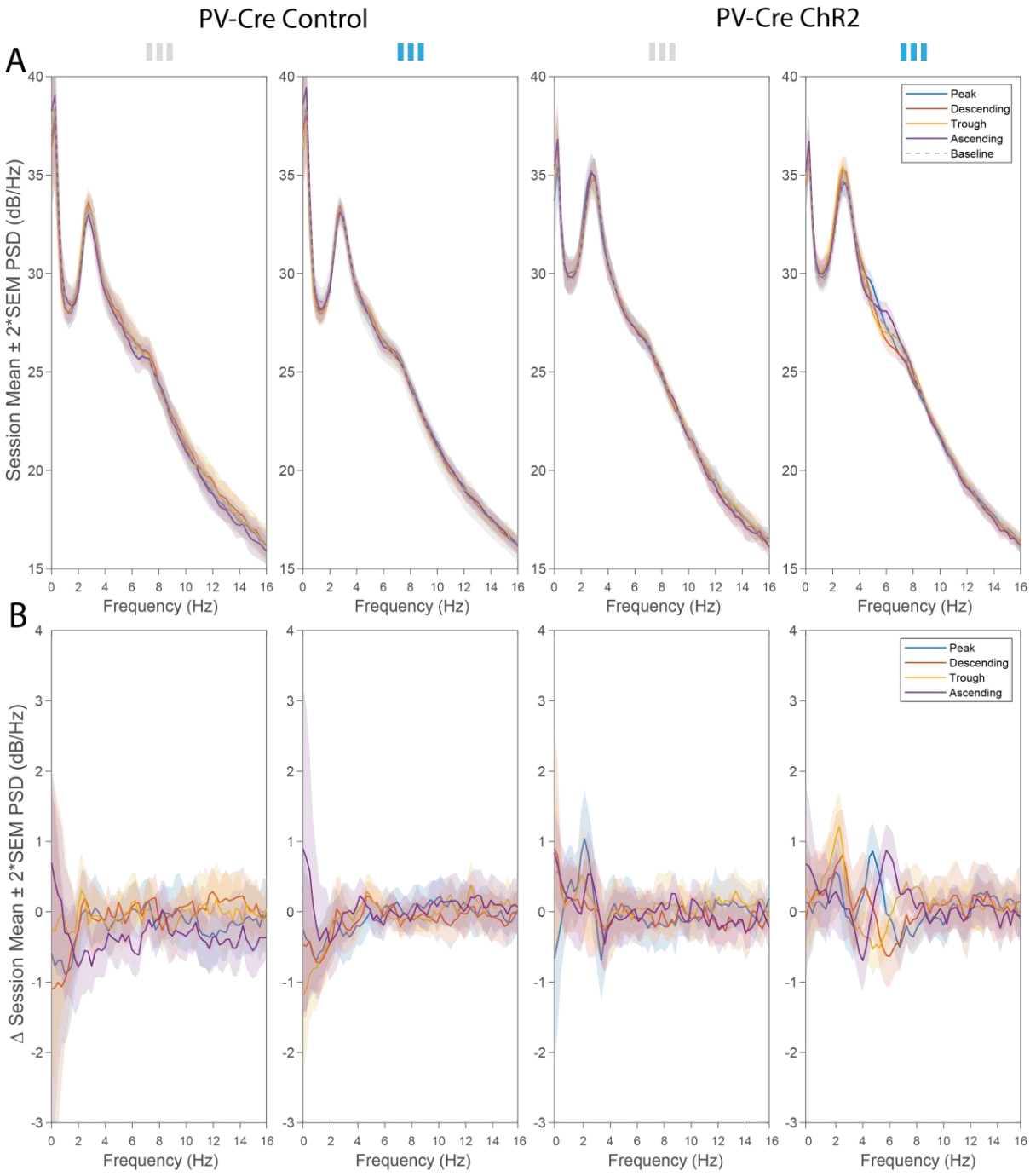


Figure 3.4 Phase-dependent effect in local LFP following closed-loop gamma stimulation of PV+ interneurons

Mean power spectral density (±2*SEM) from 0-16Hz for both PV-Cre control (n=4) and opsin mice (n=7), targeting 4 different phases of the theta oscillation with gamma stimulation (**A**). Stimulation was either off (0mW; grey pattern) or on (1 or 2mW; blue pattern). The number of sessions to calculate the mean in control mice was n=15 (14 recordings per phase stimulation off, n=29-30 recordings per phase stimulation on). In opsin mice this was n=16 (15-16 recordings per phase stimulation off, n=28-29 recordings per phase stimulation on). Within each session, a session baseline was calculated from a baseline recorded at the beginning of each session, combined with all unstimulated recordings throughout a session. The mean session baseline was then plotted on each plot for each group and stimulation on or off. The mean PSDs (±2*SEM) in which the baseline was removed from each session were also plotted for both control and opsin mice (**B**).

3.3.3.1 Closed-loop gamma stimulation of the motor cortex results in phase-specific modulation of theta power in PV-Cre mice

We next investigated the effects of our phase-specific gamma stimulation on local LFP power. Mean power spectral density (PSD) plots for each targeted phase are shown in Figure 3.4A for both control and opsin (ChR2) groups. Gamma stimulation was either off (0mW; grey bars) or on (1 or 2mW; blue bars).

To investigate whether our closed-loop stimulation protocol induced phase-specific modulation of theta power, we subtracted the baseline (Figure 3.4B) – this was the mean calculated from the baseline file recorded at the start of every session in addition to all unstimulated recordings within a session, and extracted power spectral density estimates around our target range (6Hz±1.5) (Figure 3.5). We used a linear mixed effects (LME) model to test the overarching hypothesis that there would be phase-specific differences in theta power between both experimental groups ('control' & 'opsin') and stimulation (laser power; 'off' & 'on'). The LME, with fixed effects of group, laser power & phase with interactions (random effects of subject & date) showed a significant group*phase interaction ($F(3,324)=4.29$, $p=0.006$) as expected, as we anticipated the control group to have no effect of phase, meanwhile, the opsin group to vary by phase. There was also a significant phase*laser power interaction ($F(3,324)=3.63$, $p=0.013$). This aligned with our prediction that there would be no differences in theta power when unstimulated, compared to differences when stimulation was delivered. No significant three-way interaction between the group, laser power and phase was observed ($F(3,324)=0.92$, $p=0.43$), however. These results suggest that non-specific effects do not occur within our control conditions so further analyses focus on experimental effects.

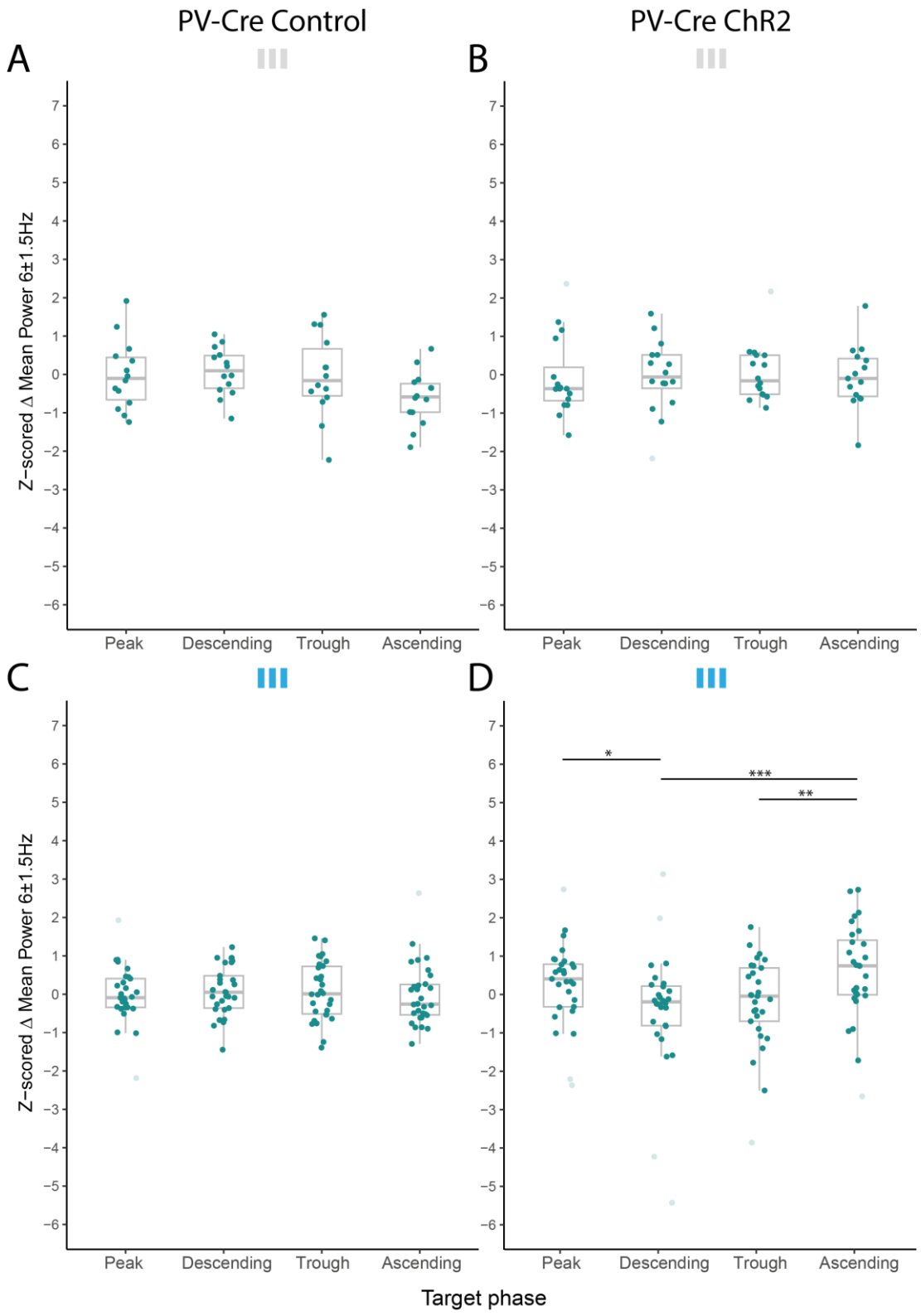


Figure 3.5 Gamma stimulation of PV+ interneurons lead to phase-dependent effects on theta power

Boxplots with the z-scored change in theta power with respect to baseline extracted between 4.5-7.5Hz (6Hz ± 1.5) for both control (n=4; **A & C**) and opsin PV-Cre mice (n=7, **B & D**) are shown when stimulation was on (1 or 2mW; blue patterns) or off (0mW; grey patterns). Stimulation was targeted to 4 phases of the ongoing theta oscillation, the peak, descending, trough, and ascending phases. A further breakdown of the total number of sessions for gamma stimulation: PV control (n=15 sessions, n=14 recordings per phase stimulation off, n=29-

30 per phase stimulation on) & PV ChR2 (n=16 sessions; n=15-16 recordings per phase stimulation off, n=28-29 per phase stimulation on). Each session will contain multiple stages - usually 1 per phase, per laser power for stimulation on data, as data was often collected at both 1 & 2mW. The baseline consisted of a mean calculated from the baseline recorded at the beginning of each session and all unstimulated recordings from within a session. The grey boxes represent the interquartile range and median values from the data set, and the whiskers extend to minimum and maximum values calculated from their quartile ±1.5*IQR for each grouped session. Session means for each laser power are plotted as individual scatter points for their respective group and stimulation type. Lighter scatter points represent data points that lie outside a threshold set as the respective quartile value ±1.5*IQR. Significant differences ($p<0.05$) were identified between the peak and descending, descending and ascending and trough and ascending phases in opsin mice (**D**) (LME followed by pairwise post hoc t-tests with Tukey adjustment).

3.3.3.2 Gamma stimulation leads to phase-specific effects on theta power in opsin mice but not control mice

To follow up the significant interactions, we first addressed the hypothesis that, when ChR2 was present in PV-Cre+ interneurons, phase-specific differences can be observed in theta power when stimulation was on. We therefore performed a LME model with fixed effects of group (opsin, control) and phase as well as their interaction, and random effects of subject and date on stimulation on data.

There was a significant group*phase interaction ($F(3,205)=6.31$, $p<0.001$), suggesting that there was a significantly greater effect of phase on theta power in opsin mice than controls, consistent with expectations. As expected, there was no significant main effect of group ($F(1,19)=0.0012$, $p=0.97$), but there was an unexpected significant main effect of phase ($F(3,205)=3.85$, $p=0.01$) indicating that when stimulation was on, phase affects band power, regardless of the group. To follow up on these significant effects and explore any differences between phase pairwise t-tests were performed (Tukey adjustment). This identified significant differences between the peak and the descending phase ($p=0.033$), the descending and ascending phases ($p=0.0001$) and the trough and the ascending phases ($p=0.003$) in opsin mice (Figure 3.5D).

3.3.3.3 Gamma stimulation in opsin mice results in phase-specific effects on theta power only when stimulation is on

Next, we investigated whether there was a significant stimulation-by-phase interaction in the opsin mice. To address this, a LME model with main effects of laser power (stimulation on/off) and phase along with their interaction term were tested on opsin only data.

We hypothesised stimulation in the opsin group would result in changes of theta band power at each phase, that wouldn't be observed when the stimulation was off. As expected there was a significant laser power*phase interaction term ($F(3,162)=3.11$, $p=0.028$), suggesting that phase-specific differences in theta band modulation were only observed when stimulation was on. There were no significant main effects (all $p>0.06$).

3.3.4 Closed-loop continuous stimulation

Having established that the effects of gamma stimulation on theta power were specific to the phase of the underlying theta on which they were delivered, we then sought to determine whether phase dependency resulted from the specific stimulation pattern or whether a different pattern of optogenetic stimulation could similarly modulate motor cortical theta power.

Therefore, we implemented a second stimulation pattern – continuous stimulation, which consisted of a single pulse delivered across ¼ of the theta cycle, the middle of the pulse was centred on the target phase of stimulation.

The following electrophysiological data were collected using continuous stimulation when the laser was off and with the laser on at a power of 1 and of 2mW (Control: n=4 mice, 16 sessions; Opsin: n=5 mice, 10 sessions).

3.3.4.1 Closed-loop continuous stimulation of the motor cortex results in phase-specific modulation of theta power in PV-Cre mice

Having combined all stimulated data, we investigated the effects of continuous phase-specific theta modulation on local LFP power. Mean PSD plots with continuous stimulation in both control and opsin (ChR2) mice at each targeted phase are shown in Figure 3.6A. Continuous stimulation was either off (0mW; grey bars) or on (1 or 2 mW; blue bars).

To investigate whether continuous closed-loop stimulation induced phase-specific theta power modulation, we subtracted the baseline (Figure 3.6B) and extracted power spectral density estimates between our 4.5-7.5Hz target range (Figure 3.7), as we did with gamma stimulation. A LME model was used to test our overarching hypothesis predicting phase-specific differences between experimental groups (‘control’ & ‘opsin’) and continuous stimulation (‘off’ & ‘on’). The LME, with fixed effects of group, laser power & phase with interactions, showed a significant interaction between group and phase ($F(3,288)=5.03$, $p=0.002$). This interaction suggests that as expected, the control group was not influenced by phase, whereas the opsin group was. Unexpectedly, there was no significant phase*laser power interaction ($F(3,288)=0.72$, $p=0.54$). Our three-way interaction between group, laser power and phase was also not significant ($F(3,288)=2.13$, $p>0.096$). However, we found significant main effects of group ($F(1,14)=8.40$, $p=0.012$) and laser power ($F(1,288)=4.82$, $p=0.029$), so further analyses focus on experimental conditions alone.

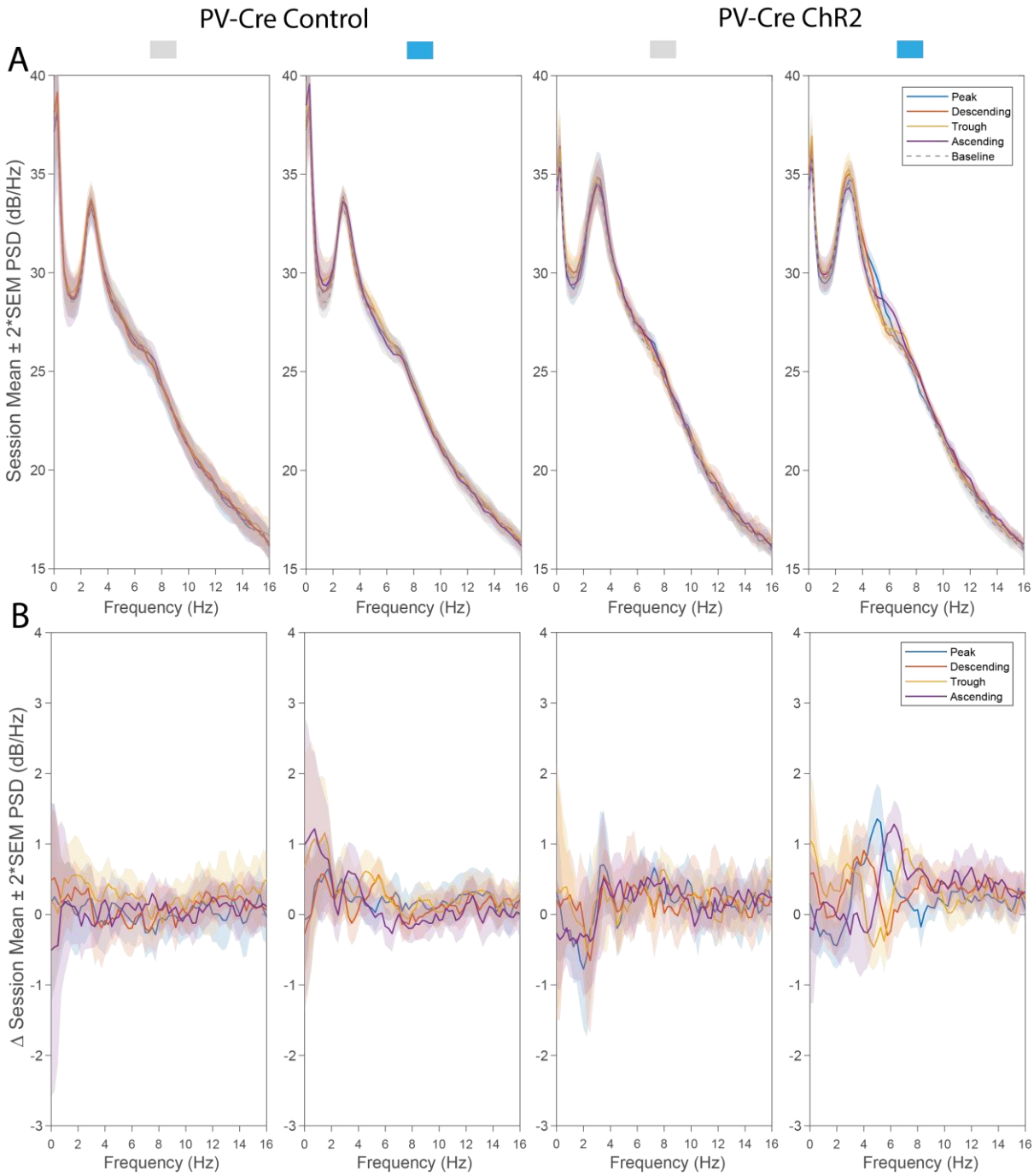


Figure 3.6 Phase-dependent effect in local LFP following closed-loop continuous stimulation of PV+ interneurons

Mean power spectral density (±2*SEM) from 0-16Hz for both PV-Cre control (n=4) and opsin mice (n=5), targeting 4 different phases of the theta oscillation with continuous stimulation (**A**). Stimulation was either off (0mW; grey pattern) or on (1 or 2mW; blue pattern). The number of sessions to calculate the mean in control mice was n=16 (16 recordings per phase stimulation off; 31 recordings per phase stimulation on). In opsin mice this was n=10 sessions (9-11 recordings per phase stimulation off; 20 recordings per phase stimulation on). Within each session, a session baseline was calculated from a baseline recorded at the beginning of each session, combined with all unstimulated recordings throughout a session. The mean session baseline was then plotted on each plot for each group and stimulation on or off. The mean PSDs (±2*SEM) in which the baseline was removed from each session were also plotted for both control and opsin mice (**B**).

3.3.4.2 Continuous stimulation leads to phase-specific effects on theta power in opsin but not control mice

To follow up on significant interactions, we first addressed the hypothesis that there are phase-specific differences in theta power when ChR2 is present in PV-Cre+ interneurons, when continuous stimulation was on. A LME was performed with fixed effects group and phase as well as their interaction and random effects of subject and date.

When continuous stimulation was on and delivered to PV+ inhibitory interneurons there was a significant group*phase interaction term ($F(3,184)=9.07$, $p<0.001$), indicative of the presence of ChR2 in driving changes in theta power across phase, and thus not an effect of visual evoked potentials. This is further supported by what we observe in Figure 3.6A & 3.6B. Additionally, there was a significant main effect of group ($F(1,13)=6.32$, $p=0.026$), while the main effect of phase was not significant ($F(3,184)=1.64$, $p=0.18$). Subsequently, pairwise t-tests (Tukey adjustment for multiple comparisons) were undertaken which found significant differences in the opsin mice between the descending and ascending phases ($p=0.0236$) as well as between the trough and ascending phases ($p=0.028$) (Figure 3.7D). Continuous stimulation targeted to the theta peak and ascending phases resulted in amplification of the theta oscillation (Figure 3.7), with respective theta peaks of 5Hz and 6Hz (Figure 3.6). This demonstrates theta phase-specificity stays consistent between the two different stimulation patterns. We had insufficient data to test for an interaction of stimulation-by-phase on theta power in the opsin group.

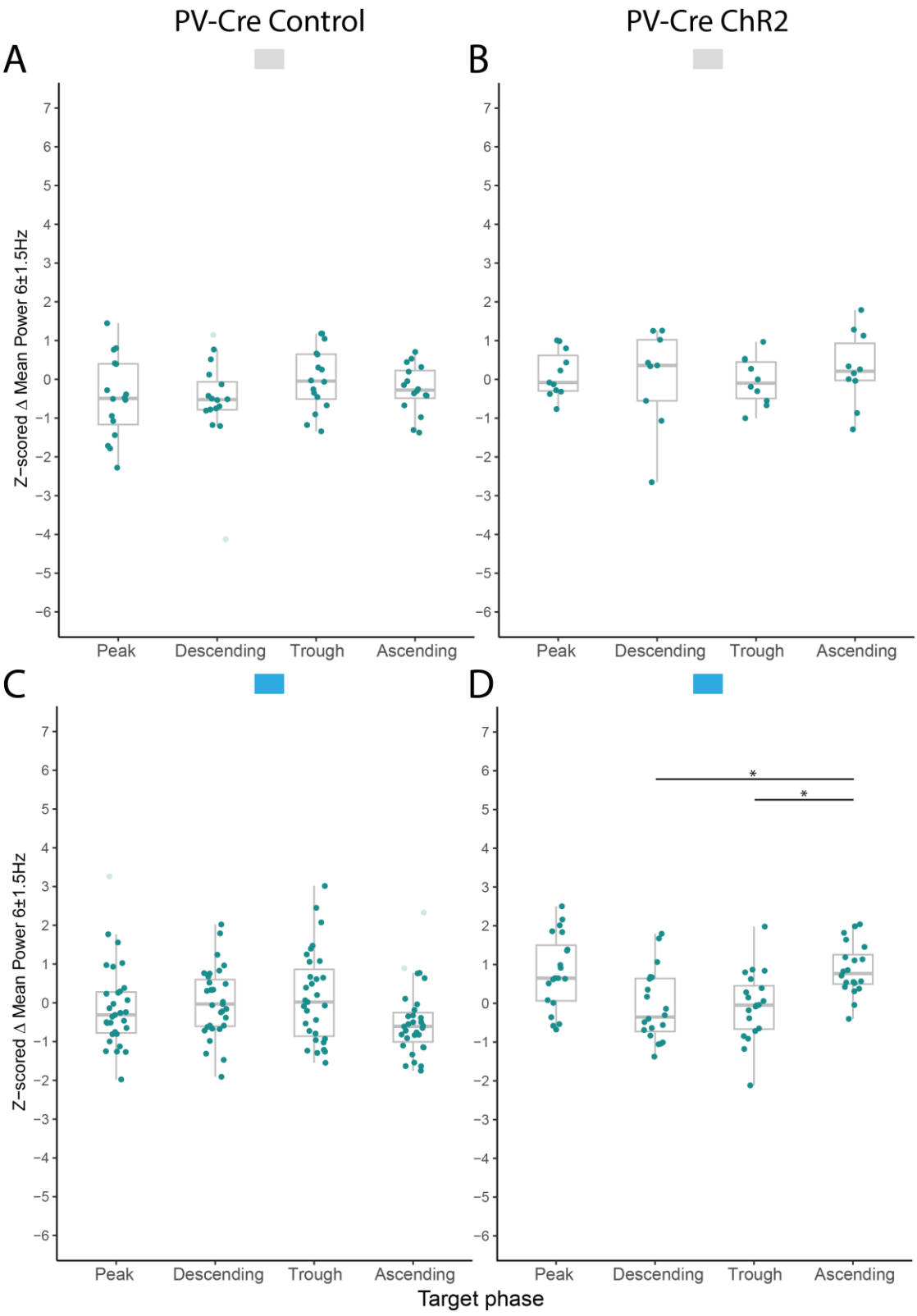


Figure 3.7 Continuous stimulation of PV+ interneurons lead to phase-dependent effects on theta power
Boxplots with the z-scored change in theta power with respect to baseline extracted between 4.5-7.5Hz (6Hz ± 1.5) for both control (n=4; **A & C**) and opsin PV-Cre mice (n=5; **B & D**) are shown when stimulation was on (1 or 2mW; blue patterns) or off (0mW; grey patterns). Stimulation was targeted to 4 phases of the ongoing theta oscillation, the peak, descending, trough, and ascending phases. A further breakdown of the total number of stages for continuous stimulation: PV control (n=16 sessions; n=16 recordings per phase stimulation off; n=31 recordings per phase stimulation on) & PV ChR2 (n=10 sessions; n=9-11 recordings per

phase stimulation off; n=20 recordings per phase stimulation on). Each session contains multiple recordings - usually 1 per phase, per laser power for stimulation on data, as data was often collected at both 1 & 2mW. The baseline consisted of a mean calculated from the baseline recorded at the beginning of each session and all unstimulated recordings from within a session. The grey boxes represent the interquartile range and median values from the data set, and the whiskers extend to minimum and maximum values calculated from their quartile ±1.5*IQR for each grouped session. Session means for each laser power are plotted as individual scatter points for their respective group and stimulation type. Lighter scatter points represent data points that lie outside a threshold set as the respective quartile value ±1.5*IQR. Significant differences were identified between the descending and ascending and trough and ascending phases in opsin mice (**D**) (LME, followed by pairwise post hoc t-tests).

3.3.5 Open-Loop Stimulation

3.3.5.1 Stimulation patterns resulting from closed-loop stimulation do not underly phase-dependent changes in theta power.

To investigate whether the changes in theta power at each phase were solely due to the pattern of stimulation received during closed-loop stimulation, we used the recordings of stimulation trains produced during closed-loop stimulation at each phase, to deliver open-loop replay of the same stimulation patterns within the same session as the closed-loop stimulation itself. This provided a direct comparison between the effects of the real-time closed-loop interaction and the stimulation pattern resulting from that interaction. In these analyses, only sessions which include open-loop replay from the same session (n=4 sessions, n=6-7 recordings per phase) were included. While closed-loop stimulation targeted to PV+ interneurons led to phase-specific changes in theta power (Figure 3.8A & 3.8C), open-loop replay does not demonstrate the same modulation (Figure 3.8B & 3.8D). In line with our previous analyses, the baseline was subtracted, and power spectral density estimates taken between 4.5-7.5Hz. These are plotted for each phase in Figure 3.8E & 3.8F. The previously shown theta peaks at 5Hz and 6Hz when targeting closed-loop continuous stimulation to the peak and ascending phases respectively (Figure 3.6B & 3.8C), are not demonstrated by open-loop replay (Figure 3.8D). Instead, it appears that targeting

the trough with the continuous replay, leads to a slight enhancement of the theta oscillation as opposed to the peak or ascending phases.

To compare the effects of closed-loop and open-loop replay stimulation, we calculated the difference in mean theta power between the most and least amplifying phases identified during each closed-loop recording session, for each stimulation pattern and laser power amplitude. For each matched open-loop recording, the phases identified as producing the most and least amplification of theta during the closed-loop recording were taken and the difference between them was calculated. In this analysis, data were only included if it was available for all four phases for comparison (Figure 3.8G). As with all previous analyses, the data was then z-scored. There was not sufficient data to use a LME, as such, we performed a paired t-test to explore how theta power responds following closed-loop continuous stimulation and subsequent open-loop replay. This was with the caveat that we were unable to control for repetition of subjects within and between sessions (n=2 mice; total n=3 sessions, 2 of these sessions had data at two different amplitudes – 1 & 2mW).

Continuous stimulation resulted in a significant difference between the z-scored change in theta power between the most and least amplifying closed-loop phases, when stimulation was delivered in a closed-loop manner and when these resultant stimulation patterns were used as open-loop replay ($p=0.01$, paired t-test). This indicates that stimulation pattern alone was not sufficient at producing the same changes between the most and least amplifying phases (Figure 3.8G).

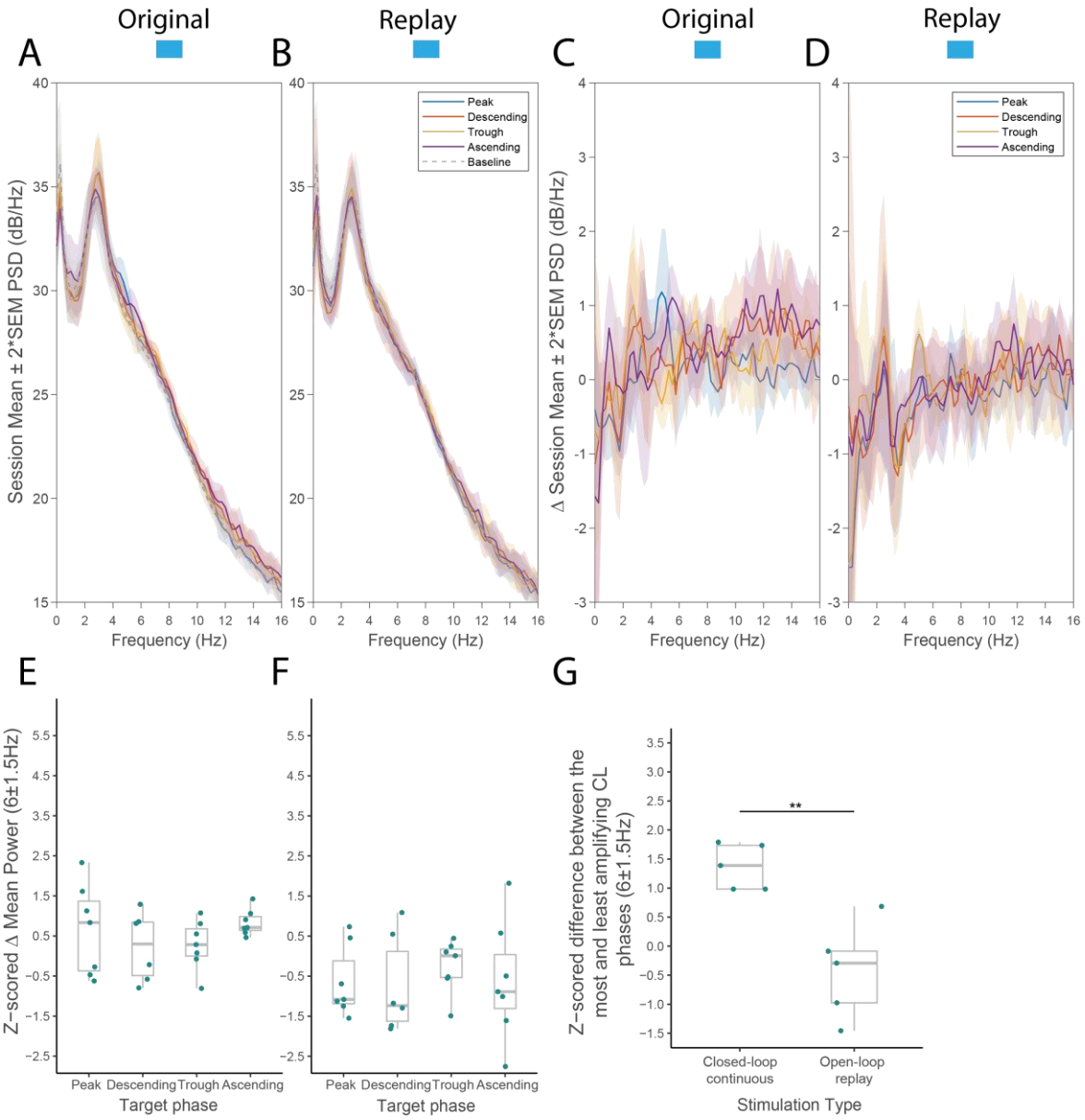


Figure 3.8 Local theta LFP and z-scored change in theta power following continuous closed-loop stimulation and its open-loop replay & the z-scored difference in theta power between the most and least amplifying closed-loop phases

Mean power spectral density (±2*SEM) from 0-16Hz in RBP4-Cre opsin mice (n=3), continuous stimulation on (1 or 2mW; blue bar) (**A & B**). Plots demonstrate PSD for closed-loop optogenetic stimulation targeting 4 different phases of the theta oscillation (original) as well as open-loop replay (replay), in which a previous closed-loop recording is played back to the mouse within the same session. More specifically, the number of sessions to calculate the mean for continuous (n=4; n=6-7 recordings per phase), some sessions have data from both 1 & 2mW. Within each session, a session baseline was calculated from a baseline recorded at the beginning of each session, combined with all unstimulated recordings throughout a session. The mean session baseline is then plotted on each plot for each group and stimulation on or off. The mean PSDs (±2*SEM) in which the baseline was removed from each session is also plotted for both control and opsin mice (**C & D**). Boxplots (**E & F**) demonstrate z-scored change in theta power with respect to baseline extracted between our target range of 4.5-7.5Hz (6Hz±1.5) (n=4 mice, n=4 sessions with a total of 6-7 recordings per phase). Grey boxes represent the interquartile range and median values from the data set, whiskers extend to the minimum and maximum values calculated as their respective quartile ±1.5*IQR. Session means for each laser power are

plotted as individual scatter points for their respective group and stimulation type. Lighter scatter points represent data points that lie outside a threshold set as the respective quartile value ±1.5*IQR. To perform statistical analyses, the minimum and maximum values extracted from the closed loop recording and the difference between them were calculated. The difference between these same phases were then calculated in the open-loop replay recording. These are both plotted as individual scatter points (**G**), grey boxes represent the interquartile range and median values from the data set, and whiskers extend to the minimum and maximum values calculated as their respective quartile ±1.5*IQR. Significant differences ($p<0.05$; paired t-test) were identified between the z-scored change in theta power from the most and least amplifying phase in each specific closed-loop recording and these phases in their open-loop counterpart. In this specific analysis only sessions that had a complete set of data for all four phases at that specific laser power were used (n=2 mice, n=3 sessions, 2 sessions contained data from both amplitudes).

3.3.5.2 Open-loop gamma and continuous stimulation do not significantly modulate theta power in opsin mice

In order to test the importance of the closed-loop interaction with the underlying theta phase, we used open-loop (OL) stimulation controls with no relationship to phase or interaction with the oscillation to determine whether open-loop stimulation elicited modulation of theta power.

Four open-loop stimulation patterns were devised from the previous closed-loop stimulation patterns (See Chapter 2, Table 2.2). The first two, OL-gamma (3 pulses at 75Hz) and OL-continuous (~41ms burst), match the previous closed-loop stimulation patterns in terms of number of pulses, their lengths and laser power amplitudes used, however, are not targeted to particular theta phases. Between subsequent stimuli were 167ms gaps. Additionally, we devised a variation of these, in which randomised 1-1.2 second gaps interleaved every 6 stimulation pulses to disrupt their regularity. Following previous analyses, stimulation at both 1 & 2mW were combined for subsequent analyses. As such, data was collected in n=3 mice, from n=7 sessions. Data with stimulation on is doubled (n=14) due to collection at both amplitudes.

Mean PDS plots with each of the four types of OL stimulation are shown in Figure 3.9 A-D, data were only collected in PV-Cre ChR2 mice. Stimulation was either off (0mW;

grey bars) or on (1 or 2mW; blue bars). Lines following the stimulation pattern denote the randomised 1-1.2 second gap following 6 bursts. To investigate whether open-loop stimulation resulted in changes in theta power the baseline was subtracted before power spectral density estimates were taken around our target band of 6±1.5Hz.

Data was split into gamma and gamma gaps for comparison as well as into continuous and continuous gaps. To determine whether there were differences between the two open-loop stimulation pattern types when stimulation was either received or not, a LME model was devised. This had main effects of stimulation pattern (either gamma or continuous, and its matching stimulation pattern with randomised 1-1.2 second gaps) and stimulation (off: 0mW; on: 1 or 2mW), their interaction and random effects of subject and date.

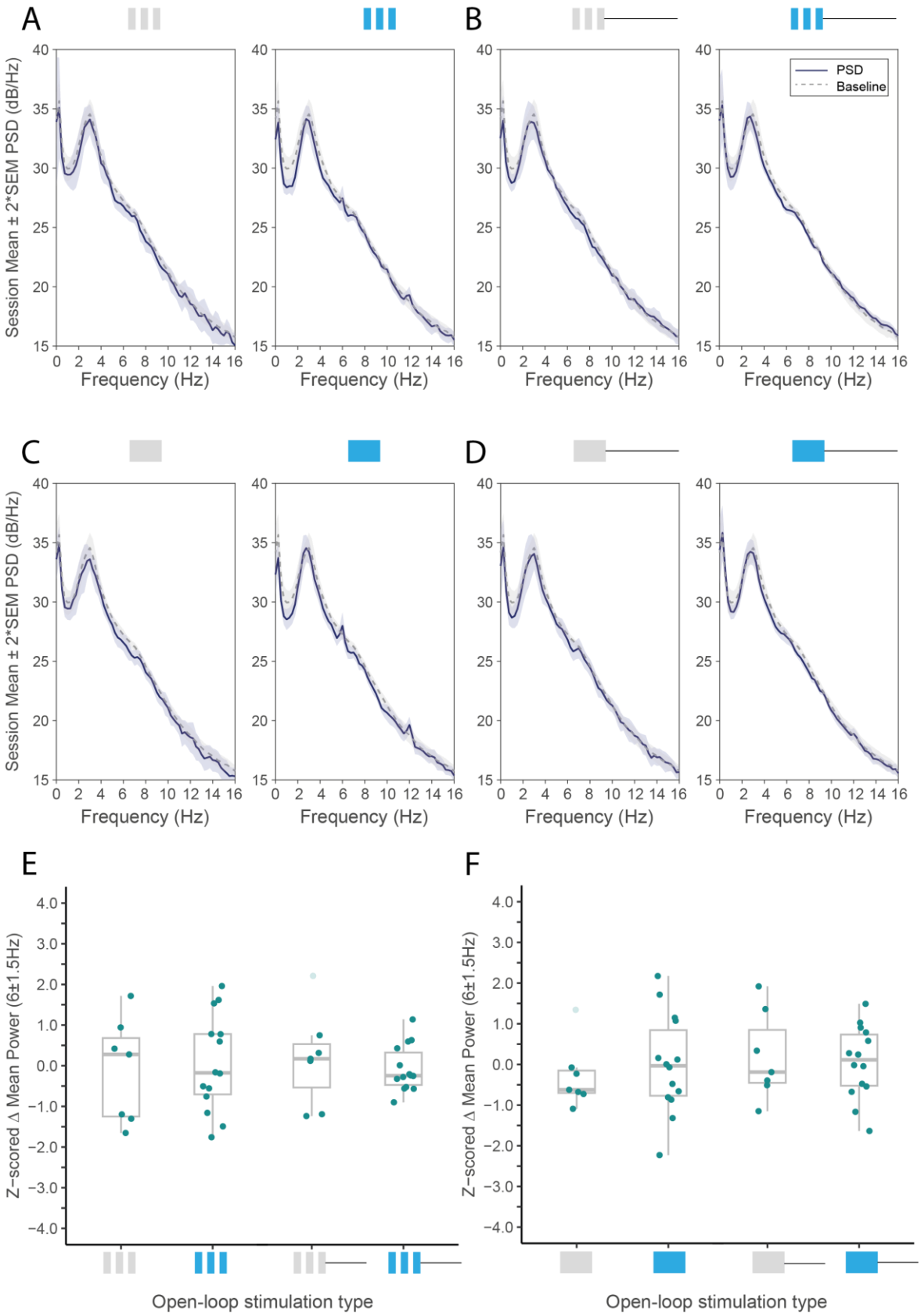


Figure 3.9 Local power spectra and z-scored change in theta power of PV-Cre opsin mice demonstrate no modulation of theta power following open-loop stimulation

To determine whether there were changes in theta power following open-loop stimulation four open-loop stimulation patterns were devised - open-loop gamma (**A**), open-loop gamma gaps (**B**), open-loop continuous

(**C**) and open-loop continuous gaps (**D**) as variations of our closed-loop patterns with no phase relationship. Mean power spectral density plots from 0-16Hz (±2*SEM) in PV-Cre opsin mice (n=3; n=7 sessions). Stimulation was either off (0mW; grey pattern) or on (1 or 2mW; blue pattern). Session means were calculated from n=3 mice, n=7 sessions (n=14 recordings when stimulation was on due to data collected at two amplitudes). Within each session, a session baseline was calculated from a baseline recorded at the beginning of each session, combined with all unstimulated recordings from throughout the session. The mean session baseline was plotted for each stimulation type. Power spectral density estimates were extracted around the 6Hz target (4.5-7.5Hz) after the baseline had been removed. The z-scored mean power was plotted (**E & F**) for each of the four open-loop stimulation patterns. No significant differences (p>0.05) were found between either stimulation patterns (OL gamma & OL gamma-gaps; OL continuous & OL continuous-gaps) (LME).

Due to lack of variance in theta power of open-loop gamma stimulation we were unable to derive conclusions and as a result simplified our model. The model was designed to test the difference between the stimulation patterns when stimulation was on (LME: stimulation pattern, random effects of subject and date). This found no significant difference ($F(1,22)=0.17$, $p=0.69$) between open-loop gamma or open-loop gamma gaps stimulation in PV-Cre ChR2 mice (Figure 3.9E). Due to a lack of data when stimulation was off, we could not test this condition.

Our original model was then applied to determine whether there were changes in theta power when using open-loop continuous or open-loop continuous gaps stimulation. The LME model found no significant main effects (stimulation pattern: ($F(1,32)=0.85$, $p=0.36$); stimulation ($F(1,32)=0.07$, $p=0.80$)) or interaction term between the stimulation pattern and stimulation (on or off) ($F(1,32)=0.54$, $p=0.47$) (Figure 3.9F).

These results suggest that open-loop stimulation of any pattern is not sufficient to drive changes in theta power, unlike the spectral plots may suggest. In these plots (Figure 3.9A & 3.9C) we also observe a 12Hz peak when stimulation was on which demonstrates harmonic effects that are not observed when stimulating using closed-loop gamma or continuous stimulation.

3.4 Discussion

We initially aimed to demonstrate the feasibility of a closed-loop set-up combined with optogenetics in head-fixed mice. To do this, we injected PV-Cre mice with a virus containing ChR2. Then, we recorded the LFP while simultaneously using OscillTrack, a new highly responsive closed-loop system to undertake phase-specific modulation. This was implemented using Intan to simultaneously track the ongoing theta oscillation from one channel, trigger optogenetic stimulation at a set theta phase, while also recording the LFP output. We tested this using two optogenetic stimulation patterns and found that we were able to stimulate across the four different phases we had selected to target – the theta peak, descending phase, ascending phase and trough using post hoc verification of the actual phase stimulated.

Using this system, we assessed whether closed-loop phase-dependent stimulation could modulate the ongoing theta oscillation when stimulating PV-interneurons in a phase-dependent manner and whether the choice of stimulation pattern was important in modulation.

In this chapter, we have demonstrated phase-specific responses in the theta oscillation when stimulating PV-Cre ChR2 mice with both gamma and continuous stimulation types, something that is not demonstrated in PV-Cre control mice. Both gamma and continuous stimulation targeted to the theta peak and ascending phases were able to amplify the ongoing theta oscillation. There is some evidence that gamma was more effective than continuous stimulation in modulating theta power. Both stimulation patterns were chosen to stimulate across ¼ of the theta cycle, therefore, this suggests that PV+ interneurons within the motor cortex respond better to shorter

stimulation pulses and less overall energy being input into the system as opposed to a longer single pulse. However, both gamma and continuous stimulation were able to modulate the theta oscillation in the same way and demonstrated the same pattern of phase response.

3.4.1 Accuracy of phase tracking does not depend on the phase of stimulation

A small but consistent peak in the resting power spectra around 6Hz in control PV-Cre mice and unstimulated PV-Cre mice is present. This demonstrates the availability of a small oscillation to target; however, this not been quantified. Previously, a 7Hz theta oscillation was observed in head-fixed rodents (Igarashi et al. 2013), indicating the presence of such an oscillation.

Within our data stimulation targeted to the peak and ascending phases amplified the underlying theta oscillation. We predicted that when the oscillation amplitude increased, it would subsequently be easier to track the phase of the oscillation therefore enhancing accuracy. However, post-hoc analyses suggests that this is not demonstrated, as the centre-point of stimulation at the ascending phase remained as accurate as in the control conditions, while at the peak it appears slightly less accurate. For each condition, the accuracy of the centre-point of stimulation appears to separate into the four phases. While there may be some overlap in accuracy across each burst of stimulation, the timeout period appears sufficient to allow the phase estimate to more precisely stimulate across subsequent oscillatory cycles. Overall, this indicates we were able to reliably track and stimulate across all four phases, however, increased variability in the accuracy of the targeted phase in the opsin mice

when stimulation was on, indicates that modulation of the oscillation may partly affect phase-tracking accuracy.

3.4.2 Closed-loop is more effective than open-loop for modulation of theta phase

Continuous stimulation pattern trains which produced amplification of the theta oscillation when phase-locked to the peak or ascending phases, did not reproduce amplification of the oscillation when delivered as open-loop replay. Quantifying the difference between the most and least amplifying closed-loop phases, demonstrated a larger change between the phases when stimulation was closed-loop, rather than in the open-loop replay of the stimulation train. The sample size for this analysis was much smaller than initial analyses, so these results should be interpreted with care. Nevertheless, the theta-phase pattern of modulation that was demonstrated when plotting all the closed-loop data is also observed in this subset of the data. This provides evidence that it is the stimulation in combination with the phase targeted, not the stimulation pattern from the resultant interaction that drives changes in theta power as expected. Following closed-loop gamma stimulation we would expect similar results; however, we did not have sufficient data to assess this.

Additionally, we have shown that open-loop stimulation with no relationship to the underlying theta oscillation does not produce significant theta modulation. We predicted that introducing randomised gaps following every 6 bursts of OL stimulation would decrease stimulation regularity, thus impacting the degree to which theta power could be modulated. However, we found no significant changes in theta power by stimulation of PV+ interneurons with regular OL-gamma or OL-continuous stimulation either. Small peaks can be observed in the power spectra at both 6Hz and

12Hz, however, the baseline is slightly higher than the stimulated PSD. By subtracting the baseline for statistical analyses, we likely remove this effect from the data. It is also possible that the variability in mean power is too large resulting from the small number of subjects we collected this data in and to properly interrogate this effect more data would be necessary.

3.4.3 Heterogeneity of optogenetically stimulated cells

3.4.3.1 Stimulated PV interneurons are spread across cortical layers

The PV-Cre mouse line we used here has been widely used and has demonstrated high efficiency and specificity for targeting cortical regions (Lima et al. 2009; Whissell et al. 2015). However, one limitation of targeting PV+ interneurons is that they are not specific to layer 5. As the main motor cortical output layer, this is the layer in which we aimed to manipulate neurons. While the viral ChR2 is injected into L5, the virus can spread and it is, therefore, possible that we are stimulating transfected PV+ interneurons from more than one specific layer, due to natural distribution of these neurons through layers 2-6 (Xu et al. 2010). The density of neurons is, however, greater in the deeper layers; therefore, it is likely the majority of neurons transfected lie within the deeper layers. Additionally, the volume of virus we inject is particularly low which may partly combat this. Furthermore, visual inspection of the region during post-hoc tissue processing has also shown the virus does not spread to other regions of the brain or widely throughout the cortex and remains local to the injection site.

3.4.3.2 Stimulated cells may not all be FS

The putative ChR2+ PV interneurons that respond to optogenetic stimulation are likely fast spiking cells, given the majority of PV+ interneurons have broadly been identified

as FS (Ascoli et al. 2008; Rudy et al. 2011). Within this data set this would need to be confirmed through analyses of the unit data. FS neurons have been shown to exert strong local inhibition (Tremblay et al. 2016), therefore, stimulation is likely to result in strong inhibition of surrounding pyramidal neurons. PV-basket cells also show reciprocal connections to other PV-interneurons (Tremblay et al. 2016), enabling greater inhibitory control through surrounding interneurons not containing ChR2, that are still involved through feedback inhibition. Reciprocal connections create a dynamic balance, in which pyramidal neuron excitability is altered over time, thereby contributing to fluctuations in excitation and inhibition that lead to neuronal oscillations. PV+ basket cells innervate surrounding neurons to provide local inhibition, as well as across cortical layers using translaminar axons (Tremblay et al. 2016). Therefore, their response is likely to be widespread.

It is possible, however, that a different subtype of non-fast spiking PV+ interneuron is involved with theta activity within the motor cortices. These are known as multipolar bursting (MB) neurons. Currently, limited knowledge exists surrounding this subtype, however, in the frontal and somatosensory cortex they have been shown to project to FS interneurons, but this was not a reciprocal (Blatow et al. 2003). MB neurons are reciprocally connected with L2/3 pyramidal neurons and to each other (Blatow et al. 2003; Tremblay et al. 2016). These neurons were shown to have a much lower natural firing frequency than that of FS interneurons, at around ~12.8Hz within the theta range (Blatow et al. 2003). Furthermore, these neurons evoked synchronised inhibition of local pyramidal neurons following carbachol induced theta oscillations between 4-7Hz (Blatow et al. 2003). These results highlight a possible role for these neurons in

driving the ongoing theta oscillation. Additionally, a small proportion of PV+ interneurons express SST and have different synaptic properties (Tremblay et al. 2016) which further complicates the pool of interneurons that could be involved. Precisely identifying the PV+ subtypes involved could only be disentangled within our data set through spike analyses, which may determine whether this subtype exists within the motor cortex.

3.4.4 Phase-specificity may be a property of the underlying microcircuitry

It is possible that if FS and MB subtypes of PV+ interneurons exist within L5 of the motor cortex, both are involved in the phase-specific theta modulation we observe. The endogenous oscillation that we track may initially be a result of the microcircuitry of MB cells. Optogenetic stimulation may then recruit many FS neurons which drive the modulation of theta power. Increases in LFP power are generally thought to be a result of increased coherence and synchrony in the underlying neurocircuitry (Buzsáki and Draguhn 2004). Optogenetically activating PV+ interneurons will ultimately drive fast and powerful inhibition of pyramidal neurons. We observe amplification of theta power only when targeting two specific phases of the oscillation. This finding indicates phase-specificity linked to the microcircuitry generating the response. One possible explanation is that the identified phases are related to the phases in which these neurons would usually produce action potentials within the microcircuitry of theta oscillations, controlling inhibition to regulate the excitation of pyramidal neurons. This would suggest in contrast, that reduced theta power following stimulation, promotes inhibitory neurons to fire out of phase and therefore reduces overall coherence and precise control over excitatory neurons.

In support of the idea that these phases are important within the microcircuitry, putative interneurons have been found phase-locked to the ascending phase of gamma oscillations of the hippocampus previously, in awake rats (Bragin et al. 1995) and *in vitro* studies (Hájos et al. 2004). However, hippocampal PV interneurons have also been shown to fire at the descending phase of the theta oscillation in anaesthetised rats (Klausberger et al. 2003). Contrastingly, PV interneurons have also been found to strongly phase lock just before the peak of CA1 theta *in vitro* (Huh et al. 2016) and descending phase *in vivo,* while somatostatin neurons which can be PV+ phase-locked to the ascending phase (Royer et al. 2012). While these results are not from within the cortex, these results align with the amplification we observe at the peak and ascending phases of the theta oscillation. Suggestive that interneurons fire at these phases to precisely control the output of the neural oscillation and therefore enhance overall synchrony which can lead to greater oscillatory power. These studies suggest that the same phases are important across multiple frequencies of oscillations and brain regions.

3.4.5 Phase-specific optogenetic stimulation outside motor cortex leads to behavioural effects

Phase-specific modulation of PV+ interneurons had not been demonstrated previously within the motor cortex, however, theta-phase specific manipulation of PV+ interneurons had been shown in the hippocampus (Siegle and Wilson 2014). In freely moving mice, PV+ interneurons were optogenetically activated during a spatial navigation exercise. Targeting stimulation to different phases of the endogenous theta rhythm resulted in improvements in performance related to different aspects of the task. Another study, targeting an endogenous theta oscillation (4Hz) that develops

during the conditioned fear response in the dmPFC, used phase-dependent optogenetic stimulation of either PV interneurons or pyramidal neurons. The authors demonstrated changes in freezing behaviour as a result of phase-specific stimulation (Dejean et al. 2016). But while stimulation at the ascending phase had opposite effects on behaviour depending on the cell type stimulated, this was not the case when the cells were stimulated at the descending phase. At the ascending phase, activation of PV+ interneurons reduced freezing behaviour whereas at the descending phase this increased freezing behaviour. Activation of pyramidal neurons at the ascending phase increased freezing behaviour, but there was no change in behaviour when pyramidal neurons were stimulated at the descending phase of the theta oscillation. This highlights a complex interplay between the microcircuitry and changes in behaviour that are highly dependent on the cell type manipulated. It is therefore vital we aim to understand how phase-specific manipulation can differentially modulate neurons at a resting state, as well as when greater complexity is introduced to the microcircuitry during tasks. Furthermore, this also provides evidence that the same phases may be important throughout different regions of the cortex for the same neuronal cell type.

3.4.6 Response of PV+ interneurons to optogenetic stimulation

Within L5, the population of fast spiking PV expressing interneurons has been associated with modulation of cortical gamma oscillations (Rudy et al. 2011; Sohal et al. 2009; Traub et al. 1996; Whittington and Traub 2003). PV-basket cells can generate an action potential roughly each gamma cycle and have been found to be precisely phase-locked to gamma oscillations (Bartos et al. 2007; Bragin et al. 1995; Csicsvari et al. 2003). As a result of these associations, it is expected these neurons can be

driven by high frequencies of stimulation. Cardin et al (2009) demonstrated optogenetic manipulation of ChR2 containing FS-interneurons, which could significantly increase LFP power between 20-80Hz stimulation. While 40Hz stimulation demonstrated the most significant alteration in LFP power (Cardin et al. 2009), the range in which they used encompasses our 75Hz gamma stimulation frequency. Sohal et al (2009) additionally manipulated PV-interneurons in the neocortex, but instead used halorhodopsin for inhibition, demonstrating *in vivo* suppression of gamma power in anaesthetised mice. These provide evidence that PV+ interneurons should be able to follow our 75Hz gamma frequency stimulation, targeted to the ongoing theta oscillation. However, it also suggests that modulation may not be specific only to theta oscillations.

3.4.7 Conclusions

Overall, the findings described in this chapter highlight phase-specific optogenetic closed-loop stimulation can be used to manipulate the motor cortical theta oscillation resulting in phase-dependent modulation. Additionally, these effects are phase-dependent and are not demonstrated when the same stimulation pattern trains are replayed to the mouse, demonstrating the importance of the underlying real-time interaction. Amplification of the underlying theta oscillation was found when stimulating at the peak and ascending phases of the oscillation, highlighting phases which may be important within the underlying microcircuitry. Understanding why we can more effectively modulate the ongoing oscillation at certain phases could be important in determining the role they play within the local circuitry.

4 Modulation of Excitatory Pyramidal Neurons

4.1 Introduction

Playing a vital role in the generation and maintenance of neuronal oscillations, pyramidal neurons are spread through the cortex from layers 2-6 (K. D. Harris & Shepherd, 2015). While all groups are heterogenous, they are commonly subdivided based on where their axons project (K. D. Harris & Shepherd, 2015). Broadly, they are either intratelencephalic (IT), pyramidal tract (PT) and corticothalamic (CT) neurons and release the excitatory neurotransmitter glutamate (K. D. Harris & Shepherd, 2015).

IT neurons in the upper cortical layers tend to project to other cortical areas, while the deeper IT neurons (L5a, 5b & 6) typically project to other cortical areas as well as the striatum (Shepherd 2013). The other two pyramidal subtypes are more restricted in location, neuronal cell bodies of PT neurons to L5b and CT neurons in L6 (K. D. Harris & Shepherd, 2015). CT neurons primarily project to the ipsilateral thalamus, whereas PT neurons send axon collaterals to a wider range of targets (K. D. Harris & Shepherd, 2015; Hooks et al., 2013; Shepherd, 2013; Winnubst et al., 2019). In the motor cortex of mice, two subtypes of PT neurons have been identified (Economo et al. 2018; Jiang et al. 2020; Winnubst et al. 2019).

The bulk of neurons in L5 are pyramidal neurons, these consist of IT and large PT neurons (K. D. Harris & Shepherd, 2015; Shepherd, 2013). Cortical L5 pyramidal neurons predominantly express a protein known as retinol-binding protein 4 (RBP4), these include both IT and PT subtypes. RBP4 is therefore used to modulate neurons located primarily in L5 using RBP4-Cre driver lines (Gerfen et al. 2013; Harris et al.

2014). Studies have shown that both IT and PT subtypes are labelled using this Cre-driver line (Gerfen et al. 2013; Khibnik, Tritsch, and Sabatini 2014).

L5 pyramidal neurons are controlled through perisomatic synapses by strong inhibition of PV+ FS basket cells. Their complex interactions lead to the effective generation of oscillations that allow for cortical information processing (Tremblay et al. 2016). While L5 is the main cortical output layer, a prominent source of intracortical excitation into L5 comes from layers 2/3. L2 neurons project to the IT neurons located in L5 whereas L3 project to the PT neurons in L5b indicating segregations between upstream cortical targets (Shepherd 2013). Optogenetic stimulation targeted to RBP4+ neurons in L5 combined with fMRI elicited strong local as well as brain-wide responses that are not found when stimulating upper layers of the motor cortex which only elicit local responses (Chan et al. 2022).

Theta phase locking of pyramidal neurons has previously been observed in moving rodents within the forelimb motor cortical region (Igarashi et al. 2013). Phase locking of pyramidal neurons was demonstrated to be dependent on the cortical layer. Pyramidal neurons in more superficial layers fired at the theta trough, but in deeper layers they instead fired broadly across the theta cycle (Igarashi et al. 2013). To study gamma oscillations in hippocampal slices, gamma phase advancing or delaying optogenetic feedback of pyramidal neurons, resulted in modulation of both the frequency and amplitude of gamma oscillations (Nicholson et al. 2018). Outside of these studies, very limited work has been undertaken using phase-specific or closed-loop stimulation methods that target pyramidal neurons.

In Chapter 3 we successfully implemented and validated our approach for tracking, optogenetically stimulating and recording electrophysiological signals in PV-Cre mice. We then proceeded to assess phase-specific modulation of pyramidal neurons in L5. We utilised an RBP4-Cre mouse line to gain precise experimental control of pyramidal neurons and injected a Cre-dependent optogenetic virus into the motor cortex (L5). Closed-loop phase-dependent optogenetic stimulation were then delivered to RBP4+ neurons to allow us to assess the phase-specific modulation of the ongoing theta oscillation and the role of RBP4+ neurons within the microcircuit. The previously used closed-loop, open-loop replay paradigm and open-loop stimulation protocols from Chapter 3 were used to assess theta modulation.

In this chapter, we additionally aimed to investigate the importance of the precise stimulation pattern used for phase-specific modulation and assess the significance of gamma rhythmicity on theta modulation. To effectively test this, we altered our original gamma stimulation pattern to make the gamma pulses less rhythmic and then assessed their ability to modulate the ongoing theta oscillation.

4.2 Methods

In brief, RBP4-Cre mice were injected with either a control or ChR2-containing virus before *in vivo* electrophysiological recordings were undertaken. During electrophysiological recordings, we used optogenetics to manipulate excitatory pyramidal neurons using closed-loop stimulation targeted to the 6Hz theta oscillation. Three different stimulation patterns were utilised to determine how these can influence changes in local theta power. These were targeted to four distinct phases of the ongoing theta oscillation (peak, descending, trough & ascending).

As well as control mice, for each stimulation condition we undertook no stimulation control recordings in both control and opsin mice as appropriate controls. Additionally, to control for the stimulation patterns received during closed-loop phase-specific stimulation we implemented another control, in which previous closed-loop stimulation patterns were utilised for 'open-loop replay' by replicating previously delivered trains of stimulation.

As data was collected using two laser power amplitudes, we examined whether there were significant differences between the modulation of theta power by stimulation at 1mW and 2mW in each group and phase, for both gamma and continuous stimulation patterns.

A linear mixed model (LME) with fixed effects of group, phase, and laser power (1mW and 2mW) and their interactions, alongside random effects of subject and date was created to test for differences in theta power modulation by laser power amplitude.

When stimulating with gamma stimulation there was no significant main effect of laser power ($F(1,334)=0.52$, $p=0.47$), and no significant interaction involving laser power [group*phase*laser power ($F(3,324)=1.54$, $p=0.20$); group*laser power ($F(1,334)=1.62$, $p=0.20$); phase*laser power ($F(3,324)=0.69$, $p=0.55$)], suggesting no significant differences between the effects on theta power for each group and phase at 1 or 2mW.

Additionally, there was no significant main effect of laser power ($F(1,336)=0.34$, $p=0.56$) or interaction terms including laser power [group*phase*laser power ($F(3,323)=0.18$, $p=0.91$); group*laser power ($F(1,336)=0.99$, $p=0.32$); phase*laser power($3,323)=1.39$, $p=0.25$)] when using continuous stimulation.

This suggests that there were no differences between these two laser powers on theta power. Therefore, as in the analyses in Chapter 3, we combined these two stimulation powers ('stimulation on') for all subsequent analyses.

In this chapter, data was collected from 4 RBP4-Cre control mice as well as 10 RBP4-Cre ChR2 mice. For a full summary of the methods and breakdown of mice used, please refer to Chapter 2.

4.3 Results

4.3.1 ChR2-GFP expression localised to cell bodies in layer 5

Firstly, it was important to verify the expression of ChR2 in RBP4-pyramidal neurons. RBP4-positive (RBP4+) pyramidal neurons in layer 5 of the motor cortex were targeted with ChR2, an excitatory opsin fused to GFP. To gain specificity of neuronal activation, Cre-dependent ChR2 & control viruses were used in conjunction with an RBP4-Cre mouse line (see methods; Chapter 2). Visual inspection of histology demonstrated that viral expression was limited to the cortex, and within the cortex, the majority of cell bodies were localised to layer 5 (Figure 4.1A & 4.1B). We could visually identify probe tracts using DiI in some sections. DiI was used primarily on the last day of recording and these sections could be compared to the Allen Brain Atlas to identify the recording location in comparison to the theoretical injection site targeted to confirm recordings were undertaken within the motor cortices. Currently, a neuronal marker for RBP4+ pyramidal neurons in layer 5 is lacking, however, we can confirm the localised expression of GFP to these neurons through detailed histology. To delineate cortical layers, FoxP2 which demonstrates strong expression within layer 6 was used. In addition, we stained for parvalbumin (PV) expression, to identify GABAergic

interneurons and verify that there was no overlap between PV and GFP to confirm GFP localisation to excitatory pyramidal neurons.

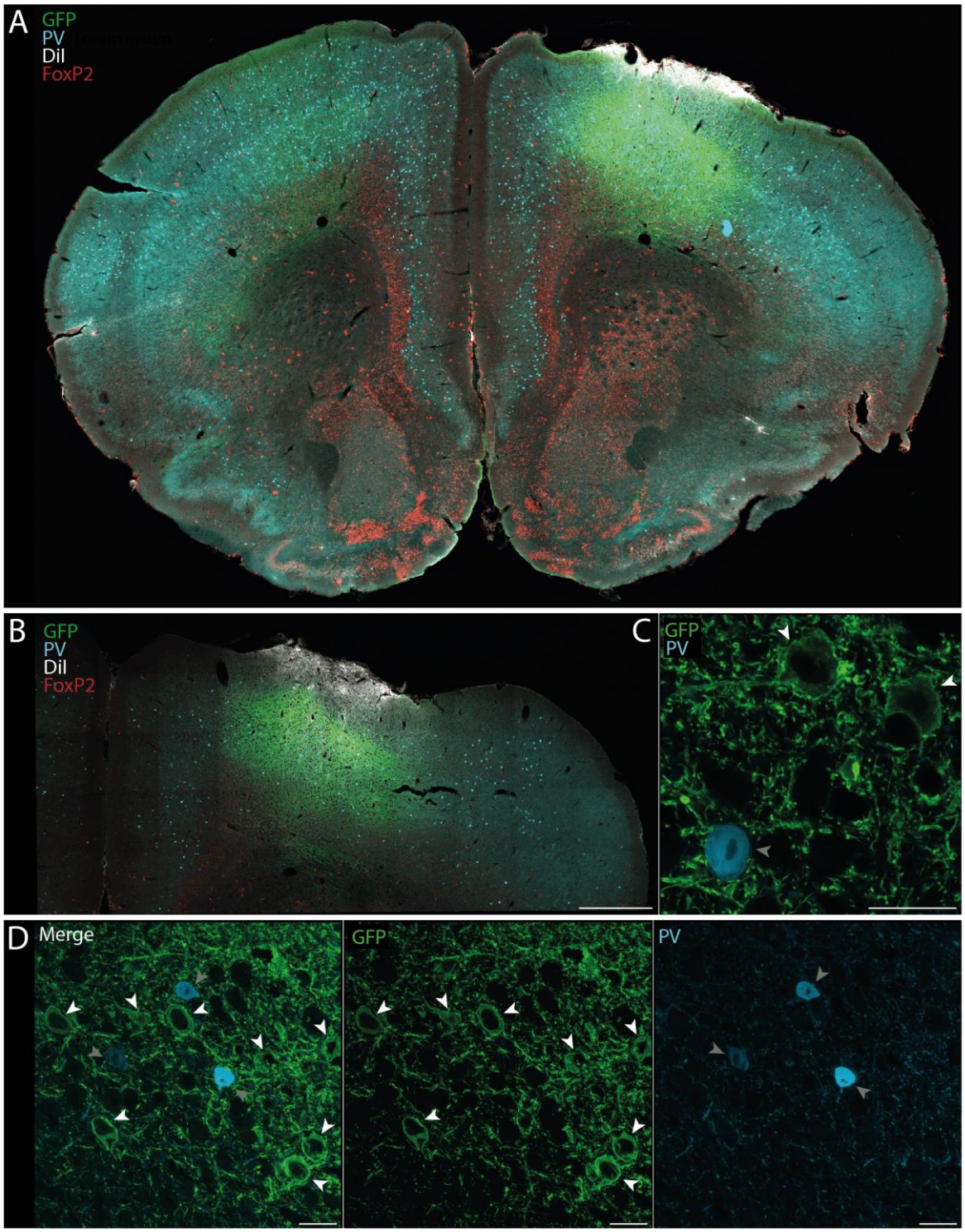


Figure 4.1 Localised expression of ChR2-GFP and no overlap with PV-expressing neurons

RBP4-Cre mice were injected either with a Cre-dependent control virus (GFP) or a virus containing ChR2-GFP. Low magnification (5x) image of PV, ChR2-GFP, and FoxP2 immunoreactivity on a whole brain coronal section alongside DiI predominantly used to mark probe location on the concluding day of recording (**A**) & within the

cortex (B; 20x magnification, scale bar = 500μm) ~1.77mm from bregma (Paxinos & Franklin's Mouse Atlas – Figure 16). The Cre-dependent virus remains within the cortex and does not spread to deeper structures, although demonstrates connections to the contralateral hemisphere (**B**). Higher magnification images (63x) of ChR2-GFP & PV expression from a section of layer 5 within the motor cortex (**C & D**; scale bar = 20μm). There is no neurochemical marker to identify the presence of RBP4, instead, we demonstrate separation between cells identified as GFP expressing pyramidal neurons expressing and inhibitory interneurons expressing the calcium-binding protein Parvalbumin (PV) - Arrows: white – GFP; grey – PV.

4.3.2 Accurate phase targeting of ongoing theta oscillations

In addition to appropriate ChR2-GFP expression, we next verified that we could accurately target theta oscillations in RBP4-Cre mice. As demonstrated in PV-Cre mice, we simultaneously recorded the LFP while performing targeted closed-loop stimulation. We delivered optogenetic stimulation targeted to four distinct phases of the ongoing theta oscillation (see Chapter 2; Figure 2.3). Post hoc analyses demonstrate accurate phase targeting for all stimulation types at each phase of the ongoing theta oscillation (Figures 4.2 & 4.3).

These demonstrate that the centre-point of the stimulation (0ms, dotted line) in the evoked potential (triggered average of the LFP) is phase-specific for both gamma (Figure 4.2) and continuous stimulation (Figure 4.3). This additionally demonstrates a high degree of alignment to each of the targeted phases. Regardless of which stimulation pattern, this was always the case in the control mice (Figure 4.2A; Figure 4.3A), as well as when stimulation was off in the opsin mice (Figure 4.2B & Figure 4.3B). When stimulation was on in opsin mice (Figure 4.2B & Figure 4.3B), the accuracy exhibited greater variability, likely a result of the stimulation effect on the LFP itself. As such, the centre-point of stimulation appears more accurate than control mice or stimulation off conditions when targeting the trough, and less accurate when targeting the peak or ascending phases (Figure 4.3B).

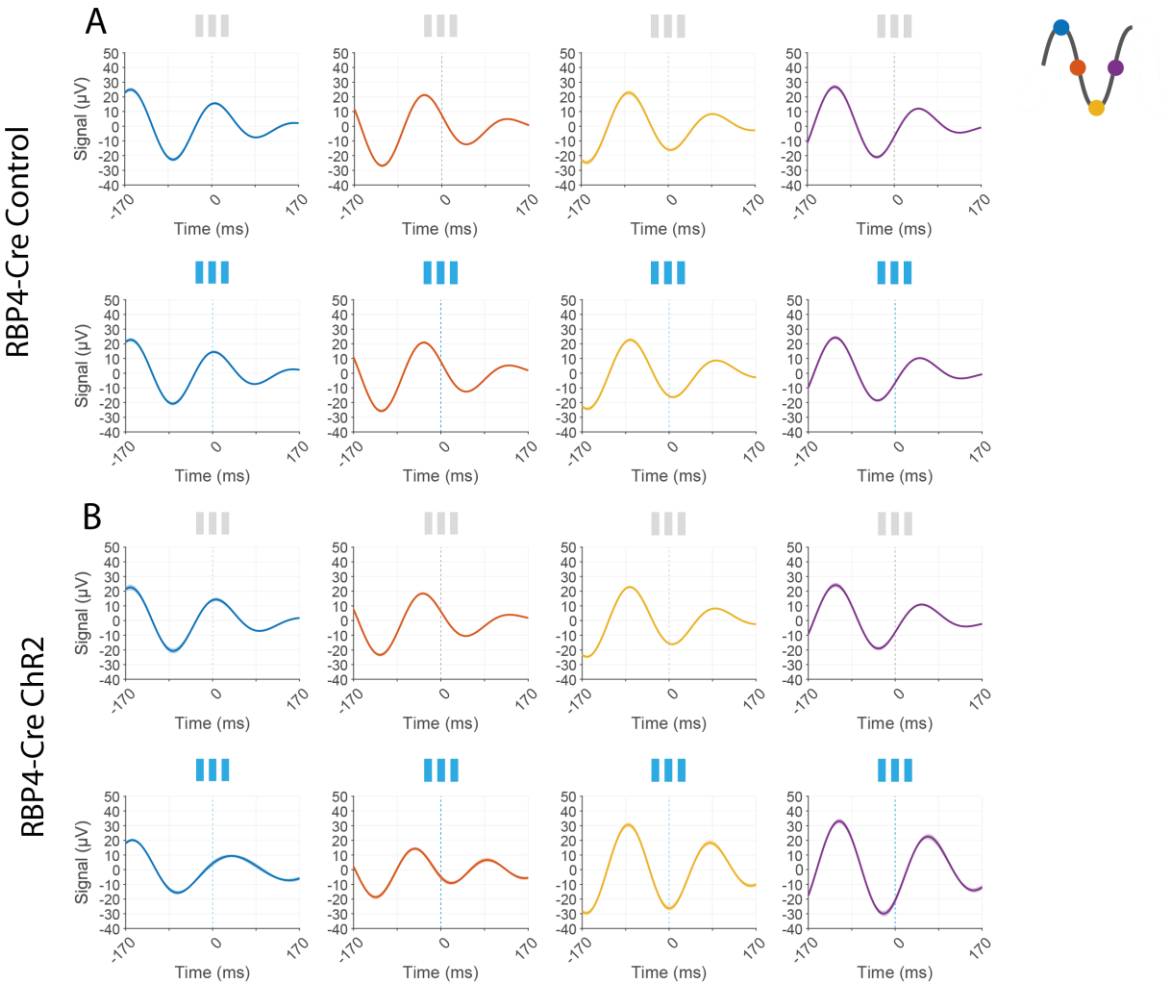


Figure 4.2 Accurate phase-targeting of ongoing theta oscillation with gamma stimulation

Stimulation triggered averages of local field potentials in response to closed-loop optogenetic gamma stimulation in RBP4-Cre mice (n=4 control (**A**); n=10 ChR2 (**B**)). The four columns denote each of the four targeted phases: peak, descending, ascending, and trough, identified with a colour-coded key. These are provided for both stimulation off (0mW; grey pulses) and stimulation on (1 or 2mW; blue pulses). The dotted line at '0' on the x-axis (Time (ms)) represents the centre-point of stimulation, which falls immediately prior to the targeted phase of the ongoing theta oscillation. This is plotted across two theta cycles one on either side of the stimulation centre-point. Mean activity in the 6±1.5Hz theta band was filtered offline with a zero-phase 4th order Butterworth filter. The coloured lines represent the mean of all the sessions for each combination of stimulation on/off and phase. Lighter shading represents the standard error of the mean (SEM). The total number of sessions used to calculate the mean & SEM in control mice was n=15 (15 recordings per phase stimulation off, n=30 recordings per phase stimulation on). In opsin mice, this was n=41 (40 recordings per phase stimulation off, n=60 recordings per phase stimulation on).

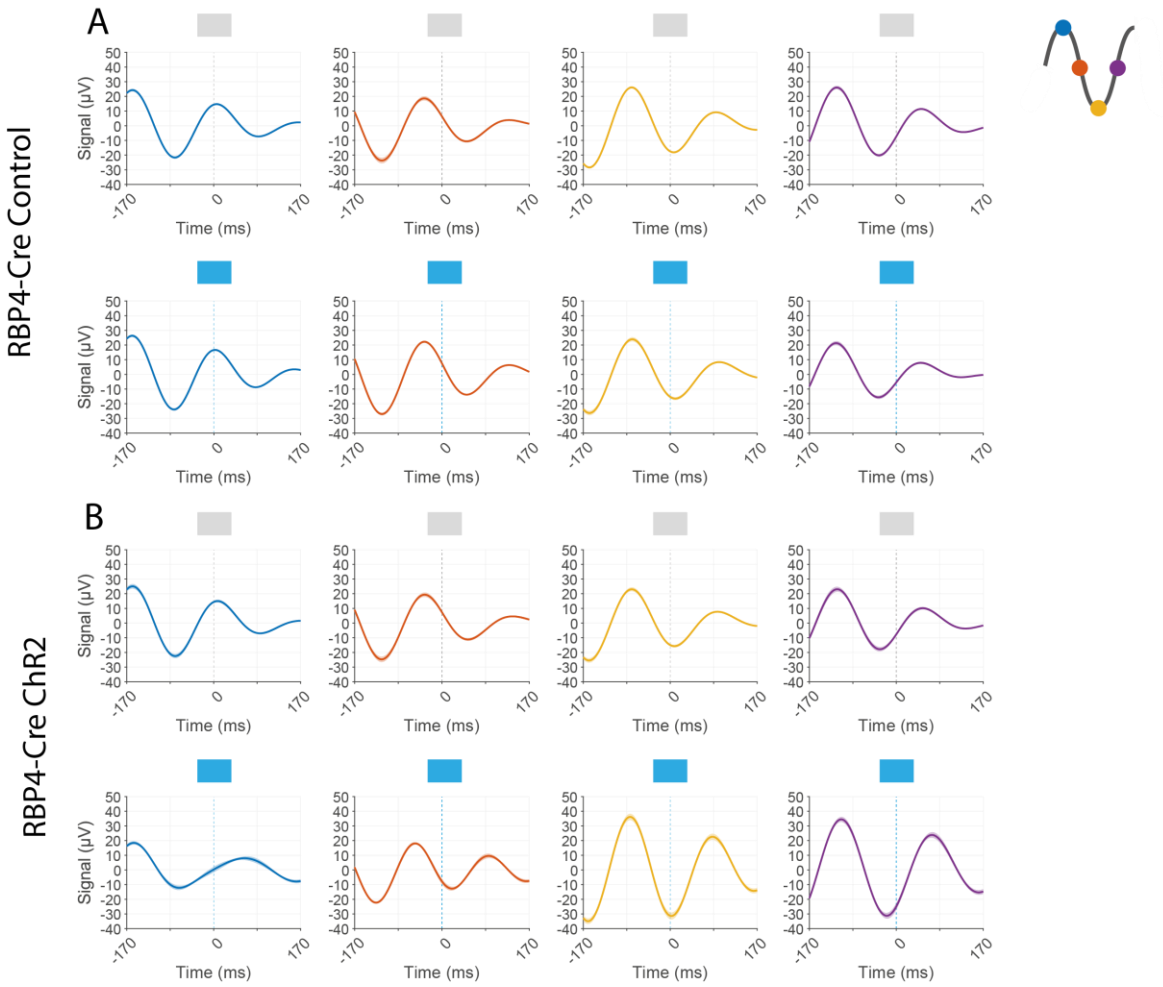


Figure 4.3 Accurate phase-targeting of ongoing theta oscillation with continuous stimulation

Stimulation triggered averages of local field potentials in response to closed-loop optogenetic gamma stimulation in RBP4-Cre mice (n=4 control (**A**); n=10 stimulation on ChR2 & n=6 stimulation off ChR2 (**B**)). The four columns denote each of the four targeted phases: peak, descending, ascending, and trough, identified with a colour-coded key. These are provided for both stimulation off (0mW; grey pulses) and stimulation on (1 or 2mW; blue pulses). The dotted line at '0' on the x-axis (Time (ms)) represents the centre-point of stimulation, which falls immediately prior to the targeted phase of the ongoing theta oscillation. This is plotted across two theta cycles one on either side of the stimulation centre-point. Mean activity in the 6±1.5Hz theta band was filtered offline with a zero-phase 4th order Butterworth filter. The coloured lines represent the mean of all the sessions for each combination of stimulation on/off and phase. Lighter shading represents the standard error of the mean (SEM). The total number of sessions used to calculate the mean & SEM in control mice was n=15 (15 recordings per phase stimulation off, n=30 recordings per phase stimulation on). In opsin mice, this was n=22 sessions (21-23 recordings per phase stimulation off) and n=41 sessions (n=60 recordings per phase stimulation on).

4.3.3 Closed-loop gamma stimulation

Having established our ability to target different phases of the theta oscillation in RBP4-Cre mice, we next determined whether we could modulate motor cortical theta power using closed-loop optogenetic stimulation, and if so, whether this was phase-

dependent. As outlined in Chapter 3 for PV+ interneurons, we aimed to test the ability of different stimulation patterns to drive phase-dependent modulation. To determine the role of the frequency and pattern of stimulation, we tested the same two stimulation patterns, gamma and continuous. Following this, to determine whether gamma rhythmicity was important for phase-specific modulation, we devised and tested a third stimulation pattern – random gamma. Closed-loop stimulation was targeted to the ongoing 6Hz theta oscillation and LFPs were measured with Neuronexus probes. The first type of stimulation we tested was gamma frequency, to simulate theta-gamma coupling.

The following data were collected when stimulation was off (0mW) and when stimulation was on (1 & 2mW) (Control: n=4 mice, 15 sessions; Opsin: n=10 mice, 41 sessions).

4.3.3.1 Closed-loop gamma stimulation of the motor cortex results in phase-specific modulation of theta power in RBP4-Cre mice

We investigated the effect closed-loop phase-specific gamma stimulation has on local LFP power. Mean power spectral density plots (PSD) are shown in Figure 4.4A for both control and opsin mouse groups at each targeted phase. Gamma stimulation was either off (0mW; grey bars) or on (1 or 2mW; blue bars). These opsin-negative and stimulation off controls allow us to pertain levels of baseline activity and a comparison between the effects of the opsin and potential non-specific effects such as visual evoked potentials.

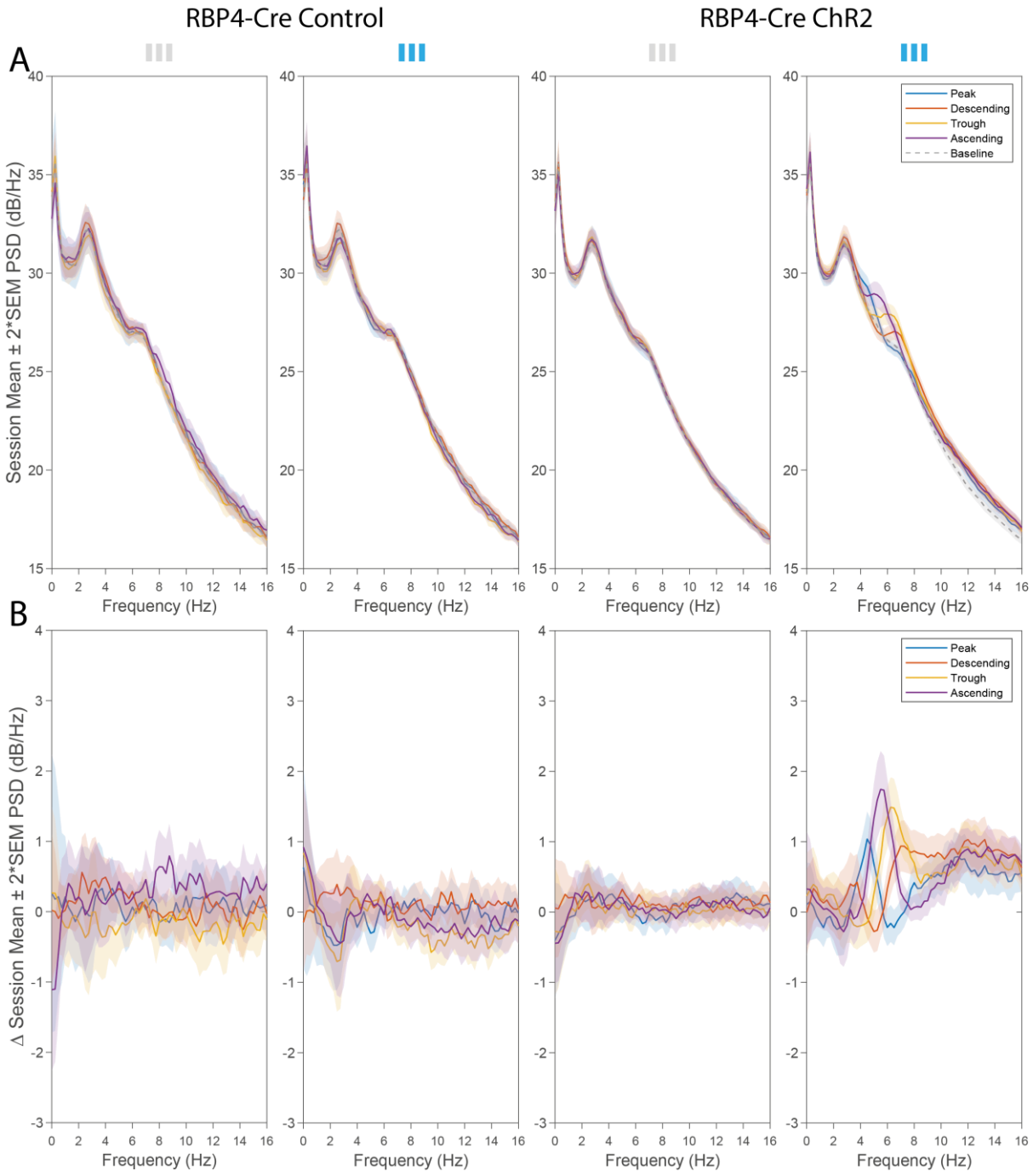


Figure 4.4 Phase-dependent effect in local LFP following closed-loop gamma stimulation of RBP4+ pyramidal neurons

Mean power spectral density (±2*SEM) from 0-16Hz for both RBP4-Cre control (n=4) and opsin mice (n=10), targeting 4 different phases of the theta oscillation with gamma stimulation (**A**). Stimulation was either off (0mW; grey pattern) or on (1 or 2mW; blue pattern). The number of sessions to calculate the mean in control mice was n=15 (15 recordings per phase stimulation off, n=30 recordings per phase stimulation on). In opsin mice this was n=41 (40 recordings per phase stimulation off, n=60 recordings per phase stimulation on). Within each session, a session baseline was calculated from a baseline recorded at the beginning of each session, combined with all unstimulated recordings throughout a session. The mean session baseline was then plotted on each plot for each group and stimulation on or off. The mean PSDs (±2*SEM) in which the baseline was removed from each session were also plotted for both control and opsin mice (**B**).

To investigate whether closed-loop stimulation could induce phase-specific effects on theta power, the baseline (mean calculated from the recorded baseline file at the start of every session and all unstimulated recordings within a session) was subtracted (Figure 4.4B) and power spectral density estimates were extracted across the target range (4.5-7.5Hz, Figure 4.5) for each target phase. We used a LME to test whether phase-dependent modulation was specific to when the opsin was present ('control' & 'opsin') and stimulation was on (laser power; 'off' and 'on'). In line with this, the LME (fixed effects of group, laser power & phase and all combinations of interactions, random effects of subject & date) showed a significant group*phase interaction ($F(3,554)=2.65$, $p=0.048$) and significant group*laser power interaction ($F(1,545)=25.45$, $p<0.001$). These interactions are as expected because we anticipated only the opsin group to vary by phase and only when stimulation is on. This is highlighted by the results in Figure 4.4A & 4.4B. Additionally the phase*laser power interaction was significant ($F(3,544)=3.36$, $p=0.018$). The main effects of phase and laser power were also significant ($F(3,544)=3.78$, $p=0.01$) & $F(1,545)=15.26$, $p<0.001$) respectively). However, there was no significant effect of the three-way interaction between group, phase, and laser power ($F(3,544)=2.53$, $p=0.056$). These results confirm that phase-dependent effects are dependent on both stimulation and opsin presence, thus further analyses focus only on experimental data.

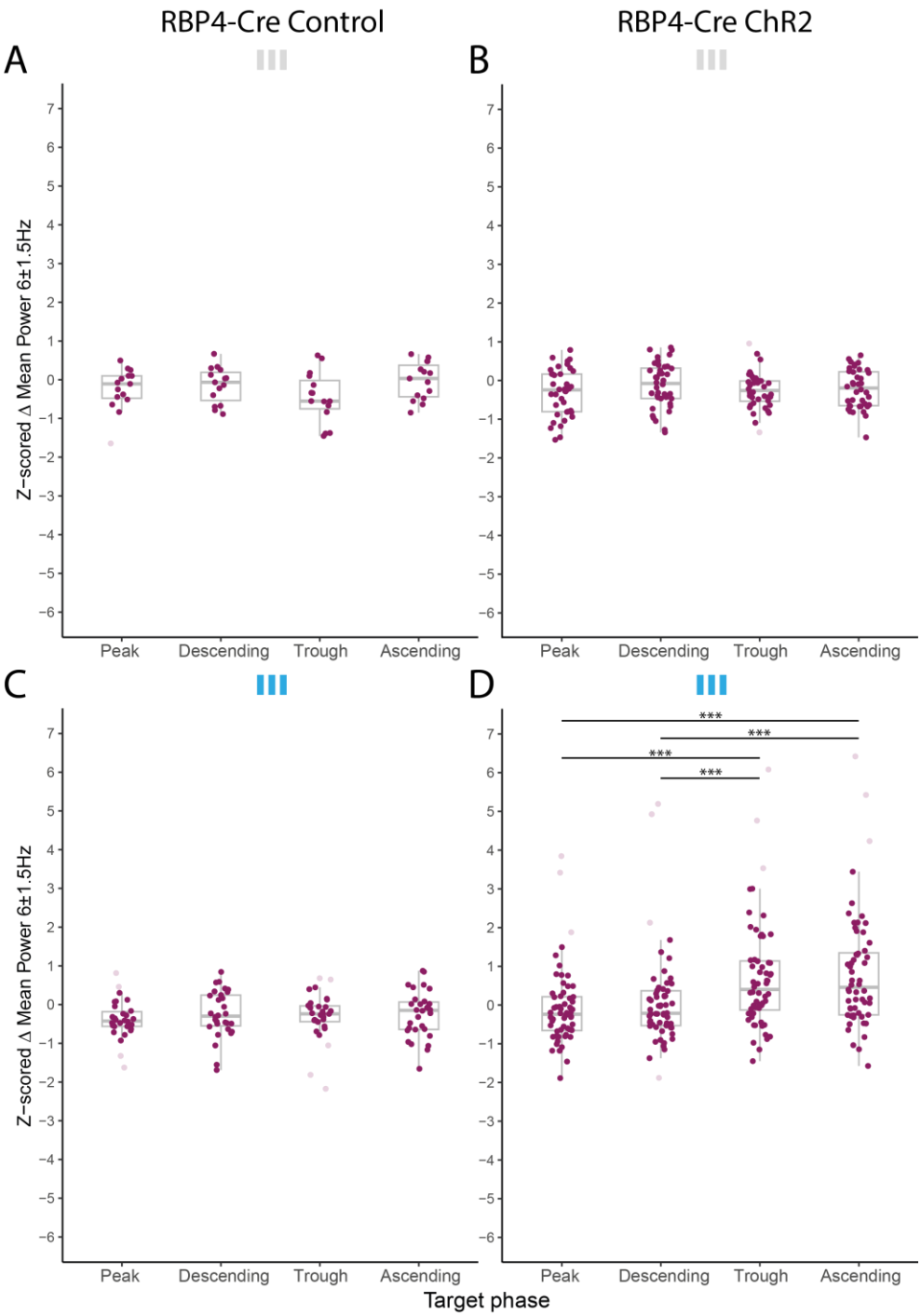


Figure 4.5 Gamma stimulation of RBP4+ pyramidal neurons lead to phase-dependent effects on theta power

Boxplots with the z-scored change in theta power with respect to baseline extracted between 4.5-7.5Hz (6Hz ± 1.5) for both control (n=4; **A & C**) and opsin RBP4-Cre mice (n=10; **B & D**) are shown when stimulation was on (1 or 2mW; blue patterns) or off (0mW; grey patterns). Stimulation was targeted to 4 phases of the ongoing theta oscillation, the peak, descending, trough, and ascending phases. A further breakdown of the total number of sessions for gamma stimulation: RBP4 control (n=15 sessions, n=15 recordings per phase stimulation off, n=30 per phase stimulation on) & RBP4 ChR2 (n=41 sessions; n=40 recordings per phase stimulation off, n=60 per phase stimulation on). Each session will contain multiple recordings - usually 1 per phase, per laser power for stimulation on data, as data was often collected at both 1 & 2mW. The baseline consisted of a mean calculated from the baseline recorded at the beginning of each session and all unstimulated recordings from

within a session. The grey boxes represent the interquartile range and median values from the data set, and the whiskers extend to minimum and maximum values calculated from their quartile ±1.5*IQR for each grouped session. Session means for each laser power are plotted as individual scatter points for their respective group and stimulation type. Lighter scatter points represent data points that lie outside a threshold set as the respective quartile value ±1.5*IQR. There were no significant effects when stimulation was off (all $p>0.05$). Significant differences ($p<0.05$) were identified when stimulation was on between the peak and trough, peak and ascending, descending and trough and ascending and descending phases in opsin mice (**D**) (LME, followed by pairwise post hoc t-tests with Tukey adjustment).

4.3.3.2 Gamma stimulation leads to phase-specific effects on theta power in opsin but not control mice

To follow up on the significant interactions presented above, we first wanted to address the hypothesis that when ChR2 is present in RBP4+ pyramidal neurons, there are phase-specific differences in theta power when stimulation is on. A LME with fixed effects of group (control, opsin) and phase as well as their interaction (random effects of subject and data) was run. We anticipated changes in theta power only within the opsin group when stimulation was on, as demonstrated by a significant group*phase interaction ($F(3,324)=5.82$, $p<0.001$). There was an additional significant main effect of phase ($F(3,324)=7.62$, $p<0.001$), indicating that stimulation differentially affected theta power at different phases regardless of the mouse group. Pairwise comparisons (t-tests with Tukey adjustment) revealed significant differences between several phases. Specifically, between the peak and trough ($p<0.0001$), peak and ascending phase ($p=0.0001$), descending phase and trough ($p=0.0005$), and finally the descending and ascending phases ($p<0.0001$) in opsin mice (Figure 4.5D). No significant differences were found between different phases in the control group (Figure 4.5C).

4.3.3.3 Gamma stimulation in opsin mice results in phase-specific effects on theta power only when stimulation is on

We then followed up on another of the significant interactions presented in our overarching LME model, stimulation-by-phase, which we investigated in the opsin mouse group.

To address this, LME models with the main effects of laser power (stimulation on (1 or 2mW) or off (0mW)) and phase were tested with their interaction term. We hypothesised that theta band power would be altered in the opsin group when stimulation was on. There was a significant interaction between laser power and phase ($F(3,369)=8.48$, $p<0.001$) as would be expected, as we anticipated no change in theta power when stimulation was off whereas when stimulation was on for theta power to change across each phase. There was additionally a significant main effect of laser power ($F(1,370)=63.46$, $p<0.001$) – this was unexpected, as we hypothesised that there would only be changes in theta power when stimulation is on in the opsin group. Along with this, the main effect of phase was also unexpectedly significant ($F(3,369)=8.44$, $p<0.001$).

4.3.4 Closed-loop continuous stimulation

Having established that gamma frequency stimulation resulted in phase-specific modulation of theta power in RBP4-Cre mice, we subsequently proceeded to determine whether phase-specific modulation was specific to stimulation pattern. We implemented our second stimulation type – continuous, as we did in PV-Cre mice, which was delivered across ¼ of the theta cycle, centred to the target phase.

The following data were collected when continuous stimulation was off (0mW) and on (1 & 2mW) (Control: n=4 mice, 15 sessions; Opsin: n=10 mice stimulation on, 41 sessions & n=6 mice stimulation off, 22 sessions).

4.3.4.1 Closed-loop continuous stimulation of the motor cortex results in phase-specific modulation of theta power in RBP4-Cre mice

Following this, we determined the effect continuous phase-specific theta stimulation had on the local LFP. In Figure 4.6 mean PSD plots for both control and opsin are shown, continuous stimulation is either off (0mW; grey bars) or on (1 or 2mW; blue bars).

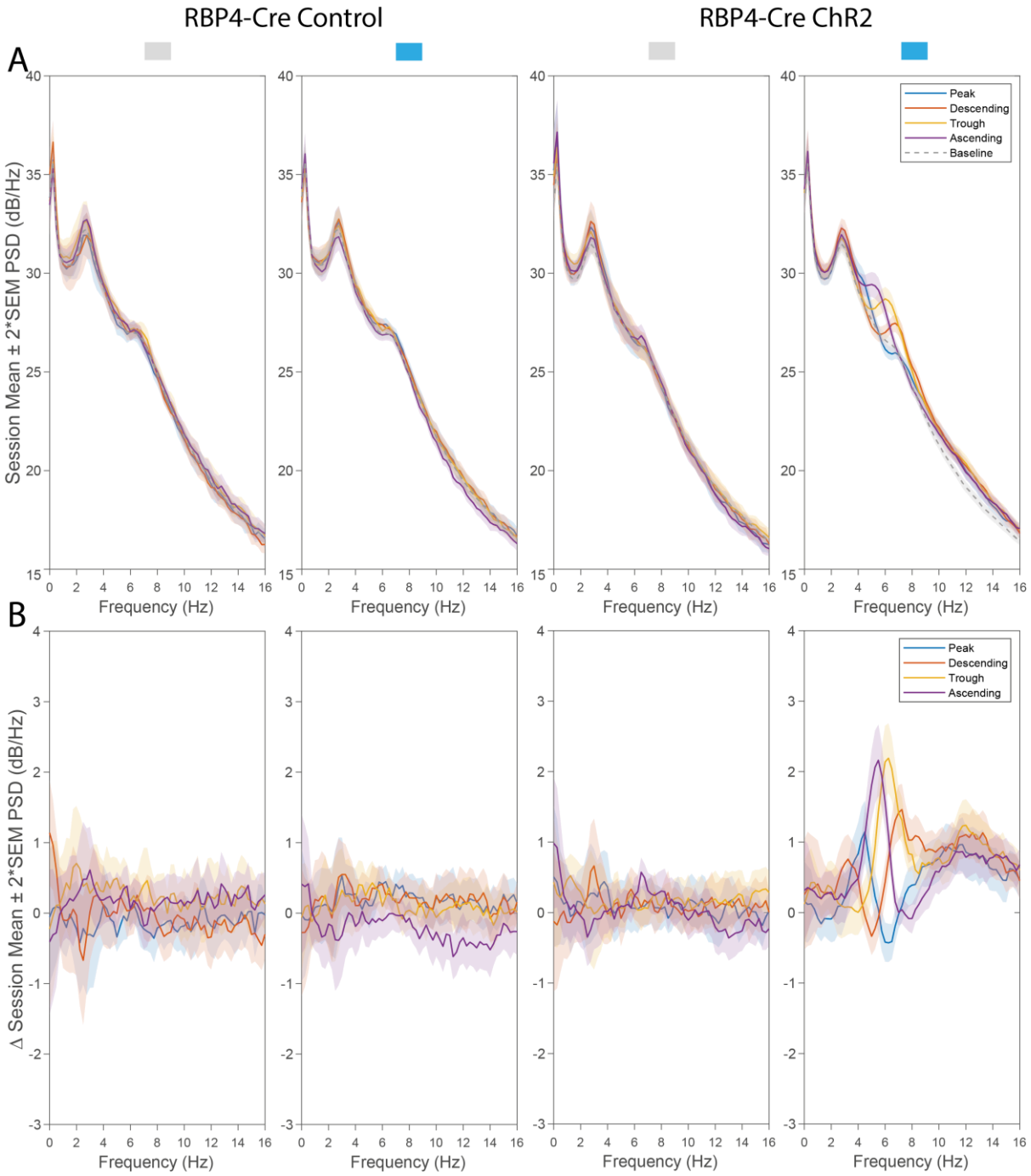


Figure 4.6 Phase-dependent effect in local LFP following closed-loop continuous stimulation of RBP4+ pyramidal neurons

Mean power spectral density (±2*SEM) from 0-16Hz for both RBP4-Cre control (n=4) and opsin mice (n=10 stimulation on, n=6 stimulation off), targeting 4 different phases of the theta oscillation with continuous stimulation (**A**). Stimulation was either off (0mW; grey pattern) or on (1 or 2mW; blue pattern). The number of sessions to calculate the mean in control mice was n=15 (15 recordings per phase stimulation off; 30 recordings per phase stimulation on). In opsin mice this was n=22 sessions (21-23 recordings per phase stimulation off) and n=41 sessions (60 recordings per phase stimulation on). Within each session, a session baseline was calculated from a baseline recorded at the beginning of each session, combined with all unstimulated recordings throughout a session. The mean session baseline was then plotted on each plot for

each group and stimulation on or off. The mean PSDs (±2*SEM) in which the baseline was removed from each session are also plotted for both control and opsin mice (**B**).

To investigate the role of continuous stimulation on theta power modulation, we subtracted the baseline (Figure 4.6B) and extracted power spectral density estimates between 4.5 and 7.5Hz (Figure 4.7). We performed a LME model to test our overarching hypothesis that when stimulating ('off' or 'on') the ongoing theta oscillation with closed-loop continuous stimulation, there would be phase-specific differences between the experimental groups of control & opsin. The LME had fixed effects of group, laser power & phase with all interaction combinations. There was a significant effect of the three-way interaction term (group*phase*laser power; $F(3,469)=6.70$, $p<0.001$), as expected, as we only anticipated a change in theta power across phase when stimulation is on in the opsin group, therefore following analyses focus on our experimental conditions. Alongside this, other interaction terms group*phase and group*laser power were also significant, [($F(3,469)=3.5$, $p=0.015$) and ($F(1,478)=12.14$, $p<0.001$) respectively]. However, the interaction between phase and laser power was not significant ($F(3,469)=0.84$, $p=0.47$). The main effects of phase and laser power were also significant [($F(3,469)=5.98$, $p<0.001$) & ($F(1,478)=20.35$, $p<0.001$) respectively].

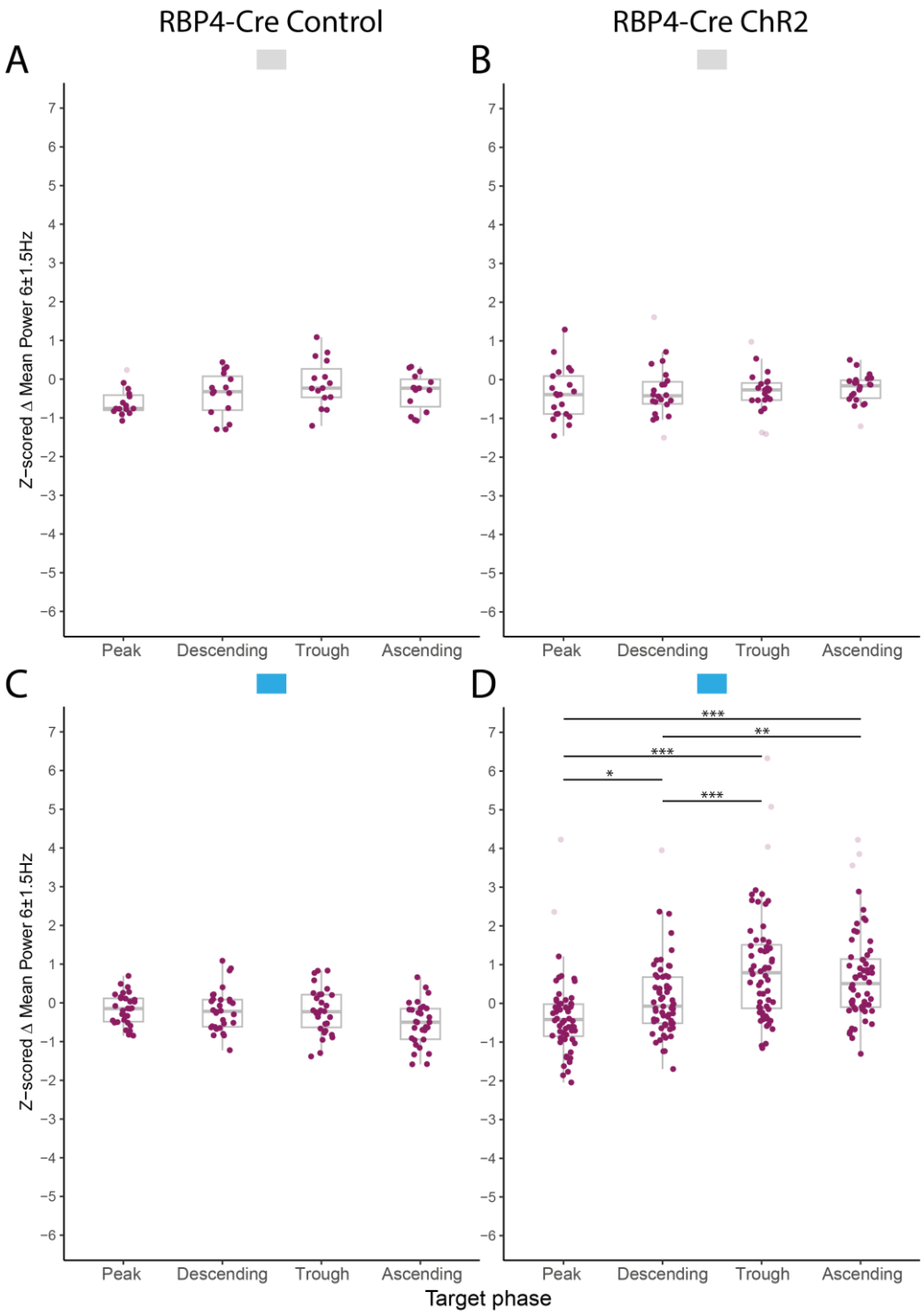


Figure 4.7 Continuous stimulation of RBP4+ pyramidal neurons lead to phase-dependent effects on theta power

Boxplots with the z-scored change in theta power with respect to baseline extracted between 4.5-7.5Hz (6Hz ± 1.5) for both control (n=4; **A & C**) and opsin RBP4-Cre mice (n=10 stimulation on; n=6 stimulation off; **B & D**) are shown when stimulation was on (1 or 2mW; blue patterns) or off (0mW; grey patterns). Stimulation was targeted to 4 phases of the ongoing theta oscillation, the peak, descending, trough and ascending phases. A further breakdown of the total number of recordings for continuous stimulation: RBP4 control (n=15 sessions; n=15 recordings per phase stimulation off; n=30 recordings per phase stimulation on) & RBP4 ChR2 (n=22 sessions stimulation off, n=21-23 recordings per phase; n=41 sessions stimulation on, n=60 recordings per phase). Each session contains multiple recordings - usually 1 per phase, per laser power for stimulation on

data, as data was often collected at both 1 & 2mW. The baseline consisted of a mean calculated from the baseline recorded at the beginning of each session and all unstimulated recordings from within a session. The grey boxes represent the interquartile range and median values from the data set, and the whiskers extend to minimum and maximum values calculated from their quartile ±1.5*IQR for each grouped session. Session means for each laser power are plotted as individual scatter points for their respective group and stimulation type. Lighter scatter points represent data points that lie outside a threshold set as the respective quartile value ±1.5*IQR. Significant differences ($p<0.05$) were found between the peak and descending, peak and trough, peak and ascending and descending and ascending phases in opsin mice (**D**) (LME, followed by pairwise post hoc t-tests with Tukey adjustment).

4.3.4.2 Continuous stimulation leads to phase-specific effects on theta power in opsin but not control mice

Following up on significant interactions, we first wanted to address whether there were phase-specific changes in theta power when stimulation was on, but only in the opsin (ChR2+) group. We performed a LME with fixed effects of group (control, opsin) and phase as well as their interaction (random effects of subject and data). In accordance with our hypothesis that stimulation targeted to ChR2+ pyramidal neurons in the opsin group would alter theta power across phase, there was a significant group and phase interaction when stimulation was on ($F(3,323)=14.93$, $p<0.001$). Additionally, there was a significant main effect of group ($F(1,16)=4.88$, $p=0.04$), which we expected as theta power was hypothesised to only change in the opsin group and not the control group. However, there was an unexpected main effect of phase ($F(3,323)=8.58$, $p<0.001$), indicating that there were differences in theta power between the phases regardless of the overall group. Following this significant group and phase interaction, post-hoc pairwise t-tests with Tukey adjustment were performed to further explore differences across phase. This analysis revealed significant differences between the peak and descending phase ($p=0.0358$), the peak and trough ($p<0.0001$), the peak and ascending phase ($p<0.0001$), the descending phase and the trough ($p<0.0001$), and the descending and ascending phases

(p=0.0025) – Figure 4.7D. There were no significant differences between any phases in the control group (Figure 4.7C).

4.3.4.3 Continuous stimulation in opsin mice leads to phase-specific effects of theta power only when stimulation is on

Next, we determined whether there was a significant stimulation-by-phase interaction in opsin mice. We hypothesised that modulation of theta power by phase would only occur when stimulation was on in the opsin group.

To address this hypothesis, a LME model was performed with the main effects of laser power (stimulation on (1 or 2mW) or off (0mW)) and phase alongside their interaction term. There was a significant interaction between laser power and phase ($F(3,297)=6.46$, $p<0.001$). This was expected as theta power was hypothesised to be modulated across different phases only when stimulation was on and not when stimulation was off. Additionally, there were significant main effects of laser power and phase [($F(1,306)=33.23$, $p<0.001$) & ($F(3,297)=9.26$, $p<0.001$) respectively] which were unexpected.

4.3.5 Open loop stimulation

4.3.5.1 Stimulation patterns resulting from closed-loop stimulation do not underly phase-dependent changes in theta power

Additionally, we investigated whether changes in theta power at each phase were a result of the stimulation pattern that was delivered when interacting with the underlying oscillation. We addressed this using our open-loop replay paradigm, in which we can directly compare the effects of real-time closed-loop stimulation to their resultant stimulation patterns. In the following analyses, only sessions in which there

were open-loop replays from within the same session were included (n=24 gamma & n=12 continuous sessions).

Closed-loop optogenetic stimulation targeted to RBP4+ pyramidal neurons in the motor cortices led to phase-specific changes in theta power as previously demonstrated (Figures 4.4-4.7). Figure 4.8 shows mean PSD plots of both gamma (blue pulses) and continuous (blue bar) stimulation, either from the original closed-loop recordings of sessions that include replay, or open-loop replay within these same sessions. The baseline was subtracted, and power spectral density estimates were extracted between 4.5 and 7.5Hz which are plotted in Figure 4.8I-L. These data demonstrate stimulation pattern alone, in the absence of phase-locking cannot reproduce phase-specific effects (Figure 4.8: B, D, F & H) demonstrated with closed-loop recordings (Figure 4.8: A, C, E & G).

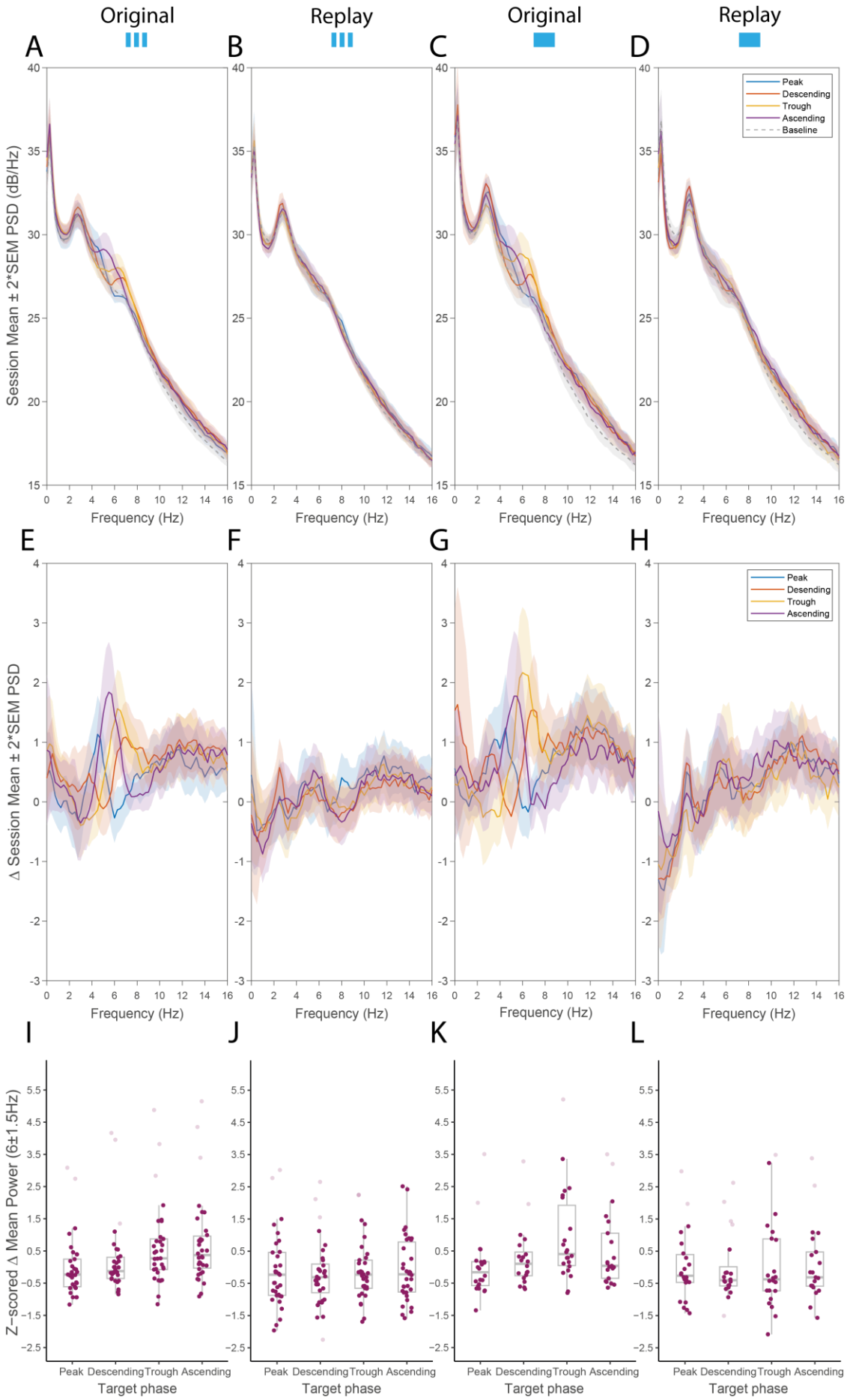

Original
Replay
Original
Replay
A
B
C
D
Peak
Descending
Trough
Ascending
Baseline
Session Mean ± 2*SEM PSD (dB/Hz)
Frequency (Hz)
E
F
G
H
Peak
Desending
Trough
Ascending
Δ Session Mean ± 2*SEM PSD
Frequency (Hz)
I
J
K
L
Z−scored Δ Mean Power (6±1.5Hz)
Peak Descending Trough Ascending
Target phase

Figure 4.8 Local theta LFP and z-scored change in theta power following gamma and continuous closed-loop stimulation and their open-loop replays

Mean power spectral density (±2*SEM) from 0-16Hz in RBP4-Cre opsin mice gamma (n=9) or continuous (n=4) stimulation on (1 or 2mW; blue patterns) (**A-D**). Plots demonstrate PSD for closed-loop optogenetic stimulation targeting 4 different phases of the theta oscillation (original) as well as open-loop replay (replay), in which a previous closed-loop recording is played back to the mouse within the same session. More specifically, the number of sessions to calculate the mean for gamma (n=24; n=32-34 recordings per phase) and continuous (n=12; n=20-22 recordings per phase), some sessions have data from both 1 & 2mW. Within each session, a session baseline was calculated from a baseline recorded at the beginning of each session, combined with all unstimulated recordings throughout a session. The mean session baseline is then plotted on each plot for each group and stimulation either on or off. The mean PSDs (±2*SEM) in which the baseline was removed from each session are also plotted for both control and opsin mice (**E-H**). Boxplots demonstrate z-scored change in theta power with respect to baseline extracted between our target range of 4.5-7.5Hz (6Hz±1.5) (Gamma: n=9 mice, n=24 sessions with a total of 32-34 recordings per phase; Continuous: n=4 mice, n=12 sessions with a total of 20-22 recordings per phase) (**I-L**). Grey boxes represent the interquartile range and median values from the data set, and whiskers extend to the minimum and maximum values calculated as their respective quartile ±1.5*IQR. Session means for each laser power are plotted as individual scatter points for their respective group and stimulation type. Lighter scatter points represent data points that lie outside a threshold set as the respective quartile value ±1.5*IQR.

To analyse the effects of closed-loop and open-loop replay stimulation, the mean change in theta power were calculated between the most and least amplifying phases during closed-loop stimulation for each stimulation pattern and amplitude. Closed-loop recordings were matched with their open-loop counterpart and the same phases were taken to calculate the difference during open-loop replay stimulation. The data was then z-scored in line with previous analyses. Data were only included if it was available for all four phases for comparison, these have been plotted in Figure 4.9A (gamma) & 4.9B (continuous). These were compared for each stimulation pattern between closed-loop and open-loop replay conditions (main effect: stimulation type) using a LME model with random effects of subject and date. Both gamma and continuous stimulation led to a significant effect [($F(1,46)=61.68$, $p<0.001$) & ($F(1, 25)=34.16$, $p<0.001$) respectively]. This indicates that stimulating with matching stimulation patterns in an open-loop manner is insufficient to drive the same differences in theta power between the most and least amplifying phases.

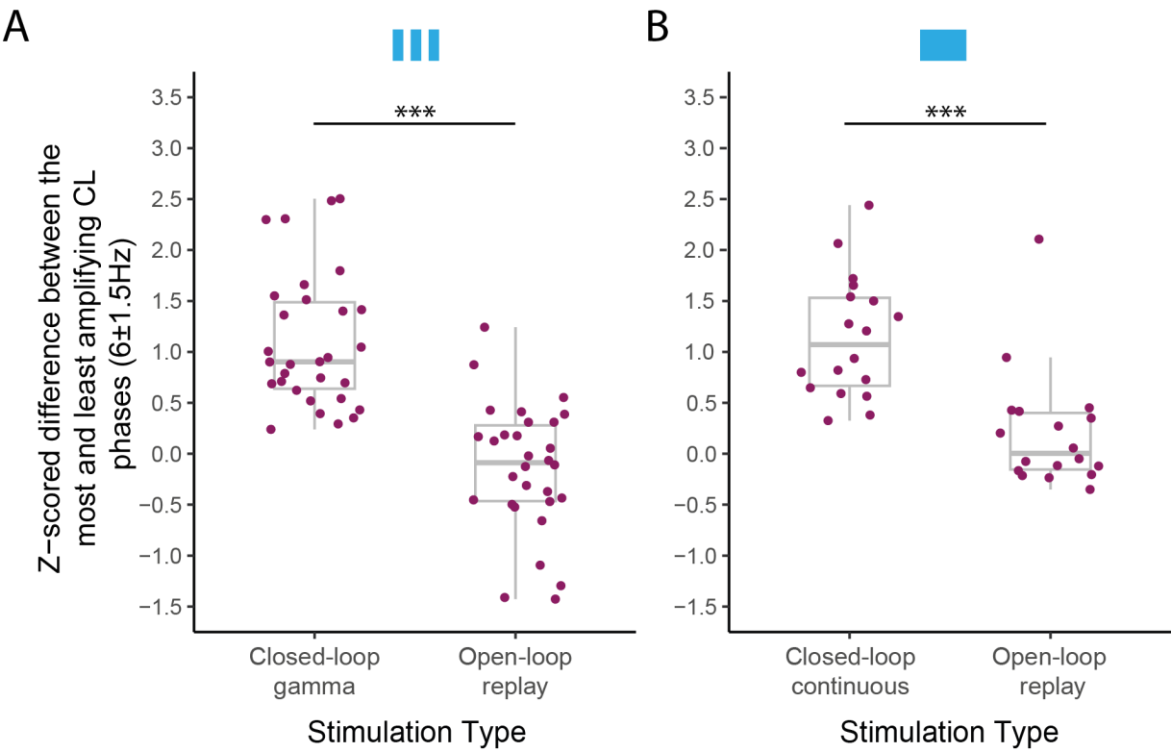


Figure 4.9 Z-scored difference in theta power between the most and least amplifying closed-loop phases identified following gamma and continuous stimulation and their open-loop replay counterparts

Grey boxes represent the interquartile range and median values from the data set, and whiskers extend to the minimum and maximum values calculated as their respective quartile ±1.5*IQR (**A & B**). For each main stimulation pattern (gamma/continuous) the difference between the most and least amplifying phase for a closed-loop recording are plotted as individual scatter points, the difference between the same phases is then taken in the open-loop recording and displayed as individual scatter points. To perform statistical analyses, the minimum and maximum values extracted from the closed loop recording and the difference between them were calculated. The difference between these same phases were then calculated in the open-loop replay recording. Significant differences ($p<0.05$) were found between the z-scored difference in theta power of the most and least amplifying phases in each specific closed-loop recording and their open-loop counterpart for both gamma (**A**) and continuous (**B**) stimulation (LME). In these specific analyses only sessions that had a complete set of data for all four phases at that specific laser power were used (Gamma: n=9 mice, n=20 sessions, 10 sessions contained data from both amplitudes; Continuous: n=4 mice, n=10 sessions, 8 sessions contained data from both amplitudes).

4.3.5.2 Open-loop gamma and continuous stimulation modulate theta power in opsin mice, but only when consistently stimulated

To examine the importance of the closed-loop relationship with the theta oscillation, we devised matching open-loop stimulation patterns that had no interaction to determine differences in modulation of theta power.

We utilised the same four patterns of OL stimulation, as with PV-Cre mice. As previously stated, OL-gamma and OL-continuous stimulation were matched to the closed-loop patterns of stimulation in terms of the number of pulses, their lengths, and the laser power amplitudes used, however, they were delivered with no relationship to an oscillation. Between subsequent stimuli were 167ms gaps. We also implemented a variation of OL-gamma and OL-continuous in which 1-1.2 second gaps were inserted between every 6 stimulation bursts (OL-gamma gaps and OL-continuous gaps). As with all previous analyses, data collected at both 1mW and 2mW were combined to enable direct comparisons.

Mean PSD plots for each of the four stimulation types are represented in Figure 4.10 for both control and opsin groups, in which stimulation is either off (0mW; grey patterns) or on (1 or 2mW; blue patterns). Lines following the stimulation pattern denote the 1-1.2 second gap following 6 bursts.

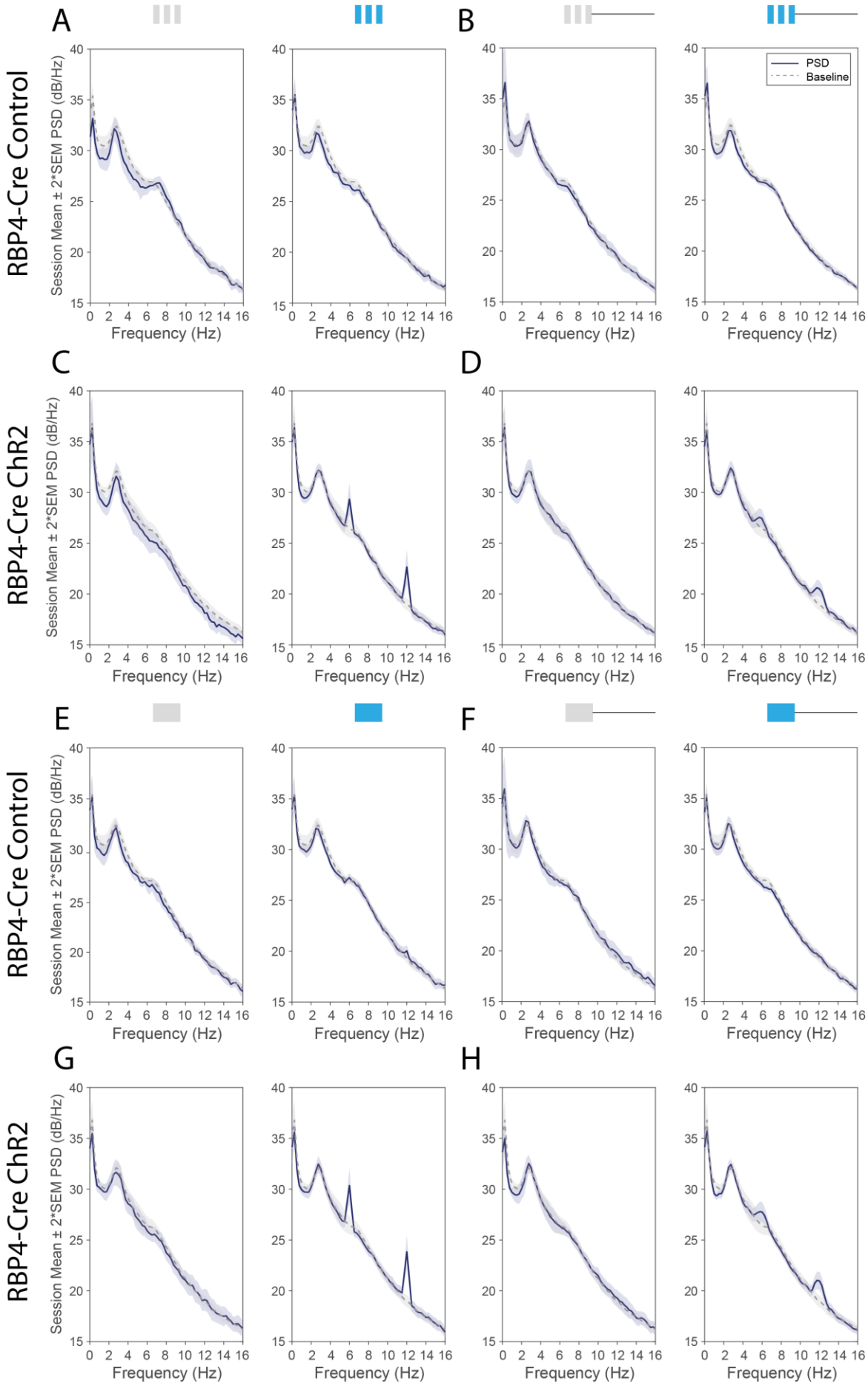

A
B
C
D
E
F
G
H
RBP4-Cre Control
RBP4-Cre ChR2
RBP4-Cre Control
RBP4-Cre ChR2
Session Mean ± 2*SEM PSD (dB/Hz)
Frequency (Hz)
PSD
Baseline

Figure 4.10 Local power spectra of RBP4-Cre opsin and control mice following open-loop stimulation patterns

To determine whether there were changes in theta power following open-loop stimulation four open-loop stimulation patterns were devised - open-loop gamma (**A & C**), open-loop gamma gaps (**B & D**), open-loop continuous (**E & G**) and open-loop continuous gaps (**F & H**) as variations of our closed-loop patterns with no phase relationship. Mean power spectral density plots from 0-16Hz (±2*SEM) in RBP4-Cre control (n=4; n=10 sessions) and opsin mice (n=4; n=13 sessions). Stimulation was either off (0mW; grey pattern) or on (1 or 2mW; blue pattern). In controls, session means were calculated from n=4 mice; from n=9-10 sessions (18-19 recordings when stimulation was on due to the two amplitudes). In opsin mice, session means were calculated from n=4 mice; from n=13 sessions (26 recordings when stimulation was on due to collection at two amplitudes). Within each session, a session baseline was calculated from a baseline recorded at the beginning of each session, combined with all unstimulated recordings from throughout the session. The mean session baseline was plotted for each stimulation type.

For statistical analyses (Figure 4.11), the baseline was removed and extracted around our theta target frequency (6±1.5Hz). A LME was devised to test how theta power changes with an open-loop stimulation pattern (OL-gamma & OL-gamma gaps/OL-continuous & OL-continuous gaps) and stimulation (0mW; 1 or 2mW) by group (opsin or control). Random effects of subject and date were modelled as usual. For analyses, data was split into gamma or continuous-type patterns. We hypothesised that there would be no effect of OL stimulation within the control group or when stimulation was off in the opsin group.

Firstly, we tested this on gamma stimulation – OL-gamma & OL-gamma gaps. As anticipated, there was a significant interaction between the group, stimulation pattern and stimulation ($F(1,114)=6.44$, $p=0.013$). The main effects of stimulation pattern (OL-gamma & OL-gamma gaps) and stimulation (0mW & 1 or 2mW) were additionally significant [$F(1,116)=5.99$, $p=0.016$) & $F(1,114)=5.28$, $p=0.02$) respectively]. The group by stimulation interaction was also significant ($F(1,114)=6.84$, $p=0.01$), expected as this highlights the role that stimulation only has an effect in the opsin mice group and as such only this experimental group are further analysed.

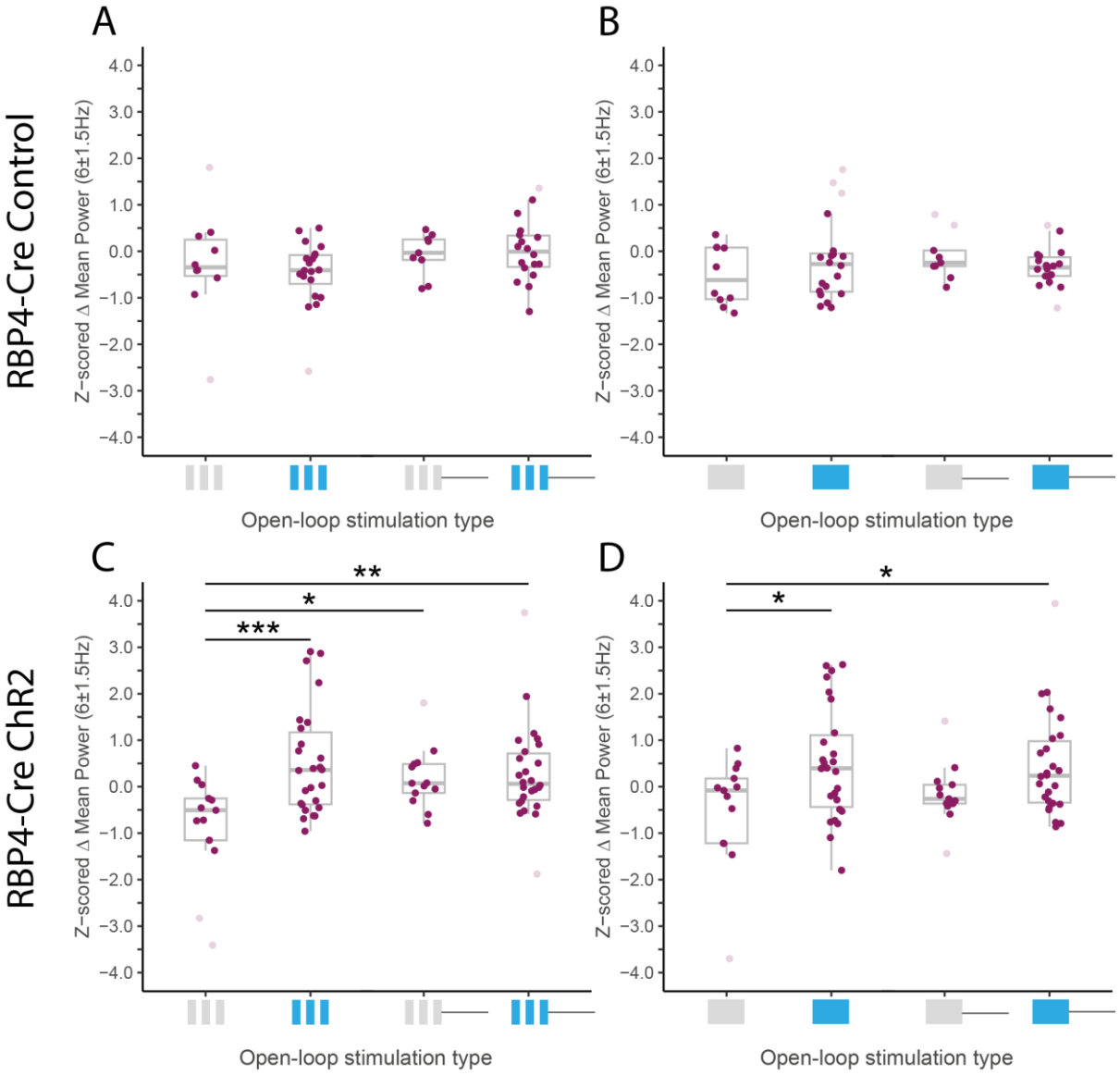


Figure 4.11 Open loop stimulation patterns can modulate theta power in RBP4-Cre opsin mice

To determine whether there were changes in theta power following open-loop stimulation four open-loop stimulation patterns were devised - open-loop gamma, open-loop gamma gaps, open-loop continuous, and open-loop continuous gaps as variations of our closed-loop patterns with no phase relationship. Stimulation was either off (0mW; grey pattern) or on (1 or 2mW; blue pattern). All open-loop data was recorded in n=5 mice, control – from 9-10 sessions (18-20 recordings when stimulation was on as data was collected at 2 amplitudes); opsin – 13 sessions (26 recordings stimulation on). For statistical analyses, power spectral density estimates were extracted around the 6Hz target (4.5-7.5Hz) after the baseline had been removed (calculated from a baseline recording and all unstimulated recordings within each session). The z-scored mean power were plotted for each of the four open-loop stimulation patterns (**A-D**). Grey boxes represent the interquartile range and median values from the data set, and whiskers extend to the minimum and maximum values calculated as their respective quartile ±1.5*IQR. Z-scored session means for each laser power are plotted as individual scatter points for their respective group and stimulation type. Lighter scatter points represent data points that lie outside a threshold set as the respective quartile value ±1.5*IQR. Statistical

analyses were performed on each overall stimulation pattern type (i.e. OL gamma to OL gamma-gaps). These demonstrated significant differences ($p<0.05$) for gamma stimulation patterns in opsin mice (**C**) between OL-gamma and OL-gamma gaps when stimulation was off, OL-gamma on vs off and OL-gamma off and OL-gamma gaps on (LME, followed by pairwise post hoc t-tests with Tukey adjustment). Similarly, for continuous stimulation patterns in opsin mice (**D**) significant differences ($p<0.05$) were identified between OL-continuous off vs on as well as OL-continuous off and OL-continuous gaps on (LME, followed by pairwise post hoc t-tests with Tukey adjustment).

To follow up on these significant interactions, the data was further split into the opsin group to test how the OL stimulation pattern and stimulation affects theta power. The LME had main effects of stimulation pattern and stimulation (on or off), their interaction, and random effects of subject and date. This found a significant main effect of stimulation ($F(1,65)=13.07$, $p<0.001$) and the interaction between stimulation pattern and stimulation ($F(1,65)=9.53$, $p=0.003$). This not only indicates that there is a difference in theta power when stimulation is on, but that there is a difference in theta power between stimulating with the two different OL gamma patterns. Pairwise post hoc tests performed (t-test with Tukey adjustment) identified a difference in theta power when stimulation was off between the two OL gamma patterns ($p=0.019$) which was unexpected as no stimulation is given in either case (Figure 4.11C). There was also a significant difference between OL gamma stimulation when on or off ($p<0.001$) as expected. Finally, a difference was found between OL gamma off and OL-gamma gaps on ($p=0.0015$).

Additionally, we carried out the same analyses on OL continuous stimulation – OL-continuous & OL-continuous gaps. Contrastingly to gamma stimulation, there was no significant effect of the group, stimulation pattern, and stimulation interaction ($F(1,117)=0.08$, $p=0.78$). The main effect of stimulation (on or off) was significant ($F(1,117)=8.08$, $p=0.005$) as was the interaction between group and stimulation

(F(1,117)=6.20, p=0.014), indicating that changes in theta power are limited to our experimental condition which further analyses focus on.

To further investigate these significant effects, we followed up with a LME model testing the OL stimulation pattern and stimulation being on or off in opsin group data. The LME with main effects of stimulation pattern and stimulation (on/off) as well as their interaction and random effects of subject and date, found a significant main effect of stimulation only (F(1,66)=12.89, p<0.001). Pairwise post hoc tests revealed significant differences between OL-continuous off and on (p=0.015; t-test with Tukey adjustment) as well as between OL-continuous off and OL-continuous gaps on (p=0.02; t-test with Tukey adjustment) (Figure 4.11D).

Overall, these statistical analyses demonstrate that stimulation elicits changes in theta power in the opsin group, but not the control group, for each of the four open-loop stimulation patterns (Figure 4.11). When observing the spectra for the opsin group (Figure 4.10: C & D; G & H), regardless of stimulation type we can observe increased mean theta power at the 6Hz target but additionally a 12Hz harmonic. The presence of this 12Hz harmonic may be a result of the regularity of the stimulation, as pulses are more rhythmical than during closed-loop stimulation. While an increase in theta power was present for all stimulation types in RBP4-Cre ChR2 mice, the largest effects were demonstrated during OL-gamma and OL-continuous stimulation compared with OL-gamma gaps and OL-continuous gaps, as anticipated (Figures 4.10 & 4.11).

4.3.6 Determining the role of gamma rhythmicity

We next wanted to investigate the importance of gamma rhythmicity in driving theta power during closed-loop stimulation. To address this, in later mice where ChR2 was still targeted to RBP4+ pyramidal neurons, we implemented a third stimulation type – random gamma. This was adapted from our 75Hz gamma stimulation pattern, by altering the timing of the middle pulse based on a set of 31 positions between the two outside pulses which remained the same (see methods, Chapter 2). As we had already confirmed there was no effect of stimulation in control mice, this cohort consisted of only ChR2 mice (5 mice, from 20 sessions). As well as our third stimulation type, to confirm the results aligned with our previous expectations and compare the effect on theta power across stimulation types, gamma and continuous stimulation pattern data were also collected.

The mean PSD plots are shown in Figure 4.12, for each stimulation type and phase with stimulation on (2mW; blue patterns) and off (0mW, grey patterns). The baseline was then removed, and power spectral density estimates were extracted from 4.5-7.5Hz for statistical analyses (Figure 4.12).

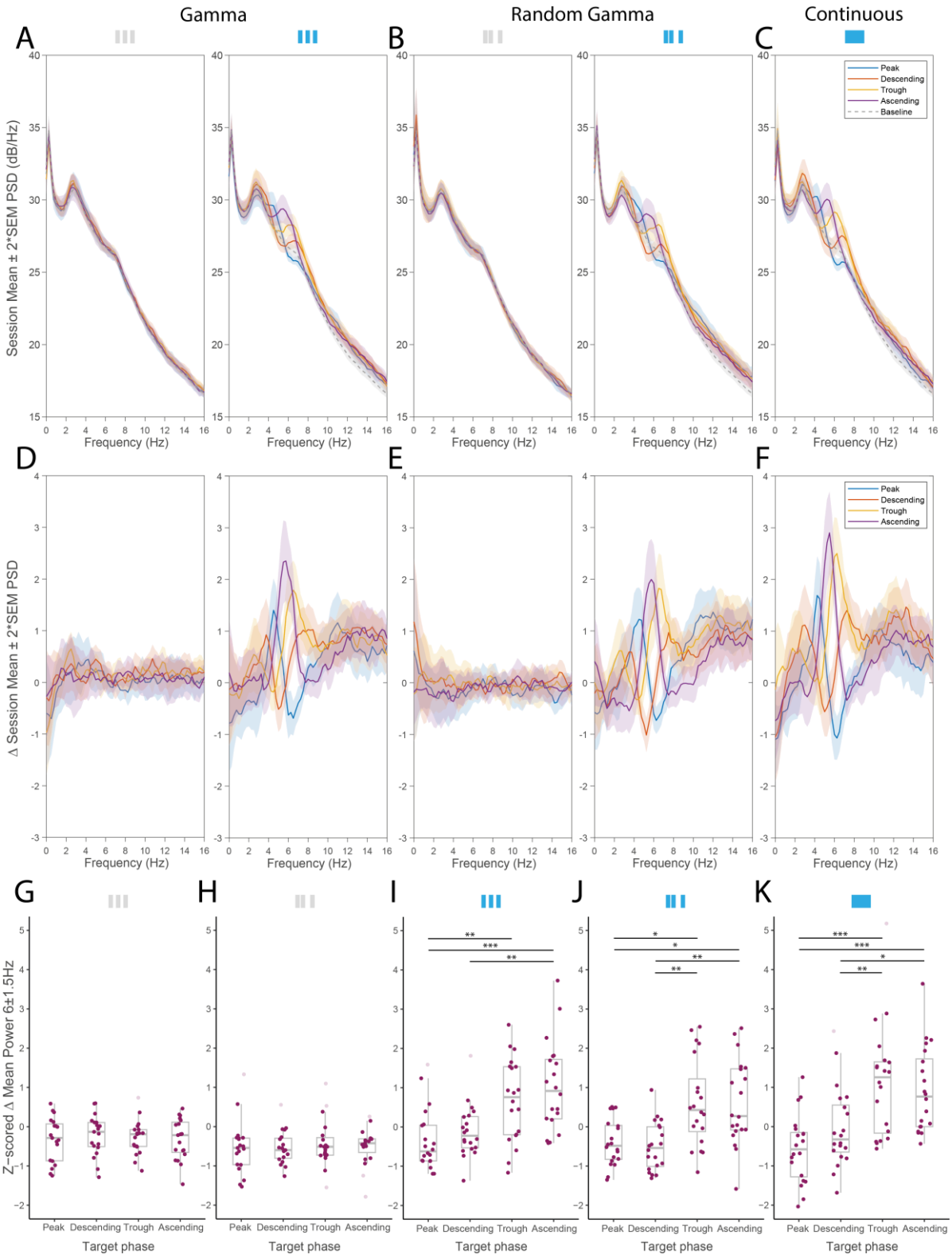


Figure 4.12 Phase-dependent effect in local LFP of opsin mice following all three closed-loop stimulation patterns

Mean power spectral density (±2*SEM) from 0-16Hz for both RBP4-Cre opsin mice (n=5), targeting 4 different phases of the theta oscillation with gamma, random gamma or continuous stimulation (**A-C**). Stimulation was either off (0mW; grey patterns) or on (2mW; blue patterns). The number of sessions to calculate the mean was n=20 (19 recordings per phase stimulation off; n=20 recordings per phase stimulation on for all stimulation

types above). Within each session, a session baseline was calculated from a baseline recorded at the beginning of each session, combined with all unstimulated recordings throughout a session. The mean session baseline was plotted on each plot for each group and stimulation either on or off. The mean PSDs (±2*SEM) in which the baseline was removed from each session are also plotted (**D-F**). Boxplots demonstrate z-scored change in theta power with respect to baseline extracted between our target range of 4.5-7.5Hz (6Hz±1.5) (n=5 mice, n=20 sessions with a total of 19 recordings per phase when stimulation was off and 20 per phase when stimulation was on) (**G-K**). Grey boxes represent the interquartile range and median values from the data set, whiskers extend to the minimum and maximum values calculated as their respective quartile ±1.5*IQR. Session means for each laser power are plotted as individual scatter points for their respective group and stimulation type. Lighter scatter points represent data points that lie outside a threshold set as the respective quartile value ±1.5*IQR. We found the following significant differences ($p<0.05$) for each stimulation pattern (LME followed by pairwise post hoc t-tests Tukey adjustment). Gamma: peak and trough, peak and ascending and the descending and ascending phases. Random gamma: peak and trough, peak and ascending, descending and trough as well as the descending and ascending. Continuous: peak and trough, peak and ascending phases, descending phase and trough and descending and ascending phases.

4.3.6.1 Gamma rhythmicity does not affect phase-dependent theta power modulation

To investigate whether random gamma stimulation had similar phase-dependent effects on theta power as gamma stimulation, we formulated a LME model with fixed effects of stimulation pattern (gamma, random gamma), laser power and phase. Subject and date were modelled as random effects.

There was a significant laser power by phase interaction ($F(3,299)=15.28$, $p<0.001$) which was expected because we hypothesised that there would only be phase-dependent changes in theta power when stimulation was on. All three main effects were significant [stimulation pattern ($F(1,300)=7.89$, $p=0.005$); laser power ($F(1,300)=60.87$, $p<0.001$); phase ($F(3,299)=16.21$, $p<0.001$)]. We had hypothesised that the main effect of laser power would be significant, as regardless of stimulation pattern and phase there was a difference when stimulation was on or off, therefore further analyses is undertaken only with stimulation on data. The three-way interaction term (stimulation pattern*laser power*phase; ($F(3,299)=0.306$, $p=0.82$)), as well as the other interaction terms - stimulation pattern*laser power and stimulation pattern*phase were not significant [($F(1,300)=0.02$, $p=0.90$) &

F(3,299)=0.61, p=0.61) respectively]. This was in line with our hypothesis that there would be no differences in theta power across phase, dependent on the type of gamma stimulation, demonstrated in Figure 4.12.

4.3.6.2 No significant differences in theta power modulation by stimulation pattern

To follow up on the significant interaction between stimulation and phase, the data was split into stimulation on (2mW; gamma, random gamma & continuous). Fixed effects of stimulation pattern and phase, their interaction and random effects of subject and date were tested using a LME model on the separated data. There was no significant stimulation pattern*phase interaction (F(6,227)=1.10, p=0.36), suggesting that all three types of stimulation modulated theta power in the same phase-dependent manner. As anticipated, there was no significant main effect of stimulation pattern (F(3,228)=2.73, p=0.07), and a significant effect of phase (F(3,227)=39.92, p<0.001), because we hypothesised change in theta power would not vary with phase for each stimulation pattern.

Additional pairwise t-tests allowed us to investigate the effects of phase within each stimulation pattern (Tukey adjustment for multiple comparisons) – Figure 4.12 G-K. For gamma stimulation, we found significant differences between the peak and the trough (p=0.009), peak and ascending (p<0.001), and the descending and ascending phases (p=0.002) (Figure 4.12I). Meanwhile for random gamma significant differences were found between the peak and trough (p=0.0115), peak and ascending (p=0.0115), descending and trough (p=0.0026) as well as the descending and ascending (p=0.0026) (Figure 4.12J). Finally, there were significant differences between the peak and trough, peak and ascending phases (both p<0.0001), descending phase and

trough (p=0.001), and descending and ascending phases (p=0.019) when stimulating using the continuous pattern (Figure 4.12K).

4.3.6.3 Gamma and random gamma stimulation resulted in significant phase-dependent modulation of theta power when stimulation was on

Additionally, to confirm differences in theta power were specific to optogenetic stimulation, the data were split by stimulation pattern for comparison to their stimulation off control. Separate LME models, with fixed effects of laser power and phase and their interaction (random effects: subject & date), were performed for each stimulation pattern (gamma & random gamma). These analyses demonstrated a significant laser power*phase interaction for both gamma and gamma random stimulation patterns [($F(3,143)=9.27$, $p<0.001$) & ($F(3,142)=7.58$, $p<0.001$) respectively]. This was expected we predicted there would only be a phase-dependent change in theta power when stimulation was on for each pattern. For gamma stimulation there were significant main effects of laser power ($F(1,144)=33.54$, $p<0.001$) and phase ($F(3,143)=8.63$, $p<0.001$). The same was found with random gamma stimulation [laser power ($F(1,143)=33.39$, $p<0.001$); phase ($F(3,143=9.64$, $p<0.001$)].

For each stimulation pattern the significant main effects of laser power were hypothesised, as they suggest a significant difference directly due to stimulation, regardless of phase. However, as we hypothesised no phase-dependent changes in theta power when stimulation was off, the effect of phase was unexpected, indicating an effect of phase regardless. Subsequent pairwise t-tests (Tukey adjustments) were performed to follow up on these significant interactions, these showed significant differences for both gamma and random gamma stimulation on between peak and

trough (p=0.0002 & p=0.0001 respectively), the peak and ascending phases (p<0.0001 & p=0.0001 respectively), the descending phase and the trough (p=0.01 & p<0.0001 respectively), and the descending and ascending phases (both p<0.0001).

4.3.6.4 Closed-loop random gamma stimulation pattern does not underly phase-specific theta modulation

As with previous data, it was necessary to confirm the random gamma stimulation pattern resulting from interaction with the oscillation using our open-loop replay paradigm does not produce phase-specific theta power modulation. Mean PSD plots can be found in Figure 4.13, demonstrating the PSD (Figure 4.13A-D) for all four phases in the original (closed-loop) and open-loop replay sessions for both gamma and random gamma stimulation patterns in this cohort. For comparison, the baseline was removed (Figure 4.13E & 4.13F), and power spectral density estimates were extracted for subsequent statistical analysis. The z-scored change in mean power are shown for each stimulation pattern (gamma/random gamma) and stimulation type (closed-loop/open-loop replay) (Figure 4.13I-L).

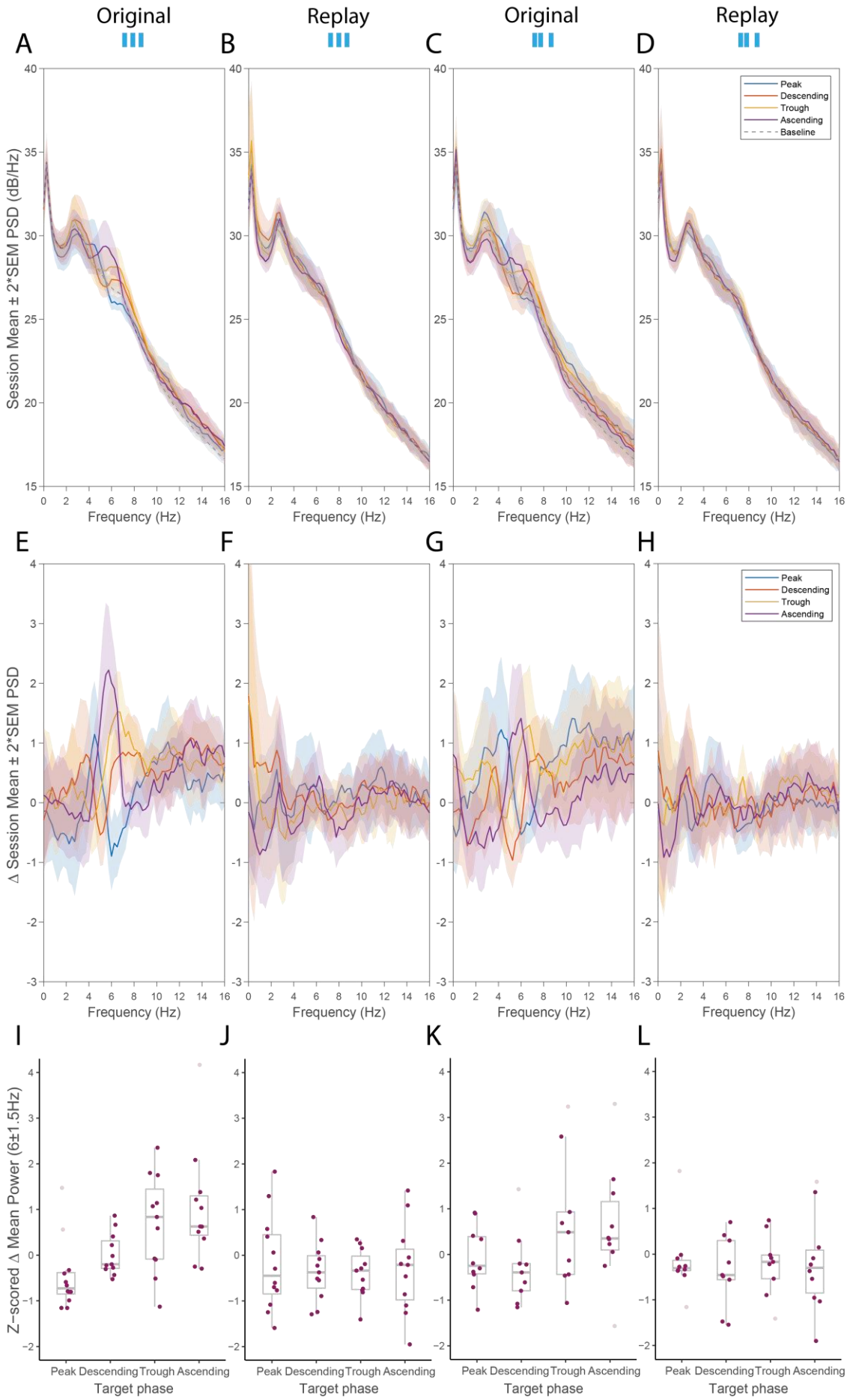

Original
Replay
Original
Replay
A
B
C
D
Peak
Descending
Trough
Ascending
Baseline
Session Mean ± 2*SEM PSD (dB/Hz)
Frequency (Hz)
E
F
G
H
Δ Session Mean ± 2*SEM PSD
I
J
K
L
Z−scored Δ Mean Power (6±1.5Hz)
Peak Descending Trough Ascending
Target phase

Figure 4.13 Local power spectra and z-scored change in theta power following gamma and random gamma closed-loop stimulation and their open-loop replays

Mean power spectral density (±2*SEM) from 0-16Hz in RBP4-Cre opsin mice (n=5), gamma or continuous stimulation on (2mW; blue patterns) (**A-D**). Plots demonstrate PSD for closed-loop optogenetic stimulation targeting 4 different phases of the theta oscillation (original; **A & C**) as well as open-loop replay (replay; **B & D**), in which a previous closed-loop recording is played back to the mouse within the same session. More specifically, the number of sessions to calculate the mean for gamma (n=5; n=12 sessions, n=11-12 recordings per phase) and random gamma (n=5; n=10 sessions, n=9-10 recordings per phase). Within each session, a session baseline was calculated from a baseline recorded at the beginning of each session, combined with all unstimulated recordings throughout a session. The mean session baseline is then plotted on each plot for each group and stimulation either on or off. The mean PSDs (±2*SEM) in which the baseline was removed from each session are also plotted for both control and opsin mice (**E-H**). Boxplots demonstrate z-scored change in theta power with respect to baseline extracted between our target range of 4.5-7.5Hz (6Hz±1.5) (n=5 mice, Gamma: n=12 sessions with a total of 11-12 recordings per phase; Random gamma: n=10 sessions, 9-10 recordings per phase) (**I-L**). Grey boxes represent the interquartile range and median values from the data set, whiskers extend to the minimum and maximum values calculated as their respective quartile ±1.5*IQR. Session means for each laser power are plotted as individual scatter points for their respective group and stimulation type. Lighter scatter points represent data points that lie outside a threshold set as the respective quartile value ±1.5*IQR.

As previously explained, the difference in mean power were calculated between the most and least amplifying phases following closed-loop stimulation. These phases were then used to calculate a difference when stimulation was replayed, matched to the stimulation pattern and amplitude. For these analyses, only data in which all four phases were collected were included and data were subsequently z-scored, boxplots are shown in Figure 4.14.

We had insufficient data to use a LME model, therefore we performed a paired t-test to get an indication of what the data suggests, with the caveat that we were unable to control for repetition of subjects within and between sessions (n=5 mice; total n=10 gamma sessions, n=9 random gamma sessions).

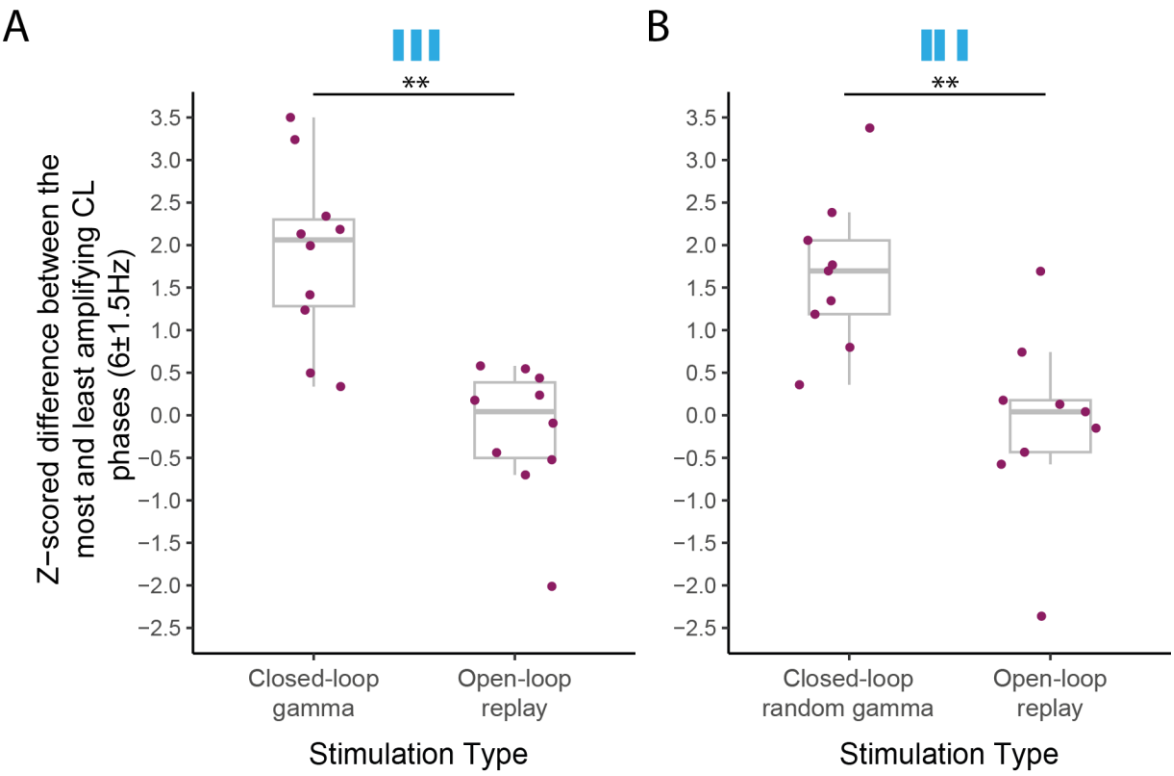


Figure 4.14 Z-scored difference in theta power between the most and least amplifying closed-loop phases identified following gamma and random gamma stimulation and their open-loop replay

Grey boxes represent the interquartile range and median values from the data set, whiskers extend to the minimum and maximum values calculated as their respective quartile ±1.5*IQR. For each main stimulation pattern (gamma (**A**)/random gamma (**B**)) the difference between the most and least amplifying phase for a closed-loop recording are plotted as individual scatter points, the difference between the same phases were then taken in the open-loop recording and displayed as individual scatter points (all stimulation delivered at 2mW). To perform statistical analyses, the minimum and maximum values were extracted from the closed loop recording and the difference between them was calculated. The difference between these same phases were then calculated for the open-loop replay recording. Significant differences ($p<0.05$, paired t-test) were found between the z-scored difference in theta power between the most and least amplifying phase in each specific closed-loop recording and it's open-loop counterpart for both gamma (A) and random gamma (B) stimulation patterns. In these specific analyses only sessions which had a complete set of data for all four phases at 2mW (n=5 mice, n=10 gamma sessions, n=9 random gamma sessions).

Gamma stimulation (Figure 4.14A) led to a significant difference between the closed and open-loop z-scored mean power change between the most and least amplifying phases following closed-loop stimulation ($p=0.002$; paired t-test). Thus, indicating the stimulation train resulting from the interaction with the underlying theta oscillation cannot drive the same changes in z-scored theta power. The same was found for random gamma stimulation ($p=0.009$; paired t-test) (Figure 4.14B) – similarly

suggesting closed-loop phase-specific optogenetic stimulation was necessary to drive changes in theta power.

4.4 Discussion

In Chapter 3 we provided evidence of phase-specific motor cortical theta modulation when stimulating PV+ interneurons. In this chapter, we aimed to assess whether closed-loop phase-specific optogenetic stimulation targeted to RBP4+ pyramidal neurons produced phase-specific theta modulation and additionally whether less rhythmic gamma stimulation altered modulation.

We have demonstrated phase-dependent modulation of the motor cortical theta oscillation when stimulating ChR2 in RBP4+ pyramidal neurons with all stimulation patterns, this is not demonstrated by control mice. Targeted stimulation producing the most theta amplification were the trough and ascending phases, while the peak was the least amplifying phase. This indicates that the stimulation pattern itself is less important than the timing of stimulation in modulation of theta power. Continuous stimulation was evidently more powerful in modulating the ongoing theta oscillation, demonstrated by a greater number of significant differences between the four stimulation phases, as well as the stronger statistical power. This can be explained by the increased power delivered into the circuitry by this pattern of stimulation.

4.4.1 Accuracy of phase-tracking is not dependent on the phase of stimulation

Within RBP4-Cre control and opsin mice a consistent peak in the power spectra around 6Hz is observed demonstrating the availability of a resting 6Hz theta oscillation to target and stimulate at particular phases, however, the presence of this oscillation

has not been quantified. This is in line with a theta oscillation observed in head-fixed rodents previously (Igarashi et al. 2013).

We hypothesised amplification of the ongoing theta oscillation would enhance phase-tracking accuracy. However, while stimulation targeted to the trough - one of the two amplifying phases, was more accurate than in control conditions, stimulation targeted to the ascending phase was less accurate. Therefore, differential effects on phase-tracking accuracy by phases that appear to amplify the ongoing theta oscillation. Visually, stimulation targeted to the ascending phase lands closer to the trough in opsin mice, which may account for modulation by both phases in a similar manner. Continuous stimulation resulted in greater variability when targeting the peak compared to gamma stimulation, however, both are indicative that suppressing the ongoing oscillation may increase variability and make tracking the oscillation more difficult.

4.4.2 Closed-loop is more effective than open-loop stimulation for theta-phase modulation

All three stimulation patterns, which produced phase-dependent amplification of the ongoing theta oscillation when phase-locked to the trough and ascending phases, did not reproduce phase-dependent effects when stimulation trains were delivered as open-loop replay. This was quantified in each case by comparing the difference in theta power between the most and least amplifying phases following closed-loop stimulation. A significant difference between changes in theta power for the stimulation paradigms indicate that replication of the stimulation trains interacting

with each phase does not reproduce the same phase-dependent effects demonstrated by closed-loop phase-dependent stimulation.

We have additionally shown that open-loop stimulation with no relationship to the underlying theta oscillation, can produce significant differences in theta power when regularly stimulated (OL-gamma & OL-continuous), something not observed in control mice. However, when these simulation patterns were made more irregular by inputting randomised 1-1.2 second gaps between every 6 stimulation bursts (OL-gamma gaps & OL-continuous gaps) we were unable to significantly modulate theta power, regardless of the little increases in the power spectra observed around 6Hz.

One clear difference between the effects of closed and open-loop stimulation, is the 12Hz harmonic demonstrated in the PSD plots for open-loop stimulation on patterns. This harmonic could be explained by the regularity of stimulation as open loop pulses are delivered more consistently than when they are delivered through phase interaction with the ongoing oscillation.

4.4.3 Phase-specific modulation is not dependent on stimulation pattern

While we determined that the specificity of the phase targeted is important, phase-specific modulation is consistent across the stimulation patterns tested - post hoc tests revealing only small differences between the phases. Continuous stimulation can most effectively modulate the theta oscillation, however, when inputting less power into the neurocircuitry with gamma or random gamma stimulation patterns we can modulate the oscillation in the same manner. Furthermore, open-loop replay of these stimulation pattern trains didn't elicit a phase-response. This suggests that the

stimulation pattern itself is not important for driving changes in the ongoing theta oscillation. Stimulation was designed for the centre of the stimulation pulse to align with the targeted phase. This was the case for both gamma and continuous stimulation, however, not for random gamma stimulation due to the inner pulse moving around within the width of the two outer pulses. As a result, in some stimulation pulses there may be no stimulation landing at the centre of the target phase. However, due to a library of stimulation patterns this would happen irregularly, perhaps therefore having less of an impact on modulation.

All stimulation patterns were designed to modulate over ¼ of the 6Hz theta cycle, the centre-point of this targeted to the identified phase. This may suggest that stimulation onset slightly preceding the target phase is important in altering theta dynamics, as neurons perhaps become maximally activated by the centre of the target phase. This may allow for greater synchrony within the microcircuit and if this aligns with the preferred firing phase of pyramidal neurons then ongoing theta power can be enhanced. Whereas, when synchrony increases but is misaligned to the preferred firing phase, theta power is less modulated by evoked gamma oscillations (Hájos et al. 2004; Mann et al. 2005).

4.4.4 Pyramidal neuron subtypes potentially involved in theta modulation within L5

The mouse line used to stimulate RBP4+ neurons is much more specific in targeting neurons that are only within L5 (Gerfen et al. 2013; Harris et al. 2014). L5 consists of two sublayers in which IT neurons are distributed across both layers, whereas PT neurons are found only in L5b (K. D. Harris & Shepherd, 2015; Li et al., 2015; Shepherd,

2013). As both types express RBP4, they both have the potential to express ChR2 and could be involved in generating the phase-specific theta modulation we observe.

These L5 pyramidal subtypes also primarily project to different regions. IT neurons to other cortical areas and the striatum, while PT neurons have collaterals in a wide range of brain targets, such as the brainstem and spinal cord, the ipsilateral cortex, and other subcortical structures (K. D. Harris & Shepherd, 2015; Shepherd, 2013; Winnubst et al., 2019). Therefore, they are involved in driving motor output from L5, IT neurons through projections to the striatum, and PT neurons in planning and execution of voluntary movement commands through the brainstem and spinal cord (Economo et al., 2018; Li et al., 2015). Previous work has additionally demonstrated optogenetic stimulation of layer 5 (RBP4+ neurons) results in brain-wide BOLD responses in fMRI as well as strong a strong local response (Chan et al. 2022). This indicates that L5 is important in driving not only local output but brain-wide responses that aren't initiated from other cortical layers.

IT neurons have both reciprocal connections and connections to the PT neurons in L5b whereas PT neurons have been shown not to have connections to IT neurons (Hooks et al., 2013; Kiritani et al., 2012; Shepherd, 2013). This may indicate that IT neurons drive excitation primarily when stimulated and can recruit other IT neurons and PT neurons producing a larger response than that of PT neurons and therefore increasing the number of excitatory post-synaptic potentials. Optogenetic phase-specific stimulation is likely to lead to increased excitation and synchrony which ultimately drives the increases in theta power that we demonstrate. Phase-specificity is

anticipated to be a property of the underlying neurocircuitry, associated with the natural firing preference of these neurons during theta oscillations.

4.4.5 Interneuron subtypes potentially involved in theta modulation within L5

Pyramidal neurons lead cortical output and interactions between different brain regions, but they are modulated by inhibitory interneurons that primarily have local connections, for instance PV-basket cells are highly connected to pyramidal neurons. The interaction of different interneurons is therefore crucial for generating oscillations. Within L5 are different subtypes of inhibitory interneurons – the majority are PV interneurons or SST neurons (Tremblay et al., 2016). Differing synaptic properties mean these two interneurons play different roles within the microcircuitry. PV-basket cells have strong fast responses to excitatory input so can exert powerful inhibition onto target neurons, but also have depressing synapses which means repeated activation doesn't lead to excessive inhibition (Tremblay et al., 2016). SST neurons, on the other hand, have facilitating synapses which means as excitatory input continues there is a progressive increase in inhibitory output (Tremblay et al., 2016). However, SST interneurons are hypothesised to deliver broad, non-specific inhibition feedback (Tremblay et al., 2016). Therefore, to synchronise the timing of action potentials and control oscillatory activity, excitatory input from optogenetic stimulation of pyramidal neurons likely recruits PV+ basket cells initially. Meanwhile as stimulation persists SST interneurons may modulate more broadly over a longer timescale, preventing overexcitation.

Recent work in the visual cortices has shown that separate SST subtypes differentially innervate and have reciprocal connections to either PT or IT neurons in L5, although

SST neurons more strongly inhibit PT neurons (Wu et al. 2023). This indicates precise roles of these inhibitory interneurons within the microcircuit. Overall, phase-specific modulation may be a direct result of increased and decreased synchrony of both excitatory and inhibitory neurons and their underlying preferred theta firing phases, as well as the specificity of different components involved within the microcircuitry.

4.4.6 Pyramidal neurons can respond to gamma frequency optogenetic stimulation

Intrinsic properties of pyramidal neurons such as firing rate can be region-specific within the cortex and likely reflect a function of their output (Groh et al., 2010; Miller et al., 2008). It is therefore possible there could be differences in the intrinsic properties specific to these RBP4+ neurons found within the motor cortex itself that are currently unknown. However, pyramidal neurons have previously been shown to respond to and were strongly phase-locked to optogenetic stimulation pulses in the prefrontal cortex, evoking gamma oscillations (Sohal et al. 2009). In addition, ~40Hz stimulation activated ChR2+ pyramidal neurons in L2/3 of the somatosensory cortex which spiked in phase with the LFP (Adesnik & Scanziani, 2010). These provide evidence that pyramidal neurons can respond to gamma frequency optogenetic stimulation. Therefore, supporting our findings that both stimulation patterns can effectively modulate RBP4+ pyramidal neurons, through increasing excitation.

4.4.7 Theta-gamma coupling is unlikely to play a role in theta power modulation in this experimental set-up

In this study we target theta oscillations, which have been found previously within the rodent motor cortex *in vivo* (Igarashi et al. 2013) and induced *in vitro* (Johnson et al. 2017) coupled to gamma oscillations. Transcranial alternating current stimulation

(tACS) simulating theta-gamma coupling has been demonstrated to significantly improve the learning of a thumb abduction task in humans (Akkad et al. 2021). Therefore, we hypothesised that theta-gamma coupling may be important in modulation of the LFP. We observe phase-dependent theta modulation from both gamma frequency and continuous stimulation patterns, which indicates theta-gamma coupling does not play an important role during theta phase-dependent modulation. If it was, we would expect gamma stimulation to preferentially modulate theta or be the only stimulation pattern that produces phase-dependent modulation. It is possible, however, that if this experiment was undertaken with a head-fixed motor learning task component, theta-gamma coupling would be important, and the stimulation patterns would interact with theta power and learning outcomes differently. Therefore, we anticipate low theta-gamma coupling in head-fixed mice without a behavioural task, however, it is possible that gamma frequency stimulation may induce gamma oscillations. If this occurs, it is possible there could be evidence of induced theta-gamma coupling at resting state in head-fixed mice.

4.4.8 Conclusions

Overall, the findings described in this chapter highlight the role RBP4+ pyramidal neurons play in theta oscillation generation. Pyramidal neurons are less frequently modulated within studies using closed-loop stimulation or phase-specific methods, as inhibitory interneurons are targeted. These data indicate that driving excitation of RBP4+ pyramidal neurons and increasing synchrony at certain phases of the ongoing oscillation can result in phase-dependent modulation of motor cortical theta power. This was not demonstrated through replayed closed-loop stimulation trains

highlighting the importance of real-time interaction in producing phase-specific effects. This may be linked to the preferred intrinsic firing properties of the neuronal subtypes involved in the generation of theta oscillations. Understanding when these cell types are most effectively modulated within the existing neurocircuitry will be vital for understanding the role they play in driving sensory, motor, and cognitive processes, as well as understanding their subsequent role in disease.

5 Cell-type dependent modulation of gamma power

5.1 Introduction

Some of the fastest neuronal oscillations in the brain are gamma oscillations (>30Hz). In the motor cortex of humans, increases in gamma power have been consistently associated with movement onset and execution (Akkad et al., 2021; Muthukumaraswamy, 2010; Nowak et al., 2017; Pfurtscheller & Lopes Da Silva, 1999).

Excitatory-inhibitory mechanisms are believed to predominate in driving gamma oscillations within the cortex, with gamma oscillations likely arising from local networks containing both PV+ basket cells, and pyramidal neurons, with reciprocal connectivity (Adesnik & Scanziani, 2010; Cardin et al., 2009; Sohal et al., 2009). The interplay between the firing patterns of FS neurons and their inhibitory feedback onto pyramidal neurons, which in turn have recurrent connections back to the FS neurons, are critical to control the precise timing of gamma oscillations (Bartos et al., 2007; Buzśaki & Wang, 2012; Cardin et al., 2009; Whittington et al., 1995). Additionally, network models that are based on mutual inhibition are implicated in the emergence of gamma oscillations if exposed to an excitatory tonic drive (Bartos et al., 2007). Typically, gamma oscillations are short-lived and arise locally, although they have also been implicated in longer-range network dynamics (Buzśaki & Wang, 2012). Of particular relevance to the work undertaken in this thesis, PV+ basket cells in layer 5 of the cortex, have been implicated in both gamma oscillation initiation and maintenance (Rudy et al. 2011).

Previous studies have shown that the firing of PV+ basket cells are precisely phase-locked to gamma oscillations, thereby generating an action potential approximately once per gamma cycle in the hippocampus (Bragin et al. 1995; Csicsvari et al. 2003). Recent *in vivo* studies in the visual cortex of awake mice also found that the firing of PV+ interneurons could phase lock to local spontaneous or visually evoked gamma oscillations (Onorato et al., 2023; Perrenoud et al., 2016).

Gamma oscillations have been robustly induced in the somatosensory (barrel) cortex of mice through 20-80Hz stimulation targeted to ChR2-containing FS-interneurons. It was found that 40Hz stimulation most significantly increased local cortical gamma power (Cardin et al. 2009). This approach demonstrates the ability of FS-interneurons to respond to gamma frequency stimulation leading to circuit-level changes in the LFP. Consistent with these findings, the opposite approach of optogenetically silencing PV+ interneurons led to the suppression of gamma oscillations in the stimulated cortex (Sohal et al. 2009). Another study showed rhythmic gamma oscillations (~40Hz) in the somatosensory cortex, that were induced through ramping stimulation of ChR2 containing pyramidal neurons in L2/3 (Adesnik & Scanziani, 2010). The authors also showed simultaneously recorded units spiked in phase with the LFP (Adesnik & Scanziani, 2010). In addition, Sohal et al (2009) found that optogenetic pulses targeting pyramidal neurons could evoke strongly phase-locked gamma oscillations. Meanwhile Lewis et al (2021) were able to induce a ~70Hz peak in the LFP when stimulating excitatory neurons in the visual cortex of anaesthetised cats with a 2-second continuous blue (excitatory) light pulse (Lewis et al., 2021). Together, these

results suggest that both inhibitory and excitatory neurons can respond to gamma frequency stimulation.

Substantial evidence suggests that gamma oscillations widely co-occur with theta oscillations in the motor cortex in both human and animal models (Canolty et al. 2006; Igarashi et al. 2013; Johnson et al. 2017; Rustamov et al. 2022; Spooner et al. 2022). In an *in vitro* study in the motor cortex of rats, for example, packets of gamma activity were found at the peak of the theta oscillation (Johnson et al. 2017). Igarashi et al (2013) also demonstrated prominent theta-gamma coupling in the forelimb area within the motor cortex of mice. Given the evidence that gamma often co-occurs with theta oscillations and that both excitatory and inhibitory neurons can be modulated through gamma frequency modulation, we hypothesised that we might see changes in the power of gamma oscillations with our optogenetic stimulation patterns.

Having already verified the feasibility of the set-up and our ability to modulate the ongoing theta oscillation through closed-loop theta phase-dependent optogenetic stimulation of two different cell types within the motor cortex, we next aimed to determine whether phase-dependent theta stimulation simultaneously modulates the local gamma oscillation.

First, we aimed to assess whether there was modulation of the local gamma oscillation in either of the cell types we have manipulated – PV+ interneurons and RBP4+ pyramidal neurons, when targeted with theta phase-specific optogenetic manipulation. Both cell types are thought to play a pivotal role in the generation of gamma oscillations (Adesnik & Scanziani, 2010; Cardin et al., 2009; Sohal et al., 2009).

As in the previous two chapters, we also aimed to determine the importance of different stimulation patterns in the potential modulation of the local gamma oscillation. For instance, to assess whether gamma frequency stimulation targeted to a specific phase of the theta oscillation would be more effective at modulating the local gamma oscillation than random gamma or continuous stimulation.

5.2 Methods

For a full summary of the methods and breakdown of mice used, please refer to Chapter 2.

In brief, to assess the effect closed-loop 6Hz theta stimulation has on the local gamma LFP, we used data collected from both PV-Cre and RBP4-Cre mice, described in Chapters 3 and 4. Optogenetic stimulation protocols used in Chapters 3 and 4 include closed-loop gamma, continuous and random gamma stimulation, and our open-loop replay paradigm.

The analyses in this chapter include data collected from 4 PV-Cre Control mice, 6 PV-Cre ChR2 (gamma) and 4 PV-Cre ChR2 (continuous). One PV-Cre mouse used in Chapter 3 was removed from this chapter due to the presence of 50Hz noise, which lies within the gamma frequency range. As well as 4 RBP4-Cre control mice, 10 RBP4-Cre ChR2 mice (gamma), 10 RBP4-Cre ChR2 (continuous stimulation on) and 6 (continuous stimulation off) were included. To examine the effect of gamma rhythmicity extra data was collected in 5 RBP4-Cre ChR2 mice.

5.3 Results

In the previous two chapters we verified the neuronal subtypes and accuracy of our phase targeting and resultant phase-dependent theta modulation. Following on from these results, we first determined whether alongside the changes we demonstrate in theta power, there was modulation in spectral power within the gamma frequency range. Consistent with our previous analyses, all data recorded at either 1 or 2mW were combined and classed as 'stimulation on'.

5.3.1 Theta phase-specific stimulation of inhibitory interneurons

5.3.1.1 No significant theta phase modulation of gamma oscillations in PV-Cre mice

First, we investigated whether there were significant differences in gamma modulation of the local LFP between each of the four targeted theta phases for each group and stimulation (On: 1 & 2mW; Off: 0mW). To address this, data was separated into respective overall stimulation patterns – gamma and continuous. Linear mixed effects (LME) models with fixed effects of group, phase, and laser power and their interactions were used. As with all previous LME models, random effects of subject and date were modelled. Figures 5.1 & 5.2 show mean PSD plots for control and opsin mice, for both gamma and continuous stimulation respectively. Stimulation was either off (0mW; grey pattern) or on (1 or 2mW; blue pattern). To investigate the effect of stimulation on gamma power, the baseline was subtracted (Figure 5.1B; Figure 5.2B) and power spectral density estimates were extracted between 75±18.75Hz (56.25-93.75Hz). This measurement was calculated as ± 25% of the stimulation frequency for consistency of the measurement extracted in the theta range.

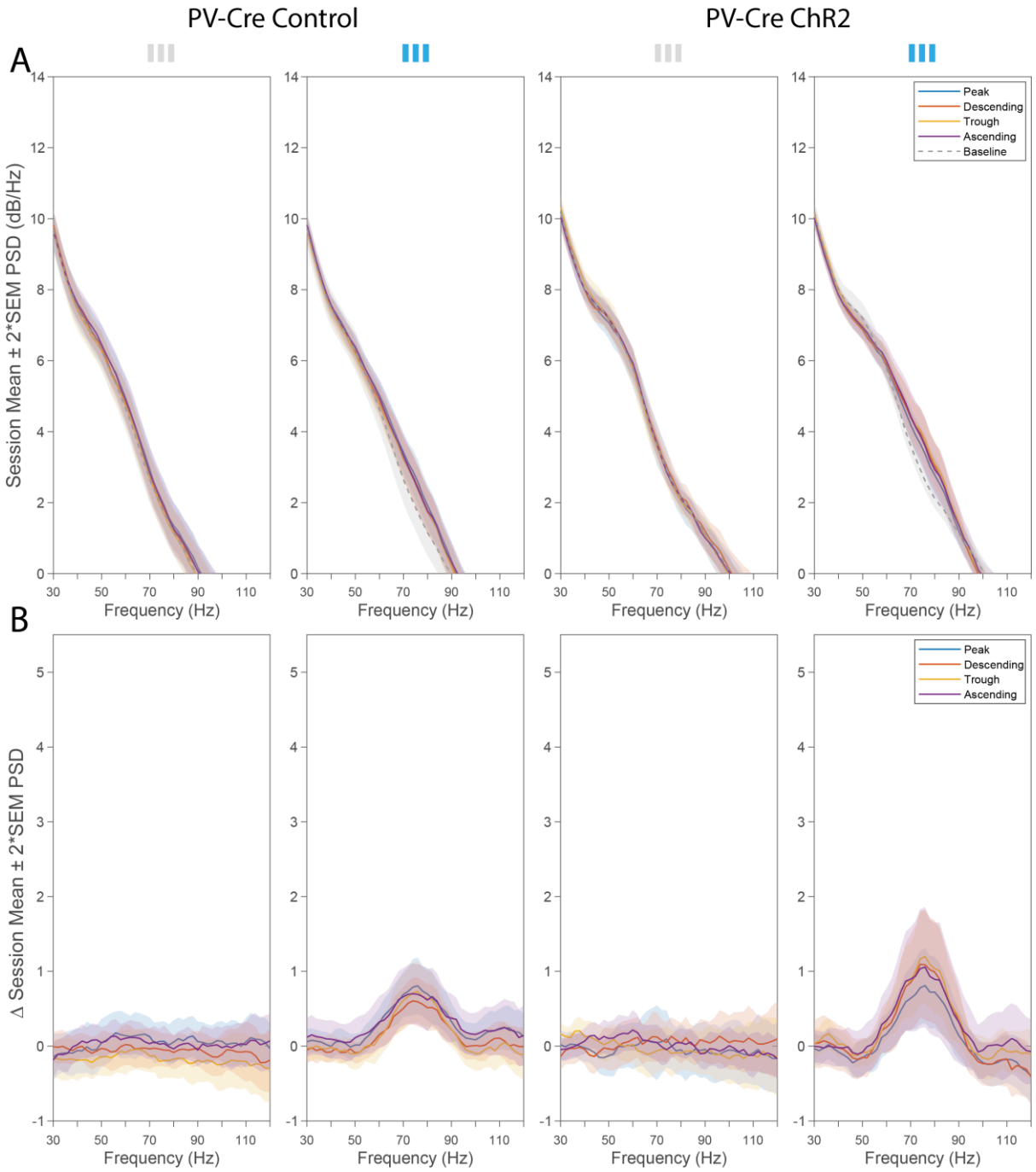


Figure 5.1 Local gamma LFP following closed-loop gamma stimulation targeted to the theta oscillation in PV-Cre mice

Mean power spectral density (±2*SEM) from 30-120Hz for both PV-Cre control (n=4) and opsin mice (n=6), targeting 4 different phases of the theta oscillation with gamma stimulation in PV-Cre mice (**A**). Stimulation was either off (0mW; grey pattern) or on (1 or 2mW; blue pattern). The number of sessions to calculate the mean in control mice was n=14 (14 recordings per phase) for stimulation off and n=15 (29-30 recordings per phase) when stimulation was on. In opsin mice, this was n=15 (14-15 recordings per phase) when stimulation was off and n=15 (26-27 recordings per phase) when stimulation was on. Within each session, a session baseline is calculated from a baseline recorded at the beginning of each session, combined with all unstimulated recordings throughout a session. The mean session baseline was then plotted on each plot for each group and stimulation was on or off. The mean PSDs (±2*SEM) in which the baseline was removed from each session are also plotted for both control and opsin mice (**B**). Statistical analyses performed demonstrated

no significant main effect or interaction terms including phase on gamma power (all p>0.05; LME), subsequently, data from all phases was combined for all further analyses.

When testing the effects of gamma frequency stimulation targeted to the theta oscillation on gamma power (Figure 5.1), unlike our findings in the theta band, there was no significant main effect of phase ($F(3,314)=0.17$, $p=0.91$) or any interaction that included phase [group*phase ($F(3,314)=0.54$, $p=0.66$); phase*laser power ($F(3,314)=0.30$, $p=0.83$); group*phase*laser power ($F(3,314)=0.03$, $p=0.99$)]. As a result, all phases were combined for subsequent analyses of gamma power modulation following gamma frequency stimulation.

Similarly, for continuous stimulation (Figure 5.2), there was no significant main effect of phase ($F(3,274)=0.16$, $p=0.93$) or any of the interactions with phase [group*phase ($F(3,274)=0.26$, $p=0.86$); phase*laser power ($F(3,274)=0.70$, $p=0.56$); group*phase*laser power ($F(3,274)=0.04$, $p=0.99$)]. Consequently, all phases were combined for further analyses of gamma modulation through continuous stimulation of the theta oscillation, as these results suggest no significant differences in gamma power modulation between the targeted theta phases.

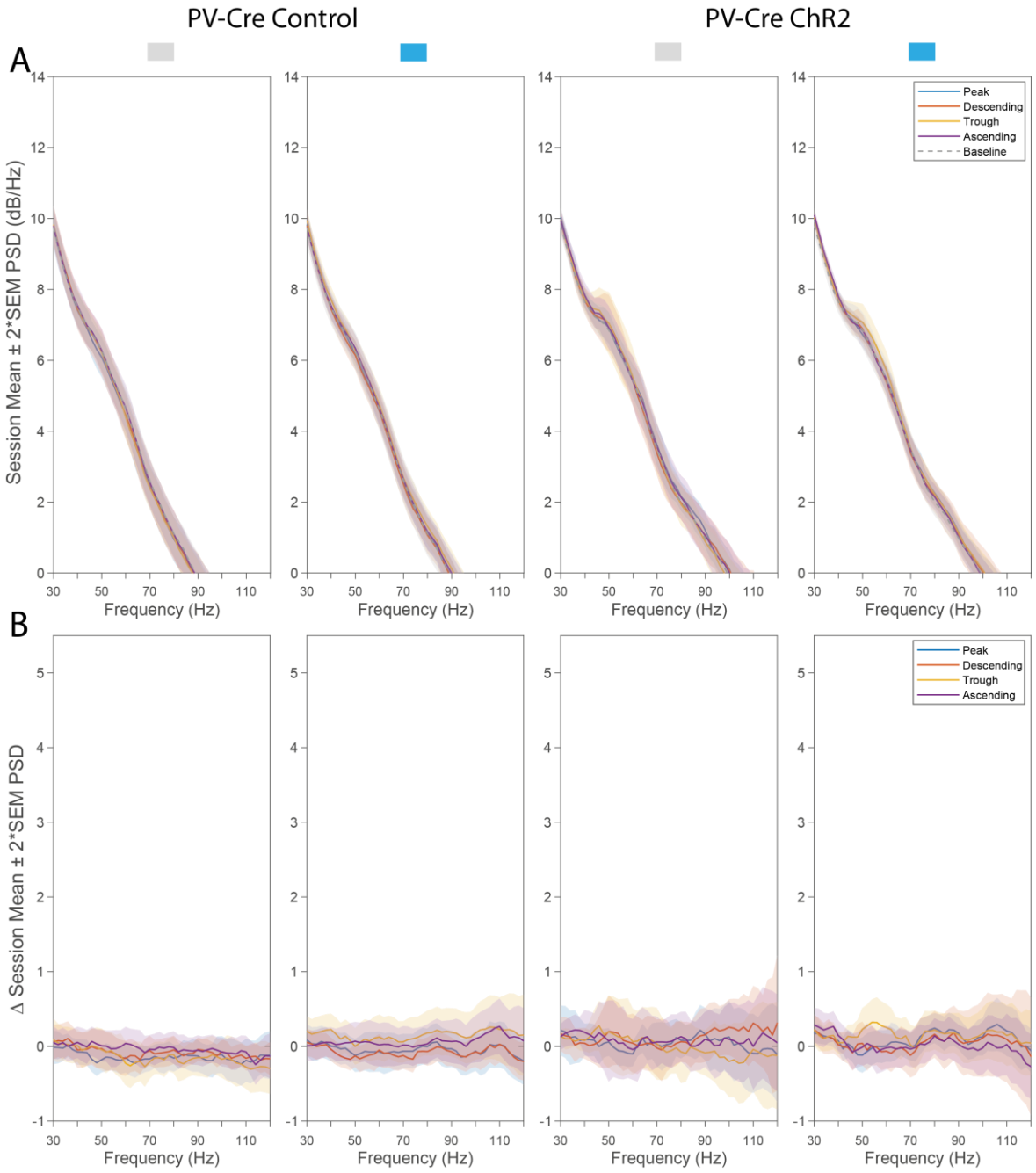


Figure 5.2 Local gamma LFP following closed-loop continuous stimulation targeted to the theta oscillation in PV-Cre mice

Mean power spectral density (±2*SEM) from 30-120Hz for both PV-Cre control (n=4) and opsin mice (n=4), targeting 4 different phases of the theta oscillation with continuous stimulation in PV-Cre mice (**A**). Stimulation was either off (0mW; grey pattern) or on (1 or 2mW; blue pattern). The number of sessions to calculate the mean in control mice was n=16 (16 recordings per phase) for stimulation off and n=16 (31 recordings per phase) when stimulation was on. In opsin mice this was n=9 (8-10 recordings per phase) when stimulation was off and n=9 (18 recordings per phase) when stimulation was on. Within each session, a session baseline is calculated from a baseline recorded at the beginning of each session, combined with all unstimulated recordings throughout a session. The mean session baseline was then plotted on each plot for each group and stimulation was on or off. The mean PSDs (±2*SEM) in which the baseline was removed from each session are also plotted for both control and opsin mice (**B**). No significant main effect or interaction terms including phase

on gamma power were found (all p>0.05; LME), subsequently, data from all phases was combined for all further analyses.

5.3.1.2 Phase-specific theta stimulation of PV-Cre ChR2 mice does not significantly modulate gamma power compared to control mice

Following this, we examined whether stimulation of PV-Cre+ interneurons could modulate gamma power. We hypothesised that gamma power would be significantly modulated during gamma frequency stimulation of the theta oscillation, but not during continuous stimulation in the opsin mice. Additionally, we only expected modulation of gamma when the stimulation was on, compared with off, in the opsin mice. We did not expect there to be any modulation in control mice when stimulation was on. Two LME models were therefore created to test these hypotheses for gamma stimulation and continuous stimulation separately, both with main effects of group (control & opsin) and laser power (stimulation off – 0mW; stimulation on – 1 or 2mW).

When stimulating PV-Cre+ interneurons with gamma frequency stimulation, there was no significant group by laser power interaction ($F(1,316)=0.30$, $p=0.58$). This was unexpected as we hypothesised gamma stimulation would modulate gamma power in opsin mice when stimulation was on. Additionally, the main effect of group was not significant ($F(1,15)=0.22$, $p=0.65$), again unexpected as we had hypothesised there would only be an effect in opsin mice. The main effect of laser power was however significant ($F(1,316)=33.90$, $p<0.001$), suggesting regardless of group there was a difference in gamma power between stimulation being on or off (Figure 5.3A). Post hoc pairwise tests (Tukey adjustment) demonstrated a significant difference between stimulation on and off in both PV-Cre control and opsin groups [$p=0.0013$ & $p=0.0001$ respectively].

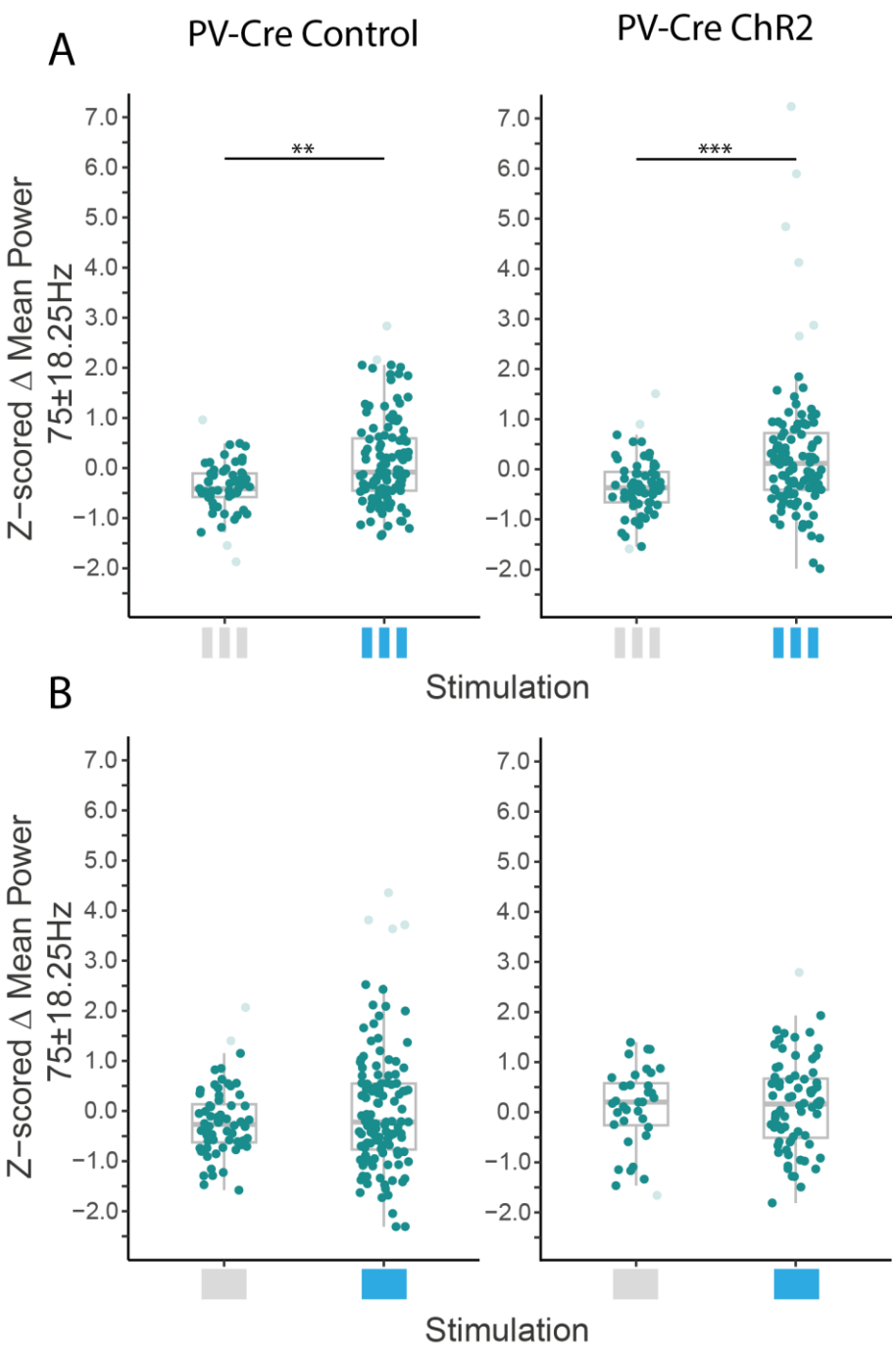


Figure 5.3 Gamma stimulation targeted to the theta oscillation leads to increased effects on gamma power in PV-Cre control and opsin mice, but not continuous stimulation

Boxplots with the z-scored change in gamma power with respect to baseline extracted between 56.25-93.75Hz (75Hz ± 18.75) for both control (n=4) and opsin PV-Cre mice (gamma n=6 (**A**); continuous n=4 (**B**)) are shown when stimulation was on (1 or 2mW; blue patterns) or off (0mW; grey patterns). Stimulation was targeted to 4 phases of the ongoing theta oscillation, statistical analyses found no significant effect of phase on gamma power and therefore as a result all phases were combined for further statistical analyses. A further breakdown of the total number of recordings for gamma stimulation: PV control (n=56 stimulation off; n=118 stimulation on) & PV ChR2 (n=59 stimulation off; n=106 stimulation on). For continuous stimulation, this was:

PV control (n=64 stimulation off; n=124 stimulation on) & PV ChR2 (n=36 stimulation off; n=72 stimulation on). Each session will contain multiple recordings - usually 1 per phase, per laser power for stimulation on data, as data was often collected at both 1 & 2mW. The baseline consisted of a mean calculated from the baseline recorded at the beginning of each session and all unstimulated recordings from within a session. The grey boxes represent the interquartile range and median values from the data set, and the whiskers extend to minimum and maximum values calculated from their quartile ±1.5*IQR for each grouped session. Session means for each laser power are plotted as individual scatter points for their respective group and stimulation type. Lighter scatter points represent data points that lie outside a threshold set as the respective quartile value ±1.5*IQR. Gamma stimulation resulted in significant differences ($p<0.05$) between stimulation on and off in both opsin and control mice (LME, followed by pairwise post hoc t-tests with Tukey adjustment for multiple comparisons). There was no significant effect of continuous stimulation (all $p>0.05$; LME).

Subsequently, when stimulating interneurons using continuous stimulation, the interaction between group and laser power was not significant ($F(1,274)=0.48$, $p=0.49$). As we had hypothesised gamma modulation to be specific to gamma frequency stimulation this was expected (Figure 5.3B). The main effects group and laser power were additionally not significant [($F(1,13)=1.11$, $p=0.31$) & ($F(1,274)=1.44$, $p=0.23$).

5.3.2 Theta phase-specific modulation of excitatory pyramidal cells

Having established that targeting PV-Cre+ interneurons does not result in gamma power modulation greater than the effects of the laser itself, we went on to examine whether this was also the case when targeting RBP4-Cre+ pyramidal neurons.

5.3.2.1 No significant theta phase modulation of gamma oscillations in RBP4-Cre mice

Mean PSD plots are found in Figures 5.4 & 5.5, which include opsin and control mice and stimulation either off (0mW; grey pattern) or on (1 or 2mW; blue pattern). All stimulation on data was combined as in previous analyses. To examine the modulation of gamma power by either gamma stimulation (Figure 5.4) or continuous stimulation (Figure 5.5), as above, the baseline was subtracted, and power spectral density estimates were extracted between 75±18.75Hz (56.25-93.75Hz). This

measurement was calculated as ± 25% of the stimulation frequency for consistency of the measurement extracted in the theta range.

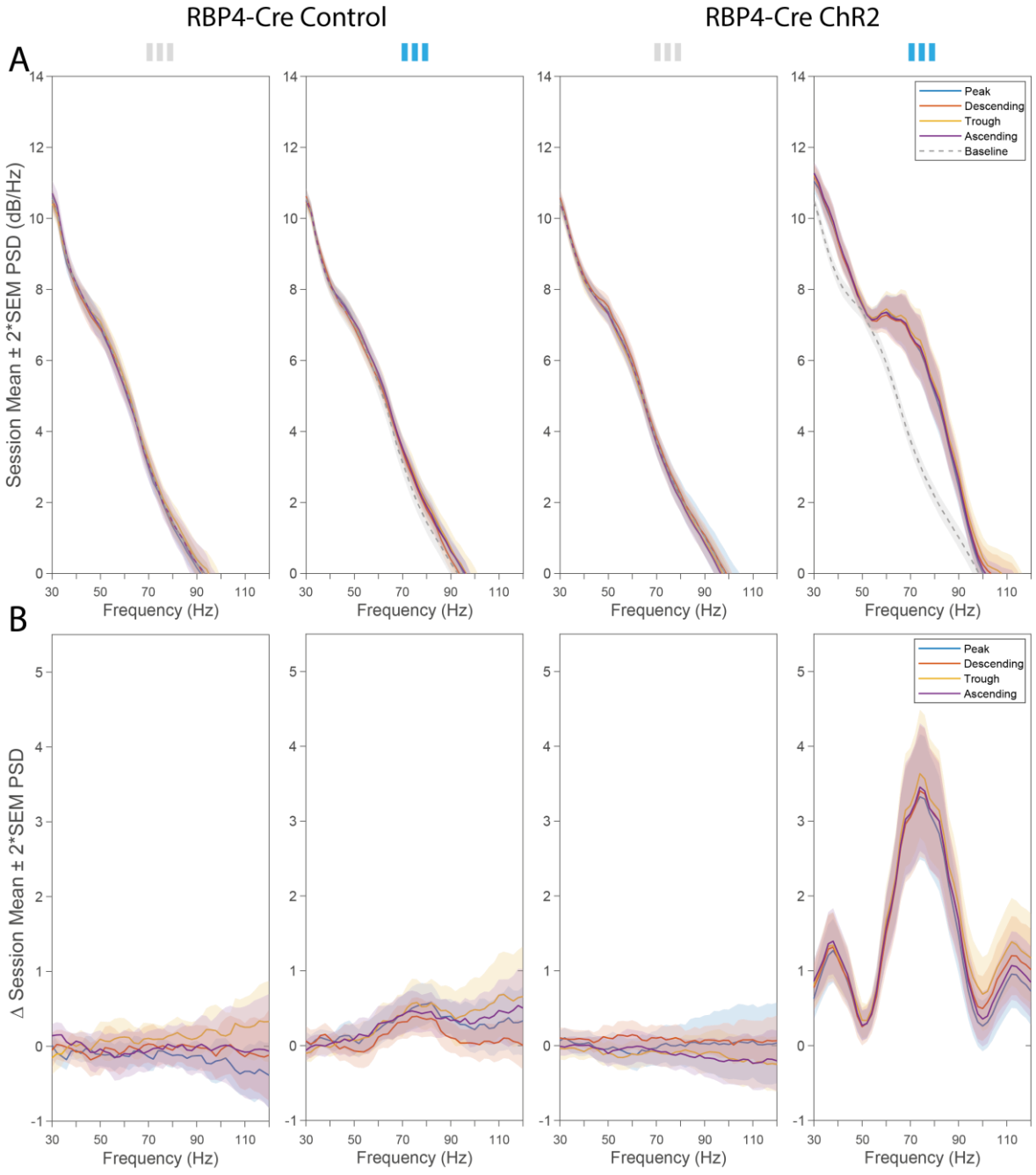


Figure 5.4 Local gamma LFP following closed-loop gamma stimulation targeted to the theta oscillation of RBP4+ pyramidal neurons

Mean power spectral density (±2*SEM) from 30-120Hz for both RBP4-Cre control (n=4) and opsin mice (n=10), targeting 4 different phases of the theta oscillation with gamma stimulation in RBP4-Cre mice (**A**). Stimulation was either off (0mW; grey pattern) or on (1 or 2mW; blue pattern). The number of sessions to calculate the mean & SEM in control mice was n=15 (15 recordings per phase) for stimulation off and n=15 (30 recordings per phase – data from both 1& 2mW) when stimulation was on. In opsin mice this was n=40 (40 recordings per phase) when stimulation was off and n=41 (60 recordings per phase) when stimulation was on. Within each

session, a session baseline was calculated from a baseline recorded at the beginning of each session, combined with all unstimulated recordings throughout a session. The mean session baseline was then plotted on each plot for each group and stimulation was on or off. The mean PSDs (±2*SEM) in which the baseline was removed from each session are also plotted for both control and opsin mice (**B**). No significant main effect or interaction terms including phase on gamma power were identified (all p>0.05; LME), subsequently, data from all phases was combined for all further analyses.

Firstly, as we had when we stimulated PV-interneurons, it was necessary to determine whether there was a difference in gamma modulation between the four different theta stimulation phases. To identify any differences in gamma modulation across phase, we implemented the same LME models as used previously, with fixed effects of group, phase, and laser power and their interactions (random effects of subject & date). Data were separated into their stimulation patterns of either gamma or continuous for this test.

Gamma frequency stimulation (Figure 5.4) resulted in no significant main effect of phase ($F(3,547)=0.14$, $p=0.94$) or interaction terms involving phase [group*phase ($F(3,547)=0.10$, $p=0.96$); phase*laser power ($F(3,547)=0.16$, $p=0.92$); group*phase*laser power ($F(3,547)=0.17$, $p=0.91$)]. Consequently, as this suggested no differences in gamma power across theta phase, all phases were combined for the following analyses.

Likewise, when stimulating theta using the continuous stimulation pattern (Figure 5.5), we found no significant main effect of phase ($F(3,471)=0.84$, $p=0.47$), or interaction terms of phase [group*phase ($F(3,471)=0.11$, $p=0.96$); phase*laser power ($F(3,471)=0.48$, $p=0.70$); group*phase*laser power ($F(3,471)=0.69$, $p=0.56$)]. This suggested no significant difference in gamma power modulation by theta phase and as such, all phases were combined for subsequent analyses.

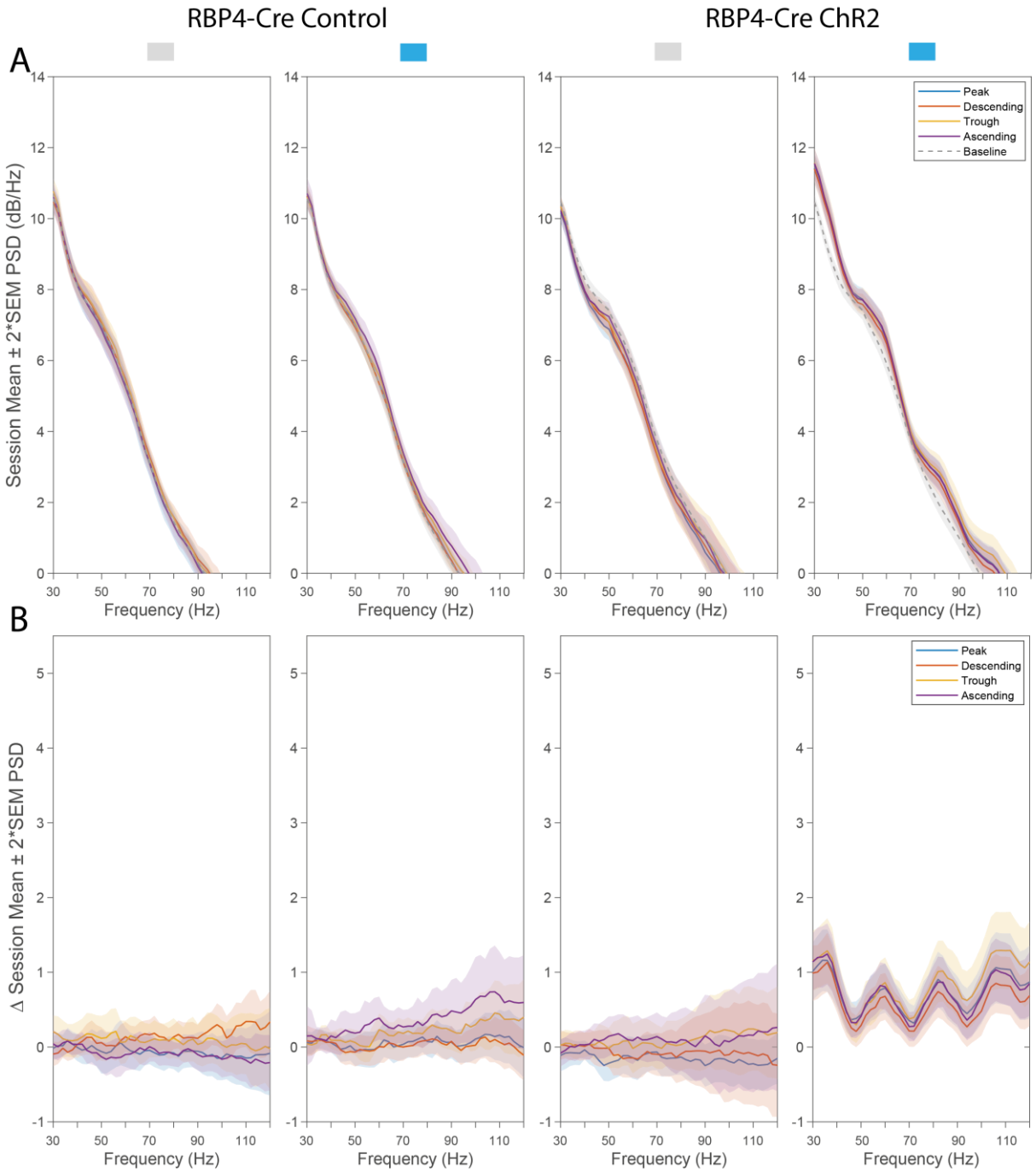


Figure 5.5 Local gamma LFP following closed-loop continuous stimulation targeted to the theta oscillation of RBP4+ pyramidal neurons

Mean power spectral density (±2*SEM) from 30-120Hz for both RBP4-Cre control (n=4) and opsin mice (n=6-10), targeting 4 different phases of the theta oscillation with continuous stimulation in RBP4-Cre mice (**A**). Stimulation was either off (0mW; grey pattern) or on (1 or 2mW; blue pattern). The number of sessions to calculate the mean in control mice was n=15 (15 recordings per phase) for stimulation off and n=15 (30 recordings per phase) when stimulation was on. In opsin mice, this was n=22 (21-23 recordings per phase) when stimulation was off and n=41 (60 sessions per phase) when stimulation was on. Within each session, a session baseline is calculated from a baseline recorded at the beginning of each session, combined with all unstimulated recordings throughout a session. The mean session baseline was then plotted on each plot for each group and stimulation was on or off. The mean PSDs (±2*SEM) in which the baseline is removed from each session are also plotted for both control and opsin mice (**B**). No significant main effect or interaction terms

including phase on gamma power were identified (all p>0.05; LME), subsequently, data from all phases was combined for all further analyses.

5.3.2.2 Phase-specific theta stimulation of pyramidal neurons significantly modulates gamma power

Next, we investigated whether gamma power could be modulated by either of our stimulation patterns (gamma & continuous) when stimulation was on and targeting pyramidal neurons in layer 5 of the motor cortex in opsin mice (Figures 5.4-5.6). We hypothesised there would be an increase in gamma power when stimulation was on, particularly when stimulating at gamma frequency, but only in opsin mice. To assess this, a LME model was devised to examine the main effects of group (control & opsin) and laser power (stimulation off – 0mW; stimulation on – 1 or 2mW) alongside their interaction.

Gamma frequency stimulation targeted to the theta oscillation resulted in modulation of gamma power, as demonstrated by a significant group and laser power interaction ($F(1,544)=69.05$, $p<0.001$). The main effect of laser power was also significant ($F(1,544)=126.06$, $p<0.001$), unexpected as it indicates that regardless of the group there was a difference between stimulation being on or off. The main effect of group was not significant ($F(1,18)=4.01$, $p=0.06$), this indicates the interaction between the group and laser power was key for modulation of gamma power by gamma stimulation of RBP4-Cre pyramidal neurons (Figure 5.6A). Further analyses using post hoc t-tests (Tukey adjustment) identified no differences between control and opsin mice when gamma stimulation was off, or between the RBP4-Cre control group when stimulation was off or on (both $p>0.30$). When stimulation was on vs off in the RBP4-Cre opsin group there was a significant difference ($p<0.0001$), as well as when comparing the

groups when stimulation was on (p=0.006), as anticipated. These results indicate the effects found are a direct result of both opsin presence and light stimulation.

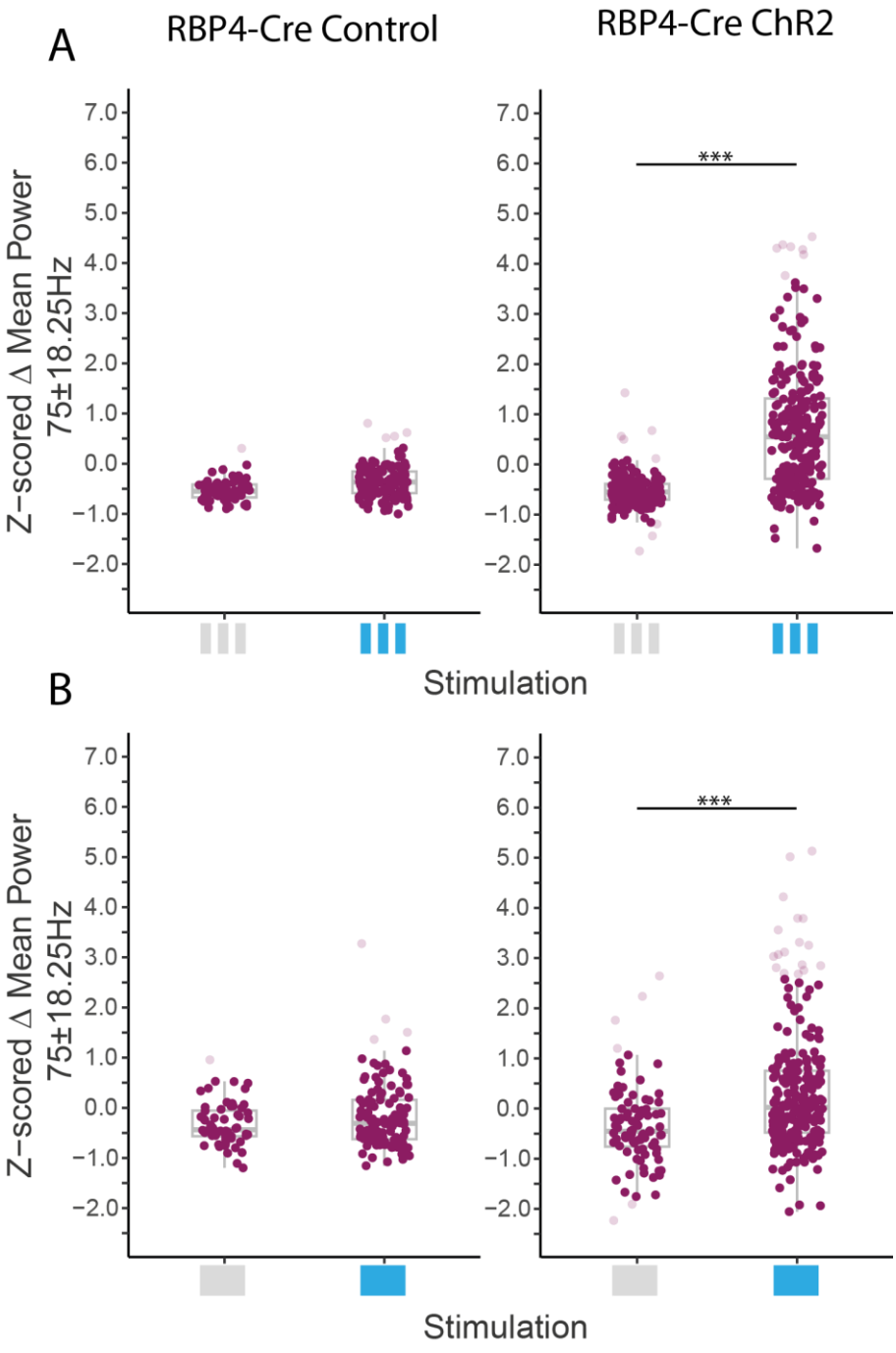


Figure 5.6 Gamma and continuous stimulation targeted to the theta oscillation lead to increased effects on gamma power in RBP4-Cre Opsin mice

Boxplots with the z-scored change in gamma power with respect to baseline extracted between 56.25-93.75Hz (75Hz ± 18.75) for both control (n=4) and opsin RBP4 mice are shown (gamma n=10 (**A**); continuous n=6 stimulation off & n=10 stimulation on (**B**)) when stimulation was on (1 or 2mW; blue patterns) or off (0mW; grey patterns). Stimulation was targeted to 4 phases of the ongoing theta oscillation, statistical analyses found no significant effect of phase on gamma power and therefore as a result all phases were combined for further

statistical analyses. A further breakdown of the total number of recordings for gamma stimulation: RBP4 control (n=60 stimulation off; n=120 stimulation on) & RBP4 ChR2 (n=160 stimulation off; n=240 stimulation on). For continuous stimulation this was: RBP4 control (n=60 stimulation off; n=120 stimulation on) & RBP4 ChR2 (n=88 stimulation off; n=240 stimulation on). Each session will contain multiple recordings - usually 1 per phase, per laser power for stimulation on data, as data was often collected at both 1 & 2mW. The baseline consisted of a mean calculated from the baseline recorded at the beginning of each session and all unstimulated recordings from within a session. The grey boxes represent the interquartile range and median values from the data set, whiskers extend to the minimum and maximum values calculated as their respective quartile ±1.5*IQR. Session means for each laser power are plotted as individual scatter points for their respective group and stimulation type. Lighter scatter points represent data points that lie outside a threshold set as the respective quartile value ±1.5*IQR. Gamma stimulation resulted in significant differences ($p<0.05$) between stimulation on and off in RBP4-Cre opsin mice, as well as when stimulation was on between the control and opsin mice. Continuous stimulation resulted in a significant difference ($p<0.05$) between stimulation on or off in the RBP4-Cre opsin mice. (LME followed up by pairwise post hoc t-tests with Tukey adjustment).

Likewise, the group and laser power interaction was significant when modulating gamma power using continuous stimulation targeted to the theta oscillation ($F(1,480)=10.36$, $p=0.001$). As with gamma frequency stimulation, there was a significant main effect of laser power ($F(1,480)=23.47$, $p<0.001$) but not of the group itself ($F(1,14)=0.467$, $p=0.50$). This again, suggests that the interaction between the group and stimulation being on is important for the modulation of gamma power (Figure 5.6B). To further explore these significant differences, post hoc t-tests (Tukey adjustment for multiple comparisons) identified no significant differences between the two groups when stimulation was off, or in the control group when stimulation was off compared to on (all $p>0.71$). With continuous stimulation, there was unexpectedly no significant difference when stimulation was on between the control and opsin groups ($p=0.30$). However, as expected, there was a significant difference between stimulation being off or on in the opsin group ($p<0.0001$).

5.3.2.3 Stimulation patterns resulting from closed-loop stimulation modulate gamma power to a lesser extent than when phase-locked

We have already demonstrated that we were able to modulate gamma power when targeting RBP4-Cre excitatory neurons, but that this was not dependent on the underlying theta phase stimulated. Therefore, we would predict that our stimulation pattern should drive changes in gamma power, regardless of the underlying phase of the theta. To address this question, we used the data from our open-loop replay paradigm. This was where identical stimulation trains were delivered within the same session without reference or interaction to the underlying theta phase.

For the following analyses, sessions were only included if they were identified as having open-loop replay within the same session. Figure 5.7 shows mean PSD plots either of the original closed-loop recording or open-loop replay from these sessions, for both gamma (Figure 5.7A & 5.7B; blue pulses) and continuous (Figure 5.7C & 5.7D; blue bar) stimulation. The baseline was subtracted (Figure 5.7E-H) and power spectral density estimates were extracted (75±18.75Hz).

LME models were created to test the fixed effects of group (control & opsin) and stimulation type (closed-loop or open-loop replay), alongside their group*stimulation type interaction for each pattern of stimulation. Random effects of subject and date were included in the model. This model compares the control group to the opsin group when stimulated with the original closed-loop stimulation pattern (theta phase-specific, however all phases are combined in these analyses) or the open-loop replay of these phase-specific stimulation patterns.

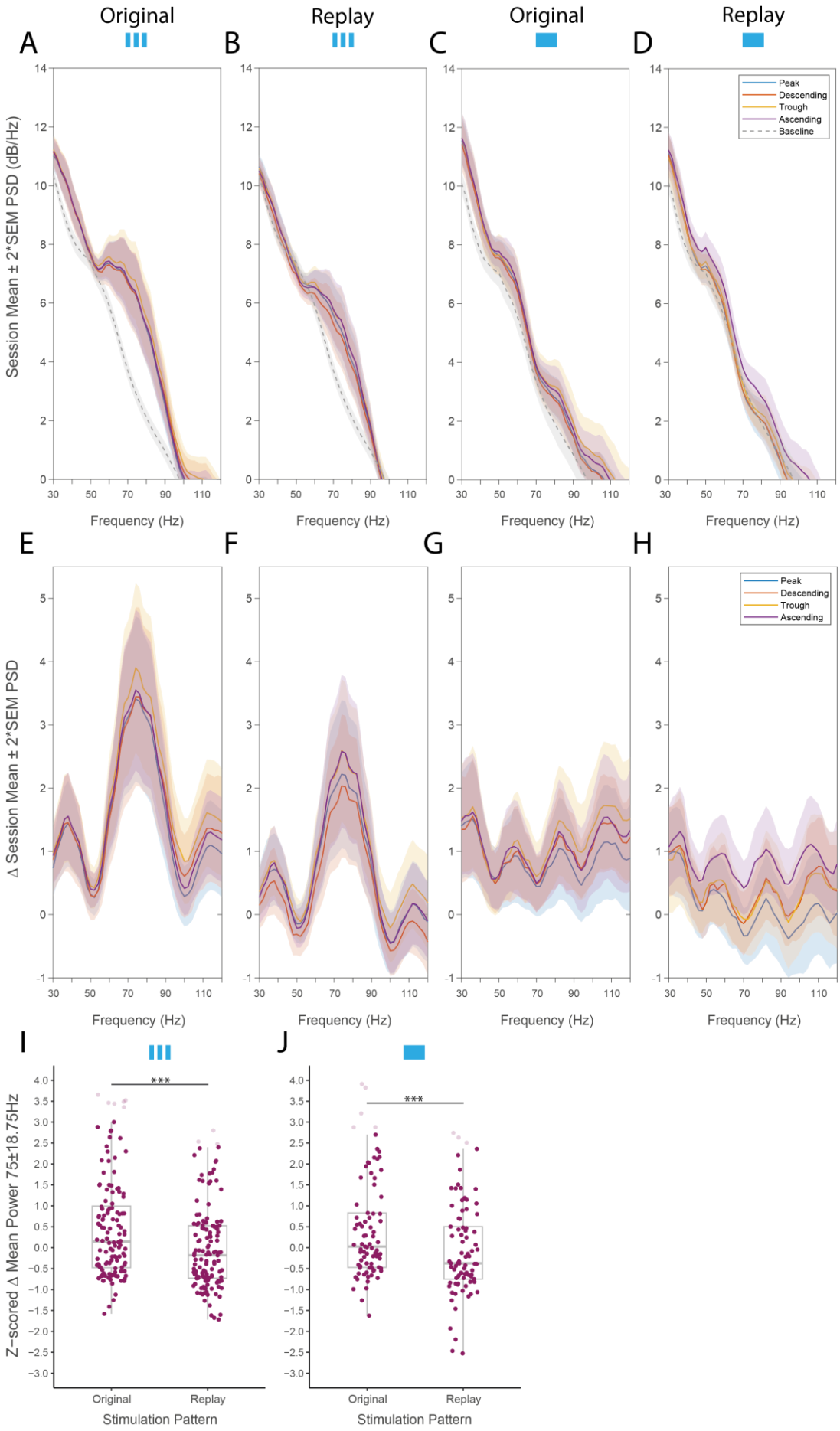

Original
Replay
Original
Replay
A
B
C
D
Session Mean ± 2*SEM PSD (dB/Hz)
Peak
Descending
Trough
Ascending
Baseline
Frequency (Hz)
E
F
G
H
Δ Session Mean ± 2*SEM PSD
I
J
Z−scored Δ Mean Power 75±18.75Hz
***
Original
Replay
Stimulation Pattern

Figure 5.7 Local gamma LFP and z-scored change in gamma power following closed-loop gamma and continuous stimulation targeted to the theta oscillation and their open-loop replays in RBP4-Cre opsin mice

Mean power spectral density (±2*SEM) from 30-120Hz in RBP4-Cre opsin mice (n=9 gamma; n=4 continuous), stimulation on (1 or 2mW; blue pattern). Plots demonstrate PSD for closed-loop optogenetic stimulation targeting 4 different phases of the theta oscillation (original) as well as open-loop replay (replay), in which a previous closed-loop recording is played back to the mouse within the same session. This is demonstrated for both gamma stimulation (original & replay; **A & B** respectively) and for continuous stimulation (original & replay; **C & D** respectively). More specifically, the number of sessions to calculate the mean for gamma (n=24; recordings n=32-34 per phase) and continuous (n=12; recordings n=20-22 per phase), some sessions will have data from both 1 & 2mW. Within each session, a session baseline was calculated from a baseline recorded at the beginning of each session, combined with all unstimulated recordings throughout a session. The mean session baseline is then plotted on each plot for each group and stimulation was on or off. The mean PSDs (±2*SEM) in which the baseline was removed from each session are also plotted for both control and opsin mice (**E-H**). Boxplots demonstrate z-scored change in gamma power with respect to baseline extracted between 56.25-93.75Hz (75Hz ± 18.75) (**I & J**). Grey boxes represent the interquartile range and median values from the data set, whiskers extend to the minimum and maximum values calculated as their respective quartile ±1.5*IQR. Session means for each laser power are plotted as individual scatter points for their respective group and stimulation type. Lighter scatter points represent data points that lie outside a threshold set as the respective quartile value ±1.5*IQR. Number of sessions for control mice (n=4): gamma n=10, recordings n=15-17 per phase; continuous n=9, recordings n=16-17 per phase. Significant differences were identified for each stimulation pattern between the closed-loop stimulation and its open-loop replay in opsin mice (both patterns $p<0.05$; LME followed up by pairwise post hoc t-tests with Tukey adjustment).

Gamma frequency stimulation demonstrated a significant group-by-stimulation type interaction ($F(1,366)=14.03$, $p<0.001$) as expected, as we hypothesised there wouldn't be any effect of stimulation in the RBP4-Cre control group. The main effect of stimulation type was significant ($F(1,366)=18.82$, $p<0.001$), indicating a difference in gamma power modulation between closed-loop stimulation and its open-loop replay counterpart. The main effect of group was not significant ($p=0.07$). Additional post hoc t-tests (Tukey adjustment for multiple comparisons) confirmed a significant difference between the original closed-loop gamma stimulation pattern and the open-loop replay ($p<0.0001$), Figure 5.7I.

To determine whether the pattern of continuous stimulation alone was sufficient for altering gamma power, we used the same LME model described above. As with gamma stimulation, there was a significant group by stimulation type (closed-loop or

open-loop replay) interaction ($F(1,281)=4.40$, $p=0.037$) as well as the main effect of stimulation type ($F(1,281)=11.31$, $p<0.001$). There was no significant main effect of group ($p=0.26$). Follow-up post hoc t-tests (Tukey adjustment) found a significant difference between the original closed-loop continuous stimulation and its open-loop replay counterpart, Figure 5.7J ($p=0.0003$).

To follow up on the significant group-by-stimulation type interactions presented above, it was necessary to identify how open-loop replay modulates gamma power separately within the opsin mice for each stimulation pattern (gamma or continuous). LME models were created to test the fixed effect of stimulation type – the difference between the original closed-loop recording and the open-loop replay recording (random effects: subject & date).

In the opsin group receiving gamma stimulation, there was a significant effect of stimulation type ($F(1,244)=49.05$, $p<0.001$), indicating a significant difference in the degree of gamma power modulation between the closed-loop recording and open-loop replay (Figure 5.7I). Similarly, when the opsin group was stimulated with continuous stimulation, there was a significant effect of stimulation type ($F(1,158)=16.59$, $p<0.001$) indicating the original closed-loop recording and the open-loop replay of this stimulation pattern modulate gamma power to different extents (Figure 5.7J).

These data (Figure 5.7I & 5.7J) demonstrate differences in the modulation of gamma power between the original closed-loop recordings and their open-loop replay counterparts for each stimulation pattern (gamma and continuous).

5.3.2.4 Theta phase-specific stimulation patterns differentially modulate gamma power when targeted to pyramidal neurons

We previously found gamma rhythmicity not to affect phase-dependent theta power modulation, however, we then proceeded to determine whether gamma rhythmicity was important for modulating gamma power. This was possible in our later cohort of RBP4-Cre ChR2 mice (n=5) in which we introduced the 'random gamma' stimulation pattern, as described in the methods (Chapter 2) and used in Chapter 4. This stimulation pattern only differed from gamma stimulation by the movement of the middle gamma pulse between the two outside pulses, which themselves stayed the same. Having previously controlled for the presence of opsin in this mouse line, this cohort only had ChR2 mice and no control group. As well as this new stimulation pattern, gamma, and continuous stimulation were also tested. We hypothesised that gamma stimulation would be more effective in modulating gamma power than either of our other two stimulation patterns, gamma random or continuous.

Although we previously determined no effect of theta phase when modulating gamma power in this mouse line which targets RBP4-Cre pyramidal neurons, we reconfirmed this in this smaller subset of the data. A LME model with fixed effects of phase, laser power, their interaction and random effects of subject and date was used. Data were separated into respective stimulation patterns for running the model. There was no significant main effect of phase ($F(3,143)=0.07$, $p=0.98$) or interaction term of phase and laser power ($F(3,143)=0.15$, $p=0.93$) when testing gamma stimulation as expected. Likewise, when testing random gamma stimulation there was no significant main effect or interaction term with phase (phase*laser power) [$F(3,144)=0.15$, $p=0.93$) & $F(3,144)=0.07$, $p=0.98$) respectively]. As we only collected data when

continuous stimulation was on, this LME model was slightly different and only had a main effect of phase. As with the other stimulation patterns, this was not significantly different ($F(3,67)=0.37$, $p=0.78$). As a result of this, data from across all the four theta phases were combined for all further analyses of stimulation patterns.

Mean PSD plots are shown in Figure 5.8, for each stimulation type, with stimulation either on (2mW, blue patterns) or off (0mW, grey patterns). The baseline was removed, and power spectral density estimates were extracted for statistical analyses (Figure 5.8C) between 75Hz ±18.75. In these analyses, 5 mice were used from a total of between 19-20 sessions depending on the stimulation pattern and stimulation on/off.

5.3.2.5 Rhythmic gamma stimulation most significantly modulates gamma power

To investigate the role gamma rhythmicity has on gamma power modulation, we formulated a LME model with fixed effects of stimulation pattern and laser power (random effects of subject & date). For this test, only data from gamma and gamma random stimulation types was used, as we did not collect 'stimulation off' data for the continuous stimulation pattern.

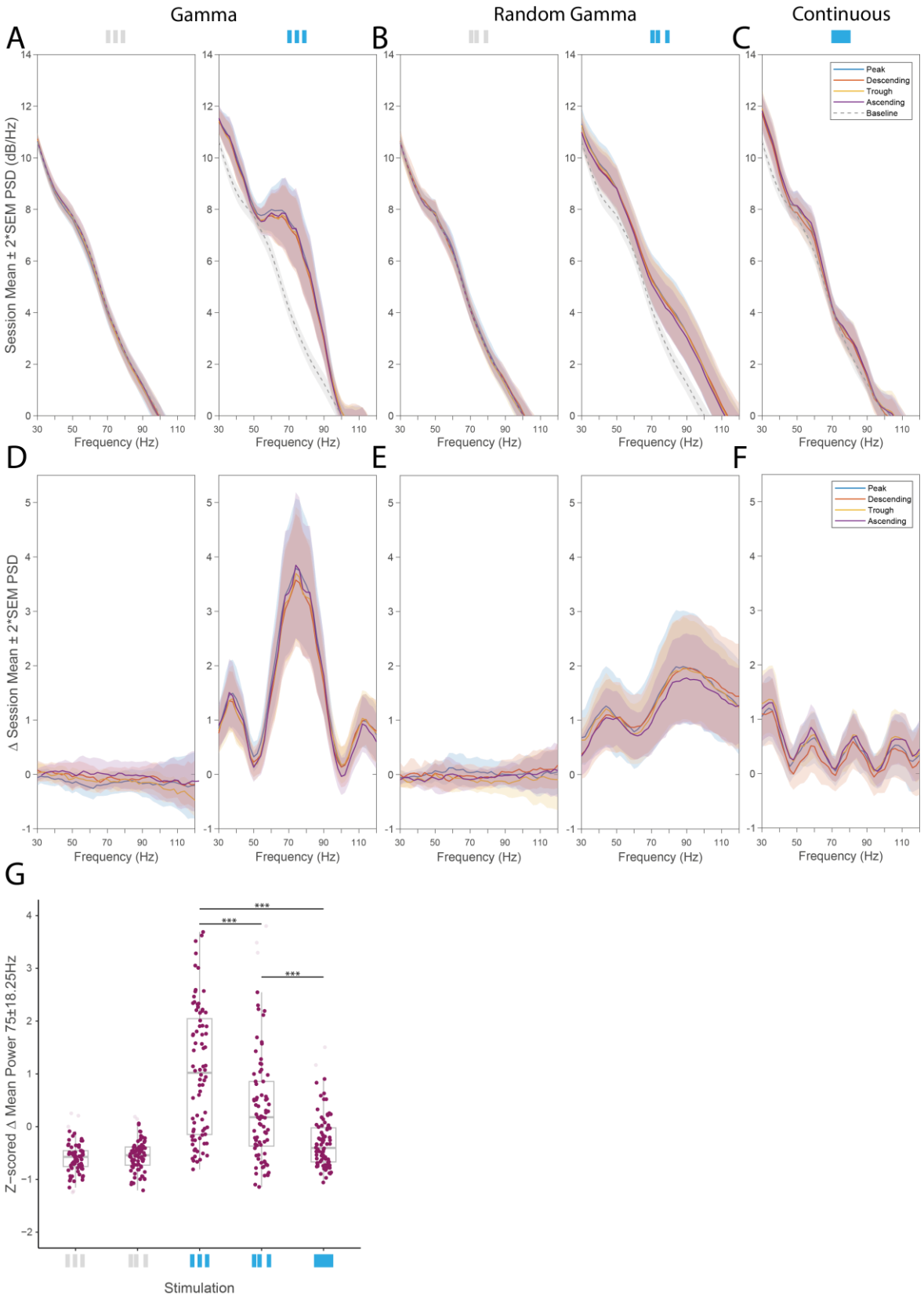


Figure 5.8 Modulation of local gamma LFP in response to gamma, random gamma, and continuous stimulation in RBP4-Cre opsin mice

Mean power spectral density (±2*SEM) from 30-120Hz in the later cohort of RBP4-Cre ChR2 mice (n=5). To test the importance of gamma rhythmicity, 4 different phases of the theta oscillation were targeted with either

gamma (**A**), random gamma (**B**), or continuous (**C**) stimulation. Stimulation was either off (0mW; grey pattern) or on (2mW; blue pattern). The number of sessions for each phase and stimulation pattern - gamma: 20 stimulation on & 19 stimulation off, random gamma: 20 stimulation on & 19 stimulation off, continuous stimulation on: 20. No data was collected when stimulation was off when stimulating with the continuous stimulation pattern. For statistical analyses data across all 4 phases were combined. Within each session, a session baseline is calculated from a baseline recorded at the beginning of each session, combined with all unstimulated recordings throughout a session. The mean session baseline is then plotted on each plot for each stimulation type. Mean PSDs (±2*SEM) in which the baseline was removed from each session are also plotted (**D-F**). Boxplots represent the z-scored change in mean power with respect to the baseline for each stimulation pattern (**G**). Grey boxes denote the interquartile range and median. Whiskers extend to the minimum and maximum values calculated from their respective quartile ±1.5*IQR. Session means are plotted as individual scatter points for their respective group and stimulation type. Lighter scatter points represent data points that lie outside a threshold set as the respective quartile value ±1.5*IQR. Significant differences were identified when stimulation was on between each stimulation pattern (all $p<0.05$; LME followed by pairwise post hoc t-tests with Tukey adjustment).

There was a significant interaction between stimulation pattern (gamma and gamma random) and laser power (stimulation on/off) ($F(1,300)=19.69$, $p<0.001$), indicating as we hypothesised that there was a difference between the two gamma stimulation patterns and the degree to which they modulate gamma power. There were also significant main effects of stimulation pattern and laser power [$F(1,300)=13.80$, $p<0.001$) & $F(1,300)=245.13$, $p<0.001$) respectively]. These were both expected, as we anticipated a difference between the stimulation patterns, but only expected these differences when stimulation was on regardless of the stimulation pattern. As a result, we ran further pairwise post hoc t-tests (Tukey adjustment) which identified no significant difference between the two gamma stimulation patterns when the laser was off ($p>0.05$). Furthermore, there were significant differences between all combinations of stimulation off and each stimulation pattern on (all $p<0.0001$) as we expected. Finally, there was a significant difference between the two gamma stimulation patterns when stimulation was on ($p<0.0001$).

5.3.2.6 *Gamma power modulation varies significantly across all three stimulation patterns*

To follow up on the significant interaction of stimulation pattern and laser power, as well as the main effect of stimulation pattern, the data were separated into stimulation on. Then tested using a LME model with a fixed effect of stimulation pattern, allowing us to compare all three stimulation patterns when the stimulation was on (gamma, random gamma & continuous – Figure 5.8G). There was a significant main effect of stimulation pattern as expected ($F(2,227)=62.75$, $p<0.001$), suggesting differences in the modulation of gamma power by each stimulation pattern. This was followed up with pairwise post hoc t-tests (Tukey adjustment), which found significant differences between gamma and gamma random, gamma and continuous, and finally gamma random and continuous stimulation patterns (all $p<0.0001$).

5.3.2.7 *Resultant random gamma closed-loop stimulation pattern leads to significantly less modulation of gamma power*

As with our other stimulation patterns, we next determined whether the random gamma stimulation pattern alone was sufficient to drive changes in gamma power. To examine this question, we utilised our open-loop replay paradigm, and sessions were only included if they were identified as having open-loop within the same session (n=12 sessions gamma (total of 45 recordings); n=10 sessions random gamma (total of 38 recordings)). Mean PSD plots are shown in Figure 5.9 of original theta phase closed-loop recordings compared to open-loop replay from these same sessions. This is demonstrated for gamma (Figure 5.9A) and random gamma (Figure 5.9B) stimulation patterns. The baseline was subtracted, and power spectral density estimates were extracted (75±18.75Hz).

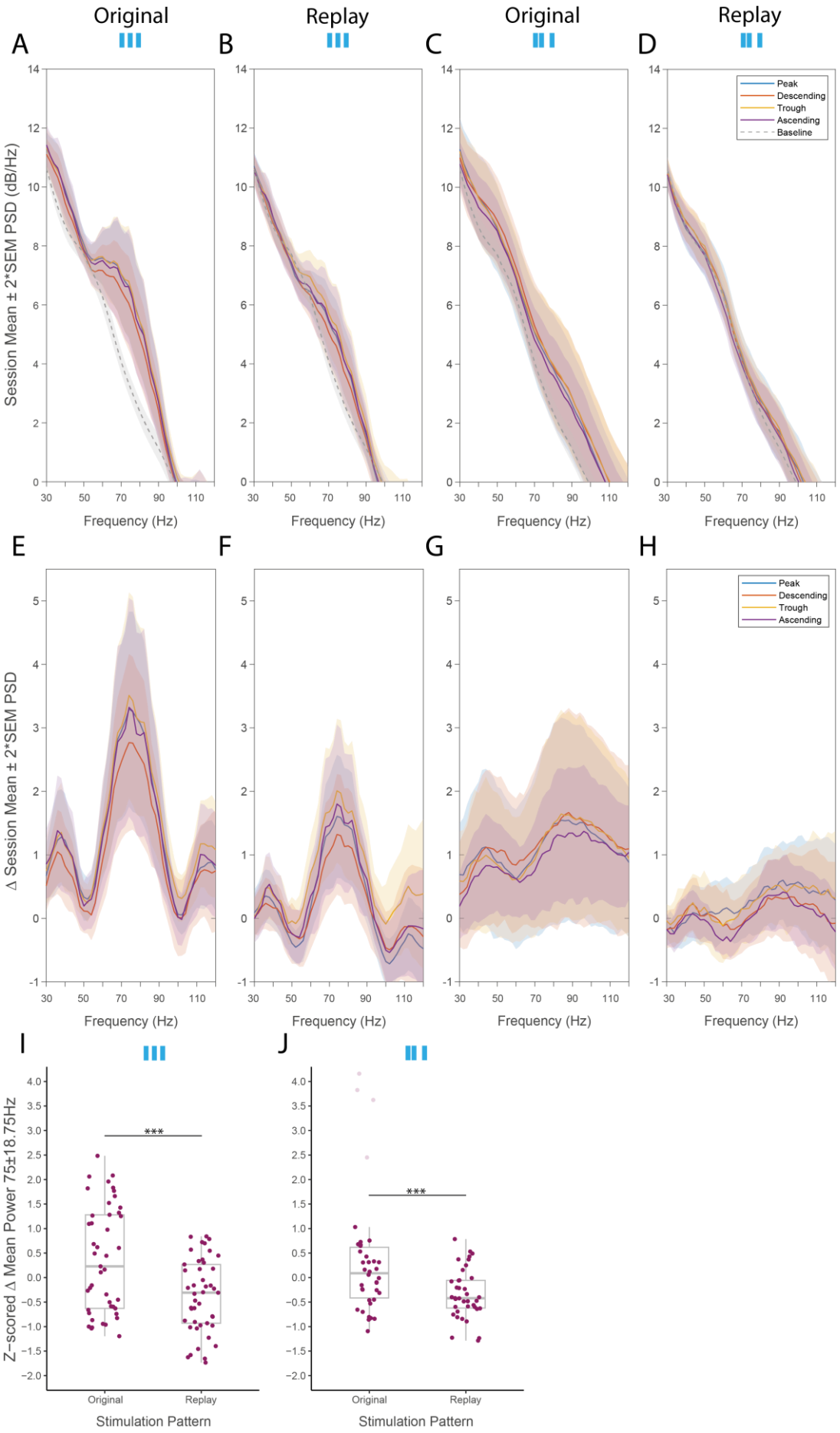

Original
Replay
Original
Replay
A
B
C
D
Session Mean ± 2*SEM PSD (dB/Hz)
Frequency (Hz)
Peak
Descending
Trough
Ascending
Baseline
E
F
G
H
Δ Session Mean ± 2*SEM PSD
I
J
Z-scored Δ Mean Power 75±18.75Hz
***
Original
Replay
Stimulation Pattern

Figure 5.9 Local gamma LFP and z-scored change in gamma power following closed-loop gamma and random gamma stimulation and their open-loop replays in RBP4-Cre opsin mice

Mean power spectral density (±2*SEM) from 30-120Hz in RBP4-Cre opsin mice (n=5), stimulation on (2mW; blue pattern). Plots demonstrate PSD for closed-loop optogenetic stimulation targeting 4 different phases of the theta oscillation (original) as well as open-loop replay (replay), in which a previous closed-loop recording is played back to the mouse within the same session. This is demonstrated for both gamma stimulation (original & replay; **A & B** respectively) and for random gamma stimulation (original & replay; **C & D** respectively). More specifically, the number of sessions to calculate the mean for gamma (n=12; n=11-12 per phase, total across all phases=45) and random gamma (n=10; n=9-10 per phase, total across all phases=38). Within each session, a session baseline was calculated from a baseline recorded at the beginning of each session, combined with all unstimulated recordings throughout a session - the mean session baselines are plotted on each plot. The mean PSDs (±2*SEM) in which this baseline was removed from each session are also plotted for both control and opsin mice (**E-H**). The change in mean power is plotted as boxplots (**I & J**) – grey lines represent the median and interquartile range. Whiskers extend to the respective quartile ±1.5*IQR. Scatter points represent a recording from a specific session, each recording has 4 scatter points as these were recorded as one for each phase for each stimulation type (previously we determined no significant effect of phase, and data from all phases were combined). Lighter colour scatter points are points that could be considered outliers, these are the quartile ±1.5*IQR. We found a significant interaction between closed-loop and open-loop replay for both stimulation patterns (both $p<0.001$; LME model).

LME models were created to test the main effect stimulation type (closed-loop vs open-loop replay), and random effects of subject and date were included. The data for each stimulation pattern, gamma, and random gamma were separated for testing. When stimulating with gamma frequency stimulation we found a significant main effect of stimulation type ($F(1,81)=49.96$, $p<0.001$), indicating a difference in gamma modulation between closed-loop gamma stimulation and modulation by its open-loop replay. Similarly, for random gamma closed-loop and open-loop replay of these stimulation patterns, we also found a significant main effect of stimulation type ($F(1,64)=23.59$, $p<0.001$), suggesting a difference between the degree of gamma power modulation between the two types. These demonstrate differences between the modulation of gamma power for both stimulation patterns delivered to these RBP4-Cre opsin mice in a closed-loop manner and their open-loop replay counterparts.

5.4 Discussion

In the previous two chapters, we provided evidence that closed-loop phase-specific modulation of motor cortical theta oscillation was possible when optogenetically stimulating both PV+ interneurons and RBP4+ pyramidal neurons. As these two neuronal types play a vital role in the generation of oscillations and have particularly been identified as key neurons for generating gamma oscillations (Rudy et al. 2011), we aimed to assess whether theta phase-specific modulation could produce additional changes in gamma power. We had anticipated that, if we were to modulate gamma oscillations in this way, this may be more effective when stimulated with gamma and not with continuous stimulation.

5.4.1 Gamma stimulation did not lead to increased gamma power when targeting PV+ interneurons

When stimulating PV+ interneurons with gamma stimulation, we found significant modulation of gamma power, although this effect was observed in both the PV-Cre ChR2 and control mice, which was unexpected. There were no significant differences between modulation in any theta phase, which suggests that the effect was driven as a direct result of laser stimulation and consequent tissue heating or photoelectric artifact in both opsin and control mice. The effect is visually smaller in control mice and statistical analyses comparing stimulation on versus off conditions within each PV-Cre mouse type indicated a higher level of statistical significance in the opsin mice. This may suggest that the opsin somewhat contributes to the modulation in PV-Cre ChR2 mice, although, this would be hard to disentangle from the potential effects of heating or optical artifact. Moreover, there was no significant modulation of gamma power when continuous stimulation was targeted to any of the theta phases in either

PV-Cre control or opsin mice. This could be explained by the fact gamma frequency stimulation is necessary for evoking changes in gamma power, and thus a single pulse across ¼ of the theta cycle is ineffective in modulating gamma. As reported in Chapter 3, we previously found no significant changes in theta power in control mice with either gamma or continuous stimulation. Therefore, these data suggest that LFP power in PV-Cre control mice is specifically modulated by gamma stimulation in the gamma frequency range, but not within the theta range, nor in either range by continuous stimulation. In summary, our data show that we were unable to produce changes in gamma power alongside theta power modulation when stimulating inhibitory interneurons.

5.4.2 Gamma and continuous stimulation lead to increased gamma power when targeting RBP4+ pyramidal neurons

In contrast, the results when targeting RBP4+ pyramidal neurons were quite different. We found that both gamma frequency and continuous stimulation targeted to all phases of the theta oscillation could drive gamma power. Significant differences between stimulation on and off were only observed in RBP4-Cre ChR2 mice. We found significant differences in gamma modulation between the two stimulation patterns. However, gamma stimulation (75Hz) produced a peak in gamma power around 75Hz, but more broadly modulated gamma frequencies between 60Hz and 90Hz. Continuous stimulation, on the other hand, produced a few smaller gamma peaks at approximately, 60Hz, 80Hz and 105Hz. This pattern of stimulation resulting in multiple gamma peaks may indicate a stimulation artifact in opsin mice, linked to the onset and offset of stimulation. However, this was not observed in control mice or when targeting

PV+ interneurons. We also found no modulation of gamma power in our stimulation off control, thus indicating this is purely an effect of stimulation being on.

5.4.3 The rhythm of gamma stimulation is important for the modulation of gamma power

In RBP4-Cre mice we were also able to test our third stimulation pattern – random gamma. This was devised to determine the role gamma rhythmicity plays in modulation. In Chapter 4, we reported that there were no significant differences between gamma and random gamma stimulation on the degree of theta power modulation. Contrastingly, this was not the case when assessing the effect random gamma stimulation of the theta oscillation had on gamma power modulation. While random gamma stimulation can drive gamma power, it does this less so than the original gamma stimulation pattern, but more than continuous stimulation. Significant differences in gamma power modulation were found between all three stimulation patterns. Random gamma could modulate theta power more than continuous stimulation, but not in the same way gamma stimulation could. Random gamma stimulation instead produced a peak in gamma power at around 90Hz, demonstrating its altered rhythmicity.

5.4.4 Open-loop replay of theta-phase locked stimulation modulated gamma power to a lesser extent

Furthermore, we found significant differences in gamma modulation between stimulation pattern trains delivered when phase-locked to the theta oscillation and when delivered as open-loop replay. This was the case for all stimulation patterns. While this indicates that some property of closed-loop stimulation is important in driving gamma power, the modulation of gamma power is not dependent on

underlying phase as we found no effect of theta phase on gamma frequency. We found that the open-loop replay spectra replicated the pattern of gamma power modulation demonstrated during closed-loop recordings, but to a lesser extent. This suggests that, at some level, the phase of theta is important for gamma power modulation as the stimulation pattern alone resulted in significantly less gamma modulation at all phases. This could perhaps suggest that theta-gamma PAC may be important and induced by stimulation without the presence of a behavioural task, although all theta phases modulated gamma power in the same way. There is evidence that the amplitude of theta can modulate the strength of theta-gamma coupling (Canolty et al. 2006; Igarashi et al. 2013), therefore, it is possible that stimulation targeted to phases that increase theta power may lead to stronger theta-gamma coupling within our set up regardless of whether the amplitude of gamma changes by phase. Future analyses of PAC will be vital to determine whether there is evidence of this within our experimental set-up. Overall, these findings may imply that some aspects of neural coding are still phase-sensitive and critical for neural activity. Therefore, our results highlight the importance of determining how these circuits encode information throughout the brain and their dynamic nature.

5.4.5 Optogenetic stimulation led to modulation of gamma power in both control and opsin PV+ mice

Overall, our results indicate that stimulation of pyramidal neurons, but not inhibitory interneurons, can effectively modulate gamma power as a direct result of optogenetic stimulation. As it has previously been shown that PV+ interneurons can be modulated at gamma frequency (Cardin et al. 2009; Gunaydin et al. 2010), and their role in the generation of gamma oscillations is well described (Rudy et al. 2011), this result was

unexpected. Moreover, in this study, we used the minimal laser power necessary to drive responses (1-2mW), which is less than the 5-10mW previously shown to alter firing or neuronal oscillations as a direct effect of heating (Stujenske et al., 2015). If the modulation of gamma power we observed in the control mice was purely a result of heating, we would expect similar results with continuous stimulation which is longer than the length of the three combined gamma pulses, and similar effects theta power in the PV-Cre control mice, neither of which we observed. We might also expect to observe significant modulation of gamma power in RBP4-Cre control mice, which we did not. Although visual inspection of the data from the RBP4-Cre control mice shows a very small modulation of gamma power with gamma stimulation, this is not statistically significant. The simplest explanation for this, is that there is rhythmic photo-artifact in the local gamma field potential due to the stimulation itself being periodic, especially given we are applying three rhythmic pulses when stimulating with the gamma pattern. This artifact could subsequently cause an increase in LFP power which could explain why we see similar effects in PV-Cre control and opsin mice.

Another reason control mice may show modulation of gamma power in response to stimulation, could be due to differences in the vascularisation of the tissue. Differences in vasculature between mice have previously been shown to contribute to significant effects of increases in tissue temperature as a result of illuminating the tissue (Arias-Gil et al. 2016). Even if the control and opsin groups are from the same mouse strain, control mice may by chance have had more blood vessels than the opsin group. However, it is unlikely that this variation would be large enough between the same genotype or litter(s) of mice to explain the result we see.

Laser heating effects have also been demonstrated to suppress neuronal activity, particularly in FS interneurons in cortical layer 5 (Owen et al., 2019). It is therefore possible that the effects of optogenetic modulation in PV-Cre ChR2 mice are masked by the heating effects of the laser.

It is also possible that gamma stimulation creates tissue heating that somehow mimics sinusoidal activity, which might putatively create small, sinusoidally varying changes in temperature at gamma frequency in both control and opsin mice. This could ultimately produce the increases in gamma LFP power we see across both PV- groups and be linked to a property of FS interneurons.

A previous study demonstrated bidirectional optogenetic modulation of gamma oscillations *in vitro* pyramidal cells, although, they were unable to replicate this effect when targeting interneurons instead (Nicholson et al. 2018). The authors propose that this was due to the out-of-phase recruitment of interneurons powerfully suppressing the oscillation (Nicholson et al. 2018). As we find an effect of only pyramidal and not interneurons, this might potentially explain our results. Activating interneurons out of phase with the ongoing gamma oscillation might effectively desynchronise and therefore suppress the underlying gamma oscillation, potentially masking the stimulation-induced modulation of gamma power in the PV-Cre opsin mice. Nicholson et al (2018) additionally suggest that optogenetic modulation of pyramidal cell activity was effective due to the weaker phase-locking of pyramidal neurons than PV+ interneurons to gamma oscillations, therefore allowing the oscillation to be more flexibly modulated. This hypothesis is potentially consistent with our results and suggests that stimulation of pyramidal neurons rather than PV+ interneurons has

greater potential to modulate network dynamics in the gamma band (Nicholson et al. 2018). Our data have the potential to add to this line of reasoning as we are able to directly determine the extent of gamma oscillatory phase-locking for individual cell types by exploring the unit data. Our model also directly reflects the complexity of the *in vivo* brain.

5.4.6 75Hz is a key frequency in the motor cortex

All three stimulation patterns targeted to RBP4+ pyramidal neurons effectively modulated gamma power, although the gamma stimulation pattern could induce the highest degree of modulation. This indicates that oscillatory firing in pyramidal neurons is driven directly by stimulation. This finding is consistent with previous research that was able to effectively drive pyramidal neurons at gamma frequency, although these frequencies were lower than our 75Hz (Adesnik & Scanziani, 2010; Sohal et al., 2009). The difference in modulation of gamma power in response to either gamma or random gamma stimulation patterns suggests that neurons are driven by the rhythmicity of all three pulses during gamma stimulation, as changing this rhythmicity very slightly significantly alters the degree to which gamma power is modulated.

In support of continuous stimulation modulating gamma power within our study, a previous study demonstrated that a 2-second continuous light pulse was able to drive excitatory neurons in the visual cortex in anaesthetised cats, producing a ~70Hz peak depending on the animal and session (Lewis et al., 2021). Whilst this experiment was performed in a different region of the cortex, in anaesthetised animals, and used a much longer stimulation than our ~41ms continuous light pulse, they also found

optogenetically-induced gamma to emerge immediately following the stimulation onset. Additionally, optogenetic white noise stimulation demonstrated that a characteristic pattern of rising and falling light intensity that had a peak-peak cycle corresponding to 75Hz could elicit spiking of neurons (Lewis et al., 2021). This highlights a causal role between 75Hz stimulation and the effect on the neuronal circuitry, demonstrating that 75Hz stimulation can play a significant role in producing gamma oscillations in the cortex. However, the authors suggest that gamma band resonance of pyramidal neurons may be a result of feedback inhibition in the network and not a direct result of the opsin or electrical properties of the neurons (Lewis et al., 2021).

5.4.7 Conclusions

In summary, these results suggest that there are key differences between how the underlying circuitry responds to theta phase optogenetic stimulation targeted to different cell types and their contribution to gamma oscillations. This may be a result of intrinsic cell properties as well as their normal contribution to gamma oscillations, which tend to be transient. There was also no effect of the theta phase stimulated on differential gamma modulation, suggesting theta-gamma coupling is not responsible for the gamma modulation observed when stimulating pyramidal neurons. It is possible, however, that this is due to the lack of a behavioural task within our experiment since theta-gamma coupling has been linked to learning and memory in addition to movement (Akkad et al., 2021; Colgin, 2015; Igarashi et al., 2013; Lasztóczi & Klausberger, 2014).

These findings highlight our ability to optogenetically stimulate different populations of neurons using a closed-loop system, which can have differing effects on the underlying neurons and circuitry. Moreover, we have demonstrated that phase-dependent theta stimulation targeted to pyramidal neurons, but not inhibitory interneurons contributes to the modulation of gamma oscillations in a non-phase-dependent manner. Therefore, specifically targeting excitatory neurons could be a more effective way of driving cortical gamma power.

6 General Discussion

6.1 Overview

In this thesis, we set out to determine the global response (LFP) of motor cortical phase-dependent closed-loop optogenetic stimulation, what this could achieve in comparison to open-loop stimulation and how modulation relates to the specific type of neuron that is stimulated. We have demonstrated phase-specific optogenetic modulation of the motor cortical theta oscillation. This was observed when stimulation was targeted to either inhibitory (PV+) or excitatory (layer 5 pyramidal) neurons. These two types of neurons are known to significantly contribute to neuronal oscillations, largely through their interplay with each other. We have shown that both neuron types can be manipulated in a phase-dependent manner when using different patterns of optogenetic stimulation and demonstrated that this is an effect of closed-loop stimulation itself and not stimulation alone.

We have additionally observed that phase-specific theta stimulation can result in local gamma frequency modulation, however, this is not phase-dependent and is only possible when stimulation was targeted to RBP4+ pyramidal neurons. In this case, the optogenetic stimulation pattern used did affect modulation within the gamma frequency range.

6.1.1 Inhibitory and excitatory neurons have a 90-degree offset in phase-dependent amplification, indicating neuronal synchronisation

Limited previous work has shown that theta oscillations are naturally found in the cortex at 6Hz in humans (Canolty et al. 2006). Additionally, 7Hz theta oscillations

coupled to gamma oscillations have been found *in vivo* in rats, although the origin of these oscillations is unknown (Igarashi et al. 2013). Here, we aimed to establish the causal roles of different neuronal types in theta and gamma oscillations in the rodent motor cortex.

We observed an offset of 90˚ in phase-dependent amplification during stimulation of excitatory versus inhibitory neurons. Maximal amplification of the theta oscillation was found when stimulating RBP4+ pyramidal neurons at the trough and ascending phases, and at the ascending phase and peak when stimulating PV+ interneurons. This finding is in line with predictions from computational models of excitatory and inhibitory circuits dominated by an excitatory-inhibitory loop (Zou & Wang, 2016). Additionally, studies in other regions of the brain, such as the hippocampus and prefrontal cortex have identified the peak firing phase of pyramidal neurons to precede the peak phase of interneurons during gamma oscillations (Csicsvari et al., 2003; Gulyás et al., 2010; Hájos et al., 2004; Hasenstaub et al., 2005). In terms of the neural circuitry, this shift generally implies that L5 RBP4+ pyramidal neurons fire around the trough of the neuronal oscillation - when inhibition from interneurons is low, then interneurons increase their activation in turn to regulate pyramidal neuron output and generate synchronised rhythmic activity. It has been suggested that such a phase shift is necessary for neural computation, similarly to theta-phase precession of place cells within the hippocampus (Buzsáki & Chrobak, 1995; Fries et al., 2007).

Amplification of the ongoing oscillation by stimulation targeted to certain phases, with an offset of 90° between cell types, indicates clear synchronisation of the underlying neuronal activity. This aligns with Buzsáki's theory describing how coordinated

assemblies of neurons facilitate effective information transfer (Buzsáki, 2010; Buzsáki & Draguhn, 2004), as synchronised activity, like phase-locking increases the power of the oscillatory signal, demonstrated by an increase in theta LFP power. Activity of excitatory pyramidal neurons preceding that of inhibitory interneurons additionally highlights the phase relationship between these two crucial cell types within the oscillatory circuitry.

Phase-locking is also central to the ideas of Fries (Fries 2015), indicating that communication is optimal when coherence is increased, thereby allowing effective information transfer. Consequently, synchronisation leads to rhythmic fluctuations of excitability and inhibition, which allows for communication. Optimal enhancement of theta power occurred when stimulating pyramidal neurons at the theta trough and ascending phase, and when stimulating interneurons at the ascending phase and peak. This indicates phase-locking within the oscillatory network that drives synchrony and therefore rhythmic fluctuations in excitability. Conversely, the absence of coherence should prevent communication, such as when stimulation targeted the non-amplifying phases for each cell type. In this case, we increase neuronal inputs, albeit out of phase with these neurons intrinsic drive to oscillate, which results in a reduction of synchrony shown as no increase in LFP power.

Within our study, we did not collect data across different brain regions to understand the influence of coherence between regions. However, one could hypothesise, that by increasing the coherence of the ongoing theta oscillation within the motor cortex, we may additionally elicit brain wide responses such as the BOLD responses found by Chan et al (2022) following optogenetic stimulation of L5 pyramidal neurons. These

responses are likely driven by the extensive connections that these neurons have to many regions of the brain (Harris & Shepherd, 2015).

In addition to targeting of particular phases leading to amplification of the theta oscillation, we observe a frequency shift in different directions when targeting optogenetic stimulation to different phases in both PV-Cre and RBP4-Cre mice. When targeting interneurons there is approximately a 1Hz decrease in frequency to 5Hz when targeting the peak, suggesting the oscillation gets slower. This decrease in frequency is not observed when either gamma or continuous stimulation are targeted to the ascending phase of theta. Targeting RBP4+ pyramidal neurons with gamma stimulation results in a shift of about 0.5Hz, resulting in a frequency of ~5.5Hz when stimulation targets the ascending phase and ~6.5Hz at the trough. Continuous stimulation of RBP4+ neurons, however, appears to result in a frequency shift only when targeting the ascending phase (5.5Hz), as the peak of the trough is at ~6Hz. This suggests that stimulation of excitatory pyramidal neurons can facilitate both slowing down or speeding up of the ongoing oscillation depending on the phase targeted and pattern of stimulation. These phase-dependent changes in frequency, may be described as a constant phase-reset of the theta oscillation, in which the oscillation changes it's timing to synchronise with the external stimulus disrupting the underlying oscillation (Canavier 2015; Hebron et al. 2024). Ultimately, whether stimulation delays or advances the oscillation seems to depend on the phase targeted. The frequency of the oscillation is then subsequently altered as a direct effect of delaying or advancing the oscillation. By constantly tracking the phase of the oscillation for stimulation in a closed-loop manner, we are likely to observe a gradual shift in the underlying theta

frequency as stimulation may not occur every single cycle and the phase targeting may not always be accurate. These factors will therefore result in the oscillation continuously adjusting to the phase of the stimulus, and as such these experimental factors may explain the only slight variation in frequency shifts demonstrated in our data. The magnitude of a phase-reset has also been found to be dependent on the amplitude of the oscillation as well as strength of the input, in which lower oscillatory power can lead to larger phase resets (Forger 2017; Hebron et al. 2024; Jaramillo et al. 2024). This aligns with the larger shift in frequency observed when targeting PV-Cre mice where the amplitude of the oscillation is less modulated than in RBP4-Cre mice.

6.1.2 Optogenetic modulation of gamma power is not theta phase-specific

Gamma oscillations have been highlighted for playing an important role in information transfer (Buzśaki & Wang, 2012). We did not quantify the presence of spontaneous gamma in our head-fixed set-up, this is therefore a limitation; however, our results indicate no evidence of spontaneous gamma. We demonstrated that theta phase-dependent modulation of pyramidal neurons increases theta power in a phase-dependent manner, while gamma power increases equally across all phases. This suggests perhaps that the presence of underlying theta oscillations through stimulation of pyramidal neurons, creates windows of excitability for gamma oscillations to occur without a phase preference in the motor cortex. These gamma oscillations may be involved in facilitating the transfer of information across networks. Fries (Fries 2005, 2009) suggests that transfer of information is most favourable when gamma oscillations are highly synchronised between regions. Therefore, it is possible

that stimulating pyramidal neurons promotes gamma oscillations that increase communication across the brain.

6.1.3 Stronger phase-specific modulation of theta power in RBP4+ mice than PV+ mice

Whilst we have clearly demonstrated phase-specific modulation in both neuron types, the phases that lead to amplification when targeting RBP4 neurons produce stronger increases in power than the phases leading to amplification when stimulation is targeted to PV+ interneurons. The accuracy of stimulation in terms of phase-specificity appears similar when targeting both neuronal cell types, so this is unlikely to be the cause of the difference between neuronal types. Neurons naturally resonate at different frequencies; therefore, it is possible more interneurons resonate at slightly different frequencies than pyramidal neurons and so don't contribute to the modulation in theta power we find when targeting interneurons.

For both cell types, however, it appears that the accuracy of successful phase tracking was more variable when stimulation was targeted to certain phases. This may be attributed to the fact that when we have successfully modulated the LFP in such a way that reduces oscillatory power, it becomes harder to track the required stimulation phase. As a result, there is likely to be more overlap between stimulation target and surrounding phases. Contrastingly, when modulating the oscillation in the opposite direction, thus strengthening LFP power, we become increasingly successful in phase-tracking more accurately. This can be explained by an increase in the amplitude of an oscillation making the phases more distinct, thereby allowing for more robust detection. However, at one of the amplifying phases in RBP4-Cre mice, the phase accuracy reduced – thereby indicating this is not always the case. Instead, it appears

that stimulation is targeted more towards the phase of optimal amplification of the oscillation, perhaps indicating greater variability in accuracy between targeting the trough or ascending phases throughout the stimulation period as a result of overall modulation.

In addition, a limitation of this study is that we have not quantified the presence of the 6Hz theta oscillation between the two mouse lines. It appears that the strength of the oscillation we target (6Hz) may be different between the mouse lines, potentially a result of genetic variation, observed as different sizes of small peaks within the power spectra of control and unstimulated mice. Variation in the strength of the underlying theta oscillation may impact the strength of theta-phase modulation between the mouse lines even if phase-accuracy is similar between the two. As such, further analyses should be considered to determine this effect.

6.1.4 Lack of a bi-directional modulation of oscillatory power

Perturbation of different phases of an ongoing oscillation has been found to result in energising or dampening ongoing neural activity (Cagnan et al., 2017; Holt et al., 2019; Kanta et al., 2019; McNamara et al., 2022; Nicholson et al., 2018). For instance, research has found both amplification and suppression of the pathological beta oscillation when targeting it with electrical stimulation in rats using an online closed-loop set-up (OscillTrack) (McNamara et al., 2022). Contrastingly, while we have “less amplifying” phases, phase-dependent optogenetic stimulation of the theta oscillation does not appear to properly suppress the ongoing oscillation when targeting stimulation to either neuronal cell type. This could be explained as a result of the underlying circuitry, linked to the utilisation of optogenetics instead of electrical

stimulation, or perhaps a result of targeting a much smaller naturally occurring oscillation opposed to the pathological beta oscillation.

6.1.5 Open-loop stimulation less effective

We employed open-loop stimulation techniques within these experiments to allow for direct comparison to phase-specific closed-loop approaches. We found that open-loop replays of the closed-loop stimulation train resulting from interactions with the underlying theta oscillation, did not lead to phase-specific modulation of the theta oscillation. This directly highlights the necessity of the real-time closed-loop approach in effectively phase-dependently modulating theta power. In addition, we demonstrate that open-loop stimulation patterns designed to examine the importance of the relationship between stimulation and the underlying theta oscillation were unable to produce significant modulation when targeted to PV+ interneurons and only produced modulation of RBP4+ pyramidal neurons when they were rhythmically stimulated. Additionally, rhythmic open-loop stimulation led to harmonic effects, demonstrating decreased specificity due to the rhythmic nature of the pulses that are more consistently delivered. This indicates that closed-loop phase-dependent stimulation has greater efficacy in modulating the ongoing theta oscillation and can be used to deliver more specific, less frequent stimulation to produce specific modulation of an oscillation.

6.1.6 Speed of optogenetic approaches

We have used optogenetics to manipulate motor cortical theta circuitry in a phase-dependent manner. This was undertaken using Cre-dependent mouse lines with a Cre-dependent ChR2 virus variant. ChR2 activates with millisecond precision in

response to optical stimulation (~473nm), in which ChR2 channels open allowing cations such as Na^+ and Ca^{2+} to flow into the ChR2-expressing neuron to depolarise it (Fenno et al., 2011). Continuous light exposure, however, does not keep ChR2 channels open permanently as they become desensitised. Therefore, such kinetics should be considered when interpreting our results. We used the ChR2(E123T/T159C; ET/TC) variant (a blue ChETA variant), which has fast activation and decay kinetics and a deactivation time constant of ~8ms (Berndt et al., 2011; Fenno et al., 2011). Compared to WT ChR2, this variant has reduced desensitisation during light exposure, which enables light pulses later in a high frequency train as likely as early light pulses for driving action potentials. Alongside this, following cessation of light, the ion channels are closed more quickly (Berndt et al., 2011; Fenno et al., 2011; Gunaydin et al., 2010). These improvements are beneficial for high frequency stimulation, ensuring reliable neuronal activation and reduced response variability. Faster kinetics reduce inactivation issues that were observed with WT ChR2, such that even during extended periods of high frequency stimulation, the ChETA variant does not accumulate as much in the inactivated state as it both responds to and recovers from light pulses more quickly (Gunaydin et al. 2010).

It was demonstrated with whole-cell recordings of acute prefrontal brain slices that PV-interneurons were able to consistently respond to sustained light stimulation at 200Hz (Gunaydin et al. 2010). Additionally, 5ms light pulses stimulated at up to 100Hz evoked 100% successful spikes, whereas spiking could not be driven by 1ms light pulses (Gunaydin et al. 2010). Sustained firing during a 40Hz train of 60 light pulses was also demonstrated in ChR2(ET/TC) expressing pyramidal neurons in whole-cell

current clamp recordings of hippocampal rat slices (Berndt et al. 2011). Additionally, 45% of neurons responded well to 60Hz stimulation, using an 80% threshold for success rate (Berndt et al. 2011).

Finally, plateau potential could also impact the results we see, this is where neurons have insufficient time to repolarise between stimulation pulses particularly at high frequencies which can make them more likely to fire subsequent action potentials. However, these ChR2 mutations had previously been shown to almost eliminate plateau potential in FS interneurons (Gunaydin et al. 2010), but evidence for pyramidal neurons was less clear. Berndt et al (2011) found that there was only a small plateau depolarisation in this variant, which increases proportionally to stimulation frequency, this could be explained by the fast off time kinetics of the variant. This was further supported by another study that also highlighted the impact that differences in temperature could have on results (Mattis et al., 2011).

These studies, alongside other experimental evidence that these neurons can be driven at high frequencies (Adesnik & Scanziani, 2010; Cardin et al., 2009; Sohal et al., 2009), indicate that both neuronal cell types should be able to effectively respond to the optogenetic stimulation in our study. We initially devised two different stimulation patterns – gamma and continuous. Both cell types should be activated quickly following the onset of either optogenetic stimulation pattern. Between each burst of stimulation, there is a timeout period greater than 3/4 of the theta cycle (~133ms) before stimulation can be re-initiated. The length of this is sufficient to allow ChR2 channels to close and prevent desensitisation or possible plateau depolarisation due to our high stimulation frequency. Continuous stimulation (~41ms) will result in rapid

depolarisation of neurons for the length of stimulation before the gap in stimulation will allow channels to inactivate. The overall response to continuous stimulation is most likely driven by the fast activation kinetics of this opsin - initial rapid depolarisation of neurons increasing their activation. As a result, the start of light stimulation is likely to recruit the most neurons. Consequently, the response may decrease across time due to desensitisation of ChR2 channels, although the variant aims to minimise this.

The response to gamma stimulation is likely a little different. Gamma pulses and the off time between each pulse is around 6.67ms, comparatively, the offset time of our ChR2 variant is ~8ms (Berndt et al., 2011; Fenno et al., 2011). This indicates that, while channels can start to inactivate, the time before the next pulse is insufficient for full inactivation, and they may remain partially activated throughout the entire stimulation burst. Therefore, if the population of neurons are responding at gamma frequency, it is more likely sequential pulses recruit neurons that were not activated by the previous stimulation pulse, otherwise the strength of the response may decrease across the pulses as channels desensitise. However, to understand how neurons in our data set respond, we would need to investigate the effect of our stimulation on the unit data.

We demonstrated that only optogenetic stimulation of pyramidal neurons could significantly alter gamma power in opsin animals and not controls. It could have been anticipated that only gamma stimulation would drive changes in gamma power, due to synchronisation of pyramidal neurons at a gamma frequency. While gamma modulation is more prominent following gamma frequency stimulation, it was still observed following random gamma or continuous stimulation. Random gamma

stimulation keeps the two outside pulses consistent and regular, which may still promote gamma oscillations. One explanation for the effect of increased gamma power when stimulating with continuous optogenetic stimulation could be that over the ~41ms, sustained action potentials are generated due to the opsin variant being less prone to desensitisation. It is therefore possible that frequent action potentials increase pyramidal neuron excitability and result in the emergence of gamma oscillations through their synchronised activity.

As we have previously highlighted the role of PV+ interneurons in the generation of gamma oscillations, it was unexpected that gamma frequency stimulation did not produce opsin-dependent changes in gamma power. Especially given these neurons have been demonstrated to respond to high frequencies of optical stimulation (Cardin et al. 2009; Gunaydin et al. 2010). For instance, Cardin et al (2009) demonstrated FS-interneurons (ChR2+) could respond to bouts of 3-second 1ms pulses between 20-200Hz. However, 40Hz stimulation drove the most reliable changes in LFP and regular spiking, and spike probability dropped as the stimulation frequency increased (Cardin et al. 2009). In this protocol, as stimulation frequency increased the time between each pulse decreased - stimulation of 80Hz for instance, where the authors observed a spike probability per cycle of ~0.25, would have 12.5ms between each 1ms pulse. Comparatively, our gamma stimulation was 3 pulses at 75Hz (6.67ms onset and offset) and used a significantly lower laser power (1-2mW opposed to 46mW/mm^2). Therefore, while it is unexpected that we do not elicit increases in gamma power by driving PV+ interneurons, perhaps this is a result of differing stimulation protocols and intensities.

In addition, there was evidence of greater modulation of theta power when modulating PV+ interneurons using gamma frequency stimulation as opposed to continuous stimulation. If modulation of the theta oscillation is stronger with gamma frequency, this would suggest that these neurons are able to respond to this frequency of stimulation on a population level. Alternatively, FS interneurons may respond better to optogenetic pulses as a result of their intrinsic membrane properties than a longer continuous pulse.

Furthermore, other studies have reported that this particular opsin variant responds to a more red-shifted activation spectrum (~505nm) (Berndt et al. 2011; Mattis et al. 2011). Therefore, while we were able to effectively modulate oscillations and these particular neuronal subtypes, it is possible that we were not using the optimal wavelength of light for this ChR2 variant. Red-shifted wavelengths of light are suggested to be more optimal for in vivo applications as these wavelengths are less scattered within brain tissue (Berndt et al. 2011). Moreover, longer wavelengths of light generate less heat (Arias-Gil et al., 2016; Owen et al., 2019; Stujenske et al., 2015), which is another potential issue when optogenetically stimulating tissue.

6.2 Technical limitations

6.2.1 Experimental

The acquisition of *in vivo* data through this method of awake head-fixed recordings provides a valuable dataset to work with and learn from. However, this method comes with the limitation of recording from an awake head-fixed animal, which is prone to movement. Therefore, to minimise the amount of movement and ultimately reduce movement artifacts within the recordings, mice were gradually habituated to the

recording set-up. Habituation, alongside periodically providing the mouse with sucrose as a reward, helps to limit the periods of restlessness within the recordings. To monitor and record large periods of movement, where possible, a piezo sensor was positioned along the side of the animal's body. This could be used for identification of periods within the recording where the animal was restless, to remove for future analyses. Mice were additionally habituated to the piezo in advance so that this did not itself induce further movement in the recordings. To further reduce the impact of electrical noise, recordings were undertaken within a Faraday cage and the probe was grounded.

Furthermore, due to the acute nature of this data acquisition set-up, repeated silicon probe insertion was required across multiple days, unlike recordings undertaken using chronic implants. To minimise cortical tissue damage resulting from multiple reinsertions with a 4-shank probe containing an optic fiber, we used slightly different coordinates for probe insertion each day. Due to restrictions in place with the license for the welfare of animals, there were limits on the amount of time data could be acquired for in each session. This meant that recordings were undertaken for a maximum of 3 to 4 hours in length, unlike those undertaking anaesthetised recordings that could yield potentially longer sessions. To enable data collection of all our experimental conditions, within each session, several shorter recordings (~2.5-7 minutes) were collected in a randomised order. Each recording was of sufficient length, to collect enough data for analysis. Data was collected from each animal for between 3-5 recording sessions, before tissue quality had deteriorated and fewer

single units were detected. This meant that there was a constraint on the volume of data that could be acquired per animal.

While we were successful in manipulating the motor cortical theta oscillation using optogenetics, this technique is not directly translatable to humans. It could additionally be said that stimulating specific neurons in this way is artificial, through activation of subsets of neurons that have had external light sensitive proteins introduced in a non-physiological manner. However, utilising precise population control to elucidate the roles different subtypes of neurons play within existing circuitry in different regions could still be useful to inform future therapeutics. This is something that would not be possible using electrical stimulation which is not selective to cell-type, has less temporal precision and often interacts with a larger less defined area. Optogenetics therefore remains a powerful tool to gain insights into neurocircuitry within the neuroscientific community.

6.2.2 Heating effect of lasers

In experiments using optogenetics, optogenetic artifacts can lead to unintended false results. In this set of experiments, we have controlled for potential optogenetic artifacts using control mice that do not express opsin as well as in stimulation off controls in both opsin and control mice. In addition to this, we reduced the intensity of stimulation to mitigate these effects. Within analyses of the data set, we removed the four channels that were closest to the optic fiber which would have been most impacted by photoelectric artifact. Data were also blindly visually inspected within the theta range to confirm resultant power spectra did not visually contain suspected photoelectric artifact; this is something that could also be done within the gamma

power spectra. Additionally, within the most recent set of recordings we utilised a probe with a special coating to further reduce the impact of photoelectric artifacts. Therefore, while there may be some impact of optogenetic artifact we have controlled for it as well as possible within these experiments.

During the use of optogenetics however, it has been documented that tissue heating often occurs alongside the delivery of light. This has been found to influence generation of action potentials in mice that do not contain opsin, particularly during prolonged optical stimulation (Cardozo Pinto & Lammel, 2019; Owen et al., 2019; Stujenske et al., 2015). Light has been previously demonstrated to result in artifactual signals in the BOLD response in fMRI when delivered to the brain, as this was linked to laser power this was perhaps a direct result of heating (Allen et al., 2015; Christie et al., 2013). The degree of heating will depend on a multitude of factors, including the intrinsic properties of the brain tissue, rate of blood flow, as well as the duration and wavelength of stimulation (Allen et al., 2015).

In these experiments we used low laser powers to try and mitigate the effects of heating alongside the delivery of light. Initial experiments determined that similar modulation could be observed when using 2mW versus 5mW of laser power. Light was then maximally delivered at 2mW to reduce the impact of heating on the tissue. Moreover, light stimulation can additionally lead to non-specific neuronal responses, this could be directly through the retina, via light escaping from the delivery apparatus or even due to light scattering within the tissue (Yizhar, Fenno, Davidson, et al. 2011).

To further verify any effects that were resulting from direct heating of the tissue or due to visual evoked potentials following laser activation, rather than due to the opsin

itself, for each genotype of mice, we included a control group that received an injection of a virus containing no opsin. Due to the lack of opsin in these mice, we would anticipate no modulation following laser stimulation. Consequently, any effect demonstrated could be linked to heating of the cortical tissue or non-specific neural responses. As an additional control, we also ran recordings without stimulation, in which a particular stimulation pattern and phase were picked, but with the laser being physically turned off, thus no light was delivered. To keep the power of light delivery as consistent as possible throughout all recordings, the power was verified before each recording session. Individual recordings ranged from around ~2.5-7 minutes in length, depending on the experimental conditions we wanted to collect within a session. Therefore, the whole duration of light delivery will not have been identical within each mouse or session. To make this experiment even more rigorous, we could have blinded the experimenter to the identity of opsin or non-opsin containing mice during the surgical preparation or through the following parts of the experiment.

In large part, we were successful in validating our approach through the use of control mice, no stimulation recordings, open-loop replay paradigm control and open-loop stimulation conditions. For all stimulation, we used values that were below the commonly used 5-10mW, which are sufficient for increasing the firing rates of neurons as a result of heat (Stujenske et al., 2015). There was additional evidence that heat could be reduced through pulsing light instead of using continuous stimulation (Stujenske et al., 2015), and modelling indicated pulses below ~100ms would produce negligible heating (Owen et al., 2019). Therefore, we would expect a more pronounced heating effect from our continuous stimulation pattern than our gamma stimulation

pattern. Contrastingly, we only found a significant effect in control mice when analysing stimulation targeted to PV-Cre interneurons in the gamma frequency range. We did not identify an effect when analysing these same mice within the theta range, which was unexpected. It is possible this effect could be due to heating, however, as mentioned there was no effect on theta power, or on gamma power when stimulating with continuous stimulation, only as a direct result of gamma pattern stimulation. This indicates that it is precisely linked only to the gamma pattern of stimulation when analyses are undertaken in the gamma frequency range, resulting in an increase in the LFP with a peak at 75Hz – our stimulation frequency.

In addition, it has been shown that the vasculature of the illuminated tissue can have a significant effect on increases in temperature found (Arias-Gil et al. 2016). Therefore, variability in optogenetic effects between mice could also be related to vasculature differences, especially since the area we recorded in often had a large blood vessel. Another experiment has demonstrated that 2mW of blue light increased cerebral blood flow in the naïve mouse brain as a result of arteriole dilation (Rungta et al. 2017). Therefore, it is possible that gamma stimulation resulted in changes in blood flow that lead to the changes we observe in the gamma range when stimulating PV+ interneurons.

6.2.3 Probes

In this set of experiments, a silicon probe was used to capitalise on our closed-loop recording system (Intan & OscillTrack). With recent technological advances, the number of channels that can be recorded using other high-density probes such as Neuropixels has taken the Neuroscience community by storm. It would be

advantageous to use such probes in these recordings, as the number of channels would mean a high yield of single units to investigate the effect of phase-stimulation.

However, within these specific experiments, using these high-density Neuropixels would have come with their drawbacks. Firstly, at the time of these experiments, Neuropixels were only one single shank. Therefore, to match our experimental set-up we would need to insert multiple Neuropixels in the same area simultaneously to record from a subset of cells across the motor cortices. Additionally, Neuropixels do not yet have an optrode version, which would have either meant separately implanting a chronic optic fiber or additional daily insertion of an optic fiber. The first method would have made less space for probe insertions, while the latter would have increased cortical tissue damage. Furthermore, less is currently known about the LFP in these high-density probes, and how these are related to the well-documented NeuroNexus probes.

To determine the feasibility of combining NeuroNexus and Neuropixel experiments, we designed a probe holder that could hold both a NeuroNexus single shank probe as well as a single Neuropixel optrode. This meant that we could insert both at the same time, enabling a high yield of single units as well as using the NeuroNexus probes as both an optic fiber and to trigger the closed-loop system. While we deemed this experimental set-up possible, due to the short nature of the recordings to allow for the constant change of experimental settings in a closed-loop manner, the data would be somewhat harder to combine and analyse. It is possible that future experiments could capitalize on this set-up, to gain unit data across a large number of brain structures.

Additionally, due to the four shanks on the probe and multiple reinsertions, we only tend to mark the probe location on the final day. This meant that fewer tracts may be identified using post-hoc histology. However, it is not always necessary to use DiI to identify probe tracts, as these tracts can sometimes be visualised within the tissue without DiI. As a result of this, we are unable to match precise recording locations across days – however, given that we are recording in a large brain structure, knowing the precise location of the probes across recordings days is not vital.

6.2.4 Inclusion of female mice

Within neuroscience research it has long been stereotyped that using female mice is more complicated due to fluctuating hormonal changes that may impede the interpretation of results (Becker et al., 2016; Clayton, 2016; Smarr & Kriegsfeld, 2022; Zucker et al., 2022). A direct outcome of this, is that drug development works better in men than women (Zucker et al., 2022; Zucker & Prendergast, 2020). Therefore, many studies are now encouraging the inclusion of both sexes in experiments.

A limitation of these results is that, within these sets of experiments, only male mice have been used. As the use of both male and female mice is now less controversial, it would be beneficial to see these results in female mice as well. However, we would not predict there to be male and female differences within this type of experiment. The headplates used in our study were originally designed for male mice, which tend to be both larger in size and weight than their female counterparts. This allows for easier headplate placement and recovery. In future work, slightly smaller headplates have been designed to allow for the fitting of headplates on female mice. However, their

smaller size could still make this kind of experiment challenging due to the potential issues with recovery and thus animal welfare.

6.3 Translational applications

Previous closed loop optogenetic stimulation methods such as that of Siegle & Wilson (2014) utilised a set-up in which phase tracking relied on a computer which impacted latency and therefore increased error. This study, while pivotal in optogenetically stimulating an oscillation based on phase, examined the output of this as a behavioural effect and did not alter the underlying theta oscillation (Siegle & Wilson, 2014). Nicholson et al (2018) demonstrated that optogenetic modulation of pyramidal neurons in hippocampal slices that produced bidirectional changes in both the power and frequency of gamma oscillations. However, this was an *in vitro* study and therefore not conducted in a living organism which presents more complexity and technical challenges (Nicholson et al. 2018). Additionally, the closed-loop circuitry similarly relied on the hippocampal LFP being processed on a computer to generate a ramp command that was fed back through to an LED driver to control neuronal activity (Nicholson et al. 2018).

Our study is the first example combining a new highly responsive closed-loop system that provides continuous online phase estimation (OsillTrack), with phase-dependent optogenetics. Experiments were undertaken by stimulating two major cell types that have been shown to contribute to neuronal oscillations (Cardin et al. 2009; Sohal et al. 2009). Therefore, our study can help to elucidate the roles and interactions of these neurons within the local microcircuitry and in the generation of neuronal oscillations. Furthermore, now that we have shown the feasibility and effectiveness of this

combined method, it could now be transferred and utilised within other areas of the brain to continue exploring the local microcircuitry at this level. Findings could then be used to inform clinically advancing closed-loop stimulation methods in humans, such as adaptive deep brain stimulation devices. This could enable a reduction in stimulation side effects and enhanced efficacy over long term treatment. Non-invasive brain stimulation protocols could be tailored in addition, which may reduce the current heterogeneity of effects observed.

6.4 Future directions

Firstly, while there was evidence that gamma stimulation modulated theta power to a greater degree during closed-loop stimulation of PV+ interneurons, this was not the case when stimulating RBP4+ pyramidal neurons. Our results, however, did not reveal a significant difference between gamma and continuous stimulation on cortical theta power. Contrastingly, we found that only pyramidal neurons could modulate motor cortical gamma power and different stimulation patterns could modulate gamma power to different degrees. A limitation of this body of work is that we haven't analysed phase-amplitude coupling to determine whether there is any evidence of theta-gamma coupled oscillations in the motor cortex with no associated behavioural task. Therefore, future work will investigate PAC within our data set to determine whether there is any evidence of an association between the 6Hz oscillation we target with gamma frequency stimulation and changes in gamma power. This will be investigated initially at resting state to determine if there is evidence of PAC during resting state (baseline recordings) in either mouse type. Following this, during the different stimulation patterns employed within the data set, particularly gamma frequency, the

stimulation pattern which would be most likely to induce PAC. Furthermore, analyses of PAC may highlight a role of pyramidal neurons and explain why we observe changes in gamma power only when stimulating this neuronal type. However, given the well-characterised role of theta-gamma PAC in learning and memory (Colgin, 2015; Lasztóczi & Klausberger, 2014), external theta-gamma PAC improving learning during a motor task (Akkad et al. 2021), and coordination of spiking activity and theta and gamma oscillations during reward motivated movement in rats (Igarashi et al. 2013), it is possible gamma stimulation would only be more effective in modulating theta power during a learning or behavioural task. Closed-loop recordings could be combined with a behavioural task such as reaching of a water droplet in the future, to determine how the circuitry and interactions differ.

Following this, to determine the role of single neurons and their contribution to modulation of the LFP of both theta and gamma oscillations the next step would be to analyse the multi-unit data collected during these experiments. This will advance our understanding of where neurons fire in relation to each targeted theta-phase and whether the two neuronal cell-types we targeted have preferential phases of theta that they normally fire at. This could facilitate our understanding of the phase-dependent effects of the theta LFP that we demonstrate. In addition, determining how both populations of neurons respond to our differing stimulation patterns may offer an explanation for the cell-type dependent effects observed within the gamma frequency range.

Finally, the power of optogenetics could be further leveraged through combination of excitatory and inhibitory opsins with simultaneous stimulation. This could enable greater dissection of the roles of these neuronal cell types within the microcircuitry.

6.5 Outlook

We have collected data from excitatory pyramidal neurons and inhibitory interneurons under identical experimental and stimulation conditions from the motor cortex. This provides researchers a unique opportunity to analyse the roles of these neuron types within the local microcircuitry and can also pave the way for computational modelling studies. These have the potential to help elucidate how the interactions between these two major neurons result in oscillatory activity within the motor cortex.

6.6 Concluding remarks

These findings demonstrate that both inhibitory and excitatory neurons can mediate phase-dependent modulation of theta power and the effects at each phase can likely be explained by interactions between these two neuronal populations. Closed-loop real-time stimulation achieves phase-dependent modulation that was not possible using open-loop replay of stimulation patterns resulting from direct interactions with the underlying theta oscillation. Furthermore, open-loop stimulation with no relationship to the theta oscillation modulated theta power only during stimulation of excitatory neurons and had reduced specificity.

We also demonstrate that closed-loop theta optogenetic stimulation of excitatory, but not inhibitory neurons could be more effective in modulating changes in cortical gamma power, however, this is independent of the theta phase. This approach can be used to inform the development of brain stimulation methods to modulate these activities in humans. The ability to drive neuronal processes into a desired state through harnessing intrinsic temporal dynamics could be crucial for therapeutics targeting a wide spectrum of brain disorders.

References

Adesnik, Hillel, and Massimo Scanziani. 2010. 'Lateral Competition for Cortical Space by Layer-Specific Horizontal Circuits'. *Nature* 464(7292):1155–60. doi: 10.1038/nature08935.

Adrian, E. D., and B. H. C. Matthews. 1934. 'THE BERGER RHYTHM: POTENTIAL CHANGES FROM THE OCCIPITAL LOBES IN MAN'. *Brain* 57(4):355–85. doi: 10.1093/BRAIN/57.4.355.

Akam, Thomas, Iris Oren, Laura Mantoan, Emily Ferenczi, and Dimitri M. Kullmann. 2012. 'Oscillatory Dynamics in the Hippocampus Support Dentate Gyrus–CA3 Coupling'. *Nature Neuroscience 2012 15:5* 15(5):763–68. doi: 10.1038/nn.3081.

Akkad, Haya, Joshua Dupont-Hadwen, Edward Kane, Carys Evans, Liam Barrett, Amba Frese, Irena Tetkovic, Sven Bestmann, and Charlotte J. Stagg. 2021. 'Increasing Human Motor Skill Acquisition by Driving Theta-Gamma Coupling'. *ELife* 10. doi: 10.7554/eLife.67355.

Aladjalova, N. A. 1957. 'Infra-Slow Rhythmic Oscillations of The Steady Potential of the Cerebral Cortex'. *Nature* 179(4567):957–59. doi: 10.1038/179957a0.

Alaverdashvili, Mariam, and Ian Q. Whishaw. 2008. 'Motor Cortex Stroke Impairs Individual Digit Movement in Skilled Reaching by the Rat'. *European Journal of Neuroscience* 28(2):311–22. doi: 10.1111/J.1460-9568.2008.06315.X.

Al-Juboori, Saif I., Anna Dondzillo, Elizabeth A. Stubblefield, Gidon Felsen, Tim C. Lei, and Achim Klug. 2013. 'Light Scattering Properties Vary across Different Regions of the Adult Mouse Brain'. *PLOS ONE* 8(7):e67626. doi: 10.1371/JOURNAL.PONE.0067626.

Alkaabi, Klaithem M., Abeer Yafea, and S. Salman Ashraf. 2005. 'Effect of PH on Thermal- and Chemical-Induced Denaturation of GFP'. *Applied Biochemistry and Biotechnology* 126(2):149–56. doi: 10.1385/ABAB:126:2:149.

Allen, Brian D., Annabelle C. Singer, and Edward S. Boyden. 2015. 'Principles of Designing Interpretable Optogenetic Behavior Experiments'. *Learning & Memory* 22(4):232–38. doi: 10.1101/LM.038026.114.

An, Su Jin, Sunah Choi, Jun Seo Hwang, Sunghyun Park, Moonyoung Jang, Minah Kim, and Jun Soo Kwon. 2024. 'Aberrant Hyperfocusing in Schizophrenia Indicated by Elevated Theta Phase-Gamma Amplitude Coupling'. *Clinical Neurophysiology* 157:88–95. doi: 10.1016/J.CLINPH.2023.11.012.

Appleby, Brian S., Patrick S. Duggan, Alan Regenberg, and Peter V Rabins. 2007. 'Psychiatric and Neuropsychiatric Adverse Events Associated with Deep Brain Stimulation: A Meta-Analysis of Ten Years' Experience'. *Movement Disorders* 22(12):1722–28. doi: 10.1002/mds.21551.

Arias-Gil, Gonzalo, Frank Walter Ohl, Kentaroh Takagaki, and Michael Thomas Lippert. 2016. 'Measurement, Modeling, and Prediction of Temperature Rise Due to Optogenetic Brain Stimulation'. *Neurophotonics* 3(4):045007. doi: 10.1117/1.NPH.3.4.045007.

Ascoli, Giorgio A., Lidia Alonso-Nanclares, Stewart A. Anderson, German Barrionuevo, Ruth Benavides-Piccione, Andreas Burkhalter, György Buzsáki, Bruno Cauli, Javier DeFelipe, Alfonso Fairén, Dirk Feldmeyer, Gord Fishell, Yves Fregnac, Tamas F. Freund, Daniel Gardner, Esther P. Gardner, Jesse H. Goldberg, Moritz Helmstaedter, Shaul Hestrin, Fuyuki Karube, Zoltán F. Kisvárday, Bertrand Lambolez, David A. Lewis, Oscar Marin, Henry Markram, Alberto Mũoz, Adam Packer, Carl C. H. Petersen, Kathleen S. Rockland, Jean Rossier, Bernardo Rudy, Peter Somogyi, Jochen F. Staiger, Gabor Tamas, Alex M. Thomson, Maria Toledo-Rodriguez, Yun Wang, David C. West, and Rafael Yuste. 2008. 'Petilla Terminology: Nomenclature of Features of GABAergic Interneurons of the Cerebral Cortex'. *Nature Reviews Neuroscience* 9(7):557–68. doi: 10.1038/nrn2402.

Baker, Stuart N. 2007. 'Oscillatory Interactions between Sensorimotor Cortex and the Periphery'. *Current Opinion in Neurobiology* 17(6):649–55. doi: 10.1016/J.CONB.2008.01.007.

Barr, Mera S., Tarek K. Rajji, Reza Zomorrodi, Natasha Radhu, Tony P. George, Daniel M. Blumberger, and Zafiris J. Daskalakis. 2017. 'Impaired Theta-Gamma Coupling during Working Memory Performance in Schizophrenia'. *Schizophrenia Research* 189:104–10. doi: 10.1016/J.SCHRES.2017.01.044.

Bartos, Marlene, Imre Vida, and Peter Jonas. 2007. 'Synaptic Mechanisms of Synchronized Gamma Oscillations in Inhibitory Interneuron Networks'. *Nature Reviews Neuroscience 2007 8:1* 8(1):45–56. doi: 10.1038/nrn2044.

Becker, Jill B., Brian J. Prendergast, and Jing W. Liang. 2016. 'Female Rats Are Not More Variable than Male Rats: A Meta-Analysis of Neuroscience Studies'. *Biology of Sex Differences* 7(1):1–7. doi: 10.1186/S13293-016-0087-5.

Belluscio, Mariano A., Kenji Mizuseki, Robert Schmidt, Richard Kempter, and György Buzsáki. 2012. 'Cross-Frequency Phase-Phase Coupling between θ and γ Oscillations in the Hippocampus'. *The Journal of Neuroscience* 32(2):423–35. doi: 10.1523/JNEUROSCI.4122-11.2012.

Benchenane, Karim, Adrien Peyrache, Mehdi Khamassi, Patrick L. Tierney, Yves Gioanni, Francesco P. Battaglia, and Sidney I. Wiener. 2010. 'Coherent Theta Oscillations and Reorganization of Spike Timing in the Hippocampal- Prefrontal Network upon Learning'. *Neuron* 66(6):921–36. doi: 10.1016/j.neuron.2010.05.013.

Berke, J. D. 2009. 'Fast Oscillations in Cortical-Striatal Networks Switch Frequency Following Rewarding Events and Stimulant Drugs'. *European Journal of Neuroscience* 30(5):848–59. doi: 10.1111/J.1460-9568.2009.06843.X.

Berndt, André, Philipp Schoenenberger, Joanna Mattis, Kay M. Tye, Karl Deisseroth, Peter Hegemann, and Thomas G. Oertner. 2011. 'High-Efficiency Channelrhodopsins for Fast Neuronal Stimulation at Low Light Levels'. *Proceedings of the National Academy of Sciences of the United States of America* 108(18):7595–7600. doi: 10.1073/PNAS.1017210108.

Biernaskie, J., and D. Corbett. 2001. 'Enriched Rehabilitative Training Promotes Improved Forelimb Motor Function and Enhanced Dendritic Growth after Focal Ischemic Injury'. *Journal of Neuroscience* 21(14):5272–80. doi: 10.1523/JNEUROSCI.21-14-05272.2001.

Blatow, Maria, Andrei Rozov, Istvan Katona, Sheriar G. Hormuzdi, Axel H. Meyer, Miles A. Whittington, Antonio Caputi, and Hannah Monyer. 2003. 'A Novel Network of Multipolar Bursting Interneurons Generates Theta Frequency Oscillations in Neocortex'. *Neuron* 38(5):805–17. doi: 10.1016/S0896-6273(03)00300-3.

Bokman, Stephen H., and William W. Ward. 1981. 'Renaturation of Aequorea Green-Fluorescent Protein'. *Biochemical and Biophysical Research Communications* 101(4):1372–80. doi: 10.1016/0006-291X(81)91599-0.

Botterill, Justin J., Abdessattar Khlaifia, Brandon J. Walters, Mark A. Brimble, Helen E. Scharfman, and Maithe Arruda-Carvalho. 2021. 'Off-Target Expression of Cre-Dependent Adeno-Associated Viruses in Wild-Type C57BL/6J Mice'. *ENeuro* 8(6):363–84. doi: 10.1523/ENEURO.0363-21.2021.

Boyden, Edward S., Feng Zhang, Ernst Bamberg, Georg Nagel, and Karl Deisseroth. 2005. 'Millisecond-Timescale, Genetically Targeted Optical Control of Neural Activity'. *Nature Neuroscience* 8(9):1263–68. doi: 10.1038/nn1525.

Braeutigam, Sven, Jessica Clare Scaife, Tipu Aziz, and Rebecca J. Park. 2022. 'A Longitudinal Magnetoencephalographic Study of the Effects of Deep Brain Stimulation on Neuronal Dynamics in Severe Anorexia Nervosa'. *Frontiers in Behavioral Neuroscience* 16:841843. doi: 10.3389/FNBEH.2022.841843.

Bragin, Anatol, Gábor Jandó, Zoltán Nádasdy, Jamille Hetke, Kensall Wise, and György Buzsáki. 1995. 'Gamma (40-100 Hz) Oscillation in the Hippocampus of the Behaving Rat'. *Journal of Neuroscience* 15(1):47–60. doi: 10.1523/JNEUROSCI.15-01-00047.1995.

Brier, Matthew R., Thomas C. Ferree, Mandy J. Maguire, Patricia Moore, Jeffrey Spence, Gail D. Tillman, John Hart, and Michael A. Kraut. 2010. 'Frontal Theta and Alpha Power and Coherence Changes Are Modulated by Semantic Complexity in Go/NoGo Tasks'. *International Journal of Psychophysiology* 78(3):215–24. doi: 10.1016/J.IJPSYCHO.2010.07.011.

Brittain, John Stuart, Penny Probert-Smith, Tipu Z. Aziz, and Peter Brown. 2013. 'Tremor Suppression by Rhythmic Transcranial Current Stimulation'. *Current Biology* 23(5):436. doi: 10.1016/J.CUB.2013.01.068.

Brown, Marie T., and Jennifer K. Bussell. 2011. 'Medication Adherence: WHO Cares?' *Mayo Clinic Proceedings* 86(4):304–14. doi: 10.4065/MCP.2010.0575.

Brown, Peter, Antonio Oliviero, Paolo Mazzone, Angelo Insola, Pietro Tonali, and Vincenzo Di Lazzaro. 2001. 'Dopamine Dependency of Oscillations between Subthalamic Nucleus and Pallidum in Parkinson's Disease'. *Journal of Neuroscience* 21(3):1033–38. doi: 10.1523/JNEUROSCI.21-03-01033.2001.

Buzsáki, György. 2002. 'Theta Oscillations in the Hippocampus'. *Neuron* 33(3):325–40. doi: 10.1016/S0896-6273(02)00586-X.

Buzsáki, György. 2004. 'Large-Scale Recording of Neuronal Ensembles'. *Nature Neuroscience* 7(5):446–51. doi: 10.1038/nn1233.

Buzsáki, György. 2010. ‘Neural Syntax: Cell Assemblies, Synapsembles, and Readers’. *Neuron* 68(3):362–85. doi: 10.1016/J.NEURON.2010.09.023.

Buzsáki, György, Costas A. Anastassiou, and Christof Koch. 2012. ‘The Origin of Extracellular Fields and Currents — EEG, ECoG, LFP and Spikes’. *Nature Reviews Neuroscience* 13(6):407–20. doi: 10.1038/nrn3241.

Buzsáki, György, and James J. Chrobak. 1995. ‘Temporal Structure in Spatially Organized Neuronal Ensembles: A Role for Interneuronal Networks’. *Current Opinion in Neurobiology* 5(4):504–10. doi: 10.1016/0959-4388(95)80012-3.

Buzsáki, György, and Andreas Draguhn. 2004. ‘Neuronal Oscillations in Cortical Networks’. *Science* 304(5679):1926–29. doi: 10.1126/SCIENCE.1099745.

Buzsáki, György, Nikos Logothetis, and Wolf Singer. 2013. ‘Scaling Brain Size, Keeping Timing: Evolutionary Preservation of Brain Rhythms’. *Neuron* 80(3):751–64. doi: 10.1016/J.NEURON.2013.10.002.

Buzsáki, György, and Edvard I. Moser. 2013. ‘Memory, Navigation and Theta Rhythm in the Hippocampal-Entorhinal System’. *Nature Neuroscience 2013 16:2* 16(2):130–38. doi: 10.1038/nn.3304.

Buzsáki, György, and Erik W. Schomburg. 2015. ‘What Does Gamma Coherence Tell Us about Inter-Regional Neural Communication?’ *Nature Neuroscience* 18(4):484–89. doi: 10.1038/nn.3952.

Buzśaki, Gÿorgy, and Xiao Jing Wang. 2012. ‘Mechanisms of Gamma Oscillations’. *Annu Rev Neuroscience* 35:203–25. doi: 10.1146/ANNUREV-NEURO-062111-150444.

Cagnan, Hayriye, David Pedrosa, Simon Little, Alek Pogosyan, Binith Cheeran, Tipu Aziz, Alexander Green, James Fitzgerald, Thomas Foltynie, Patricia Limousin, Ludvic Zrinzo, Marwan Hariz, Karl J. Friston, Timothy Denison, and Peter Brown. 2017. ‘Stimulating at the Right Time: Phase-Specific Deep Brain Stimulation’. *Brain* 140(1):132–45. doi: 10.1093/BRAIN/AWW286.

Canavier, Carmen C. 2015. ‘Phase-Resetting as a Tool of Information Transmission’. *Current Opinion in Neurobiology* 31:206–13. doi: 10.1016/J.CONB.2014.12.003.

Canolty, R. T., E. Edwards, S. S. Dalal, M. Soltani, S. S. Nagarajan, H. E. Kirsch, M. S. Berger, N. M. Barbare, and R. T. Knight. 2006. ‘High Gamma Power Is Phase-Locked to Theta Oscillations in Human Neocortex’. *Science* 313(5793):1626–28. doi: 10.1126/SCIENCE.1128115.

Cao, Vania Yu, Yizhou Ye, Surjeet Mastwal, Ming Ren, Matthew Coon, Qing Liu, Rui M. Costa, and Kuan Hong Wang. 2015. ‘Motor Learning Consolidates Arc-Expressing Neuronal Ensembles in Secondary Motor Cortex’. *Neuron* 86(6):1385–92. doi: 10.1016/J.NEURON.2015.05.022.

Cardin, Jessica A., Marie Carlén, Konstantinos Meletis, Ulf Knoblich, Feng Zhang, Karl Deisseroth, Li Huei Tsai, and Christopher I. Moore. 2009. ‘Driving Fast-Spiking Cells Induces Gamma Rhythm and Controls Sensory Responses’. *Nature 2009 459:7247* 459(7247):663–67. doi: 10.1038/nature08002.

Cardin, Jessica A., Marie Carlén, Konstantinos Meletis, Ulf Knoblich, Feng Zhang, Karl Deisseroth, Li Huei Tsai, and Christopher I. Moore. 2010. 'Targeted Optogenetic Stimulation and Recording of Neurons in Vivo Using Cell-Type-Specific Expression of Channelrhodopsin-2'. *Nature Protocols* 5(2):247. doi: 10.1038/NPROT.2009.228.

Cardozo Pinto, Daniel F., and Stephan Lammel. 2019. 'Hot Topic in Optogenetics: New Implications of in Vivo Tissue Heating'. *Nature Neuroscience* 22(7):1039–41. doi: 10.1038/s41593-019-0426-z.

Carmichael, James E., Jimmie M. Gmaz, and Matthijs A. A. van der Meer. 2017. 'Gamma Oscillations in the Rat Ventral Striatum Originate in the Piriform Cortex'. *Journal of Neuroscience* 37(33):7962–74. doi: 10.1523/JNEUROSCI.2944-15.2017.

Carracedo, Lucy M., Henrik Kjeldsen, Leonie Cunnington, Alastair Jenkins, Ian Schofield, Mark O. Cunningham, Ceri H. Davies, Roger D. Traub, and Miles A. Whittington. 2013. 'A Neocortical Delta Rhythm Facilitates Reciprocal Interlaminar Interactions via Nested Theta Rhythms'. *Journal of Neuroscience* 33(26):10750–61. doi: 10.1523/JNEUROSCI.0735-13.2013.

Chan, Russell W., Greg O. Cron, Mazen Asaad, Bradley J. Edelman, Hyun Joo Lee, Hillel Adesnik, David Feinberg, and Jin Hyung Lee. 2022. 'Distinct Local and Brain-Wide Networks Are Activated by Optogenetic Stimulation of Neurons Specific to Each Layer of Motor Cortex'. *NeuroImage* 263:119640. doi: 10.1016/J.NEUROIMAGE.2022.119640.

Chen, Tsai Wen, Nuo Li, Kayvon Daie, and Karel Svoboda. 2017. 'A Map of Anticipatory Activity in Mouse Motor Cortex'. *Neuron* 94(4):866–79. doi: 10.1016/j.neuron.2017.05.005.

Chow, Brian Y., Xue Han, Allison S. Dobry, Xiaofeng Qian, Amy S. Chuong, Mingjie Li, Michael A. Henninger, Gabriel M. Belfort, Yingxi Lin, Patrick E. Monahan, and Edward S. Boyden. 2010. 'High-Performance Genetically Targetable Optical Neural Silencing by Light-Driven Proton Pumps'. *Nature* 463(7277):98–102. doi: 10.1038/nature08652.

Christie, Isabel N., Jack A. Wells, Paul Southern, Nephtali Marina, Sergey Kasparov, Alexander V. Gourine, and Mark F. Lythgoe. 2013. 'FMRI Response to Blue Light Delivery in the Naïve Brain: Implications for Combined Optogenetic FMRI Studies'. *NeuroImage* 66:634–41. doi: 10.1016/J.NEUROIMAGE.2012.10.074.

Clayton, Janine Austin. 2016. 'Studying Both Sexes: A Guiding Principle for Biomedicine'. *The FASEB Journal* 30(2):519. doi: 10.1096/FJ.15-279554.

Clayton, Michael S., Nick Yeung, and Roi Cohen Kadosh. 2018. 'The Many Characters of Visual Alpha Oscillations'. *European Journal of Neuroscience* 48(7):2498–2508. doi: 10.1111/EJN.13747.

Cochin, S., C. Barthelemy, B. Lejeune, S. Roux, and J. Martineau. 1998. 'Perception of Motion and QEEG Activity in Human Adults'. *Electroencephalography and Clinical Neurophysiology* 107(4):287–95. doi: 10.1016/S0013-4694(98)00071-6.

Cochin, S., C. Barthelemy, S. Roux, and J. Martineau. 1999. 'Observation and Execution of Movement: Similarities Demonstrated by Quantified Electroencephalography'. *European Journal of Neuroscience* 11(5):1839–42. doi: 10.1046/J.1460-9568.1999.00598.X.

Colgin, Laura Lee. 2013. 'Mechanisms and Functions of Theta Rhythms'. *Annu Rev Neuroscience* 36:295–312. doi: 10.1146/ANNUREV-NEURO-062012-170330.

Colgin, Laura Lee. 2015. 'Theta–Gamma Coupling in the Entorhinal–Hippocampal System'. *Current Opinion in Neurobiology* 31:45–50. doi: 10.1016/J.CONB.2014.08.001.

Colgin, Laura Lee. 2016. 'Rhythms of the Hippocampal Network'. *Nature Reviews Neuroscience* 17(4):239–49. doi: 10.1038/nrn.2016.21.

Cooper, Jonathan A. 2008. 'A Mechanism for Inside-out Lamination in the Neocortex'. *Trends in Neurosciences* 31(3):113–19. doi: 10.1016/j.tins.2007.12.003.

Cornwell, Brian R., Linda L. Johnson, Tom Holroyd, Frederick W. Carver, and Christian Grillon. 2008. 'Human Hippocampal and Parahippocampal Theta during Goal-Directed Spatial Navigation Predicts Performance on a Virtual Morris Water Maze'. *The Journal of Neuroscience* 28(23):5983–90. doi: 10.1523/JNEUROSCI.5001-07.2008.

Corrigan, Frances, Ing Chee Wee, and Lyndsey E. Collins-Praino. 2023. 'Chronic Motor Performance Following Different Traumatic Brain Injury Severity—A Systematic Review'. *Frontiers in Neurology* 14:1180353. doi: 10.3389/FNEUR.2023.1180353.

Corripio, Iluminada, Alexandra Roldán, Peter McKenna, Salvador Sarró, Anna Alonso-Solís, Laura Salgado, Enric Álvarez, Joan Molet, Edith Pomarol-Clotet, and Maria Portella. 2022. 'Target Selection for Deep Brain Stimulation in Treatment Resistant Schizophrenia'. *Progress in Neuro-Psychopharmacology and Biological Psychiatry* 112(110436). doi: 10.1016/J.PNPBP.2021.110436.

Corripio, Iluminada, Alexandra Roldán, Salvador Sarró, Peter J. McKenna, Anna Alonso-Solís, Mireia Rabella, Anna Díaz, Dolors Puigdemont, Víctor Pérez-Solà, Enric Álvarez, Antonio Arévalo, Pedro P. Padilla, Jesus M. Ruiz-Idiago, Rodrigo Rodríguez, Joan Molet, Edith Pomarol-Clotet, and Maria J. Portella. 2020. 'Deep Brain Stimulation in Treatment Resistant Schizophrenia: A Pilot Randomized Cross-over Clinical Trial'. *EBioMedicine* 51(102568). doi: 10.1016/j.ebiom.2019.11.029.

van der Cruijsen, Joris, Mana Manoochehri, Zeb D. Jonker, Eleni Rosalina Andrinopoulou, Maarten A. Frens, Gerard M. Ribbers, Alfred C. Schouten, and Ruud W. Selles. 2021. 'Theta but Not Beta Power Is Positively Associated with Better Explicit Motor Task Learning'. *NeuroImage* 240:118373. doi: 10.1016/J.NEUROIMAGE.2021.118373.

Csicsvari, Jozsef, Brian Jamieson, Kensall D. Wise, and György Buzsáki. 2003. 'Mechanisms of Gamma Oscillations in the Hippocampus of the Behaving Rat'. *Neuron* 37(2):311–22. doi: 10.1016/S0896-6273(02)01169-8.

Dave, S., T. A. Brothers, and T. Y. Swaab. 2018. '1/f Neural Noise and Electrophysiological Indices of Contextual Prediction in Aging'. *Brain Research* 1691:34–43. doi: 10.1016/J.BRAINRES.2018.04.007.

David, François, Melodie Borel, Suleman Ayub, Patrick Ruther, and Luc J. Gentet. 2023. 'Layer-Specific Stimulations of Parvalbumin-Positive Cortical Interneurons in Mice Entrain Brain Rhythms to Different Frequencies'. *Cerebral Cortex* 33(13):8286–99. doi: 10.1093/CERCOR/BHAD114.

Deisseroth, Karl. 2010. ‘Optogenetics’. *Nature Methods* 8(1):26–29. doi: 10.1038/nmeth.f.324.

Deisseroth, Karl, Guoping Feng, Ania K. Majewska, Gero Miesenböck, Alice Ting, and Mark J. Schnitzer. 2006. ‘Next-Generation Optical Technologies for Illuminating Genetically Targeted Brain Circuits’. *Journal of Neuroscience* 26(41):10380–86. doi: 10.1523/JNEUROSCI.3863-06.2006.

Dejean, Cyril, Julien Courtin, Nikolaos Karalis, Fabrice Chaudun, Hélène Wurtz, Thomas C. M. Bienvenu, and Cyril Herry. 2016. ‘Prefrontal Neuronal Assemblies Temporally Control Fear Behaviour’. *Nature* 535(7612):420–24. doi: 10.1038/nature18630.

Donoghue, Thomas, Matar Haller, Erik J. Peterson, Paroma Varma, Priyadarshini Sebastian, Richard Gao, Torben Noto, Antonio H. Lara, Joni D. Wallis, Robert T. Knight, Avgusta Shestyuk, and Bradley Voytek. 2020. ‘Parameterizing Neural Power Spectra into Periodic and Aperiodic Components’. *Nature Neuroscience 2020 23:12* 23(12):1655–65. doi: 10.1038/s41593-020-00744-x.

Du, J., L. Tian, W. Liu, J. Hu, G. Xu, M. Ma, X. Fan, R. Ye, Y. Jiang, Q. Yin, W. Zhu, Y. Xiong, F. Yang, and X. Liu. 2016. ‘Effects of Repetitive Transcranial Magnetic Stimulation on Motor Recovery and Motor Cortex Excitability in Patients with Stroke: A Randomized Controlled Trial’. *European Journal of Neurology* 23(11):1666–72. doi: 10.1111/ENE.13105.

Du, Minghui, Jiajun Zheng, Yicong Huang, Xiaoli Wang, Yankun Qi, Jianrong Qiu, Lu Huang, Chaoran Ren, Zhuliang Yu, and Shifeng Zhou. 2024. ‘Closed-Loop Optogenetic Modulation of Neural Activities in Freely Moving Mice with Multimodal Fibers’. *Advanced Optical Materials* 12(2302044). doi: 10.1002/ADOM.202302044.

Dupret, David, Joseph O’Neill, and Jozsef Csicsvari. 2013. ‘Dynamic Reconfiguration of Hippocampal Interneuron Circuits during Spatial Learning’. *Neuron* 78(1):166–80. doi: 10.1016/j.neuron.2013.01.033.

Dymecki, Susan M., and Jun Chul Kim. 2007. ‘Molecular Neuroanatomy’s “Three Gs”: A Primer’. *Neuron* 54(1):17–34. doi: 10.1016/J.NEURON.2007.03.009.

Ebbesen, Christian Laut, and Michael Brecht. 2017. ‘Motor Cortex — to Act or Not to Act?’ *Nature Reviews Neuroscience* 18(11):694–705. doi: 10.1038/nrn.2017.119.

Economo, Michael N., Sarada Viswanathan, Bosiljka Tasic, Erhan Bas, Johan Winnubst, Vilas Menon, Lucas T. Graybuck, Thuc Nghi Nguyen, Kimberly A. Smith, Zizhen Yao, Lihua Wang, Charles R. Gerfen, Jayaram Chandrashekar, Hongkui Zeng, Loren L. Looger, and Karel Svoboda. 2018. ‘Distinct Descending Motor Cortex Pathways and Their Roles in Movement’. *Nature* 563(7729):79–84. doi: 10.1038/s41586-018-0642-9.

Einevoll, Gaute T., Christoph Kayser, Nikos K. Logothetis, and Stefano Panzeri. 2013. ‘Modelling and Analysis of Local Field Potentials for Studying the Function of Cortical Circuits’. *Nature Reviews Neuroscience* 14(11):770–85. doi: 10.1038/nrn3599.

Engel, Andreas K., and Pascal Fries. 2010. ‘Beta-Band Oscillations — Signalling the Status Quo?’ *Current Opinion in Neurobiology* 20(2):156–65. doi: 10.1016/J.CONB.2010.02.015.

Engel, Andreas K., Pascal Fries, and Wolf Singer. 2001. 'Dynamic Predictions: Oscillations and Synchrony in Top–down Processing'. *Nature Reviews Neuroscience* 2(10):704–16. doi: 10.1038/35094565.

Fenno, Lief, Ofer Yizhar, and Karl Deisseroth. 2011. 'The Development and Application of Optogenetics'. *Annu Rev Neuroscience* 34:389–412. doi: 10.1146/ANNUREV-NEURO-061010-113817.

Figee, Martijn, Patricio Riva-Posse, Ki Sueng Choi, Lucia Bederson, Helen S. Mayberg, and Brian H. Kopell. 2022. 'Deep Brain Stimulation for Depression'. *Neurotherapeutics* 19(4):1229–45. doi: 10.1007/S13311-022-01270-3.

Fischer, Kyle B., Hannah K. Collins, and Edward M. Callaway. 2019. 'Sources of Off-Target Expression from Recombinasedependent AAV Vectors and Mitigation with Cross-over Insensitive ATG-out Vectors'. *Proceedings of the National Academy of Sciences of the United States of America* 116(52):27001–10. doi: 10.1073/PNAS.1915974116.

Fisher, Robert, Roy Bakay, Jaimie Henderson, Jacqueline French, Gordon Baltuch, William Rosenfeld, Andrew Youkilis, Babu Krishnamurthy, Steven Papavassiliou, Charles Epstein, John Pollard, Lisa Tonder, Joan Grebin, Robert Coffey, Nina Graves, and the SANTE Study Group. 2010. 'Electrical Stimulation of the Anterior Nucleus of Thalamus for Treatment of Refractory Epilepsy'. *Epilepsia* 51(5):899–908. doi: 10.1111/j.1528-1167.2010.02536.x.

Fitzgerald, Paul B., Kate E. Hoy, David Elliot, R. N. Susan McQueen, Lenore E. Wambeek, and Zafiris J. Daskalakis. 2018. 'Accelerated Repetitive Transcranial Magnetic Stimulation in the Treatment of Depression'. *Neuropsychopharmacology* 43(7):1565. doi: 10.1038/S41386-018-0009-9.

Florez, C. M., R. J. McGinn, V. Lukankin, I. Marwa, S. Sugumar, J. Dian, L. N. Hazrati, P. L. Carlen, L. Zhang, and T. A. Valiante. 2015. 'In Vitro Recordings of Human Neocortical Oscillations'. *Cerebral Cortex* 25(3):578–97. doi: 10.1093/CERCOR/BHT235.

Forger, Daniel B. 2017. 'How to Shift an Oscillator Optimally'. in *Biological Clocks, Rhythms, and Oscillations: The Theory of Biological Timekeeping.* Cambridge(MA): MIT Press.

Fries, P., J. H. Reynolds, A. E. Rorie, and R. Desimone. 2001. 'Modulation of Oscillatory Neuronal Synchronization by Selective Visual Attention'. *Science* 291(5508):1560–63. doi: 10.1126/SCIENCE.1055465.

Fries, Pascal. 2005. 'A Mechanism for Cognitive Dynamics: Neuronal Communication through Neuronal Coherence'. *Trends in Cognitive Sciences* 9(10):474–80. doi: 10.1016/J.TICS.2005.08.011.

Fries, Pascal. 2009. 'Neuronal Gamma-Band Synchronization as a Fundamental Process in Cortical Computation'. *Annu Rev Neuroscience* 32:209–24. doi: 10.1146/ANNUREV.NEURO.051508.135603.

Fries, Pascal. 2015. 'Rhythms For Cognition: Communication Through Coherence'. *Neuron* 88(1):220–35. doi: 10.1016/J.NEURON.2015.09.034.

Fries, Pascal, Danko Nikolić, and Wolf Singer. 2007. 'The Gamma Cycle'. *Trends in Neurosciences* 30(7):309–16. doi: 10.1016/J.TINS.2007.05.005.

Gao, Richard, Erik J. Peterson, and Bradley Voytek. 2017. 'Inferring Synaptic Excitation/Inhibition Balance from Field Potentials'. *NeuroImage* 158:70–78. doi: 10.1016/J.NEUROIMAGE.2017.06.078.

Gardner, John. 2013. 'A History of Deep Brain Stimulation: Technological Innovation and the Role of Clinical Assessment Tools'. *Social Studies of Science* 43(5):707. doi: 10.1177/0306312713483678.

Gastaut, Henri J., and Jacques Bert. 1954. 'EEG Changes during Cinematographic Presentation (Moving Picture Activation of the EEG)'. *Electroencephalography and Clinical Neurophysiology* 6(C):433–44. doi: 10.1016/0013-4694(54)90058-9.

Gerfen, Charles R., Ronald Paletzki, and Nathaniel Heintz. 2013. 'GENSAT BAC Cre-Recombinase Driver Lines to Study the Functional Organization of Cerebral Cortical and Basal Ganglia Circuits'. *Neuron* 80(6):1368–83. doi: 10.1016/J.NEURON.2013.10.016.

Glickfeld, Lindsey L., J. David Roberts, Peter Somogyi, and Massimo Scanziani. 2008. 'Interneurons Hyperpolarize Pyramidal Cells along Their Entire Somatodendritic Axis'. *Nature Neuroscience* 12(1):21–23. doi: 10.1038/nn.2230.

Gong, Shiaoching, Martin Doughty, Carroll R. Harbaugh, Alexander Cummins, Mary E. Hatten, Nathaniel Heintz, and Charles R. Gerfen. 2007. 'Targeting Cre Recombinase to Specific Neuron Populations with Bacterial Artificial Chromosome Constructs'. *Journal of Neuroscience* 27(37):9817–23. doi: 10.1523/JNEUROSCI.2707-07.2007.

Gordon, Evan M., Roselyne J. Chauvin, Andrew N. Van, Aishwarya Rajesh, Ashley Nielsen, Dillan J. Newbold, Charles J. Lynch, Nicole A. Seider, Samuel R. Krimmel, Kristen M. Scheidter, Julia Monk, Ryland L. Miller, Athanasia Metoki, David F. Montez, Annie Zheng, Immanuel Elbau, Thomas Madison, Tomoyuki Nishino, Michael J. Myers, Sydney Kaplan, Carolina Badke D'Andrea, Damion V. Demeter, Matthew Feigelis, Julian S. B. Ramirez, Ting Xu, Deanna M. Barch, Christopher D. Smyser, Cynthia E. Rogers, Jan Zimmermann, Kelly N. Botteron, John R. Pruett, Jon T. Willie, Peter Brunner, Joshua S. Shimony, Benjamin P. Kay, Scott Marek, Scott A. Norris, Caterina Gratton, Chad M. Sylvester, Jonathan D. Power, Conor Liston, Deanna J. Greene, Jarod L. Roland, Steven E. Petersen, Marcus E. Raichle, Timothy O. Laumann, Damien A. Fair, and Nico U. F. Dosenbach. 2023. 'A Somato-Cognitive Action Network Alternates with Effector Regions in Motor Cortex'. *Nature* 617(7960):351–59. doi: 10.1038/s41586-023-05964-2.

Gould, T. J., W. B. Rowe, K. L. Heman, M. H. Mesches, D. A. Young, G. M. Rose, and P. C. Bickford. 2002. 'Effects of Hippocampal Lesions on Patterned Motor Learning in the Rat'. *Brain Research Bulletin* 58(6):581–86. doi: 10.1016/S0361-9230(02)00832-8.

Goutagny, Romain, Jesse Jackson, and Sylvain Williams. 2009. 'Self-Generated Theta Oscillations in the Hippocampus'. *Nature Neuroscience* 12(12):1491–93. doi: 10.1038/nn.2440.

Gray, Charles M., Peter König, Andreas K. Engel, and Wolf Singer. 1989. 'Oscillatory Responses in Cat Visual Cortex Exhibit Inter-Columnar Synchronization Which Reflects Global Stimulus Properties'. *Nature* 338(6213):334–37. doi: 10.1038/338334a0.

Grillner, Sten. 2006. 'Biological Pattern Generation: The Cellular and Computational Logic of Networks in Motion'. *Neuron* 52(5):751–66. doi: 10.1016/J.NEURON.2006.11.008.

Groh, Alexander, Hanno S. Meyer, Eric F. Schmidt, Nathaniel Heintz, Bert Sakmann, and Patrik Krieger. 2010. 'Cell-Type Specific Properties of Pyramidal Neurons in Neocortex Underlying a Layout That Is Modifiable Depending on the Cortical Area'. *Cerebral Cortex* 20(4):826–36. doi: 10.1093/CERCOR/BHP152.

Guerin, Karen, Meghan Rego, Daniela Bourges, Ina Ersing, Leila Haery, Kate Harten Demaio, Erin Sanders, Meron Tasissa, Maya Kostman, Michelle Tillgren, Luke Makana Hanley, Isabelle Mueller, Alanna Mitsopoulos, and Melina Fan. 2020. 'A Novel Next-Generation Sequencing and Analysis Platform to Assess the Identity of Recombinant Adeno-Associated Viral Preparations from Viral DNA Extracts'. *Human Gene Therapy* 31(11–12):664–78. doi: 10.1089/HUM.2019.277.

Guidetti, Matteo, Sara Marceglia, Aaron Loh, Irene E. Harmsen, Sara Meoni, Guglielmo Foffani, Andres M. Lozano, Elena Moro, Jens Volkmann, and Alberto Priori. 2021. 'Clinical Perspectives of Adaptive Deep Brain Stimulation'. *Brain Stimulation* 14(5):1238–47. doi: 10.1016/J.BRS.2021.07.063.

Gulyás, Attila I., Gergely G. Szabó, István Ulbert, Noémi Holderith, Hannah Monyer, Ferenc Erdélyi, Gábor Szabó, Tamás F. Freund, and Norbert Hájos. 2010. 'Parvalbumin-Containing Fast-Spiking Basket Cells Generate the Field Potential Oscillations Induced by Cholinergic Receptor Activation in the Hippocampus'. *Journal of Neuroscience* 30(45):15134–45. doi: 10.1523/JNEUROSCI.4104-10.2010.

Gunaydin, Lisa A., Ofer Yizhar, André Berndt, Vikaas S. Sohal, Karl Deisseroth, and Peter Hegemann. 2010. 'Ultrafast Optogenetic Control'. *Nature Neuroscience* 13(3):387–92. doi: 10.1038/nn.2495.

Guo, Jian-Zhong, Austin R. Graves, Wendy W. Guo, Jihong Zheng, Allen Lee, Juan Rodríguez-Gonzá Lez, Nuo Li, John J. Macklin, James W. Phillips, Brett D. Mensh, Kristin Branson, and Adam W. Hantman. 2015. 'Cortex Commands the Performance of Skilled Movement'. *ELife* 4(DECEMBER):e10774. doi: 10.7554/ELIFE.10774.

Guo, Zengcai V., Nuo Li, Daniel Huber, Eran Ophir, Diego Gutnisky, Jonathan T. Ting, Guoping Feng, and Karel Svoboda. 2014. 'Flow of Cortical Activity Underlying a Tactile Decision in Mice'. *Neuron* 81(1):179–94. doi: 10.1016/J.NEURON.2013.10.020.

Guru, Akash, Ryan J. Post, Yi Yun Ho, and Melissa R. Warden. 2015. 'Making Sense of Optogenetics'. *International Journal of Neuropsychopharmacology* 18(11):1–8. doi: 10.1093/IJNP/PYV079.

Hájos, Norbert, János Pálhalini, Edward O. Mann, Beáta Nèmeth, Ole Paulsen, and Tamas F. Freund. 2004. 'Spike Timing of Distinct Types of GABAergic Interneuron during Hippocampal Gamma Oscillations In Vitro'. *Journal of Neuroscience* 24(41):9127–37. doi: 10.1523/JNEUROSCI.2113-04.2004.

Hamada, Masashi, Nagako Murase, Alkomiet Hasan, Michelle Balaratnam, and John C. Rothwell. 2013. 'The Role of Interneuron Networks in Driving Human Motor Cortical Plasticity'. *Cerebral Cortex* 23(7):1593–1605. doi: 10.1093/CERCOR/BHS147.

Hariz, Marwan I., Stig Rehncrona, Niall P. Quinn, Johannes D. Speelman, and Carin Wensing. 2008. 'Multicenter Study on Deep Brain Stimulation in Parkinson's Disease: An Independent Assessment of Reported Adverse Events at 4 Years'. *Movement Disorders* 23(3):416–21. doi: 10.1002/mds.21888.

Harris, Julie A., Karla E. Hirokawa, Staci A. Sorensen, Hong Gu, Maya Mills, Lydia L. Ng, Phillip Bohn, Marty Mortrud, Benjamin Ouellette, Jolene Kidney, Kimberly A. Smith, Chinh Dang, Susan Sunkin, Amy Bernard, Seung Wook Oh, Linda Madisen, and Hongkui Zeng. 2014. 'Anatomical Characterization of Cre Driver Mice for Neural Circuit Mapping and Manipulation'. *Frontiers in Neural Circuits* 8(76). doi: 10.3389/FNCIR.2014.00076.

Harris, Kenneth D., and Thomas D. Mrsic-Flogel. 2013. 'Cortical Connectivity and Sensory Coding'. *Nature* 503(7474):51–58. doi: 10.1038/nature12654.

Harris, Kenneth, and Gordon Shepherd. 2015. 'The Neocortical Circuit: Themes and Variations'. *Nature Neuroscience* 18(2):170–81. doi: 10.1038/nn.3917.

Hasenstaub, Andrea, Yousheng Shu, Bilal Haider, Udo Kraushaar, Alvaro Duque, and David A. McCormick. 2005. 'Inhibitory Postsynaptic Potentials Carry Synchronized Frequency Information in Active Cortical Networks'. *Neuron* 47(3):423–35. doi: 10.1016/j.neuron.2005.06.016.

He, Biyu J. 2014. 'Scale-Free Brain Activity: Past, Present, and Future'. *Trends in Cognitive Sciences* 18(9):480–87. doi: 10.1016/j.tics.2014.04.003.

Hebron, Henry, Beatrice Lugli, Radost Dimitrova, Valeria Jaramillo, Lisa R. Yeh, Edward Rhodes, Nir Grossman, Derk Jan Dijk, and Ines R. Violante. 2024. 'A Closed-Loop Auditory Stimulation Approach Selectively Modulates Alpha Oscillations and Sleep Onset Dynamics in Humans'. *PLOS Biology* 22(6):e3002651. doi: 10.1371/JOURNAL.PBIO.3002651.

Hippenmeyer, Simon, Eline Vrieseling, Markus Sigrist, Thomas Portmann, Celia Laengle, David R. Ladle, and Silvia Arber. 2005. 'A Developmental Switch in the Response of DRG Neurons to ETS Transcription Factor Signaling'. *PLOS Biology* 3(5):e159. doi: 10.1371/JOURNAL.PBIO.0030159.

Holt, Abbey B., Eszter Kormann, Alessandro Gulberti, Monika Pötter-Nerger, Colin G. McNamara, Hayriye Cagnan, Magdalena K. Baaske, Simon Little, Johannes A. Köppen, Carsten Buhmann, Manfred Westphal, Christian Gerloff, Andreas K. Engel, Peter Brown, Wolfgang Hamel, Christian K. E. Moll, and Andrew Sharott. 2019. 'Phase-Dependent Suppression of Beta Oscillations in Parkinson's Disease Patients'. *The Journal of Neuroscience* 39(6):1119–34. doi: 10.1523/JNEUROSCI.1913-18.2018.

Hooks, Bryan M., Tianyi Mao, Diego A. Gutnisky, Naoki Yamawaki, Karel Svoboda, and Gordon M. G. Shepherd. 2013. 'Organization of Cortical and Thalamic Input to Pyramidal Neurons in Mouse Motor Cortex'. *Journal of Neuroscience* 33(2):748–60. doi: 10.1523/JNEUROSCI.4338-12.2013.

Hovde, Karoline, Michele Gianatti, Menno P. Witter, and Jonathan R. Whitlock. 2019. 'Architecture and Organization of Mouse Posterior Parietal Cortex Relative to Extrastriate Areas'. *European Journal of Neuroscience* 49(10):1313–29. doi: 10.1111/EJN.14280.

Howard, Allyson, Gabor Tamas, and Ivan Soltesz. 2005. 'Lighting the Chandelier: New Vistas for Axo-Axonic Cells'. *Trends in Neurosciences* 28(6 SPEC. ISS.):310–16. doi: 10.1016/j.tins.2005.04.004.

Huh, Carey Y. L., Bénédicte Amilhon, Katie A. Ferguson, Frédéric Manseau, Susana G. Torres-Platas, John P. Peach, Stephanie Scodras, Naguib Mechawar, Frances K. Skinner, and Sylvain Williams. 2016. 'Excitatory Inputs Determine Phase-Locking Strength and Spike-Timing of CA1 Stratum Oriens/Alveus Parvalbumin and Somatostatin Interneurons during Intrinsically Generated Hippocampal Theta Rhythm'. *Journal of Neuroscience* 36(25):6605–22. doi: 10.1523/JNEUROSCI.3951-13.2016.

Igarashi, Jun, Yoshikazu Isomura, Kensuke Arai, Rie Harukuni, and Tomoki Fukai. 2013. 'A θ–γ Oscillation Code for Neuronal Coordination during Motor Behavior'. *Journal of Neuroscience* 33(47):18515–30. doi: 10.1523/JNEUROSCI.2126-13.2013.

Isaacson, Jeffry S., and Massimo Scanziani. 2011. 'How Inhibition Shapes Cortical Activity'. *Neuron* 72(2):231–43. doi: 10.1016/J.NEURON.2011.09.027.

Jaramillo, Valeria, Henry Hebron, Sara Wong, Giuseppe Atzori, Ullrich Bartsch, Derk-Jan Dijk, and Ines R. Violante. 2024. 'Closed-Loop Auditory Stimulation Targeting Alpha and Theta Oscillations during Rapid Eye Movement Sleep Induces Phase-Dependent Power and Frequency Changes'. *Sleep* zsae193. doi: 10.1093/SLEEP/ZSAE193.

Jasper, Herbert, and Wilder Penfield. 1949. 'Electrocorticograms in Man: Effect of Voluntary Movement upon the Electrical Activity of the Precentral Gyrus'. *Archiv Für Psychiatrie Und Nervenkrankheiten* 183(1–2):163–74. doi: 10.1007/BF01062488.

Jensen, Ole, and Laura L. Colgin. 2007. 'Cross-Frequency Coupling between Neuronal Oscillations'. *Trends in Cognitive Sciences* 11(7):267–69. doi: 10.1016/j.tics.2007.05.003.

Jensen, Ole, Jochen Kaiser, and Jean Philippe Lachaux. 2007. 'Human Gamma-Frequency Oscillations Associated with Attention and Memory'. *Trends in Neurosciences* 30(7):317–24. doi: 10.1016/j.tins.2007.05.001.

Jiang, Siqi, Yue Guan, Shangbin Chen, Xueyan Jia, Hong Ni, Yalun Zhang, Yutong Han, Xue Peng, Can Zhou, Anan Li, Qingming Luo, and Hui Gong. 2020. 'Anatomically Revealed Morphological Patterns of Pyramidal Neurons in Layer 5 of the Motor Cortex'. *Scientific Reports* 10(1):1–10. doi: 10.1038/s41598-020-64665-2.

Johnson, Nicholas W., Mazhar Özkan, Adrian P. Burgess, Emma J. Prokic, Keith A. Wafford, Michael J. O'Neill, Stuart D. Greenhill, Ian M. Stanford, and Gavin L. Woodhall. 2017. 'Phase-Amplitude Coupled Persistent Theta and Gamma Oscillations in Rat Primary Motor Cortex in Vitro'. *Neuropharmacology* 119:141–56. doi: 10.1016/J.NEUROPHARM.2017.04.009.

Jones, Matthew W., and Matthew A. Wilson. 2005. 'Theta Rhythms Coordinate Hippocampal-Prefrontal Interactions in a Spatial Memory Task'. *PLoS Biol.* 3(12):e402. doi: 10.1371/journal.pbio.0030402.

Jurkiewicz, Michael T., William C. Gaetz, Andreea C. Bostan, and Douglas Cheyne. 2006. 'Post-Movement Beta Rebound Is Generated in Motor Cortex: Evidence from Neuromagnetic Recordings'. *NeuroImage* 32(3):1281–89. doi: 10.1016/J.NEUROIMAGE.2006.06.005.

Kahana, Michael J., David Seelig, and Joseph R. Madsen. 2001. 'Theta Returns'. *Current Opinion in Neurobiology* 11(6):739–44. doi: 10.1016/S0959-4388(01)00278-1.

Kamondi, Anita, László Acsády, and György Buzsáki. 1998. 'Dendritic Spikes Are Enhanced by Cooperative Network Activity in the Intact Hippocampus'. *Journal of Neuroscience* 18(10):3919–28. doi: 10.1523/JNEUROSCI.18-10-03919.1998.

Kanta, Vasiliki, Denis Pare, and Drew B. Headley. 2019. 'Closed-Loop Control of Gamma Oscillations in the Amygdala Demonstrates Their Role in Spatial Memory Consolidation'. *Nature Communications* 10(1):1–14. doi: 10.1038/s41467-019-11938-8.

Karni, Avi, Gundela Meyer, Christine Rey-Hipolito, Peter Jezzard, Michelle M. Adams, Robert Turner, and Leslie G. Ungerleider. 1998. 'The Acquisition of Skilled Motor Performance: Fast and Slow Experience-Driven Changes in Primary Motor Cortex'. *Proceedings of the National Academy of Sciences of the United States of America* 95(3):861. doi: 10.1073/PNAS.95.3.861.

Kätzel, Dennis, Boris V. Zemelman, Christina Buetfering, Markus Wölfel, and Gero Miesenböck. 2010. 'The Columnar and Laminar Organization of Inhibitory Connections to Neocortical Excitatory Cells'. *Nature Neuroscience* 14(1):100–107. doi: 10.1038/nn.2687.

Katzner, Steffen, Ian Nauhaus, Andrea Benucci, Vincent Bonin, Dario L. Ringach, and Matteo Carandini. 2009. 'Local Origin of Field Potentials in Visual Cortex'. *Neuron* 61(1):35–41. doi: 10.1016/j.neuron.2008.11.016.

Kawai, Risa, Timothy Markman, Rajesh Poddar, Raymond Ko, Antoniu L. Fantana, Ashesh K. Dhawale, Adam R. Kampff, and Bence P. Ölveczky. 2015. 'Motor Cortex Is Required for Learning but Not for Executing a Motor Skill'. *Neuron* 86(3):800–812. doi: 10.1016/J.NEURON.2015.03.024.

Kessler, K., R. A. Seymour, and G. Rippon. 2016. 'Brain Oscillations and Connectivity in Autism Spectrum Disorders (ASD): New Approaches to Methodology, Measurement and Modelling'. *Neuroscience & Biobehavioral Reviews* 71:601–20. doi: 10.1016/J.NEUBIOREV.2016.10.002.

Khibnik, Lena A., Nicolas X. Tritsch, and Bernardo L. Sabatini. 2014. 'A Direct Projection from Mouse Primary Visual Cortex to Dorsomedial Striatum'. *PLoS ONE* 9(8):104501. doi: 10.1371/JOURNAL.PONE.0104501.

Kim, Jaekyung, Tanuj Gulati, and Karunesh Ganguly. 2019. 'Competing Roles of Slow Oscillations and Delta Waves in Memory Consolidation versus Forgetting'. *Cell* 179(2):514-526.e13. doi: 10.1016/J.CELL.2019.08.040.

Kirihara, Kenji, Anthony J. Rissling, Neal R. Swerdlow, David L. Braff, and Gregory A. Light. 2012. 'Hierarchical Organization of Gamma and Theta Oscillatory Dynamics in Schizophrenia'. *Biological Psychiatry* 71(10):873–80. doi: 10.1016/J.BIOPSYCH.2012.01.016.

Kiritani, Taro, Ian R. Wickersham, H. Sebastian Seung, and Gordon M. G. Shepherd. 2012. 'Hierarchical Connectivity and Connection-Specific Dynamics in the Corticospinal–Corticostriatal Microcircuit in Mouse Motor Cortex'. *Journal of Neuroscience* 32(14):4992–5001. doi: 10.1523/JNEUROSCI.4759-11.2012.

Klausberger, Thomas, Peter J. Magill, László F. Márton, J. David B. Roberts, Philip M. Cobden, György Buzsáki, and Peter Somogyi. 2003. 'Brain-State- and Cell-Type-Specific Firing of Hippocampal Interneurons in Vivo'. *Nature* 421(6925):844–48. doi: 10.1038/nature01374.

Kleim, Jeffrey A., Erich Lussnig, Edward R. Schwarz, Thomas A. Comery, and William T. Greenough. 1996. 'Synaptogenesis and FOS Expression in the Motor Cortex of the Adult Rat after Motor Skill Learning'. *Journal of Neuroscience* 16(14):4529–35. doi: 10.1523/JNEUROSCI.16-14-04529.1996.

Knyazev, Gennady G. 2012. 'EEG Delta Oscillations as a Correlate of Basic Homeostatic and Motivational Processes'. *Neuroscience & Biobehavioral Reviews* 36(1):677–95. doi: 10.1016/J.NEUBIOREV.2011.10.002.

Korotkova, Tatiana, Alexey Ponomarenko, Caitlin K. Monaghan, Steven L. Poulter, Francesca Cacucci, Tom Wills, Michael E. Hasselmo, and Colin Lever. 2018. 'Reconciling the Different Faces of Hippocampal Theta: The Role of Theta Oscillations in Cognitive, Emotional and Innate Behaviors'. *Neuroscience & Biobehavioral Reviews* 85:65–80. doi: 10.1016/J.NEUBIOREV.2017.09.004.

Kravitz, Alexxai V., Benjamin S. Freeze, Philip R. L. Parker, Kenneth Kay, Myo T. Thwin, Karl Deisseroth, and Anatol C. Kreitzer. 2010. 'Regulation of Parkinsonian Motor Behaviours by Optogenetic Control of Basal Ganglia Circuitry'. *Nature* 466(7306):622–26. doi: 10.1038/nature09159.

Krishnan, Giri P., Jenifer L. Vohs, William P. Hetrick, Christine A. Carroll, Anantha Shekhar, Marcia A. Bockbrader, and Brian F. O'Donnell. 2005. 'Steady State Visual Evoked Potential Abnormalities in Schizophrenia'. *Clinical Neurophysiology* 116(3):614–24. doi: 10.1016/J.CLINPH.2004.09.016.

Kumari, Lekshmy Sudha, and Abbas Z. Kouzani. 2021. 'Phase-Dependent Deep Brain Stimulation: A Review'. *Brain Sciences* 11(4). doi: 10.3390/BRAINSCI11040414.

Kuo, Min Fang, Walter Paulus, and Michael A. Nitsche. 2014. 'Therapeutic Effects of Non-Invasive Brain Stimulation with Direct Currents (TDCS) in Neuropsychiatric Diseases'. *NeuroImage* 85:948–60. doi: 10.1016/J.NEUROIMAGE.2013.05.117.

Kwan, H. C., W. A. MacKay, J. T. Murphy, and Y. C. Wong. 1978. 'Spatial Organization of Precentral Cortex in Awake Primates. II. Motor Outputs.' *J Neurophysiol* 41(5):1120–31. doi: 10.1152/JN.1978.41.5.1120.

Langhorne, Peter, Julie Bernhardt, and Gert Kwakkel. 2011. 'Stroke Rehabilitation'. *The Lancet* 377(9778):1693–1702. doi: 10.1016/S0140-6736(11)60325-5.

Larrain-Valenzuela, Josefina, Francisco Zamorano, Patricia Soto-Icaza, Ximena Carrasco, Claudia Herrera, Francisca Daiber, Francisco Aboitiz, and Pablo Billeke. 2017. 'Theta and Alpha Oscillation Impairments in Autistic Spectrum Disorder Reflect Working Memory Deficit'. *Scientific Reports 2017 7:1* 7(1):1–11. doi: 10.1038/s41598-017-14744-8.

Lasztóczi, Bálint, and Thomas Klausberger. 2014. 'Layer-Specific GABAergic Control of Distinct Gamma Oscillations in the CA1 Hippocampus'. *Neuron* 81(5):1126–39. doi: 10.1016/j.neuron.2014.01.021.

Ledochowitsch, P., A. Yazdan-Shahmorad, K. E. Bouchard, C. Diaz-Botia, T. L. Hanson, J. W. He, B. A. Seybold, E. Olivero, E. A. K. Phillips, T. J. Blanche, C. E. Schreiner, A. Hasenstaub, E. F. Chang, P. N. Sabes, and M. M. Maharbiz. 2015. 'Strategies for Optical Control and Simultaneous Electrical Readout of Extended Cortical Circuits'. *Journal of Neuroscience Methods* 256:220–31. doi: 10.1016/J.JNEUMETH.2015.07.028.

Lee, Chaery, Yeonjun Kim, and Bong Kiun Kaang. 2022. 'The Primary Motor Cortex: The Hub of Motor Learning in Rodents'. *Neuroscience* 485:163–70. doi: 10.1016/J.NEUROSCIENCE.2022.01.009.

Lee, Jin Hyung, Remy Durand, Viviana Gradinaru, Feng Zhang, Inbal Goshen, Dae Shik Kim, Lief E. Fenno, Charu Ramakrishnan, and Karl Deisseroth. 2010. 'Global and Local FMRI Signals Driven by Neurons Defined Optogenetically by Type and Wiring'. *Nature* 465(7299):788–92. doi: 10.1038/nature09108.

Lee, Soo Hyun, Jens Hjerling-Leffler, Edward Zagha, Gord Fishell, and Bernardo Rudy. 2010. 'The Largest Group of Superficial Neocortical GABAergic Interneurons Expresses Ionotropic Serotonin Receptors'. *Journal of Neuroscience* 30(50):16796–808. doi: 10.1523/JNEUROSCI.1869-10.2010.

Lefaucheur, Jean Pascal, André Aleman, Chris Baeken, David H. Benninger, Jérôme Brunelin, Vincenzo Di Lazzaro, Saša R. Filipović, Christian Grefkes, Alkomiet Hasan, Friedhelm C. Hummel, Satu K. Jääskeläinen, Berthold Langguth, Letizia Leocani, Alain Londero, Raffaele Nardone, Jean Paul Nguyen, Thomas Nyffeler, Albino J. Oliveira-Maia, Antonio Oliviero, Frank Padberg, Ulrich Palm, Walter Paulus, Emmanuel Poulet, Angelo Quartarone, Fady Rachid, Irena Rektorová, Simone Rossi, Hanna Sahlsten, Martin Schecklmann, David Szekely, and Ulf Ziemann. 2020. 'Evidence-Based Guidelines on the Therapeutic Use of Repetitive Transcranial Magnetic Stimulation (RTMS): An Update (2014–2018)'. *Clinical Neurophysiology* 131(2):474–528. doi: 10.1016/J.CLINPH.2019.11.002.

Leopold, David A., Yusuke Murayama, and Nikos K. Logothetis. 2003. 'Very Slow Activity Fluctuations in Monkey Visual Cortex: Implications for Functional Brain Imaging'. *Cerebral Cortex* 13(4):422–33. doi: 10.1093/CERCOR/13.4.422.

Lewis, Christopher Murphy, Jianguang Ni, Thomas Wunderle, Patrick Jendritza, Andreea Lazar, Ilka Diester, and Pascal Fries. 2021. 'Cortical Gamma-Band Resonance Preferentially Transmits Coherent Input'. *Cell Reports* 35(5):109083. doi: 10.1016/J.CELREP.2021.109083.

Lewis, David A., Takanori Hashimoto, and David W. Volk. 2005. 'Cortical Inhibitory Neurons and Schizophrenia'. *Nature Reviews Neuroscience* 6(4):312–24. doi: 10.1038/nrn1648.

Li, Lucia M., Kazumasa Uehara, and Takashi Hanakawa. 2015. 'The Contribution of Interindividual Factors to Variability of Response in Transcranial Direct Current Stimulation Studies'. *Frontiers in Cellular Neuroscience* 9(181). doi: 10.3389/FNCEL.2015.00181.

Li, Nuo, Tsai Wen Chen, Zengcai V. Guo, Charles R. Gerfen, and Karel Svoboda. 2015. 'A Motor Cortex Circuit for Motor Planning and Movement'. *Nature 2015 519:7541* 519(7541):51–56. doi: 10.1038/nature14178.

Li, Nuo, Kayvon Daie, Karel Svoboda, and Shaul Druckmann. 2016. 'Robust Neuronal Dynamics in Premotor Cortex during Motor Planning'. *Nature 2016 532:7600* 532(7600):459–64. doi: 10.1038/nature17643.

Lima, Susana Q., Tomáš Hromádka, Petr Znamenskiy, and Anthony M. Zador. 2009. 'PINP: A New Method of Tagging Neuronal Populations for Identification during in Vivo Electrophysiological Recording'. *PLoS ONE* 4(7). doi: 10.1371/journal.pone.0006099.

Little, Simon, Alex Pogosyan, Spencer Neal, Baltazar Zavala, Ludvic Zrinzo, Marwan Hariz, Thomas Foltynie, Patricia Limousin, Keyoumars Ashkan, James FitzGerald, Alexander L. Green, Tipu Z. Aziz, and Peter Brown. 2013. 'Adaptive Deep Brain Stimulation in Advanced Parkinson Disease'. *Annals of Neurology* 74(3):449–57. doi: 10.1002/ANA.23951.

Little, Simon, Elina Tripoliti, Martijn Beudel, Alek Pogosyan, Hayriye Cagnan, Damian Herz, Sven Bestmann, Tipu Aziz, Binith Cheeran, Ludvic Zrinzo, Marwan Hariz, Jonathan Hyam, Patricia Limousin, Tom Foltynie, and Peter Brown. 2016. 'Adaptive Deep Brain Stimulation for Parkinson's Disease Demonstrates Reduced Speech Side Effects Compared to Conventional Stimulation in the Acute Setting'. *Journal of Neurology, Neurosurgery & Psychiatry* 87(12):1388–89. doi: 10.1136/JNNP-2016-313518.

Llinás, Rodolfo R. 1988. 'The Intrinsic Electrophysiological Properties of Mammalian Neurons: Insights into Central Nervous System Function'. *Science* 242(4886):1654–64. doi: 10.1126/SCIENCE.3059497.

Logothetis, Nikos K., Christoph Kayser, and Axel Oeltermann. 2007. 'In Vivo Measurement of Cortical Impedance Spectrum in Monkeys: Implications for Signal Propagation'. *Neuron* 55(5):809–23. doi: 10.1016/j.neuron.2007.07.027.

Long, Hua, Hongbin Wang, Chenguang Zhao, Qiang Duan, Feng Feng, Nan Hui, Li Mao, Huiling Liu, Xiang Mou, and Hua Yuan. 2018. 'Effects of Combining High- and Low-Frequency Repetitive Transcranial Magnetic Stimulation on Upper Limb Hemiparesis in the Early Phase of Stroke'. *Restorative Neurology and Neuroscience* 36(1):21–30. doi: 10.3233/RNN-170733.

Lopes-dos-Santos, Vítor, Gido M. van de Ven, Alexander Morley, Stéphanie Trouche, Natalia Campo-Urriza, and David Dupret. 2018. 'Parsing Hippocampal Theta Oscillations by Nested Spectral Components during Spatial Exploration and Memory-Guided Behavior'. *Neuron* 100(4):940-952.e7. doi: 10.1016/J.NEURON.2018.09.031.

López-Alonso, Virginia, Binith Cheeran, Dan Río-Rodríguez, and Miguel Fernández-Del-Olmo. 2014. 'Inter-Individual Variability in Response to Non-Invasive Brain Stimulation Paradigms'. *Brain Stimulation* 7(3):372–80. doi: 10.1016/J.BRS.2014.02.004.

Macías, Martín, Verónica Lopez-Virgen, Rafael Olivares-Moreno, and Gerardo Rojas-Piloni. 2022. 'Corticospinal Neurons from Motor and Somatosensory Cortices Exhibit Different Temporal Activity Dynamics during Motor Learning'. *Frontiers in Human Neuroscience* 16:1043501. doi: 10.3389/FNHUM.2022.1043501.

Madisen, Linda, Theresa A. Zwingman, Susan M. Sunkin, Seung Wook Oh, Hatim A. Zariwala, Hong Gu, Lydia L. Ng, Richard D. Palmiter, Michael J. Hawrylycz, Allan R. Jones, Ed S. Lein, and Hongkui Zeng. 2009. 'A Robust and High-Throughput Cre Reporting and

Characterization System for the Whole Mouse Brain'. *Nature Neuroscience* 13(1):133–40. doi: 10.1038/nn.2467.

Maeda, Fumiko, Julian P. Keenan, Jose M. Tormos, Helge Topka, and Alvaro Pascual-Leone. 2000. 'Interindividual Variability of the Modulatory Effects of Repetitive Transcranial Magnetic Stimulation on Cortical Excitability'. *Experimental Brain Research* 133(4):425–30. doi: 10.1007/S002210000432.

Maetzler, Walter, Inga Liepelt, and Daniela Berg. 2009. 'Progression of Parkinson's Disease in the Clinical Phase: Potential Markers'. *The Lancet Neurology* 8(12):1158–71. doi: 10.1016/S1474-4422(09)70291-1.

Makino, Hiroshi, Chi Ren, Haixin Liu, An Na Kim, Neehar Kondapaneni, Xin Liu, Duygu Kuzum, and Takaki Komiyama. 2017. 'Transformation of Cortex-Wide Emergent Properties during Motor Learning'. *Neuron* 94(4):880-890.e8. doi: 10.1016/j.neuron.2017.04.015.

Manita, Satoshi, Takayuki Suzuki, Chihiro Homma, Takashi Matsumoto, Maya Odagawa, Kazuyuki Yamada, Keisuke Ota, Chie Matsubara, Ayumu Inutsuka, Masaaki Sato, Masamichi Ohkura, Akihiro Yamanaka, Yuchio Yanagawa, Junichi Nakai, Yasunori Hayashi, Matthew E. Larkum, and Masanori Murayama. 2015. 'A Top-Down Cortical Circuit for Accurate Sensory Perception'. *Neuron* 86(5):1304–16. doi: 10.1016/j.neuron.2015.05.006.

Mann, Edward O., Jillian M. Suckling, Norbert Hajos, Susan A. Greenfield, and Ole Paulsen. 2005. 'Perisomatic Feedback Inhibition Underlies Cholinergically Induced Fast Network Oscillations in the Rat Hippocampus in Vitro'. *Neuron* 45(1):105–17. doi: 10.1016/j.neuron.2004.12.016.

Mansouri, Farrokh, Alaa Shanbour, Frank Mazza, Peter Fettes, José Zariffa, and Jonathan Downar. 2019. 'Effect of Theta Transcranial Alternating Current Stimulation and Phase-Locked Transcranial Pulsed Current Stimulation on Learning and Cognitive Control'. *Frontiers in Neuroscience* 13:470531. doi: 10.3389/FNINS.2019.01181.

Mao, Tianyi, Deniz Kusefoglu, Bryan M. Hooks, Daniel Huber, Leopoldo Petreanu, and Karel Svoboda. 2011. 'Long-Range Neuronal Circuits Underlying the Interaction between Sensory and Motor Cortex'. *Neuron* 72(1):111–23. doi: 10.1016/J.NEURON.2011.07.029.

Markram, Henry, Maria Toledo-Rodriguez, Yun Wang, Anirudh Gupta, Gilad Silberberg, and Caizhi Wu. 2004. 'Interneurons of the Neocortical Inhibitory System'. *Nature Reviews Neuroscience* 5(10):793–807. doi: 10.1038/nrn1519.

Mateos-Aparicio, Pedro, and Antonio Rodríguez-Moreno. 2019. 'The Impact of Studying Brain Plasticity'. *Frontiers in Cellular Neuroscience* 13:66. doi: 10.3389/FNCEL.2019.00066.

Matsuno-Yagi, Akemi, and Yasuo Mukohata. 1977. 'Two Possible Roles of Bacteriorhodopsin; a Comparative Study of Strains of Halobacterium Halobium Differing in Pigmentation'. *Biochemical and Biophysical Research Communications* 78(1):237–43. doi: 10.1016/0006-291X(77)91245-1.

Mattis, Joanna, Kay M. Tye, Emily A. Ferenczi, Charu Ramakrishnan, Daniel J. O'Shea, Rohit Prakash, Lisa A. Gunaydin, Minsuk Hyun, Lief E. Fenno, Viviana Gradinaru, Ofer Yizhar, and Karl Deisseroth. 2011. 'Principles for Applying Optogenetic Tools Derived from

Direct Comparative Analysis of Microbial Opsins'. *Nature Methods* 9(2):159–72. doi: 10.1038/nmeth.1808.

Mazuir, Elisa, Desdemona Fricker, and Nathalie Sol-Foulon. 2021. 'Neuron–Oligodendrocyte Communication in Myelination of Cortical GABAergic Cells'. *Life (Basel)* 11(3):216. doi: 10.3390/LIFE11030216.

McConnell, George C., Rosa Q. So, Justin D. Hilliard, Paola Lopomo, and Warren M. Grill. 2012. 'Effective Deep Brain Stimulation Suppresses Low-Frequency Network Oscillations in the Basal Ganglia by Regularizing Neural Firing Patterns'. *Journal of Neuroscience* 32(45):15657–68. doi: 10.1523/JNEUROSCI.2824-12.2012.

McNamara, C., and A. Sharott. 2022. 'OscillTrack – Real-Time Neuronal Oscillation Tracking for Closed-Loop Stimulation'.

McNamara, Colin G., Max Rothwell, and Andrew Sharott. 2022. 'Stable, Interactive Modulation of Neuronal Oscillations Produced through Brain-Machine Equilibrium'. *Cell Reports* 41(6):111616. doi: 10.1016/J.CELREP.2022.111616.

Meissner, Sarah Nadine, Vanessa Krause, Martin Südmeyer, Christian Johannes Hartmann, and Bettina Pollok. 2018. 'The Significance of Brain Oscillations in Motor Sequence Learning: Insights from Parkinson's Disease'. *NeuroImage: Clinical* 20:448–57. doi: 10.1016/J.NICL.2018.08.009.

Miller, Mark N., Benjamin W. Okaty, and Sacha B. Nelson. 2008. 'Region-Specific Spike-Frequency Acceleration in Layer 5 Pyramidal Neurons Mediated by Kv1 Subunits'. *The Journal of Neuroscience* 28(51):13716. doi: 10.1523/JNEUROSCI.2940-08.2008.

Mitchell, S. J., J. N. P. Rawlins, O. Steward, and D. S. Olton. 1982. 'Medial Septal Area Lesions Disrupt Theta Rhythm and Cholinergic Staining in Medial Entorhinal Cortex and Produce Impaired Radial Arm Maze Behavior in Rats'. *Journal of Neuroscience* 2(3):292–302. doi: 10.1523/JNEUROSCI.02-03-00292.1982.

Mizuno, Yoshikuni, Satoe Shimoda, and Hideki Origasa. 2018. 'Long-Term Treatment of Parkinson's Disease with Levodopa and Other Adjunctive Drugs'. *Journal of Neural Transmission* 125(1):35–43. doi: 10.1007/s00702-016-1671-x.

Monto, Simo, Satu Palva, Juha Voipio, and J. Matias Palva. 2008. 'Very Slow EEG Fluctuations Predict the Dynamics of Stimulus Detection and Oscillation Amplitudes in Humans'. *Journal of Neuroscience* 28(33):8268–72. doi: 10.1523/JNEUROSCI.1910-08.2008.

Muñoz-Castañeda, Rodrigo, Brian Zingg, Katherine S. Matho, Xiaoyin Chen, Quanxin Wang, Nicholas N. Foster, Anan Li, Arun Narasimhan, Karla E. Hirokawa, Bingxing Huo, Samik Bannerjee, Laura Korobkova, Chris Sin Park, Young Gyun Park, Michael S. Bienkowski, Uree Chon, Diek W. Wheeler, Xiangning Li, Yun Wang, Maitham Naeemi, Peng Xie, Lijuan Liu, Kathleen Kelly, Xu An, Sarojini M. Attili, Ian Bowman, Anastasiia Bludova, Ali Cetin, Liya Ding, Rhonda Drewes, Florence D'Orazi, Corey Elowsky, Stephan Fischer, William Galbavy, Lei Gao, Jesse Gillis, Peter A. Groblewski, Lin Gou, Joel D. Hahn, Joshua T. Hatfield, Houri Hintiryan, Junxiang Jason Huang, Hideki Kondo, Xiuli Kuang, Philip Lesnar, Xu Li, Yaoyao Li, Mengkuan Lin, Darrick Lo, Judith Mizrachi, Stephanie Mok, Philip R. Nicovich, Ramesh Palaniswamy, Jason Palmer, Xiaoli Qi, Elise Shen, Yu Chi Sun, Huizhong W. Tao, Wayne Wakemen, Yimin Wang, Shenqin Yao, Jing Yuan, Huiqing Zhan, Muye Zhu, Lydia Ng, Li I. Zhang, Byung Kook Lim, Michael Hawrylycz, Hui

Gong, James C. Gee, Yongsoo Kim, Kwanghun Chung, X. William Yang, Hanchuan Peng, Qingming Luo, Partha P. Mitra, Anthony M. Zador, Hongkui Zeng, Giorgio A. Ascoli, Z. Josh Huang, Pavel Osten, Julie A. Harris, and Hong Wei Dong. 2021. 'Cellular Anatomy of the Mouse Primary Motor Cortex'. *Nature* 598(7879):159–66. doi: 10.1038/s41586-021-03970-w.

Murata, Yumi, Noriyuki Higo, Takao Oishi, Akiko Yamashita, Keiji Matsuda, Motoharu Hayashi, and Shigeru Yamane. 2008. 'Effects of Motor Training on the Recovery of Manual Dexterity after Primary Motor Cortex Lesion in Macaque Monkeys'. *Journal of Neurophysiology* 99(2):773–86. doi: 10.1152/JN.01001.2007.

Murthy, Venkatesh N., and Eberhard E. Fetz. 1996. 'Oscillatory Activity in Sensorimotor Cortex of Awake Monkeys: Synchronization of Local Field Potentials and Relation to Behavior'. *J Neurophysiol* 76(6):3949–67. doi: 10.1152/JN.1996.76.6.3949.

Muthukumaraswamy, Suresh D. 2010. 'Functional Properties of Human Primary Motor Cortex Gamma Oscillations'. *Journal of Neurophysiology* 104(5):2873–85. doi: 10.1152/JN.00607.2010.

Muthuraman, Muthuraman, Manuel Bange, Nabin Koirala, Dumitru Ciolac, Bogdan Pintea, Martin Glaser, Gerd Tinkhauser, Peter Brown, Gunther Deuschl, and Sergiu Groppa. 2020. 'Cross-Frequency Coupling between Gamma Oscillations and Deep Brain Stimulation Frequency in Parkinson's Disease'. *Brain* 143(11):3393–3407. doi: 10.1093/BRAIN/AWAA297.

Nagel, Georg, Doris Ollig, Markus Fuhrmann, Suneel Kateriya, Anna Maria Musti, Ernst Bamberg, and Peter Hegemann. 2002. 'Channelrhodopsin-1: A Light-Gated Proton Channel in Green Algae'. *Science* 296(5577):2395–98. doi: 10.1126/SCIENCE.1072068.

Nicholson, Elizabeth, Dmitry A. Kuzmin, Marco Leite, Thomas E. Akam, and Dimitri Michael Kullmann. 2018. 'Analogue Closed-Loop Optogenetic Modulation of Hippocampal Pyramidal Cells Dissociates Gamma Frequency and Amplitude'. *ELife* 7(e38346). doi: 10.7554/ELIFE.38346.

Nowak, Magdalena, Emily Hinson, Freek Van Ede, Alek Pogosyan, Andrea Guerra, Andrew Quinn, Peter Brown, and Charlotte J. Stagg. 2017. 'Driving Human Motor Cortical Oscillations Leads to Behaviorally Relevant Changes in Local GABAA Inhibition: A TACS-TMS Study'. *Journal of Neuroscience* 37(17):4481–92. doi: 10.1523/JNEUROSCI.0098-17.2017.

Nucifora, Frederick C., Edgar Woznica, Brian J. Lee, Nicola Cascella, and Akira Sawa. 2019. 'Treatment Resistant Schizophrenia: Clinical, Biological, and Therapeutic Perspectives'. *Neurobiology of Disease* 131:104257. doi: 10.1016/J.NBD.2018.08.016.

Nuñez, Angel, and Washington Buño. 2021. 'The Theta Rhythm of the Hippocampus: From Neuronal and Circuit Mechanisms to Behavior'. *Frontiers in Cellular Neuroscience* 15:649262. doi: 10.3389/FNCEL.2021.649262.

O'Keefe, John, and Michael L. Recce. 1993. 'Phase Relationship between Hippocampal Place Units and the EEG Theta Rhythm'. *Hippocampus* 3(3):317–30. doi: 10.1002/HIPO.450030307.

Onorato, Irene, Athanasia Tzanou, Marius Schneider, Cem Uran, Ana Broggini, and Martin Vinck. 2023. 'Distinct Roles of PV and Sst Interneurons in Visually-Induced Gamma Oscillations'. *BioRxiv* 2023.04.08.535291. doi: 10.1101/2023.04.08.535291.

Orekhova, Elena V., Tatiana A. Stroganova, Gudrun Nygren, Marina M. Tsetlin, Irina N. Posikera, Christopher Gillberg, and Mikael Elam. 2007. 'Excess of High Frequency Electroencephalogram Oscillations in Boys with Autism'. *Biological Psychiatry* 62(9):1022–29. doi: 10.1016/J.BIOPSYCH.2006.12.029.

Osinski, Bolesław L., Alex Kim, Wenxi Xiao, Nisarg M. Mehta, and Leslie M. Kay. 2018. 'Neural Circuits: Pharmacological Manipulation of the Olfactory Bulb Modulates Beta Oscillations: Testing Model Predictions'. *Journal of Neurophysiology* 120(3):1090. doi: 10.1152/JN.00090.2018.

Oudijn, M. S., J. T. W. Linders, A. Lok, P. R. Schuurman, P. van den Munckhof, A. A. van Elburg, G. A. van Wingen, R. J. T. Mocking, and D. Denys. 2023. 'Neural Effects of Deep Brain Stimulation on Reward and Loss Anticipation and Food Viewing in Anorexia Nervosa: A Pilot Study'. *Journal of Eating Disorders* 11(1):1–12. doi: 10.1186/S40337-023-00863-3.

Owen, Scott F., Max H. Liu, and Anatol C. Kreitzer. 2019. 'Thermal Constraints on in Vivo Optogenetic Manipulations'. *Nature Neuroscience* 22(7):1061–65. doi: 10.1038/s41593-019-0422-3.

Paxinos, George, and Keith B. J. Franklin. 2019. *Paxinos and Franklin's The Mouse Brain in Stereotaxic Coordinates*. Vol. Fifth Edition.

Penfield, Wilder, and Edwin Boldrey. 1937. 'SOMATIC MOTOR AND SENSORY REPRESENTATION IN THE CEREBRAL CORTEX OF MAN AS STUDIED BY ELECTRICAL STIMULATION'. *Brain* 60(4):389–443. doi: 10.1093/BRAIN/60.4.389.

Penttonen, M., N. Nurminen, R. Miettinen, J. Sirviö, D. A. Henze, J. Csicsvári, and G. Buzsáki. 1999. 'Ultra-Slow Oscillation (0.025 Hz) Triggers Hippocampal Afterdischarges in Wistar Rats'. *Neuroscience* 94(3):735–43. doi: 10.1016/S0306-4522(99)00367-X.

Penttonen, Markku, and György Buzsáki. 2003. 'Natural Logarithmic Relationship between Brain Oscillators'. *Thalamus & Related Systems* 2(2):145–52. doi: 10.1016/S1472-9288(03)00007-4.

Perrenoud, Quentin, Cyriel M. A. Pennartz, and Luc J. Gentet. 2016. 'Membrane Potential Dynamics of Spontaneous and Visually Evoked Gamma Activity in V1 of Awake Mice'. *PLOS Biology* 14(2):e1002383. doi: 10.1371/JOURNAL.PBIO.1002383.

Pfurtscheller, G., and A. Aranibar. 1977. 'Event-Related Cortical Desynchronization Detected by Power Measurements of Scalp EEG'. *Electroencephalography and Clinical Neurophysiology* 42(6):817–26. doi: 10.1016/0013-4694(77)90235-8.

Pfurtscheller, G., and F. H. Lopes Da Silva. 1999. 'Event-Related EEG/MEG Synchronization and Desynchronization: Basic Principles'. *Clinical Neurophysiology* 110(11):1842–57. doi: 10.1016/S1388-2457(99)00141-8.

Pinault, D., and M. Deschênes. 1992. 'Voltage-Dependent 40-Hz Oscillations in Rat Reticular Thalamic Neurons in Vivo'. *Neuroscience* 51(2):245–58. doi: 10.1016/0306-4522(92)90312-P.

Pineda, Jaime A. 2005. 'The Functional Significance of Mu Rhythms: Translating "Seeing" and "Hearing" into "Doing"'. *Brain Research Reviews* 50(1):57–68. doi: 10.1016/J.BRAINRESREV.2005.04.005.

Pisanello, Ferruccio, Leonardo Sileo, Ian A. Oldenburg, Marco Pisanello, Luigi Martiradonna, John A. Assad, Bernardo L. Sabatini, and Massimo De Vittorio. 2014. 'Multipoint-Emitting Optical Fibers for Spatially Addressable In Vivo Optogenetics'. *Neuron* 82(6):1245–54. doi: 10.1016/J.NEURON.2014.04.041.

Pisano, Filippo, Marco Pisanello, Suk Joon Lee, Jaeeon Lee, Emanuela Maglie, Antonio Balena, Leonardo Sileo, Barbara Spagnolo, Marco Bianco, Minsuk Hyun, Massimo De Vittorio, Bernardo L. Sabatini, and Ferruccio Pisanello. 2019. 'Depth-Resolved Fiber Photometry with a Single Tapered Optical Fiber Implant'. *Nature Methods* 16(11):1185–92. doi: 10.1038/s41592-019-0581-x.

Popescu, Andrei T., Daniela Popa, and Denis Paré. 2009. 'Coherent Gamma Oscillations Couple the Amygdala and Striatum during Learning'. *Nature Neuroscience* 12(6):801–7. doi: 10.1038/nn.2305.

Ramanathan, Dhakshin, James M. Conner, and Mark H. Tuszynski. 2006. 'A Form of Motor Cortical Plasticity That Correlates with Recovery of Function after Brain Injury'. *Proceedings of the National Academy of Sciences of the United States of America* 103(30):11370–75. doi: 10.1073/PNAS.0601065103.

Rapinesi, Chiara, Georgios D. Kotzalidis, Stefano Ferracuti, Gabriele Sani, Paolo Girardi, and Antonio Del Casale. 2019. 'Brain Stimulation in Obsessive-Compulsive Disorder (OCD): A Systematic Review'. *Current Neuropharmacology* 17(8):787–807. doi: 10.2174/1570159X17666190409142555.

Ridding, M. C., and U. Ziemann. 2010. 'Determinants of the Induction of Cortical Plasticity by Non-Invasive Brain Stimulation in Healthy Subjects'. *The Journal of Physiology* 588(13):2291–2304. doi: 10.1113/JPHYSIOL.2010.190314.

Rizzolatti, Giacomo, Leonardo Fogassi, and Vittorio Gallese. 2001. 'Neurophysiological Mechanisms Underlying the Understanding and Imitation of Action'. *Nature Reviews Neuroscience* 2(9):661–70. doi: 10.1038/35090060.

Rosson, Stella, Renato de Filippis, Giovanni Croatto, Enrico Collantoni, Simone Pallottino, Daniel Guinart, Andre R. Brunoni, Bernardo Dell'Osso, Giorgio Pigato, Joshua Hyde, Valerie Brandt, Samuele Cortese, Jess G. Fiedorowicz, Georgios Petrides, Christoph U. Correll, and Marco Solmi. 2022. 'Brain Stimulation and Other Biological Non-Pharmacological Interventions in Mental Disorders: An Umbrella Review'. *Neuroscience & Biobehavioral Reviews* 139(104743). doi: 10.1016/J.NEUBIOREV.2022.104743.

Rothwell, Patrick E., Scott J. Hayton, Gordon L. Sun, Marc V. Fuccillo, Byung Kook Lim, and Robert C. Malenka. 2015. 'Input- and Output-Specific Regulation of Serial Order Performance by Corticostriatal Circuits'. *Neuron* 88(2):345–56. doi: 10.1016/j.neuron.2015.09.035.

Roux, Franck Emmanuel, Mahamadou Niare, Saloua Charni, Carlo Giussani, and Jean Baptiste Durand. 2020. 'Functional Architecture of the Motor Homunculus Detected by Electrostimulation'. *The Journal of Physiology* 598(23):5487–5504. doi: 10.1113/JP280156.

Royer, Sébastien, Boris V. Zemelman, Attila Losonczy, Jinhyun Kim, Frances Chance, Jeffrey C. Magee, and György Buzsáki. 2012. 'Control of Timing, Rate and Bursts of Hippocampal Place Cells by Dendritic and Somatic Inhibition'. *Nature Neuroscience* 15(5):769–75. doi: 10.1038/nn.3077.

Rozengurt, Roman, Anat Barnea, Sunao Uchida, and Daniel A. Levy. 2016. 'Theta EEG Neurofeedback Benefits Early Consolidation of Motor Sequence Learning'. *Psychophysiology* 53(7):965–73. doi: 10.1111/PSYP.12656.

Rudy, Bernardo, Gordon Fishell, Soo Hyun Lee, and Jens Hjerling-Leffler. 2011. 'Three Groups of Interneurons Account for Nearly 100% of Neocortical GABAergic Neurons'. *Developmental Neurobiology* 71(1):45–61. doi: 10.1002/DNEU.20853.

Rungta, Ravi L., Bruno Félix Osmanski, Davide Boido, Mickael Tanter, and Serge Charpak. 2017. 'Light Controls Cerebral Blood Flow in Naive Animals'. *Nature Communications 2017 8:1* 8(1):1–9. doi: 10.1038/ncomms14191.

Rustamov, Nabi, Joseph Humphries, Alexandre Carter, and Eric C. Leuthardt. 2022. 'Theta-Gamma Coupling as a Cortical Biomarker of Brain-Computer Interface-Mediated Motor Recovery in Chronic Stroke'. *Brain Communications* 4(3):fcac136. doi: 10.1093/BRAINCOMMS/FCAC136.

Salanova, Vicenta, Thomas Witt, Robert Worth, Thomas R. Henry, Robert E. Gross, Jules M. Nazzaro, Douglas Labar, Michael R. Sperling, Ashwini Sharan, Evan Sandok, Adrian Handforth, John M. Stern, Steve Chung, Jaimie M. Henderson, Jacqueline French, Gordon Baltuch, William E. Rosenfeld, Paul Garcia, Nicholas M. Barbaro, Nathan B. Fountain, W. Jeffrey Elias, Robert R. Goodman, John R. Pollard, Alexander I. Tröster, Christopher P. Irwin, MS Kristin Lambrecht, Pa-c Nina Graves, PharmD Robert Fisher, St Luke, and St Louis. 2015. 'Long-Term Efficacy and Safety of Thalamic Stimulation for Drug-Resistant Partial Epilepsy'. *Neurology* 84(10):1017–25. doi: 10.1212/WNL.0000000000001334.

Sanes, Jerome N., and John P. Donoghue. 2000. 'PLASTICITY AND PRIMARY MOTOR CORTEX'. *Annu. Rev. Neurosci* 23:393–415.

Scaife, Jessica C., John Eraifej, Alexander L. Green, Beth Petric, Tipu Z. Aziz, and Rebecca J. Park. 2022. 'Deep Brain Stimulation of the Nucleus Accumbens in Severe Enduring Anorexia Nervosa: A Pilot Study'. *Frontiers in Behavioral Neuroscience* 16:842184. doi: 10.3389/FNBEH.2022.842184.

Schreglmann, Sebastian R., David Wang, Robert L. Peach, Junheng Li, Xu Zhang, Anna Latorre, Edward Rhodes, Emanuele Panella, Antonino M. Cassara, Edward S. Boyden, Mauricio Barahona, Sabato Santaniello, John Rothwell, Kailash P. Bhatia, and Nir Grossman. 2021. 'Non-Invasive Suppression of Essential Tremor via Phase-Locked Disruption of Its Temporal Coherence'. *Nature Communications* 12(1):1–15. doi: 10.1038/s41467-020-20581-7.

Schuepbach, W. M. M., J. Rau, K. Knudsen, J. Volkmann, P. Krack, L. Timmermann, T. D. Hälbig, H. Hesekamp, S. M. Navarro, N. Meier, D. Falk, M. Mehdorn, S. Paschen, M. Maarouf, M. T. Barbe, G. R. Fink, A. Kupsch, D. Gruber, G. H. Schneider, E. Seigneuret, A. Kistner, P. Chaynes, F. Ory-Magne, C. Brefel Courbon, J. Vesper, A. Schnitzler, L. Wojtecki, J. L. Houeto, B. Bataille, D. Maltête, P. Damier, S. Raoul, F. Sixel-Doering, D. Hellwig, A. Gharabaghi, R. Krüger, M. O. Pinsker, F. Amtage, J. M. Régis, T. Witjas, S. Thobois, P. Mertens, M. Kloss, A. Hartmann, W. H. Oertel, B. Post, H. Speelman, Y. Agid, C. Schade-Brittinger, and G. Deuschl. 2013. 'Neurostimulation for Parkinson's Disease with Early Motor Complications'. *The New England Journal of Medicine* 368(7):610–22. doi: 10.1056/NEJMOA1205158.

Schürmann, Martin, and Erol Başar. 2001. 'Functional Aspects of Alpha Oscillations in the EEG'. *International Journal of Psychophysiology* 39(2–3):151–58. doi: 10.1016/S0167-8760(00)00138-0.

Semahegn, Agumasie, Kwasi Torpey, Adom Manu, Nega Assefa, Gezahegn Tesfaye, and Augustine Ankomah. 2020. 'Psychotropic Medication Non-Adherence and Its Associated Factors among Patients with Major Psychiatric Disorders: A Systematic Review and Meta-Analysis'. *Systematic Reviews* 9(1). doi: 10.1186/S13643-020-1274-3.

Sharott, Andrew, Peter J. Magill, Daniel Harnack, Andreas Kupsch, Wassilios Meissner, and Peter Brown. 2005. 'Dopamine Depletion Increases the Power and Coherence of β-Oscillations in the Cerebral Cortex and Subthalamic Nucleus of the Awake Rat'. *European Journal of Neuroscience* 21(5):1413–22. doi: 10.1111/J.1460-9568.2005.03973.X.

Shepherd, Gordon M. G. 2013. 'Corticostriatal Connectivity and Its Role in Disease'. *Nature Reviews Neuroscience* 14(4):278–91. doi: 10.1038/nrn3469.

Sheth, Sameer A., Kelly R. Bijanki, Brian Metzger, Anusha Allawala, Victoria Pirtle, Joshua A. Adkinson, John Myers, Raissa K. Mathura, Denise Oswalt, Evangelia Tsolaki, Jiayang Xiao, Angela Noecker, Adriana M. Strutt, Jeffrey F. Cohn, Cameron C. McIntyre, Sanjay J. Mathew, David Borton, Wayne Goodman, and Nader Pouratian. 2022. 'Deep Brain Stimulation for Depression Informed by Intracranial Recordings'. *Biological Psychiatry* 92(3):246–51. doi: 10.1016/j.biopsych.2021.11.007.

Shu, Yousheng, Andrea Hasenstaub, and David A. McCormick. 2003. 'Turning on and off Recurrent Balanced Cortical Activity'. *Nature* 423(6937):288–93. doi: 10.1038/nature01616.

Siapas, Athanassios G., Evgueniy V. Lubenov, and Matthew A. Wilson. 2005. 'Prefrontal Phase Locking to Hippocampal Theta Oscillations'. *Neuron* 46(1):141–51. doi: 10.1016/J.NEURON.2005.02.028.

Siegel, Markus, Tobias H. Donner, and Andreas K. Engel. 2012. 'Spectral Fingerprints of Large-Scale Neuronal Interactions'. *Nature Reviews Neuroscience* 13(2):121–34. doi: 10.1038/nrn3137.

Siegle, Joshua H., and Matthew A. Wilson. 2014. 'Enhancement of Encoding and Retrieval Functions through Theta Phase-Specific Manipulation of Hippocampus'. *ELife* 3(e03061). doi: 10.7554/ELIFE.03061.001.

Silberberg, Gilad, and Henry Markram. 2007. 'Disynaptic Inhibition between Neocortical Pyramidal Cells Mediated by Martinotti Cells'. *Neuron* 53(5):735–46. doi: 10.1016/J.NEURON.2007.02.012.

Silva, Laurie R., Yael Amitai, and Barry W. Connors. 1991. 'Intrinsic Oscillations of Neocortex Generated by Layer 5 Pyramidal Neurons'. *Science (New York, N.Y.)* 251(4992):432–35. doi: 10.1126/SCIENCE.1824881.

Simon, David M., and Mark T. Wallace. 2016. 'Dysfunction of Sensory Oscillations in Autism Spectrum Disorder'. *Neuroscience and Biobehavioral Reviews* 68:848–61. doi: 10.1016/J.NEUBIOREV.2016.07.016.

Singer, Wolf. 1993. 'Synchronization of Cortical Activity and Its Putative Role in Information Processing and Learning'. *Annual Review of Physiology* 55:349–74. doi: 10.1146/ANNUREV.PH.55.030193.002025.

Sirota, Anton, Sean Montgomery, Shigeyoshi Fujisawa, Yoshikazu Isomura, Michael Zugaro, and György Buzsáki. 2008. 'Entrainment of Neocortical Neurons and Gamma Oscillations by the Hippocampal Theta Rhythm'. *Neuron* 60(4):683–97. doi: 10.1016/j.neuron.2008.09.014.

Smarr, Benjamin, and Lance J. Kriegsfeld. 2022. 'Female Mice Exhibit Less Overall Variance, with a Higher Proportion of Structured Variance, than Males at Multiple Timescales of Continuous Body Temperature and Locomotive Activity Records'. *Biology of Sex Differences* 13(1):1–10. doi: 10.1186/S13293-022-00451-1.

Sohal, Vikaas S., and Jessica A. Cardin. 2016. 'Snapshots of the Brain in Action: Local Circuit Operations through the Lens of γ Oscillations'. *Journal of Neuroscience* 36(41):10496–504. doi: 10.1523/JNEUROSCI.1021-16.2016.

Sohal, Vikaas S., Feng Zhang, Ofer Yizhar, and Karl Deisseroth. 2009. 'Parvalbumin Neurons and Gamma Rhythms Enhance Cortical Circuit Performance'. *Nature* 459(7247):698–702. doi: 10.1038/nature07991.

Somogyi, Peter, Linda Katona, Thomas Klausberger, Bálint Lasztóczi, and Tim J. Viney. 2014. 'Temporal Redistribution of Inhibition over Neuronal Subcellular Domains Underlies State-Dependent Rhythmic Change of Excitability in the Hippocampus'. *Philosophical Transactions of the Royal Society B: Biological Sciences* 369(1635):20120518. doi: 10.1098/RSTB.2012.0518.

Spooner, Rachel K, Tony W Wilson, R K Spooner, and T W Wilson. 2022. 'Cortical Theta–Gamma Coupling Governs the Adaptive Control of Motor Commands'. *Brain Communications* 4(6):fcac249. doi: 10.1093/BRAINCOMMS/FCAC249.

Stahlberg, Markus A., Charu Ramakrishnan, Katrin I. Willig, Edward S. Boyden, Karl Deisseroth, and Camin Dean. 2019. 'Investigating the Feasibility of Channelrhodopsin Variants for Nanoscale Optogenetics'. *Neurophotonics* 6(1):1. doi: 10.1117/1.NPH.6.1.015007.

Stark, Eran, Tibor Koos, and György Buzsáki. 2012. 'Diode Probes for Spatiotemporal Optical Control of Multiple Neurons in Freely Moving Animals'. *Journal of Neurophysiology* 108(1):349–63. doi: 10.1152/JN.00153.2012.

Stiles, Joan, and Terry L. Jernigan. 2010. ‘The Basics of Brain Development’. *Neuropsychology Rev* 20(4):327–48. doi: 10.1007/s11065-010-9148-4.

Stujenske, Joseph M., Timothy Spellman, and Joshua A. Gordon. 2015. ‘Modeling the Spatiotemporal Dynamics of Light and Heat Propagation for In Vivo Optogenetics’. *Cell Reports* 12(3):525–34. doi: 10.1016/J.CELREP.2015.06.036.

Swann, Nicole C., Coralie De Hemptinne, Svjetlana Miocinovic, Salman Qasim, Sarah S. Wang, Nathan Ziman, Jill L. Ostrem, Marta San Luciano, Nicholas B. Galifianakis, and Philip A. Starr. 2016. ‘Gamma Oscillations in the Hyperkinetic State Detected with Chronic Human Brain Recordings in Parkinson’s Disease’. *Journal of Neuroscience* 36(24):6445–58. doi: 10.1523/JNEUROSCI.1128-16.2016.

Swann, Nicole C., Coralie De Hemptinne, Margaret C. Thompson, Svjetlana Miocinovic, Andrew M. Miller, Ro’Ee Gilron, Jill L. Ostrem, Howard J. Chizeck, and Philip A. Starr. 2018. ‘Adaptive Deep Brain Stimulation for Parkinson’s Disease Using Motor Cortex Sensing’. *Journal of Neural Engineering* 15(4):046006. doi: 10.1088/1741-2552/AABC9B.

Szabadics, János, Csaba Varga, Gábor Molnár, Szabolcs Oláh, Pál Barzó, and Gábor Tamás. 2006. ‘Excitatory Effect of GABAergic Axo-Axonic Cells in Cortical Microcircuits’. *Science* 311(5758):233–35. doi: 10.1126/SCIENCE.1121325.

Tachibana, Yoshihisa, Hitoshi Kita, Satomi Chiken, Masahiko Takada, and Atsushi Nambu. 2008. ‘Motor Cortical Control of Internal Pallidal Activity through Glutamatergic and GABAergic Inputs in Awake Monkeys’. *European Journal of Neuroscience* 27(1):238–53. doi: 10.1111/J.1460-9568.2007.05990.X.

Tan, Enda, Sonya V. Troller-Renfree, Santiago Morales, George A. Buzzell, Marco McSweeney, Martín Antúnez, and Nathan A. Fox. 2024. ‘Theta Activity and Cognitive Functioning: Integrating Evidence from Resting-State and Task-Related Developmental Electroencephalography (EEG) Research’. *Developmental Cognitive Neuroscience* 67:101404. doi: 10.1016/J.DCN.2024.101404.

Taniguchi, Hiroki, Miao He, Priscilla Wu, Sangyong Kim, Raehum Paik, Ken Sugino, Duda Kvitsani, Yu Fu, Jiangteng Lu, Ying Lin, Goichi Miyoshi, Yasuyuki Shima, Gord Fishell, Sacha B. Nelson, and Z. Josh Huang. 2011. ‘A Resource of Cre Driver Lines for Genetic Targeting of GABAergic Neurons in Cerebral Cortex’. *Neuron* 71(6):995–1013. doi: 10.1016/J.NEURON.2011.07.026.

Topalovic, Uros, Sam Barclay, Chenkai Ling, Ahmed Alzuhair, Wenhao Yu, Vahagn Hokhikyan, Hariprasad Chandrakumar, Dejan Rozgic, Wenlong Jiang, Sina Basir-Kazeruni, Sabrina L. Maoz, Cory S. Inman, Matthias Stangl, Jay Gill, Ausaf Bari, Aria Fallah, Dawn Eliashiv, Nader Pouratian, Itzhak Fried, Nanthia Suthana, and Dejan Markovic. 2023. ‘A Wearable Platform for Closed-Loop Stimulation and Recording of Single-Neuron and Local Field Potential Activity in Freely Moving Humans’. *Nature Neuroscience* 26(3):517–27. doi: 10.1038/s41593-023-01260-4.

Traub, Roger D., Miles A. Whittington, Ian M. Stanford, and John G. R. Jeffreys. 1996. *A Mechanism for Generation of Long-Range Synchronous Fast Oscillations in the Cortex*. doi: 10.1038/383621a0.

Tremblay, Robin, Soohyun Lee, and Bernardo Rudy. 2016. 'GABAergic Interneurons in the Neocortex: From Cellular Properties to Circuits'. *Neuron* 91(2):260–92. doi: 10.1016/J.NEURON.2016.06.033.

Tsai, Hsing Chen, Feng Zhang, Antoine Adamantidis, Garret D. Stuber, Antonello Bond, Luis De Lecea, and Karl Deisseroth. 2009. 'Phasic Firing in Dopaminergic Neurons Is Sufficient for Behavioral Conditioning'. *Science* 324(5930):1080–84. doi: 10.1126/SCIENCE.1168878.

Uhlhaas, Peter J., David E. J. Linden, Wolf Singer, Corinna Haenschel, Michael Lindner, Konrad Maurer, and Eugenio Rodriguez. 2006. 'Dysfunctional Long-Range Coordination of Neural Activity during Gestalt Perception in Schizophrenia'. *Journal of Neuroscience* 26(31):8168–75. doi: 10.1523/JNEUROSCI.2002-06.2006.

Uhlhaas, Peter J., and Wolf Singer. 2006. 'Neural Synchrony in Brain Disorders: Relevance for Cognitive Dysfunctions and Pathophysiology'. *Neuron* 52(1):155–68. doi: 10.1016/J.NEURON.2006.09.020.

Uhlhaas, Peter J., and Wolf Singer. 2010. 'Abnormal Neural Oscillations and Synchrony in Schizophrenia'. *Nature Reviews Neuroscience* 11(2):100–113. doi: 10.1038/nrn2774.

Vanderwolf, C. H. 1969. 'Hippocampal Electrical Activity and Voluntary Movement in the Rat'. *Electroencephalography and Clinical Neurophysiology* 26(4):407–18. doi: 10.1016/0013-4694(69)90092-3.

Velligan, Dawn I., Martha Sajatovic, Ainslie Hatch, Pavel Kramata, and John P. Docherty. 2017. 'Why Do Psychiatric Patients Stop Antipsychotic Medication? A Systematic Review of Reasons for Nonadherence to Medication in Patients with Serious Mental Illness'. *Patient Preference and Adherence* 11:449–68. doi: 10.2147/PPA.S124658.

Veuthey, T. L., K. Derosier, S. Kondapavulur, and K. Ganguly. 2020. 'Single-Trial Cross-Area Neural Population Dynamics during Long-Term Skill Learning'. *Nature Communications* 11(1):1–15. doi: 10.1038/s41467-020-17902-1.

Vierock, Johannes, Silvia Rodriguez-Rozada, Alexander Dieter, Florian Pieper, Ruth Sims, Federico Tenedini, Amelie C. F. Bergs, Imane Bendifallah, Fangmin Zhou, Nadja Zeitzschel, Joachim Ahlbeck, Sandra Augustin, Kathrin Sauter, Eirini Papagiakoumou, Alexander Gottschalk, Peter Soba, Valentina Emiliani, Andreas K. Engel, Peter Hegemann, and J. Simon Wiegert. 2021. 'BiPOLES Is an Optogenetic Tool Developed for Bidirectional Dual-Color Control of Neurons'. *Nature Communications* 12(1):1–20. doi: 10.1038/s41467-021-24759-5.

Voytek, Bradley, Mark A. Kramer, John Case, Kyle Q. Lepage, Zechari R. Tempesta, Robert T. Knight, and Adam Gazzaley. 2015. 'Age-Related Changes in 1/f Neural Electrophysiological Noise'. *Journal of Neuroscience* 35(38):13257–65. doi: 10.1523/JNEUROSCI.2332-14.2015.

Van Vreeswijk, C., and H. Sompolinsky. 1996. 'Chaos in Neuronal Networks with Balanced Excitatory and Inhibitory Activity'. *Science* 274(5293):1724–26. doi: 10.1126/SCIENCE.274.5293.1724.

Walker, William C., and Treven C. Pickett. 2007. 'Motor Impairment after Severe Traumatic Brain Injury: A Longitudinal Multicenter Study'. *Journal of Rehabilitation Research and Development* 44(7):975–82. doi: 10.1682/JRRD.2006.12.0158.

Wang, Yingxue, Sandro Romani, Brian Lustig, Anthony Leonardo, and Eva Pastalkova. 2014. 'Theta Sequences Are Essential for Internally Generated Hippocampal Firing Fields'. *Nature Neuroscience* 18(2):282–88. doi: 10.1038/nn.3904.

Whishaw, Ian Q. 2000. 'Loss of the Innate Cortical Engram for Action Patterns Used in Skilled Reaching and the Development of Behavioral Compensation Following Motor Cortex Lesions in the Rat'. *Neuropharmacology* 39(5):788–805. doi: 10.1016/S0028-3908(99)00259-2.

Whissell, Paul D., Janine D. Cajanding, Nicole Fogel, and Jun Chul Kim. 2015. 'Comparative Density of CCK- and PV-GABA Cells within the Cortex and Hippocampus'. *Frontiers in Neuroanatomy* 9(September). doi: 10.3389/fnana.2015.00124.

Whittington, Miles A., and Roger D. Traub. 2003. 'Interneuron Diversity Series: Inhibitory Interneurons and Network Oscillations in Vitro'. *Trends in Neurosciences* 26(12):676–82.

Whittington, Miles A., Roger D. Traub, and Natalie E. Adams. 2018. 'A Future for Neuronal Oscillation Research'. *Brain and Neuroscience Advances* 2:239821281879482. doi: 10.1177/2398212818794827.

Whittington, Miles A., Roger D. Traub, and John G. R. Jefferys. 1995. 'Synchronized Oscillations in Interneuron Networks Driven by Metabotropic Glutamate Receptor Activation'. *Nature* 373(6515):612–15. doi: 10.1038/373612a0.

Wiethoff, Sarah, Masashi Hamada, and John C. Rothwell. 2014. 'Variability in Response to Transcranial Direct Current Stimulation of the Motor Cortex'. *Brain Stimulation* 7(3):468–75. doi: 10.1016/J.BRS.2014.02.003.

Winnubst, Johan, Erhan Bas, Tiago A. Ferreira, Zhuhao Wu, Michael N. Economo, Patrick Edson, Ben J. Arthur, Christopher Bruns, Konrad Rokicki, David Schauder, Donald J. Olbris, Sean D. Murphy, David G. Ackerman, Cameron Arshadi, Perry Baldwin, Regina Blake, Ahmad Elsayed, Mashtura Hasan, Daniel Ramirez, Bruno Dos Santos, Monet Weldon, Amina Zafar, Joshua T. Dudman, Charles R. Gerfen, Adam W. Hantman, Wyatt Korff, Scott M. Sternson, Nelson Spruston, Karel Svoboda, and Jayaram Chandrashekar. 2019. 'Reconstruction of 1,000 Projection Neurons Reveals New Cell Types and Organization of Long-Range Connectivity in the Mouse Brain'. *Cell* 179(1):268-281.e13. doi: 10.1016/J.CELL.2019.07.042.

Wojcik, S. M., J. S. Rhee, E. Herzog, A. Sigler, R. Jahn, S. Takamori, N. Brose, and C. Rosenmund. 2004. 'An Essential Role for Vesicular Glutamate Transporter 1 (VGLUT1) in Postnatal Development and Control of Quantal Size'. *Proceedings of the National Academy of Sciences of the United States of America* 101(18):7158–63. doi: 10.1073/PNAS.0401764101.

Woodruff, Alan R., Laura M. McGarry, Tim P. Vogels, Melis Inan, Stewart A. Anderson, and Rafael Yuste. 2011. 'State-Dependent Function of Neocortical Chandelier Cells'. *Journal of Neuroscience* 31(49):17872–86. doi: 10.1523/JNEUROSCI.3894-11.2011.

Wu, Sherry Jingjing, Elaine Sevier, Deepanjali Dwivedi, Giuseppe Antonio Saldi, Ariel Hairston, Sabrina Yu, Lydia Abbott, Da Hae Choi, Mia Sherer, Yanjie Qiu, Ashwini Shinde, Mackenzie Lenahan, Daniella Rizzo, Qing Xu, Irving Barrera, Vipin Kumar, Giovanni Marrero, Alvar Prönneke, Shuhan Huang, Klas Kullander, David A. Stafford, Evan Macosko, Fei Chen, Bernardo Rudy, and Gord Fishell. 2023. 'Cortical Somatostatin Interneuron Subtypes Form Cell-Type-Specific Circuits'. *Neuron* 111(17):2675-2692.e9. doi: 10.1016/J.NEURON.2023.05.032.

Xu, Xiangmin, Keith D. Roby, and Edward M. Callaway. 2010. 'Immunochemical Characterization of Inhibitory Mouse Cortical Neurons: Three Chemically Distinct Classes of Inhibitory Cells'. *Journal of Comparative Neurology* 518(3):389–404. doi: 10.1002/CNE.22229.

Yamawaki, Naoki, Jelena Radulovic, and Gordon M. G. Shepherd. 2016. 'A Corticocortical Circuit Directly Links Retrosplenial Cortex to M2 in the Mouse'. *The Journal of Neuroscience* 36(36):9365–74. doi: 10.1523/JNEUROSCI.1099-16.2016.

Yizhar, Ofer, Lief E. Fenno, Thomas J. Davidson, Murtaza Mogri, and Karl Deisseroth. 2011. 'Optogenetics in Neural Systems'. *Neuron* 71(1):9–34. doi: 10.1016/J.NEURON.2011.06.004.

Yizhar, Ofer, Lief E. Fenno, Matthias Prigge, Franziska Schneider, Thomas J. Davidson, Daniel J. Ogshea, Vikaas S. Sohal, Inbal Goshen, Joel Finkelstein, Jeanne T. Paz, Katja Stehfest, Roman Fudim, Charu Ramakrishnan, John R. Huguenard, Peter Hegemann, and Karl Deisseroth. 2011. 'Neocortical Excitation/Inhibition Balance in Information Processing and Social Dysfunction'. *Nature* 477(7363):171–78. doi: 10.1038/nature10360.

Zaaimi, B., M. Turnbull, A. Hazra, Y. Wang, C. Gandara, F. McLeod, E. E. McDermott, E. Escobedo-Cousin, A. Shah Idil, R. G. Bailey, S. Tardio, A. Patel, N. Ponon, J. Gausden, D. Walsh, F. Hutchings, M. Kaiser, M. O. Cunningham, G. J. Clowry, F. E. N. LeBeau, T. G. Constandinou, S. N. Baker, N. Donaldson, P. Degenaar, A. O'Neill, A. J. Trevelyan, and A. Jackson. 2023. 'Closed-Loop Optogenetic Control of the Dynamics of Neural Activity in Non-Human Primates'. *Nature Biomedical Engineering* 7(4):559–75. doi: 10.1038/s41551-022-00945-8.

Zangiabadi, Nasser, Lady Diana Ladino, Farzad Sina, Juan Pablo Orozco-Hernández, Alexandra Carter, and José Francisco Téllez-Zenteno. 2019. 'Deep Brain Stimulation and Drug-Resistant Epilepsy: A Review of the Literature'. *Frontiers in Neurology* 1:601. doi: 10.3389/fneur.2019.00601.

Zavala, Baltazar, Anthony Jang, Michael Trotta, Codrin I. Lungu, Peter Brown, and Kareem A. Zaghloul. 2018. 'Cognitive Control Involves Theta Power within Trials and Beta Power across Trials in the Prefrontal-Subthalamic Network'. *Brain* 141(12):3361–76. doi: 10.1093/BRAIN/AWY266.

Zeng, Ke, Jiannan Kang, Gaoxiang Ouyang, Jingqing Li, Junxia Han, Yao Wang, Estate M. Sokhadze, Manuel F. Casanova, and Xiaoli Li. 2017. 'Disrupted Brain Network in Children with Autism Spectrum Disorder'. *Scientific Reports* 7(1):1–12. doi: 10.1038/s41598-017-16440-z.

Zhang, Feng, Alexander M. Aravanis, Antoine Adamantidis, Luis De Lecea, and Karl Deisseroth. 2007. 'Circuit-Breakers: Optical Technologies for Probing Neural Signals and Systems'. *Nature Reviews Neuroscience* 8(8):577–81. doi: 10.1038/nrn2192.

Ziemann, Ulf, and Hartwig R. Siebner. 2015. 'Inter-Subject and Inter-Session Variability of Plasticity Induction by Non-Invasive Brain Stimulation: Boon or Bane?' *Brain Stimulation* 8(3):662–63. doi: 10.1016/J.BRS.2015.01.409.

Zou, Xiaolong, and Da Hui Wang. 2016. 'On the Phase Relationship between Excitatory and Inhibitory Neurons in Oscillation'. *Frontiers in Computational Neuroscience* 10(DEC):138. doi: 10.3389/FNCOM.2016.00138.

Zrenner, Christoph, Debora Desideri, Paolo Belardinelli, and Ulf Ziemann. 2018. 'Real-Time EEG-Defined Excitability States Determine Efficacy of TMS-Induced Plasticity in Human Motor Cortex'. *Brain Stimulation* 11(2):374–89. doi: 10.1016/J.BRS.2017.11.016.

Zucker, Irving, and Brian J. Prendergast. 2020. 'Sex Differences in Pharmacokinetics Predict Adverse Drug Reactions in Women'. *Biology of Sex Differences* 11(1):1–14. doi: 10.1186/S13293-020-00308-5.

Zucker, Irving, Brian J. Prendergast, and Annaliese K. Beery. 2022. 'Pervasive Neglect of Sex Differences in Biomedical Research'. *Cold Spring Harbor Perspectives in Biology* 14(4):a039156. doi: 10.1101/CSHPERSPECT.A039156.